Bentonite Barriers – New Experiments and State of the Art

Bentonite as Barrier Material for the Sealing of Underground Disposal Sites

Final Report

GRS - 300

Gesellschaft für Anlagen-
und Reaktorsicherheit
(GRS) mbH

Bentonite Barriers – New Experiments and State of the Art

Bentonite as Barrier Material for the Sealing of Underground Disposal Sites

Final Report

Mingliang Xie (GRS)
Rüdiger Miehe (GRS)
Jörn Kasbohm (Universität Greifswald)
Horst-Jürgen Herbert (GRS)
Lothar Meyer (GRS)
Udo Ziesche (GRS)

June 2012

Remark:

This report was prepared under the contract No. 02 C 1638 with the German Federal Ministry of Education and Research (BMBF).

The work was conducted by the Gesellschaft für Anlagen- und Reaktorsicherheit (GRS) mbH.

The authors are responsible for the content of the report.

GRS - 300
ISBN 978-3-939355-79-3

Keywords:
Diffusion, Gas Diffusion, Gas Dissolution, Heavy Metal, IP21 Solution, MX-80 Bentonite, Saturated NaCl Solution

Preface

From January 2009 to December 2011, the project “Bentonit Barrier” was performed by GRS to investigate the migration parameters of heavy metals in saline solution, and gas diffusion processes through densely compacted bentonite. The summary of current research status and further research gaps provided a thorough overview of research activities on bentonite.

Table of contents

Kurzfassung

Im Rahmen des vom Bundesministerium für Bildung und Forschung (BMBF) geförderten FuE-Projektes 02 C 1638 wurden von der GRS und der Universität Greifswald, im Zeitraum 2009 – 2011, abschließende Untersuchungen an kompaktierten Bentoniten als Verschlussmaterialien für technische Bauwerke in Untertagedeponien durchgeführt.

Mit den theoretisch und experimentell ausgerichteten Arbeiten wurde das Verständnis über die gekoppelten, komplex ablaufenden Prozesse in Bentoniten, die in Kontakt mit salinaren Lösungen stehen, erweitert. Schwerpunktmäßig wurden Wechselwirkungen modelliert, die beim Transport von Schwermetallen und Gasen in Bentoniten auftreten. In Diffusions- und Batch-Versuchen wurde das Sorptionsverhalten ermittelt. Im Ergebnis werden Auswahlkriterien für den effektiven Einsatz von Bentoniten als Verschlussmaterial aufgezeigt.

Bentonite kommen bei der Verfüllung und Abdichtung von Untertagedeponien (UTD) sowie im Altbergbau bei der Verwahrung von Schächten zur Anwendung. Mit ausschlaggebend für ihre langfristige Dichtwirkung und die Beibehaltung ihrer Rückhalteeigenschaften gegenüber Schadstoffen ist die milieuabhängige Stabilität ihrer Mikrostruktur. Salzlösungen und ihre Inhaltsstoffe beeinflussen die Auflösung dieser Mineralstruktur und führen damit langfristig zu einer Veränderung der intrinsischen Eigenschaften der Bentonite.

In modifizierten THROUGH-DIFFUSION-Experimenten mit MX-80-Bentonit wurde der Einfluss verschieden konzentrierter (50 %/90 %iger) NaCl- und IP21-Lösungen auf die Diffusion von Blei (Pb), Cäsium (Cs) und Cadmium (Cd) im Ton untersucht. Im Experiment wurden dazu durch mechanische Kompaktion der trockenen MX-80-Proben Einbaudichten (ρ) von 1,200, 1,400, 1,600 und 1,800 kg/m³ voreingestellt. Die unter den verschiedenen Versuchsbedingungen ermittelten Diffusionskoeffizienten ($D_{koef.}$) für Pb, Cs und Cd liegen in der Größenordnung von $D_{koef.} \sim 10^{-11}/10^{-10}$ m²/s. Trendmäßig zeichnet sich mit steigender Salzkonzentration eine Abnahme der $D_{koef.}$ ab, wobei die Unterschiede zwischen NaCl- und IP21-Lösung nur marginal in Erscheinung treten. Die höchsten Werte für die $D_{koef.}$ wurden an Proben mit einer geringen Einbaudichte (ρ = 1,200 kg/m³) gemessen. Eine Übersicht über alle ermittelten Diffusionskoeffizienten und die Diskussion der Einzelwerte sowie ein Vergleich mit Literaturwerten sind im Bericht aufgeführt.

Die im Projekt weiterentwickelte Standard-Messmethode ermöglicht eine Verkürzung der Versuchszeit und eine effektive Konditionierung (u. a. Dichte, Wassersättigung) der Proben sowie eine verbesserte Kontrolle der Elementdotierung.

Das Sorptionspotenzial von MX-80-Bentonit gegenüber Cd, Cs und Pb wurde für unterschiedlich konzentrierte NaCl-Lösungen (10 % bis 100 %) durch Bestimmung der spezifischen Sorptionskoeffizienten (k_d-Werte) untersucht. Insgesamt führt die Zunahme der Salinität der Lösung bei allen drei untersuchten Schwermetallen zu niedrigeren k_d -Werten, wobei Cd und Pb am stärksten von der NaCl-Konzentration beeinflusst wird. Auf eine vergleichsweise geringe Sensitivität gegenüber der Salzkonzentration deuten die ermittelten k_d-Werte für Cs hin. Die Entwicklung aller experimentell ermittelten k_d-Werte konnte modelltechnisch sowohl mit dem LINEAREN- als auch FREUNDLICH-Modell nachvollzogen werden.

Der vorliegende Bericht gibt eine Übersicht über die in der Literatur beschriebenen Charakteristika der Smektit-Fraktion von Bentoniten und ihre spezifischen rheologischen Eigenschaften. Dazu wurden die mineralogische Zusammensetzung natürlich vorkommender Bentonite und ihre Herkunft als Indikator für spezifische technische Eigenschaften in Beziehung gesetzt.

Im analytischen Ansatz können Bentonite aufgrund ihres spezifischen Auflösungspotenzials in die beiden Haupttypen Typ A „SPRINTER“ und Typ B „SLEEPER“ eingeteilt werden. „SPRINTER“ stehen für Bentonite, die ein relativ hohes Auflösungspotenzial aufweisen, während „SLEEPER“ verzögert auf Änderungen des geochemischen Milieus reagieren. Typ A und Typ B unterscheiden sich auch aufgrund der Milieubedingungen bei ihrer Entstehung durch Verwitterung des mafischen Muttergesteins. Während die Bildung von Typ A niedrige Temperaturen voraussetzt, führen höhere z. B. hydrothermale Temperaturen zur Bildung von Typ B. Auch die Verwitterung saurer vulkanischer Aschen, die als marine Sedimente abgelagert wurden, führt zur Bildung von Typ B.

Im Ergebnis kann ein sogenannter „FOOTPRINT“ abgeleitet werden, der die ermittelte Abhängigkeit der Stabilität der Bentonite im Sinne eines Auflösungspotenzials /HER 11/ mit ihrer Herkunft widerspiegelt. Das Heranziehen eines „FOOTPRINTS“ eröffnet die Möglichkeit zur Vor-Auswahl geeigneter Bentonite für ihre spezifische Anwendung.

1 Introduction

Chemical and toxic wastes are deposited in underground landfills in Germany in deep potash and rock salt formations /SCH 08/. At the end of operation time the underground landfill has to be closed under the German legislation (TA Abfall) under the general concept of multibarrier system to ensure the isolation of the hazardous chemotoxic waste from leaching out and migrating into the biosphere /TAA 91/. The key compartments of such multibarrier system are technical barriers in the form of pit closures and sealing. The technical barriers prevent the intrusion of solutions and thus prevent leaching of waste and the transport of dissolved contaminants from the underground landfills in the biosphere. For such landfills in deep potash and rock salt formations, it is essential to keep the waste dry and enclosed with effective barrier systems. However, for the long-term safety assessment, special scenarios have to be considered such as solution intrusion into the repository. The related processes are the interaction of the solution with rock salt, the chemotoxic waste as well as the engineered barriers. Consequently, this could lead to the release and transport of liquid and gaseous chemotoxic contaminants. Similar problems can occur for the deep underground nuclear waste repositories, especially for HLW (high-level nuclear waste) repositories with the special characteristics for heat generating waste. The potential contaminants will then be not only heavy metal, chemotoxic but also radioactive with extremely long half-life. Such contaminants will migrate around and through engineered barrier material (Fig. 1.1). The transport parameters like diffusion and sorption coefficient are crucial for the safety assessment of chemotoxic contaminants.

Bentonite is widely used as engineered barrier material for various constructions (e. g. landfill liner and cover system, water storage facilities) owing to its favourite properties – low permeability, self-sealing through swelling when water enters, long-term stability. Based on the good engineering experiences, it is also extensively studied worldwide for decades to investigate its suitability as engineered barrier material in the near field of HLW (**H**igh-**L**evel nuclear **W**aste) repositories. However, most of the studies are based on dilute groundwater solution (e. g. in Opalinus Clay as) or oceanic solutions (e. g. in granite as formation rock under see in Sweden). In Germany, several underground repositories in deep potash and rock salt formations have been in operation since 70s /SCH 08/. Bentonite is considered to be a potential sealing material in shaft to close such repositories especially around the contact area between the rock salt and soil layers above it.

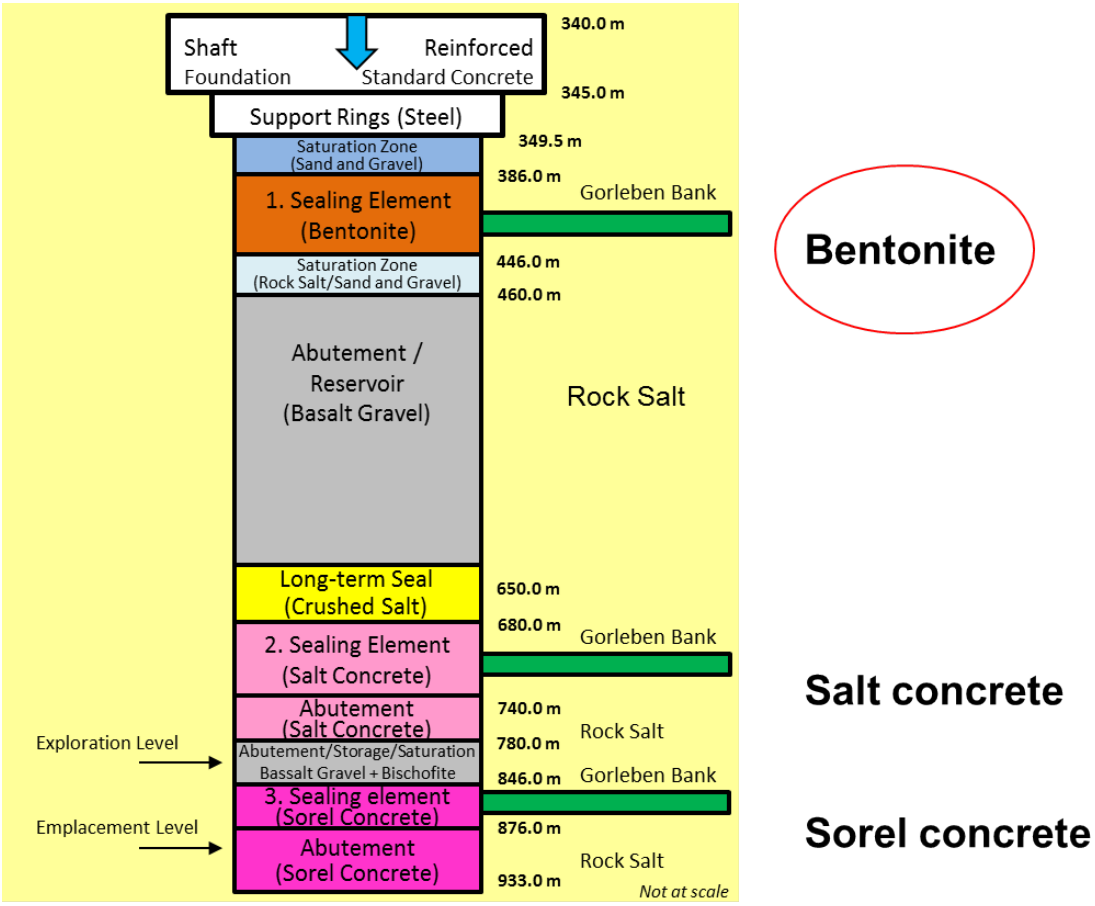

Fig. 1.1 Betonite as sealing material for the closure of the shafts in Gorleben repository /MUE 12/

In such cases, the resulted solution to seep into bentonite barrier material will be most probably saturated NaCl-solution, or Mg^{2+}, SO_4^{2-} rich solutions like IP9 or IP21 solutions. All of these kinds of solutions have much higher corrosion potential to metals (waste canisters). Some metals (e. g. Pb, Cd etc.) can form complexes like $PbCl^+$, $PbCl_2$, $PbCl_3^-$ or even $PbCl_4^{2-}$. Consequently, the total dissolution amount of such elements in solution can be much higher as in dilute solution. The change of the ions in th solution for the charge from positive to negative can affect the migration parameters through highly compacted bentonite owing to the negative surface charge of smectite mineral. On the other hand side, the hydraulic permeability of bentonite increases with the ionic strength of the solution. Therefore, it is crucial to investigate the diffusion coefficient of chemotoxic elements through the bentonite, which is the main part of the report.

In the underground landfill different kinds of gases can be generated at various rates and amount /MUE 97/, /SCH 98/, /JOC 97/.

2 Scientific status of bentonite as engineered barrier material

2.1 Strategy of bentonite-review

Bentonites are a suitable buffer- and backfill-material in the multibarrier-concept for HLW-repositories. The scientific task is to predict the behavior of geotechnical properties of such bentonite barriers for the next 1 million of years.

Generally, it is to expect that the mineralogical and chemical composition of bentonite should determine also its starting geotechnical properties. Otherwise, the different geological processes of bentonite formation affect its mineralogical and chemical composition. Following this concept, the results of literature review to properties and origin of bentonites have been organized under the main topics “Geological History” → “Mineralogical & Chemical Properties” → “Geotechnical Properties”. Fig. 2.1 offers a first impression about the opportunities of this system.

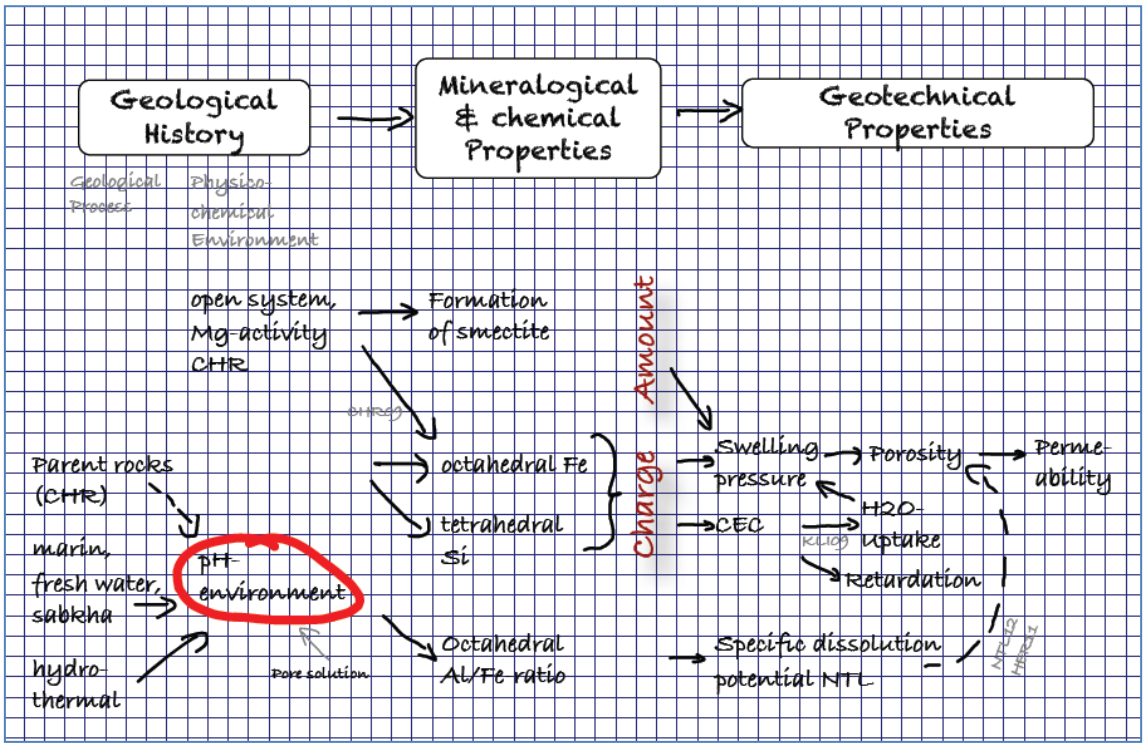

Fig. 2.1 Worksheet „Strategy of Bentonite Review I“: The geological processes during the formation of bentonite affect its mineralogical and chemical properties, which determine finally the geotechnical parameter

This concept would be applied also to organize identified processes in the barrier, to recognize than their impact on alteration of mineralogical, chemical and structural composition of bentonite and to understand finally again the future development of geotechnical parameter ("Barrier Processes" → "Mineralogical & Chemical Properties" → "Geotechnical Properties").

2.2 Formation of bentonites and its impact on bentonite properties

2.2.1 Origin of bentonites

The following explanations to the origin of bentonites have a focus to typical genesis mainly of economic deposits.

Millot /MIL 70/ developed a general concept for clays to explain their origin. He divided the different geological environments for clay formation in weathering environment, sedimentary environment and diagenetic-hydrothermal environment. The weathering environment and especially the sedimentary environment represent typical conditions for the formation of the most economic deposits of bentonite.

Weathering environment (low temperature) should be linked mostly with low pH (acidic) /JAS 93/. Only in case of weathering of mafic rocks, high pH (alkalic) determines the alteration processes to smectite. The reduction potential of Fe^{2+}-oxidation into Fe^{3+} is supporting this development /HER 11/. Four geological or geomorphological variables determine the weathering process: rock type (= chemical factor), climate (with precipitation as chemical factor and temperature as physical factor), topography or flow rate (with ratio of water to rock as chemical factor) and age (with time as physical parameter) /VEL 92/. Weathering is determined by dissolution and erosion processes. Hydrolysis reactions, processes of interaction between minerals and aqueous solution, are mainly responsible to form the new clay phases from different mineral species. Alkali and Ca are lost but the minerals tend to conserve Mg and Fe in the silicate or oxide state. Low precipitation causes formation of smectite for basic and acid rocks /VEL 92/, /JAS 93/. Saponite and Fe-rich dioctahedral montmorillonite would be typical smectitic neoformation in weathering profiles of basic rocks. Beidellite is a common product of soil formation under tropical conditions and limited precipitation.

Hydrothermal alteration can be considered also as weathering process, but under increased temperature conditions. So called high temperature hydrothermal alteration occurs at depths great enough to be at temperatures above 250 °C. It will occur also along few and large pathways created by fractures in the rock. In hydrothermal smectite formation by alteration of volcanic glass, solutions were characterized by neutral to alkaline pH (Fig. 2.2). The higher the temperature, the more the selectivity for Ca in smectite increases /INO 95/. The type of clay produced depends upon the ratio rock to water and the anion content of the aqueous solution. Other authors pronounced that the hydrothermal alteration is frequently one of hydrogen exchange in the presence of strong anionically controlled solutions /VEL 92/. It is a systematic loss of alkali ions (Ca, Mg and eventually Fe). White and Fe-poor clays are common under these conditions. This is very different from the situation of rainwater interaction. Parent rocks affect also the composition of smectite. Smectite originated from hydrothermal alteration of felsic rocks contains more Na and K, but less Mg and Fe. Smectites from altered mafic rocks are originally rich in Mg, Fe and Ca /INO 95/, /CHR 09/.

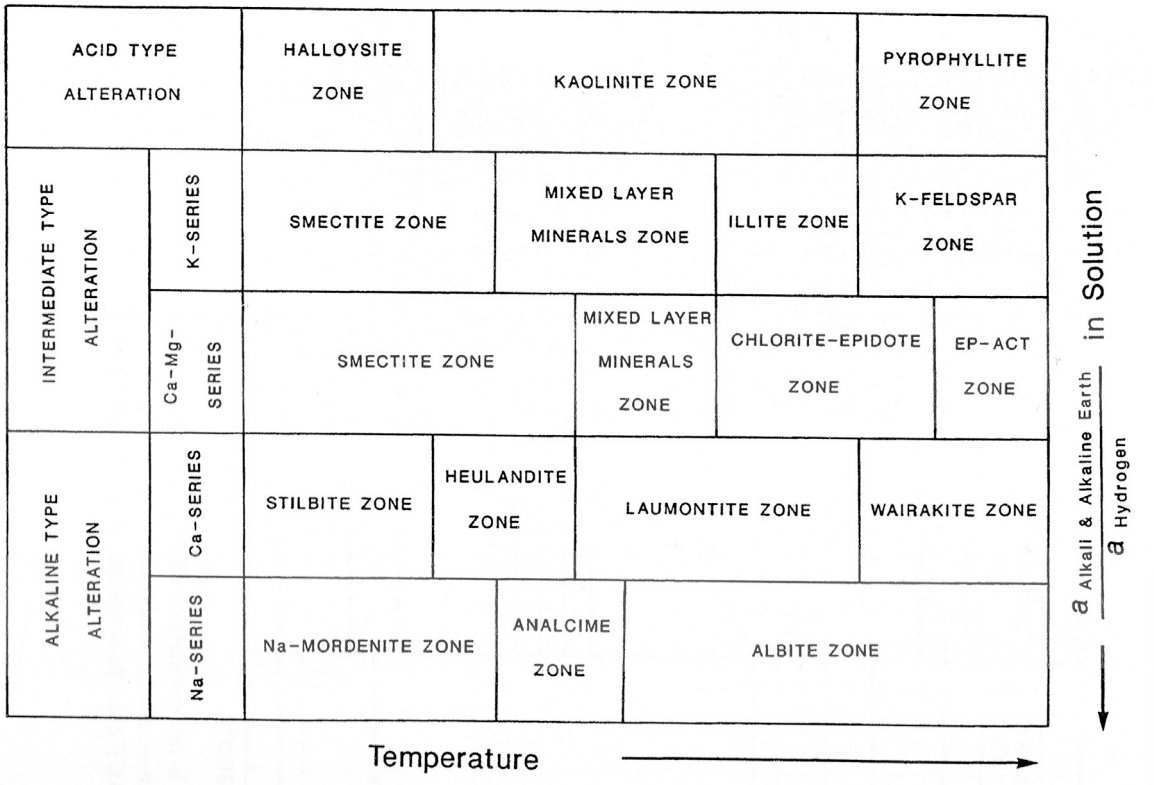

Fig. 2.2 Division of zones in three types of hydrothermal alteration; Utada 1980 cited in /INO 95/ (K-series linked with acidic and intermediate parent rocks; Ca-Mg-series associated with mafic parent rocks)

Deep-sea alteration would be a special case of hydrothermal alteration. In the alteration of deep-sea basalts in contact with sea salt-water, the clays are in fact iron-rich at very low temperatures (below 300 °C) and become more alkali-rich. Velde /VEL 92/ described a temperature-related development of alteration products. The first clay minerals to form are saponites. The intermediate-temperature clay-forming processes give aluminous and iron-rich beidellitic smectites (and celadonites). The lowest-temperature clay forming processes give nontronite (usually of a K-form). The general trend of deep-sea alteration of basalts is shown in Fig. 2.3. Meunier /MEU 05/ noted also the impact of O_2-fugacity for the formation of nontronite for a temperature below 70 °C (Fig. 2.4). Seawater-basalt interaction experiments show acid (under high water/rock-ratios) or neutral pH-environment (under low water/rocks-ratios) caused by removal of Mg^{2+} via $Mg^{2+} + 2\ H_2O = Mg(OH)_2 + 2\ H^+$ /MOT 83/.

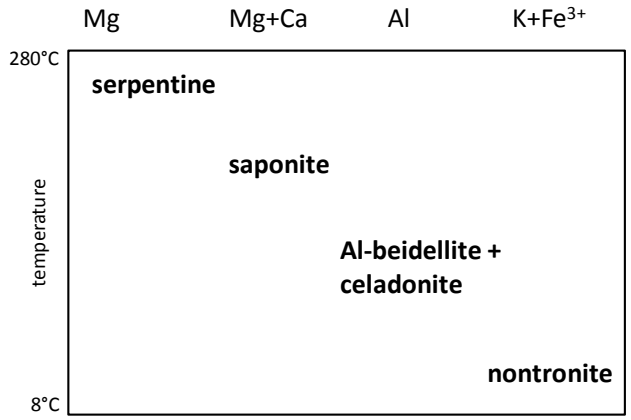

Fig. 2.3 Deep sea basalt alteration: Composition of clays and temperature conditions /VEL 92/

Sedimentary Environment (according to /MEU 05/): Clays in sediments are derived from different sources: (1) erosion of soils and weathered rocks, and (2) crystallization by reaction between saline solutions and silicates. The first form rocks whose granulometric and mineralogical characteristics depend on transport and deposit processes. The second replace minerals in rocks that are already formed. The first are inherited from disintegrated rocks; the second are totally neoformed. Accordingly, clays formed in a continental environment by dissolution of silicates under the influence of diluted solutions undergo chemical modifications – and even recrystallisations – when settled in a saline environment (early diagenesis or neodiagenesis). No clay mineral reaction during suspension, transport and sedimentation could be clearly identified /MEU 05/. The interactions with the transporting agent seem to be insignificant and reduced to ion ex-

changes. The exchange capacity of smectites formed in soils and alterites is saturated by several cations – Ca^{2+}, Mg^{2+}, and K^{+} principally. In rivers, saturation is dominated by Ca^{2+} ions. In oceans, saturation is dominated by Na^{+} (50 %), the remaining part being shared between Mg^{2+} (30 – 40 %), Ca^{2+} (10 – 20 %) and K^{+} (5 %) /SAY 77/.

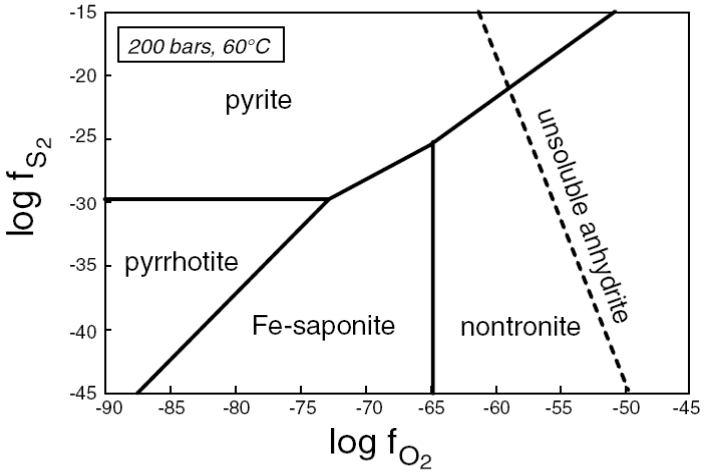

Fig. 2.4 Deep sea basalt alteration: Phase diagram in the Fe–Al–Na–Si–O–S system at 200 bars, 60 °C showing the stability fields of nontronite and anhydrite /MEU 05/ in according to /ZIE 83/

2.2.1.1 Bentonite formed from weathered material in salt lakes and sabkhas

Salt lakes in desert areas are closed sedimentary basins in which detrital inputs are essentially composed of kaolinite, and to a lesser extent of illite, chlorite and Al-rich smectite. These minerals are derived from the erosion of tropical soils. Their Fe, Ca and Na content is relatively low. The waters supplying these lakes are rich in Mg, Ca, Si and alkaline elements /MIL 64/. The progressive evaporation of lakes leading to the precipitation of gypsum is accompanied by the formation of saponite, stevensite and sepiolite (Fig. 2.5). Palygorskite formation needs high pH values and high Si and Mg activities (Fig. 2.6) /WEA 77/. Since palygorskite and saponite contain more aluminium than sepiolite and stevensite, they are generally considered as resulting from the reaction between detrital minerals and Si- and Mg-rich solutions /JON 88/.

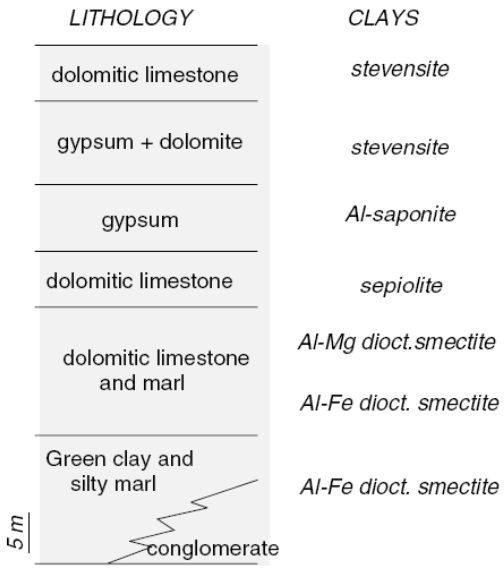

Fig. 2.5 Sedimentation in salt lakes – pH-stratigraphic sequence formed by evaporation /TRA 77/

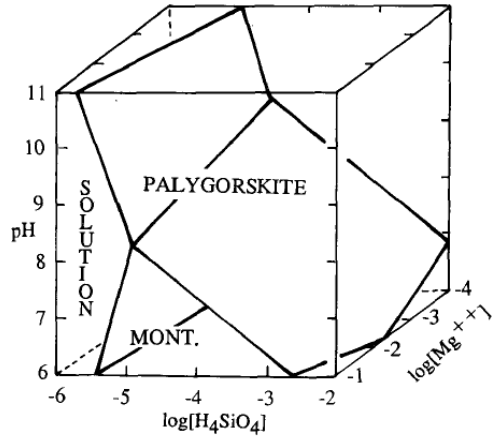

Fig. 2.6 Stability fields of palygorskite, montmorillonite and aqueous solution at 25 °C, log[$Al(OH)_4$] = -5.5 /WEA 77/

2.2.1.2 Bentonite formed from volcanic ash in lakes, swamps, lagoons or shallow sea areas

Ashes deposited on the surface of continents are subjected to weathering and to andosol-type pedogenesis /MEU 05/. Ash alteration should run very rapidly (a few hours to a few days /BER 99/ and is not due to weathering /GRI 68/. Under marine conditions, the rate of transformation of volcanic glass into smectite decreases with depth and remains

constant at about 50 % at 250 cm from the interface with seawater /CHA 71/. The sedimentary environment for smectite formation is mainly characterized by medium pH-level /JAS 93/.

Christidis and other authors described different micro-environmental conditions in rock/water interface, which prefer the smectite formation in opposite to zeolite formation. They pronounced the occurrence of high Mg^{2+}/H^{+}-ratio, otherwise zeolite were formed during alteration of volcanic glass /SEN 84/, /CHR 98/. Furthermore, a low H_4SiO_4-activity is demanded in the pore fluids. Otherwise, it is drawn a preferred formation of opal-CT and zeolites /CHR 09/. Additionally, an open system is necessary to form smectites, regardless of the parent rock /MEU 05/, /CHR 09/.

There are several alternative solutions which should be taken into consideration: ash alteration may take place either at the time of deposition in waters that are more saline or alkaline than seawater or before deposition inside the volcano hydrothermal system itself, or after deposition during burial by diagenetic reaction. In the first case, ashes are transformed in lagoons where solutions are concentrated by evaporation. In the second case, glass is altered very early in its volcanic context and sedimentation involves already transformed ashes. In the last case, origin of bentonites is a diagenetic-like reaction. The rhyolitic glass gets hydrated, and then yields smectite in a longer process by a dissolution-recrystallisation process.

2.2.1.3 Bentonite by diagenetic alteration of weathered detrital material or volcanic glas

Diagenesis begins right after the sediment-seawater interface; it is referred to as “early” when this burial does not lead to a noteworthy temperature rise /CHA 89/. This mostly involves thicknesses of several hundreds of meters. In the present case, the term “early diagenesis” refers to the first tens of centimeters from the surface of the soft sediments. Their very high porosity (over 50 %.) allows for easy exchanges with seawater by chemical diffusion from the interface. This phenomenon has also been referred to as “reverse weathering” /SIL 61/.

Continental clay minerals remain seemingly inert when settled in oceans. Nevertheless, their exchange capacity is no longer saturated by the same ions. The neogenesis of phyllosilicates is a proved phenomenon in marine sediments. It is expressed by over-

growths on detrital clays (illite, smectite, and kaolinite) or by the formation of lath-shaped smectites. The main factor in the formation of these minerals does not seem to be the burial depth but rather the duration of the exchanges with seawater by diffusion. In many of the bentonite beds one finds a chemical gradation in potassium content which shows changes in the illite content of the I/S mineral. The most potassic (illite-rich) portions are found in contact with the enclosing sedimentary rock layers. This indicates also the presence of a diffusion process which gradually transforms the smectite clay into the I/S phase over long periods of time /VEL 92/. Bentonites from tuffs are formed initially at or near the surface from volcanic ash materials.

In all systems, the rate of smectite crystallization versus the rate of amorphous SiO_2 precipitation determines the final mineral assemblage. Finally, during diagenesis, high-grade bentonites are produced if fluid flow is maintained /CHR 09/. Dioctahedral smectites formed in sedimentary environment and which undergone no more when only a low temperature impact have a trans-vacant occupation of octahedral layer /CHR 06/.

Christidis /CHR 08/ investigated in detail the possible impact of parent rocks on the final chemical composition of smectites. He found that its Fe-amount mirrors parent rocks (Fig. 2.7): smectites from basic rocks were characterized by an averaged Fe^{3+} content of 0.63 atoms per half unit cell (phuc), from intermediate rocks by 0.21 Fe^{3+}-atoms phuc and from acidic rocks by 0.12 Fe^{3+}-atoms phuc. Fe^{3+} is mobile only at very acid pH and very high Eh /GAR 65/. Furthermore, tetrahedral Si mirrors also parent rocks, but with limitations. Following that, smectites from basic rocks have shown a trend with 3.73 Si-atoms phuc, from intermediate rocks with 3.82 Si-atoms phuc and from acidic rocks with 3.92 Si-atoms phuc.

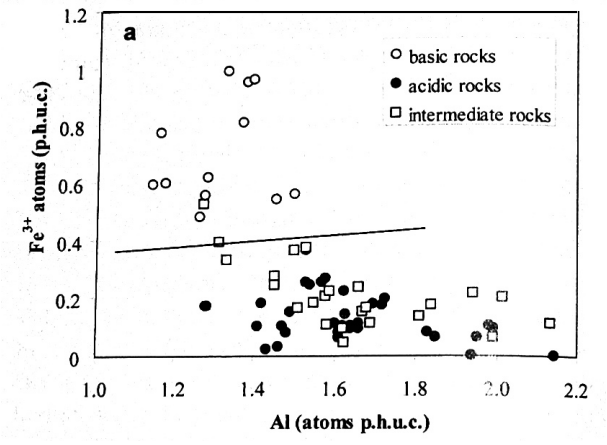

Fig. 2.7 Impact of parent rocks on octahedral chemistry of bentonite /CHR 08/

Diagenetic alteration processes run mostly under alkalic pH-environment /JAS 93/.

The above summarized discussion about the different origin of economic bentonite deposits concerning its impact to mineralogy and chemistry of smectitic phases is sketched for weathering environment (Fig. 2.8) and sedimentary environment (Fig. 2.9). It is to see that certain conditions during the formation prefer the development of certain mineral associations. The environmental framework during the bentonite formation affects amount of formed smectite, the chemistry of octahedral sheet (Al, Mg, Fe-composition), the composition of tetrahedral sheet (Si-amount or in case of surplus causing a cementation of neighbored particles by additional Si-precipitation) and the occupation of interlayer space by alkali or earth alkali cations.

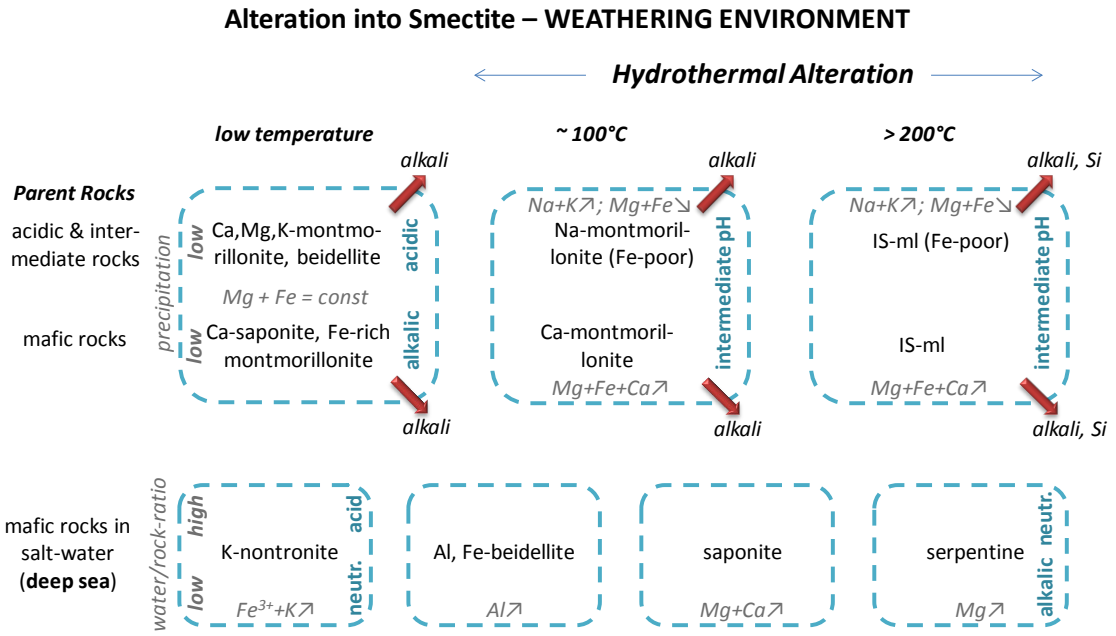

Fig. 2.8 Sketch-like overview concerning Smectite Formation in Weathering Environment (temperature-controlled) under viewpoint of economic bentonite deposits in according to /MIL 64/, /MIL 70/, /CHA 71/, /TRA 77/, /WEA 77/, /MOT 83/, /CHA 89/, /VEL 92/, /JAS 93/, /INO 95/, /BER 99/, /MEU 05/, /CHR 09/, /HER 11/ – explanations see text (dashed boxes – demand for open reaction system)

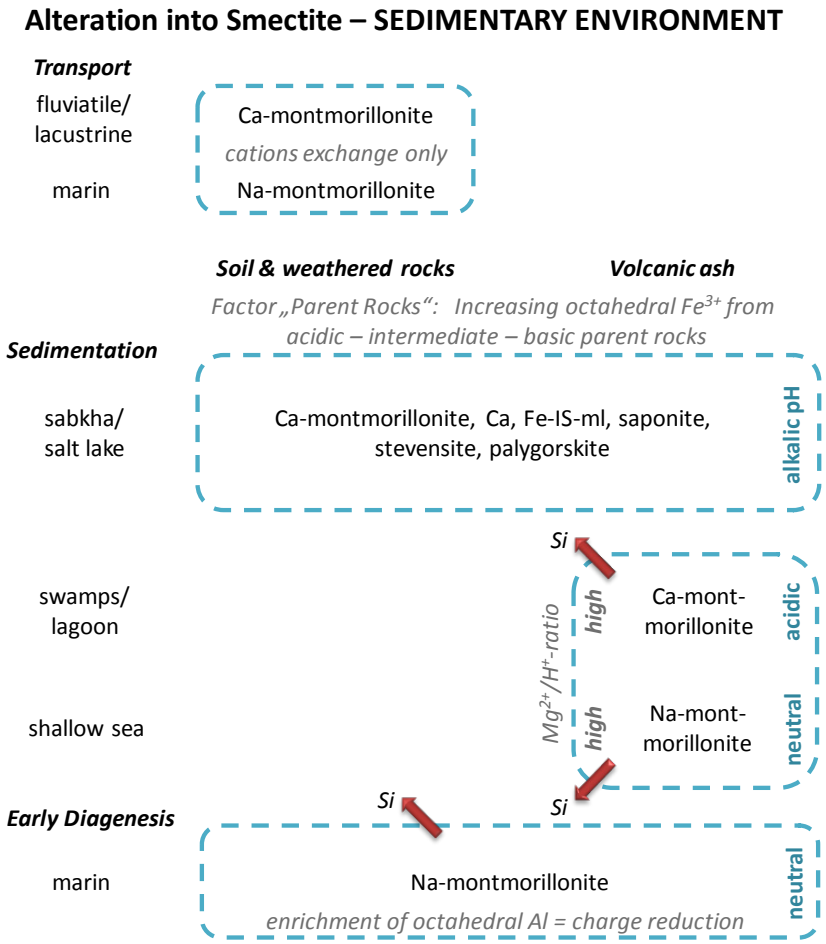

Fig. 2.9 Sketch-like overview concerning Smectite Formation in Sedimentary Environment under viewpoint of economic bentonite deposits in according to /SIL 61/, /GRI 68/, /MIL 70/, /SAY 77/, /JON 88/, /VEL 92/, /CHA 89/, /BER 99/, /MEU 05/, /CHR 06/, /CHR 08/, /CHR 09/

Fluviatile or lacustrine conditions are responsible for Ca and Mg in the interlayer space and marine environment is mainly arranging a cation exchange by Na (exception for alteration of mafic rocks in deep sea). Higher temperature in hydrothermal alterations is responsible for a loss of Si resulting formation of IS-ml. Mafic parent rocks are mirrored in smectite by higher Fe- and Mg-content.

Stevensite or palygorskite are typical additional clay mineral phases for formation of bentonites in salt lakes or sabkhas or volcanish ash is falling down into lakes or lagoon and the heat of this ash is evaporating this lake/lagoon. Furthermore, the different milieu during the formation of bentonite is also arranging different pH-conditions.

2.2.2 Changing of Bentonite in the Bentonite Deposit

Christidis /CHR 09/ has discussed the distribution of some parameter of bentonite like CEC and charge in the deposit. He mentioned two recent reports, which demonstrate cryptic variation of smectites in bentonites. Variation that was not visible macroscopically, but it could be seen microscopic trends in composition and, more specifically, layer charge. Data from a 1 m thick bentonite bed in Charente, France have shown that $(Al_2O_3 + Fe_2O_3)/MgO$ in smectite decreased from the center towards the margin of the deposit, whereas the cation exchange capacity (CEC) increased (Fig. 2.10). Because layer charge is derived mainly from substitution in the octahedral sheet, the observed compositional trend also suggested that layer charge increased toward the margins.

A similar, clearer trend was observed by /CHR 07/ in a bentonite from Milos, Aegean, Greece (Fig. 2.11). The layer charge increases also here towards the top of the deposit, but the authors /CHR 07/ interpreted this higher charge as caused by increasing tetrahedral charge (development into beidellite). Neither Milos deposit shows a systematic change in macroscopic characteristics (colour, rock texture) that would reflect a systematic change in composition. The parent rocks were different from in two cases. In Charente, the bentonite formed from a thin ash fall, whereas in Milos, a thick pyroclastic flow was the parent rock.

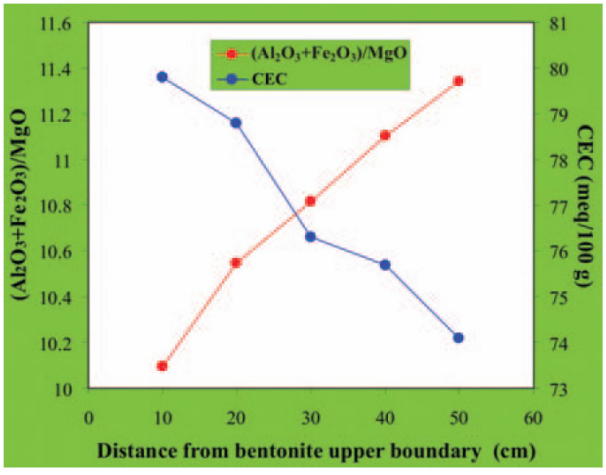

The CEC increases as the $(Al_2O_3 + Fe_2O_3)/MgO$ ratio decreases toward the upper boundary, suggesting increasing smectite layer charge from the center of the bentonite bed to the top (Data from /MEU 04/ /CHR 09/)

Fig. 2.10 Variation of cation exchange capacity (CEC) (milliequivalents/100 g) and the $(Al_2O_3 + Fe_2O_3)/MgO$ ratio with depth in smectites from a bentonite deposit in Charente, France

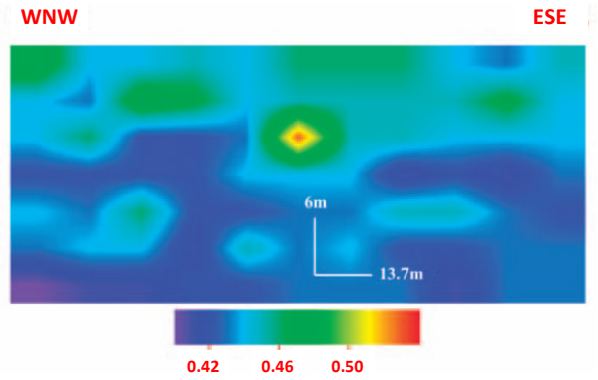

Smectites have layer charge between 0.3 and 0.6 charge equivalents, increasing towards the top of the profile. Smectite layer charge is defined as low for less than 0.425 equivalents per half unit cell (blue), intermediate between 0.425 and 0.47 (blue to green) and high for more than 0.47 equivalents (green to red) /CHR 09/.

Fig. 2.11 Cross-section of a bentonite profile (21 m × 120 m) from a deposit in Eastern Milos, Greece, showing evolution of smectite layer charge (the colour scale indicates charge equivalents per half unit cell)

Otherwise, the above discussed two cases of development in deposit into increased charges at the top of the bentonite layers may mirror similar processes from different experiments with engineered barriers /HER 04/, /HER 08/, /HER 11/. These authors reported in close reaction systems a substitution of Mg by Al in octahedral sheet. This replacement is causing than a lower charge. This process could be to identify in the bottom parts of the two cases described by /CHR 09/. The upper parts of the bentonite deposit were considered as open reaction system. So, Si could migrate and would cause an increasing layer charge by increasing tetrahedral charge. Additionally, Mg can enter the octahedral sheet in an open reaction system replacing octahedral Al. The former Al is partially substituting in the tetrahedral sheet the before migrated Si.

2.2.3 The footprints of bentonite's origin in specific dissolution potential

Herbert and his co-workers /HER 11/ found that bentonites have a specific dissolution potential. Some bentonites have shown in interaction with water a very fast alteration of chemical composition (these bentonites were called as "Sprinter"), other one were nearby unchanged under the same experimental conditions (called as "Sleeper"). This potential was identified by degree of "illitization" or smectitization for each sample (proofed by TEM-EDX, FT-IR). Bentonites with illite-smectite mixed layer phase in the original material have shown commonly smectitization. It seems that such mixed layer phases can buffer dissolved Si. Otherwise, fast reacting bentonites with a tetrahedral Si-amount

close to 4 per half unit cell (phuc) are preferred for cementation of aggregates by precipitated Si. This cementation can have a drastically impact to the properties of engineered barrier.

The following parameters were identified as driving forces for the mentioned specific dissolution potential:

- original distribution of Al, Fe and Mg in octahedral sheet and
- Na/(Ca + Mg)-ratio in cationic composition of interlayer space.

Increasing octahedral Fe- and Mg-amounts are promoting a faster dissolution of smectite. Two types of dissolution behavior were identified for 21 different bentonites. High Na amount in interlayer space has acted in some cases as stabilizator (group A). In other cases Ca + Mg-cations in interlayer space stabilized the aggregates. These two groups are characterized by specific composition of octa-hedral sheet and by a specific signature in FT-IR-spectroscopy.

The Al-Fe ratio in the octahedral sheet influences the stability of the interlayer:

a) $Al_{oct} > 1.4$ and $Fe_{oct} > 0.2$ (per $(OH)_2\ O_{10}$) favour delamination of quasicrystals. The swelling pressure increases by a co-volume process between the delaminated layers with higher numbers of quasicrystals for Na-dominant population of the interlayer space /LAI 06/. The microstructural components including both small and large particles and parts of them have a very small ability to move and undergo free rotation. Such Na-montmorillonites are considered as stable phases and have only a low specific dissolution potential. They are „Sleepers“.

b) $Al_{oct} > 1.4$ and $Fe_{oct} < 0.2$ or $Al_{oct} < 1.4$ and $Fe_{oct} > 0.2$ (per $(OH)_2\ O_{10}$) promote demixing of monovalent and divalent interlayer cations /LAI 06/. In the case of Ca and Mg-dominant interlayers, quasicrystal can break at Na-bearing interlayers and help to maintain the quasicrystal structure. Such Ca and Mg-montmorillonites can also be taken as „Sleepers“, because of their low specific dissolution potential.

It is assumed that the original composition of octahedral sheet is representing mainly the pH-environment (Fig. 2.12) during the formation of the smectite clay and therefore it serves as a geological fingerprint. The “Al/Fe” ratio in the octahedral sheet of investigated bentonites was linked with the assumed pH-conditions (Fig. 2.12). It is to recognize there that especially Wyoming bentonite would be a member of group A (with Na

stabilizing the smectite against alteration). A further comparison (Fig. 2.13) of the pH-controlled octahedral composition in according to /HER 11/ (Fig. 2.14) and the parent rocks controlled composition of octahedral composition (Fig. 2.7) in according to allows following conclusions:

a) The investigated series of bentonites in /HER 11/ meets mainly only the fields of acidic and intermediate rocks drawn by /CHR 08/.

b) The pH-zones /HER 11/ do not distinguish between acidic and intermediate parent rocks /CHR 08/.

c) It seems that pH-conditions during the bentonite formation and the composition of parent rocks affect together the later chemistry of bentonites.

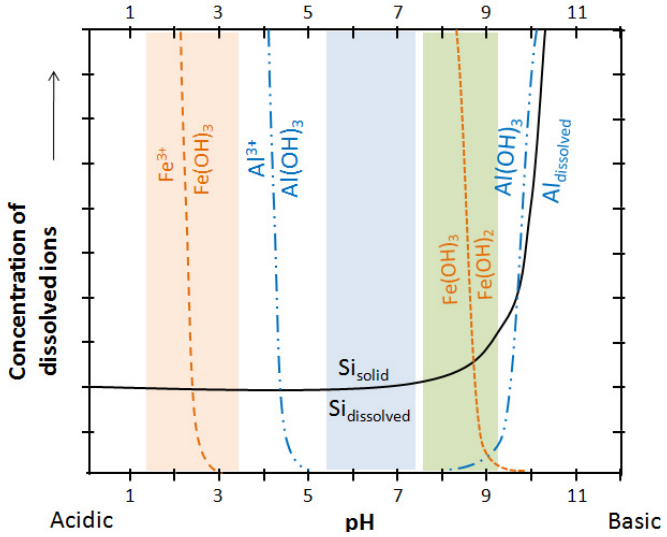

Colored boxes represent the three typical pH-zones (acidic, neutral, alkaline) summarized in Fig. 2.7 and Fig. 2.8

Fig. 2.12 pH-controlled dissolubility of selected elements in according to /SEI 90/.

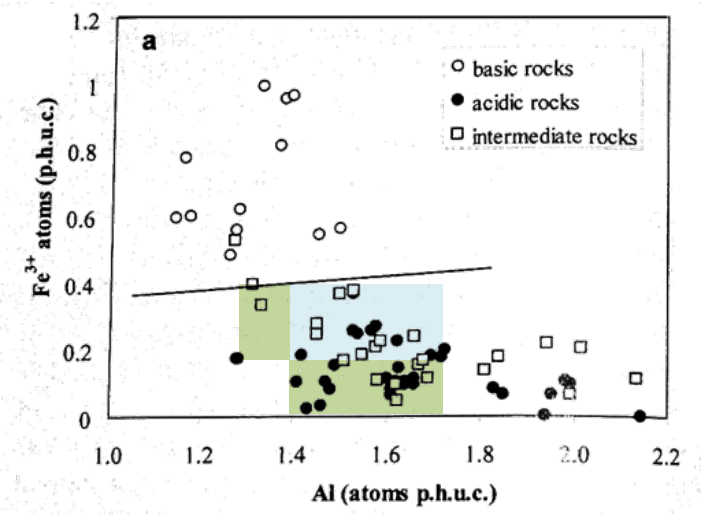

blue box – group A with Na as stabilization, intermediate pH; green boxes – group B with Ca, Mg as stabilization, alkaline pH

Fig. 2.13 Integration "Specific dissolution potential controlled by pH" (Fig. 2.14 /HER 11/ into "Mirroring of parent rocks in chemistry of smectite" (Fig. 2.7 /CHR 09/

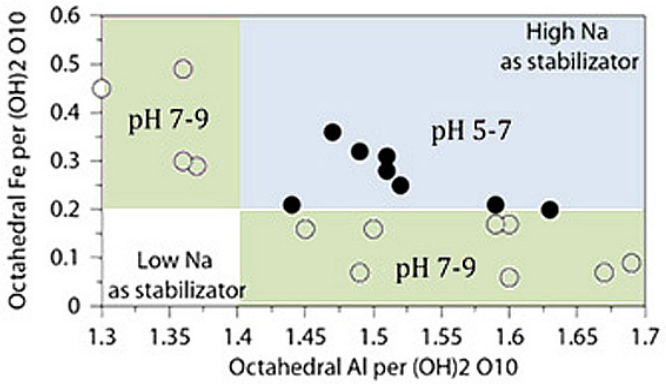

Blue box – group A: high Na-amount in interlayer space is reducing the rate of alteration; green box – group B: high Ca+Mg-amount in interlayer space is reducing the rate of alteration

Fig. 2.14 Specific dissolution potential controlled by pH-milieu during bentonite formation /HER 11/

2.2.4 Typical bentonites investigated as HLW-barrier material

A literature review about bentonites as possible HLW-barrier material has shown publications to series of natural bentonites (Tab. 2.1). Other well documented bentonites would be reference samples certified by American Petroleum Institute Clay Mineral

Standards (API), the bentonites from Clay Mineral Society (CMS) source clays as well as the bentonite collection from BGR Hannover.

Tab. 2.1 Overview about natural bentonites investigated as possible HLW-barrier material

Na-Bentonites		
Europe		
Holmehus	Bjerreby/Danmark	/KAR 06/
Ölst	Bjerreby/Danmark	/KAR 06/
Friedland Clay	Friedland/Germany	/HEN 98/, /HIC 09/, /KAR 10/
Asia		
AZM	China	/XIA 11/
Asha	India	/SHA 97/, /KAR 06/
Kunigel	Japan	/HIC 09/, /DEL 10/
Kunipia	Japan	/HIC 09/, /WIL 11/
?Kyungju	ROK	/HIC 09/

K-Bentonites		
Europe		
Dolná Ves	Slovakia	/ŠUC 05/, /ADA 09/
Kinnekule	Kinnekule/Sweden	/BRU 86/, /MÜL 90/, /MÜL 91/, /PUS 95/, /SOM 09/, /WIL 11/

Ca-Bentonites		
Europe		
Dnesice	Plzen/Czech	/KAR 06/, /PRI 02/
Rokle	Kadan Ba-sin/Czech	/KAR 06/, /PRI 02/, /KON 86/
Skalna	Cheb/Czech	/KAR 06/, /PRI 02/
Strance	Most/Czech	/KAR 06/, /PRI 02/
Rösnes	Bjerreby/Danmark	/KAR 06/
Montigel Calcigel	Germany	/MAD 98/, /VOG 80/, /PUS 01/
Deponit-Ca-N	Milos/Greece	/CHR 95/, /DEC 96/, /KAR 06/
Ibeco RWC	Greece	/KAR 10/, /KOC 08/
Jelšový Potok	St. Kremnička/ Slovakia	/ŠUC 05/, /ADA 09/
Kopernica	Slovakia	/ŠUC 05/, /ADA 09/
Lieskovec	Polana Region/ Slovakia	/ŠUC 05/, /ADA 09/
Lastovce	Slovakia	/ŠUC 05/, /ADA 09/
Febex	Almería/Spain	/FER 04/, /CAB 05/, /HIC 09/,

List of authors concerning contribution to geological background and characterization of original material

Literature Review

Locality and geological background of the identified bentonites were summarized in Tab. 2.2. They represented mainly sedimentary deposits, where bentonite was formed under submarine or fluviatile/lacustrine alteration of volcanic glass mainly under low temperature impact.

API-Standards (summarized in /HER 11/)

The Belle Fourche (API #27, South Dakota), Otay (API #24, California) and Cameron (API #31, Arizona) bentonites contained Na-montmorillonite while Pioche (API #32 Nevada), Chambers (API #23, Apache County - Arizona) and Bayard (API #30, New Mexico), Amory (API #22a, Mississippi), Polkville (API #20, Mississippi) bentonite were Ca-montmorillonite.

Tab. 2.2 Overview to locality and origin of typical bentonites, which were investigated as possible HLW-barrier material

Bentonite	Type	Locality	Origin	Sources
CZECH				
Dnesice	Ca-bentonite	Dnesice deposit in the Plzen basin, c. 100 km SW Prague	sedimentary type, and the clay is therefore often classified as bentonitic rather than as a true bentonite.	/KAR 06/, /PRI 02/
Rokle (RMN)	Ca-bentonite {cv}	Kadan basin, c. 100 km WNW of Prague (Doupovské Hory Mountains)	series of argillized basaltic volcanoclastic accumulations of Tertiary age, formed in shallow lacustrine basins within the stratovolcano complex of Doupovské Mountains; bentonite is capped by basaltic lava-flows (> 40 million tons)	/KAR 06/, /KON 86/, /PRI 02/, /PUS 07a/, /STR 09/
Skalna	Ca-bentonite	Zelena-Skalna deposit in the Cheb basin, near the western Czech border	Sedimentary smectite-bearing, so called “Green clay” of Tertiary age (~ 130 ktons)	/KAR 06/, /PRI 02/
Strance	Ca-bentonite	Ceske Stredohori area, 4 km SE of Most	formed by argillization of tuffites and pyroclastic rocks during the Tertiary (~ 7 million tons)	/KAR 06/, /PRI 02/
DANMARK				
Holmehus	Na-bentonite	opened quarry at Bjerreby on island of Tåsinge, south of Fyn	Tertiary sediments of various age; sequence has been glacially tectonized (~1 million tons)	/KAR 06/
Rösnäs	Ca-bentonite			
Ölst	Na-bentonite			
GERMANY				
Montigel, Calcigel	Nat. Ca-bentonite	Region of Moosburg-Landshut-Mainburg (NE of Munich), Bavaria	Volcanic acidic vitreous tuff decomposed under freshwater conditions, volcanic activity in the Carpathian Mountains some 12 to 14 million years ago; easterly winds prevailing at that time blew the volcanic ash over a distance of some 3,000 km	/VOG 80/, /PUS 01/
Friedland Clay	Nat. Na-bentonite	Quarry in Friedland near the town of Neubrandenburg, NE Germany	Tertiary sediments derived through erosion of the pre-existing Baltic weathering mantle, alteration by early diagenesis (100 million tons)	/HEN 98/

Tab. 2.2 [continued] Overview to locality and origin of typical bentonites, which were investigated as possible HLW-barrier material

Bentonite	Type	Locality	Origin	Sources
GREECE				
IBECO RWC (Deponit CA-N)	Nat. Ca-bentonite	Island of Milos in the Aegean Sea (part of the Hellenic Arc volcanic province)	pyroclastic tuffs and lavas of andesitic to dacitic composition as parent rocks; bentonite by hydrothermal reactions with percolating groundwater heated to below 90 °C during volcanic activity [DEC96] or submarine alteration of the parent volcanoclastic rocks took place under low temperatures and is probably not related to hydrothermal alteration (a separate event modifying the bentonite) [CHR95]	/CHR 95/, /DEC 96/, /KAR 06/, /KAR 10/
INDIA				
ASHA	Nat. Na-bentonite	Kutch area, 60–80 km from the ports of Kandla & Mandvi on the NW-coast	associated with the basaltic Deccan Trap rocks of Tertiary age and formed through hydrothermal alteration of volcanic ash in saline water (~ 25 million tons)	/KAR 06/, /SHA 97/
SLOVAKIA				
Jelšový Potok Kopernica Lieskovec Lastovce	Nat. Ca-bentonites	Stará Kremnička Po'lana region	products of the Neogene volcanic activity (rhyolite tuffs and tuffites, andesites), and of different subsequent alteration processes and/or redeposition (JP ~ 2.3 million tons; LI ~ 4.5 million tons)	/ADA 09/, /ŠUC 05/
Dolná Ves	Nat. K-bentonite			
SPAIN				
FEBEX	Nat. Ca-bentonite	Cortijo de Archidona deposit (Serrata de Níjar, Almería)	submarine, associated with low-temperature hydrothermal alteration processes (~ 100 °C) that took place in rhyodacitic tuffaceous volcanic rocks	/FER 04/, /CAB 05/
SWEDEN				
Kinnekulle	Nat. K-bentonite	Kinnekulle region, southwest Sweden (common in Baltic basin)	Ordovician marine bentonite beds; Magma intruded parallel to the bedding planes about 90 m above the bentonite beds in Permian time; bentonite beds were thereby heated to 120-140 °C in the first 500 years after the magma intrusion, followed by a successive drop to about 90 °C after 1000 years	/BRU 86/, /MÜL 90/, /MÜL 91/, /PUS 95/, /SOM 09/, /WIL 11/
MX-80	Nat. Na-bentonite	Wyoming, parts of Montana and South Dakota	bentonite occurs as layers in marine shales and formed through alteration of rhyolitic tephra deposited in ancient Mowry Sea basin during the Cretaceous; tephra altered in contact with the Mowry seawater	/SLA 65/, /ELZ 89/, /ELZ 89/
Volclay	Nat. Na-bentonite	Wyoming		

Garfield nontronite (API #33a) is a weathering product of the basalt zone in the Garfield area, Washington/USA.

CMS-source clays (summarized in /MOL 01/)

The CMS-source clay “SAz-1 Montmorillonite, Arizona (Cheto)” represents deposits of Ca-bentonites from the non-marine Bidahochi Formation of Pliocene age in northeastern Arizona. In according to /KIE 55/, the SAz-1 montmorillonite was the result of redeposited smectite after alteration of vitric ash of quartz-latitic composition in lacustrine/fluviatile environment.

The CMS-source clay “SHCa-1: Hectorite, California” is associated with volcanic rocks in the Mohave Desert near Hector, California. The actual structure and mineral associations of the hectorite deposit and its genesis, remain controversial. Probably, vitric ash fell into a partially restricted and protected environment of a linear, shallow lake. The deposition of the tuff was contemporaneous with extensive hot-spring activity that provided hot, Li-rich solutions. Crystallization of hectorite apparently occurred only near the on-shore zone. Off shore, in the lake, a brown mud containing a non-hectorite smectite formed.

In Gonzales County (east central Texas), the bentonite of the CMS-Source clay “STx-1: Montmorillonite, Texas” occurs in commercially mineable amounts. The general consensus is that this white Ca-bentonite resulted from alteration of volcanic ash of rhyolitic composition. The transformation mechanism, however, is controversial. It is assumed finally that subterranean brines ascended along fault planes and into the ash. The rich quantities of alkaline earths in the brines would aid in the alteration.

'Wyoming bentonite' (“SWy-1,2: Montmorillonite, Wyoming) does not imply a single occurrence, and involves a number of geological units from Wyoming, Montana and South Dakota, and consists largely of Na-rich smectite. The two Source Clays “SWy-1” and “SWy-2” are from single sites in the Newcastle Formation. All authors agree that the Wyoming bentonites resulted from volcanic ash falling into the sea, or in the possible exception of the Newcastle Formation, a lake. The source of the ash lay to the west. All investigators believe these characteristics indicate a near-shore environment. The volcanic ash fell near the beach and into lagoons. The bentonite resulted from a latitic or rhyolitic volcanic ash that fell into the Mowry sea, or possibly in the case of the Newcastle Formation, onto fresh-water lakes, near the shore /ELZ 94/. Alteration from ash to bentonite probably occurred immediately after deposition. Slaughter & Early /SLA 65/ proposed that Na-rich solutions must have passed through the deposit after alteration.

BGR-collection

Different bentonites perform rather different in most fields of applications. These differences cannot always be explained by the dominating exchangeable cation only. So, the Federal Institute of Geological Raw Materials (Bundesanstalt für Geologische Rohstoffe – BGR) in Hannover, Germany, has collected bentonites from nearby 40 different deposits. This collection was used by BGR to analyze different parameter of bentonites under comparable conditions. The BGR has published already following parameter: chemical composition, degree of detachment of colloid particles, pH caused mainly by Na-cations in interlayer space /KAU 08a/; qualitative and quantitative mineralogy by XRD and Rietveld-refinement /UFE 08/; pH, carbonate and sulfur concentration/ /KAU 08b/ as well as CEC, charge by alkylammonium method and charge by structural formula method /KAU 11a/.

2.2.5 Composition of smectite as footprint of its origin and indicator for technical properties

Chapter 2.2.2 has tried to summarize the typical types of origin for economic bentonites. It was indicated in this chapter that certain environments of bentonite formation are characterized also by a certain pH-milieu. A new aspect of possible differences in pH at the time of bentonite's formation and its impact of a specific dissolution potential of bentonites were discussed in chapter 2.2.3. Furthermore, it was studied the literature to information about type of origin as well as chemical and mineralogical composition for the common bentonites considered as possible HLW-buffer or backfill material (chapter 2.2.4).

Now, all this dataset is to discuss under the viewpoint: What is the impact of the environment during the formation of bentonite on the chemistry of smectite? Is that than also related to typical pH-milieus?

A series of mineral formulae from smectite of different bentonites is summarized in Tab. 2.3.

The identification of the origin of bentonites is not yet completed. Actually, it is to recognize that bentonites in marine, sedimentary environment with acidic or intermediate parent rocks represent the "specific dissolution"-group A. The formation of this type is

linked with a neutral pH-milieu. Some Wyoming bentonites (e. g., MX-80[1998], MX-80[2005]) would be typical bentonites of this series.

The variability of Wyoming bentonites would assumed by diverse authors by changing situations of sedimentation of volcanic ash into marine lagoons or lakes and by different composition of ash. Otherwise, it was focused already in chapter 2.2.2 that the fall of hot volcanic ash into water will result in another development in comparison to fall of cooled ash. The hot ash is evaporating the water and an increasing of pH is to expect slight similar to the processes under salt lakes or sabkha conditions. A closer or farther origin of volcanic ash would be in this case the only key difference to explain the different behavior of Wyoming bentonites on one side with MX-80 charges analyzed by [HEN98] and [KAR06] and Belle Fourche (all: group B) and on the other hand the before mentioned MX-80[1998] and MX-80[2005] (all: group A).

The main impact of hot ash during the formation of bentonite is mirrored mainly by formation of IS-ml instead of pure montmorillonite as smectite phase. This development seems to see for the bentonites Rokle, Lieskovec and Jelsovy Potok in comparison to the Bavarian bentonites like Montigel.

Hydrothermal alteration is mirrored by formation of IS-ml (Kunipia-F > IBECO RWC, FEBEX). The low temperature weathering of mafic rocks represents the general chemical composition of parent rocks: low Al & Si and high amount of Fe, Mg and Ca. Especially, the oxidation of Fe^{2+} from parent rocks is forcing an alkali pH-milieu during the formation of bentonite.

2.2.6 Conclusions

The origin of bentonite formation seems to affect the specific dissolution potential in sense of /HER 11/ via parent rocks and pH-milieu.

It seems possible to develop a new strategy for pre-selection of suitable bentonites using the origin of bentonites as key parameter.

Tab. 2.3 Mineral formula of different bentonites and as far as possible relation to the origin of deposits

	Ca	Mg	Na	K	Al	Fe^{3+}	Mg	Ti	Al	Si	XII	nVI	ΔS % total	ΔS % prec	diss_ group	assumed origin	authors	
Polkville (API #20)	0,01	0,10	0,10	0,02	1,52	0,25	0,22	0,01	0,08	3,92	0,34	1,99	-11 %	0 %	A	sedi_acid_brines	/HER 11/	cv
Amory (API #22a)	0,02	0,04	0,18	0,11	1,42	0,33	0,22	0,01	0,13	3,87	0,40	1,98	-10 %	0 %	A	sedi_acid_brines	/HER 11/	
Otay (API #24)	0,03	0,02	0,20	0,06	1,43	0,32	0,19	0,02	0,07	3,93	0,36	1,96	-8 %	0 %	A	sedi_acid_marin_hot	/HER 11/	
Cameron (API #31)	0,02	0,07	0,15	0,26	1,51	0,33	0,14	0,01	0,40	3,60	0,59	1,99	-9 %	0 %	A		/HER 11/	tv
Pioche (API #32)	0,01	0,12	0,16	0,06	1,44	0,21	0,33	0,01	0,13	3,87	0,48	1,99	-11 %	0 %	A		/HER 11/	cv
Bayard (API #30)	0,02	0,14	0,11	0,01	1,49	0,06	0,44	0,01	0,02	3,98	0,44	2,01	-6 %	2 %	B		/HER 11/	
Chambers (API #23)	0,15	0,04	0,05	0,01	1,45	0,16	0,38	0,01	0,06	3,94	0,44	2,00	-5 %	0 %	B	sedi_acid_lacu	/HER 11/	cv
MX-801998			0,30		1,55	0,20	0,25		0,04	3,96	0,30	2,00	-1 %	0 %	A	sedi_acid_marin	/MAD 98/	cv
MX-802005	0,04	0,04	0,01	0,02	1,59	0,21	0,16	0,04	0,05	3,95	0,19	2,00	-21 %	11 %	A	sedi_acid_marin	/HER 11/	
Friedland Clay (Burgfeld)	0,01	0,11	0,03	0,23	1,54	0,31	0,12	0,02	0,4	3,6	0,53	1,96	-29 %	0 %	A	sedi_acid_marin	/HER 11/	
IBECO RWC	0,09	0,05	0,09	0,01	1,43	0,22	0,29	0,04	0,10	3,90	0,38	1,98	-13 %	0 %	A	sedi_acid_marin	/KAR 10/	
Belle Fourche (API #27)	0,04	0,03	0,16	0,04	1,60	0,17	0,19	0,01	0,06	3,94	0,34	1,97	0 %	0 %	B	sedi_acid_brack?_hot?	/HER 11/	cv
MX-80	0,07		0,22	0,01	1,54	0,17	0,26	0,02	0,05	3,95	0,36	1,99	-1 %	0 %	B	sedi_acid_brack?_hot?	/HEN 98/	cv
MX-80	0,02	0,01	0,23	0,01	1,55	0,18	0,25	0,01	0,03	3,97	0,30	1,99	-1 %	0 %	B	sedi_acid_brack?_hot?	/KAR 06/	
Rokle, Czech	0,04	0,07	0,05	0,07	1,32	0,45	0,18	0,02	0,10	3,90	0,33	1,97	-20 %	3 %	B	sedi_mafic_lacu	own	cv
Lieskovec, Slovakia	0,23				1,32	0,53	0,14		0,28	3,72	0,45	1,99	-3 %	0 %	B	sedi_acid_lacu_?vhot	/MIS 99/	
Jelšový potok, Slovakia	0,22				1,50	0,19	0,32		0,15	3,85	0,44	2,01	-2 %	0 %	B	sedi_acid_lacu_?vhot	/MIS 99/	
Montigel	0,14				1,36	0,31	0,36			4,00	0,56	2,03	-2 %	2 %	B	sedi_acid_lacu	/MAD 98/	tv/cv
Friedland Clay (Siedlungsscholle)	0,05	0,07	0,03	0,28	1,19	0,56	0,19	0,01	0,20	3,80	0,55	1,96	-29 %	0 %	B	sedi_mari_diag	/HEN 98/	tv/cv
Kunipia-F	0,03	0,01	0,48	0,01	1,54	0,09	$^{+}$0.35		0,13	3,87	0,57	1,98	-3 %	0 %	B	weat_hydr_vhot	/WIL 11/	
Febex	0,12	0,12	0,11	0,01	1,32	0,20	0,46		0,08	3,92	0,6	1,98	-16 %	1 %	B	weat_mafic_hydo_100	/FER 10/	
Asha / India	0,01		0,41		1,22	0,42	0,36	0,02	0,15	3,85	0,43	2,02	-29 %	13 %	B	weat_mafic_marin	/KAR 06/	
GeoHellas di smectite	0,09	0,13	0,00	0,12	1,06	0,55	0,36	0,02	0,32	3,77	0,56	1,99	-8 %	0 %	B	weath_mafic_sabkha	/HER 11/	
VN-Clay	0,03	0,09	0,00	0,03	0,57	*1.27	0,15	0,02	0,15	3,85	0,27	2,01	-60 %	31 %	B	weat_mafic_fluv	/HER 11/	
Garfield Nontronite (API #33a)	0,02	0,08	0,07	0,02	0,20	1,79	0,00	0,01	0,40	3,60	0,29	2,00	-94 %	27 %	B	weat_mafic	/HER 11/	

Legend see next page

Legend to Tab. 2.3

ΔS%total	total specific dissolution potential of bentonite (so lower the value so faster the process of dissolution
ΔS%prec	precipitation by dissolved Si as result of ΔS%total and the ability of bentonite to buffer dissolved Si into new montmorillonitic layers)
diss_group	type of mechanism to prevent dissolution (A – Na acts as stabilizer, B – Ca + Mg acts as stabilizer)
type of last impact	the last reported main impact on bentonite formation; authors – authors concerning the mineral formulas

sedi	sedimentary environment
weat	weathering environment
hydr	hydrothermal alteration
100	hydrothermal alteration at intermediate temperatures
Vhot	a) hydrothermal alteration > 200 °C b) very hot volcanic ash was settling into water
hot	warm volcanic ash was settling into water (< 100 °C)
mafic	mafic parent rocks
acid	acidic or intermediate parent rocks
fluv	sedimentation in fluviatile water
lacu	sedimentation in lacustrine water
marin	sedimentation in marine water
?	assumed sub-topic
+	incl. Fe^{2+} 0.02
*	incl. Cr^{3+} 0.08

Following the system (Tab. 2.3) than it should be possible to identify slow reacting bentonites (sleepers) of dissolution-type B in case of mafic parent rocks under hydrothermal alteration. A low temperature weathering of mafic rocks is linked more with fast reacting bentonites (sprinters).

The alteration of hot acidic volcanic ash as parent rocks in a marine, sedimentation environment forms mainly sleepers following until now available examples.

SKB has removed his decision to apply MX-80 as buffer or backfill material (oral information by R. Pusch). Recently, SKB is looking for few Danish bentonites (Holmehus, Rösnaes, Ölst). Accepting the mineral formula of smectite in these bentonites /KAR 06/, these bentonites are characterized by high octahedral Fe^{3+} and Mg-contents. Following the system from Tab. 2.3, Holmehus represents alteration of cold volcanic ash in marine milieu, Ölst would be the result of alteration of hot volcanish ash in marine environment and Rösnaes should be characterized by alteration of hot volcanic ash in fresh water facies. Only Rösnaes as Ca-bentonite could offer an option as sleeper of the dissolution type B. The other two bentonites are to expect as sprinters of dissolution type B.

2.3 Solute transport and retardation

Solute transport and retardation are the important processes in porous media for substances migration in the underground. The main processes of solute transport include diffusion and advection. The general retardation process is adsorption.

2.3.1 Diffusion and advection

Advection is a transport mechanism of a substance by a fluid due to the fluid's bulk motion. This is induced by the hydraulic gradient and can be described by Darcy Law for most soil material. Diffusion in liquid is a transport mechanism induced by concentration gradient and requires no bulk motion of the liquid. Advection is sometimes confused with convection. In fact, convective transport is the sum of advective transport and diffusive transport. The equation for mass transport with geochemical reaction in saturated porous media is:

$$\frac{\partial C_i}{\partial t} = -v_a \nabla C_i + \nabla \cdot (D \nabla C_i) + Q_{C_i} + React(C_1, \dots C_n) \quad (2.1)$$

C_i	concentration of the chemical component or element i
v_a	flow velocity (advection), v_a = permeability · hydraulic gradient
D	diffusion coefficient
Q_{C_i}	source term of the chemical component or element i
$React(C_1, \dots C_n)$	concentration change owing to chemical reactions

In porous media with extremely low permeability but relatively high porosity like bentonite, diffusion is the dominant mass transport process. Contaminants may migrate in the interparticle as well as the interlayer pore spaces. Details of diffusion can be found in section 3.

2.3.2 Sorption

Adsorption is the fluid/solid interaction process with the adhesion of atoms, ions, or molecules from a gas, liquid, or dissolved solid to a solid surface, which leads to the formation of a film of the adsorbate on the surface of the adsorbent. Adsorption is one

of the most important processes leading to the retardation of contaminants migrating through clayey substances like bentonite as engineered barrier material. Owing to the net negative charge on the surface, clay minerals (especially montmorillonite) tend to adsorb cations with positive charge. The main factors influencing the sorption are the surface properties of the adsorbent e. g. specific surface, surface charge, CEC (Cation Exchange Capacity) etc.; the properties of the adsorbate e. g. the charge, diameter of the ion, hydration properties, interaction with coexisting ions, initial concentration etc.; other factors like the temperature, pH, Eh, solid/liquid ratio, adsorption time, stirring speed, mineral pre-treatment etc. An overview of the possible mechanism for sorption can be found in /VIL 09/: non-specific Coulombic sorption in diffuse layer, Coulombic sorption in Stern layer, specific chemical sorption in Stern layer, surface induced precipitation, chemical substitution, structural penetration, isotopic exchange, physical sorption or physisorption.

One of the most common adsorption reactions in soils is ion exchange. Such reactions result in the replacement of ionic species on the surface of a solid phase by another ionic species existing in an aqueous solution in contact with the solid. This is also the main form of adsorption of metals by clay minerals like bentonite. It is also reverse process and desorption occurs by lowing the contaminant concentration in the solution. Ion exchange can be chemically determined and described by equilibrium constant /STU 96/. In a multicomponent solution with competing ions, the ion exchange process becomes more complex and depending on the activities of each cations and charge, ion radius and even kinetic together with ion interaction parameters.

Another common adsorption reaction is precipitation reaction of dissolved species in the solution, which is also referred to be a special case of the complexation reaction in forming solids by mixing two or more aqueous species. Owing to the low solubility of many heavy metal components (e. g. Ni and Pb components) in soil/groundwater systems, precipitation is particularly important for the groundwater environment science.

As sedimentary rocks in der deep underground saturated with highly saline solution in Canada, and salt rock in Germany and USA are potential host rocks for chemotoxic and/or nuclear wastes, there is a need to establish an understanding of how brine solutions affect sorption on sedimentary rocks and sealing materials (e. g. bentonite) /VIL 09/, /VIL 11/, /WAR 94/. According to the experiments by /VIL 11/, the sorption of some cations like strontium and radium was not observed in highly concentrated brine solutions, indicating the sorption coefficients of such elements should be assigned val-

ues of 0 for sedimentary rocks. However, transition metals such as Ni(II), Cu(II), Eu(III) and even U(IV) sorb by surface complexation mechanisms to bentonite, shale and limestone.

Sorption properties can be described with different models:

1. The constant distribution coefficient (k_d) model: k_d, is a measure of sorption and is defined as the ratio of the quantity of the adsorbate (i. e., metal) adsorbed per unit mass of solid to the quantity of the adsorbate remaining in solution at equilibrium.

$$K_d = \frac{A_i - A_e}{A_e} \times \frac{V}{W} \tag{2.2}$$

in which k_d is the distribution coefficient in [ml/g], A_i and A_e are the initial and equilibrium activities of the adsorbate in solution in [mg/L], V is the volume of the solution in [ml], and W is the weight of adsorbent (e. g. clay) in [g].

This equation can be rewritten as:

$$A_j = K_d C_j \tag{2.3}$$

In which $\mathrm{A_j}$ refers to the amount of adsorbate adsorbed per unit mass of solid in [mg/g], $\mathrm{C_j}$ is the equilibrium solution concentration of the adsorbate in [mg/L], $\mathrm{K_d}$ is the constant adsorption constant in [L/g] or [ml/g].

2. The FREUNDLICH isotherm model: In order to evaluate the factors affecting the sorption properties, systematic experiments of sorption have to be conducted. The results of a suite of such experiments evaluating the influence of main factors like initial concentration of the contaminant on adsorption, while other factors are held constant, are called an “adsorption isotherm”. One of the isotherm model is the FREUNDLICH isotherm model /FRE 26/. This model is defined as:

$$A_j = K_f C_j^n \tag{2.4}$$

In which $\mathrm{A_j}$ refers to the amount of adsorbate adsorbed per unit mass of solid in [mg/g], $\mathrm{C_j}$ is the equilibrium solution concentration of the adsorbate in [mg/L], $\mathrm{K_f}$ is the FREUNDLICH adsorption constant in [(mg/g)/(mg/L)^n], n is the dimensionless coefficient.

3. The Langmuir model: this model was initially introduced to describe adsorption of gas molecules onto homogeneous solid surfaces like crystalline materials with one type of adsorption site /LAN 18/. This model is later on extended to describe adsorption of solution species onto solid adsorbents including heterogeneous solids like soils as the following /EPA 99/:

$$A_j = \frac{K_L A_m C_j}{1 + K_L C_j} \tag{2.5}$$

where A_j refers to the amount of adsorbate adsorbed per unit mass of solid, K_L is the Langmuir adsorption constant related to the energy of adsorption, A_m is the maximum adsorption capacity of the solid, C_j is the equilibrium solution concentration of the adsorbate.

Substituting 1/B for K_L , the equation (2.5) can be rewritten as:

$$A_j = \frac{A_m C_j}{B + C_j} \tag{2.6}$$

or

$$A_j = -B\frac{A_j}{C_j} + A_m \tag{2.7}$$

in which B and A_m can be obtained by plotting the $A_j - (A_j/C_j)$ diagram if the adsorption can be well described by Langmuir model.

2.4 Interaction of bentonite and canister corrosion products (Fe, gas, chemotoxic substance; radiation, radioactive nuclides etc.)

2.4.1 Iron-induced impacts on alteration of smectite

WIL11 reviewed the latest state of art in literature also concerning iron/steel-bentonite interactions. They summarized, there are a number of physico-chemical processes that could occur should steel/iron waste containers be used in an EBS along with bentonite. Steel is likely to corrode and react with the smectite component of the bentonite. Depending on dissolved carbonate, chloride and sulphide concentrations and redox, pos-

sible steel corrosion products under low oxygen conditions include magnetite (which may form via metastable $Fe(OH)_2$ or 'green rust' compounds), iron carbonates (such as siderite), iron sulphides and iron (oxy)hydroxides (e. g., /TAM 84/, /ANT 03/, /REF 03/, /WER 03/, /KIN 08/.

The interaction of iron with bentonite has few, if any, natural analogues due to the lack of native Fe in the Earth's crust /WIL 03/, /WIL 06a/.

Wersin & co-authors /WER 08/ described that the iron-bentonite interaction under reducing conditions may involve different processes including sorption, redox and dissolution/precipitation reactions. One process to consider is the sorption of corrosion-derived Fe(II). This process is fast and leads to strong binding of Fe(II) at the smectite surface. A further process to consider under very reducing conditions is the reduction of structural Fe(III) in the clay which may destabilize the montmorillonite structure. The process of greatest relevance for the buffer's performance is montmorillonite transformation in contact with reduced iron. Current data suggest that the trans-formation process may either lead to a Fe-rich smectite (e. g. saponite) or to non-swelling clay (berthierine or chlorite). In addition, cementation due to precipitation of iron corrosion products or of SiO_2 resulting from montmorillonite transformation may occur.

Physical properties of the buffer may in principle be affected by montmorillonite transformation or cementation processes. CAR06 reported in their oxygen-free experiments about increasing hydraulic conductivities also for high swelling pressure conditions in case of high iron/bentonite ratios (wire experiments). They expected an inhomogeneous system with localized high density volumes and low density volumes /BÖR 03/. In such systems, the high density volumes lead to higher swelling pressure and the low density volumes lead to higher hydraulic conductivity compared to a homogenous material. Similar results with high swelling pressure and increased hydraulic conductivity were also described in experiments with oxidative environment /BÖR 05/.

Like summarized in /WIL 11/, the results of low temperature experiments (< 250 °C) do not give an unequivocal indication of the most likely reaction pathway that may occur in an engineered backfill system. However, it appears to be the case that Fe(II) produced from Fe(0) oxidation reacts with smectite which may lose tetrahedral units to form disordered smectite/gel regions with re-crystallization occurring to produce either Fe-rich smectite/1:1 minerals (e. g. berthierine, odinite, cronstedtite). These minerals are prob-

ably metastable with respect to Fe-rich chlorite, which is observed to form under higher temperature conditions.

The mentioned equivocal indication from low temperature experiments is mirrored also in the literature review presented in Fig. 2.15. Publications detecting changing in some bulk properties of bentonite like CEC, swelling pressure and hydraulic conductivity are in balance with papers, which concluded no impact by Fe on bentonite behavior. A minority of publications has shown experimental proofs also for mineralogical alteration of smectite into new Fe-rich sheet silicates.

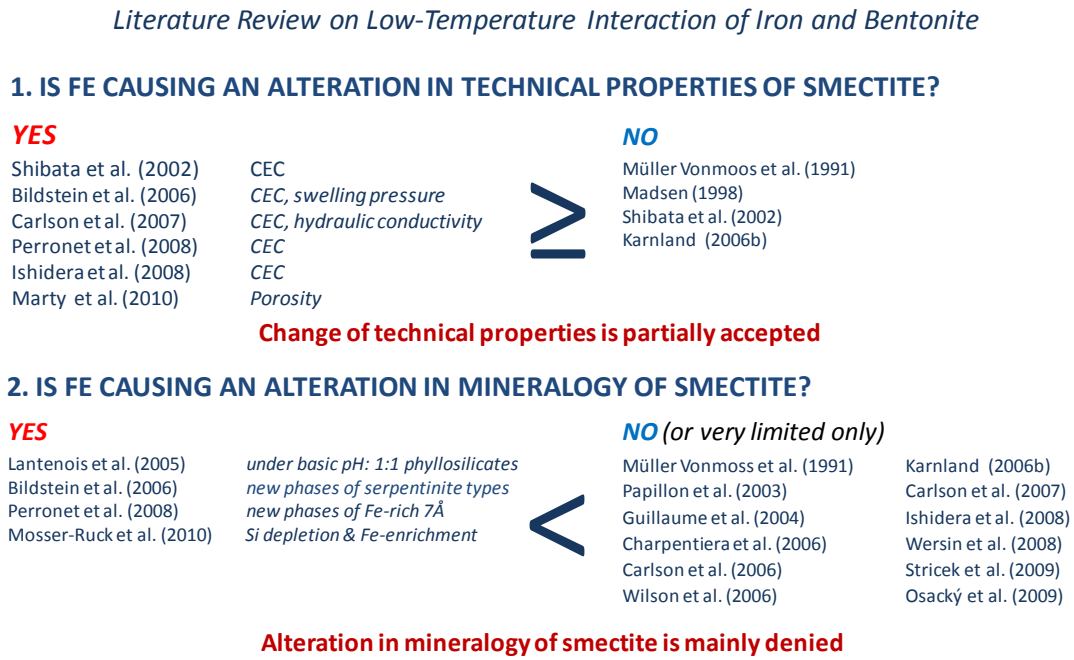

Fig. 2.15 Literature review about published experiments at < 250 °C mirroring the discussion about Fe-impact on technical properties of bentonite and mineralogical changing of smectite

What could be the key to dissolve these mentioned equivocal indications?

2.4.1.1 Key 1 "Different Fe-activities cause different reaction products"

/KRU 01/ has drawn a simplified Fe-Pourbaix-diagram (Fig. 2.16). This diagram visualizes pH-related two fields of Fe-corrosion separated from a field of passivity (at 25 °C).

Authors like /LAN 05/ described the Fe-corrosion and the alteration of smectite under different pH-ranges. They have shown in their experiments (45 days, 80 °C):

- when initial pH is mildly acidic to neutral, a large proportion of metal iron is dissolved, whereas iron oxides, identified as magnetite using XRD, precipitate extensively. In addition, smectite appears unaffected;
- when initial pH is basic (8 – 12 pH range), the reaction is dramatically different as dioctahedral smectites are involved in the reaction.

Under basic pH, dioctahedral smectites are then destabilized to form new clay phases like 1 : 1 iron-rich phyllosilicates and iron oxides.

However, smectite plays a catalytic role as in the same experimental conditions (45 days, 80 °C, initial pH = 6) metal iron is not destabilized in the absence of smectite whereas in presence of smectite metal iron is oxidized /LAN 05/.

Fe-corrosion is causing an environment with increasing pH-range by OH--formation. So, higher activity of Fe (e. g., by higher Fe-concentration, higher temperature or higher concentration of electrolytes) is responsible for higher pH-range in such reaction cells. The higher Fe-activity caused by increased temperature and the additional catalytic effect of smectite seem also to reduce the passivity field drawn in Fig. 2.16.

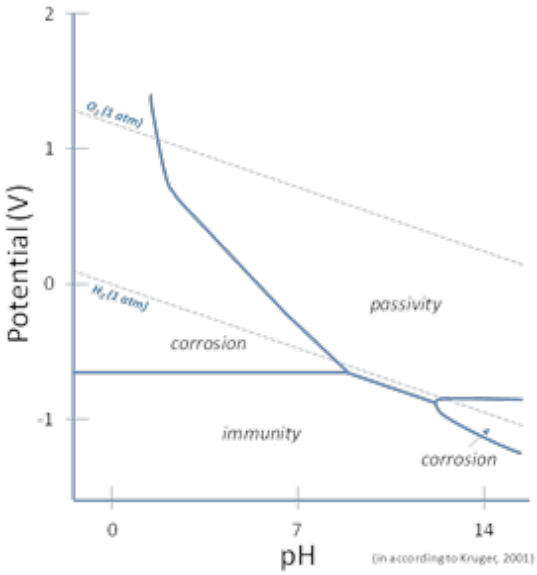

Fig. 2.16 Simplified Fe-Pourbaix-diagram under focus of O_2-poor conditions (in according to /KRU 01/ visualizing two possible fields of Fe-corrosion

Some authors like /PER 08/ caught the topic concentration by variable ratio between iron (Fe^0) and clay and described a strong relation between iron/clay (Fe^0/C)-ratio with CEC and neoformed Fe-rich sheet silicates. They have applied the FoCa7 bentonite for their experiments with varying Fe^0/clay mass ratio (Fe^0/C) tested in Evian mineral water at 80 °C during 45 days. This study shows that the exchange capacity of samples decreases with increasing Fe^0/C-ratio. For Fe^0/C = 1/30 and 1/7.5, secondary iron oxides are formed whereas from Fe^0/C = 1/3.75, initial iron oxides are strongly consumed to participate in Fe^{2+} and Fe^{3+} incorporation in gels or new phyllosilicates octahedral. When Fe^0/C = 1/3, a Fe-rich 7 Å clay appears, whose mean structural formula is close to odinite.

In a second part, the influence of duration and temperature are tested for the mixture with Fe^0/C = 1/3, i. e. for which a reactivity has been evidenced at 80 °C after 1.5 months. The experiments are conducted in one hand at 25, 80 and 150 °C during 1 month and in the other hand during 1, 3 and 12 months at 80 °C. When the run is longer than 1 month and the temperature is over 80 °C, new Fe-rich 7 Å phases crystallize at the expense of smectite and kaolinite.

/MOS10/ have extended such experiments for parameters like temperature, pH, iron/clay and liquid/clay ratios. They carried out batch experiments using MX-80 bentonite (< 2 µm) in contact with magnetite and Fe metal saturated in dilute chlorine solution, NaCl or $CaCl_2$. The experiment was carried out in an autoclave under an Ar atmosphere at temperature of 80, 150 and 300 °C for 3 to 12 months. The mass ratio of liquid/clay was 5 and 10 and the ratio of Fe^0/clay was 0.5 and 0.1. A plate of metallic Fe (~1 cm²) was added in all experiments. The observed mineral composition at each temperature released in different mineral sequences:

A higher Fe^0/C-ratio is causing an increasing basic pH by the reduction potential of Fe-oxidation. This high basic pH-range is also supporting a faster dissolution process of smectite.

- MX-80 bentonite → 1:1 Fe-rich phase like berthierine, odinite – cronstedtite for high iron/clay ratio (> 0.5)
- MX-80 bentonite → Fe-rich trioctahedral smectite for low iron/clay ratio (0.1) at temperature up to 150 °C, neutral pH and ratio of liquid/clay > 5.
- MX-80 → palygorskite for a small ratio of iron/clay = 0.1 in the case of higher than 150 °C under alkaline pH and ratio of liquid/clay > 5.

- MX-80 → Fe-rich saponite → trioctahedral chlorite + feldspar + zeolite at 300 °C, ratio small ratio of iron/clay = 0.1 and ratio of liquid/clay > 5.
- MX-80 → Fe rich vermiculite + mordenite at 300 °C, ratio small ratio of iron/clay = 0.1 and ratio of liquid/clay > 5 and at pH = 10 to 12

In general, Si and interlayer charge slightly decreased in comparison to an increase of Fe in the octahedral sheet at 80 °C. At 300 °C, Si in the tetrahedral sheet was markedly depleted. This showed that the increase in temperature caused Si depletion and enrichment of Fe in run products /MOS10/.

Summarizing the above introduced experiments, a higher Fe^0-activity is increasing the pH-range. That means a lower Fe^0-activity is related with middle to neutral pH-range, where smectite is catalyzing the corrosion, but smectite itself is not altered. High Fe^0-activity is promoting an increasing pH into high basic environment. This situation could dissolve also clay minerals because of the dissolubility of Al and Si in this pH-range (Fig. 2.17). Future experiments should outline the typical ranges for Fe-activities and the applied Fe-activity (concerning Fe^0/clay-ratio, temperature).

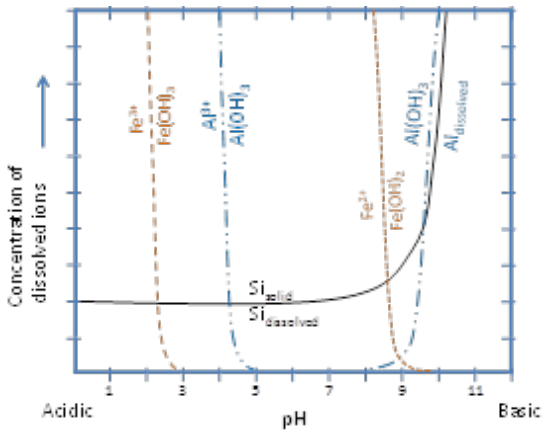

Fig. 2.17 Diagram for pH-related dissolution behavior (in according to /SEI 90/ visualizing the dissolution potential for clay minerals under high alkali conditions (see: Al & Si)

2.4.1.2 Key 2 "Different smectites have different chemical reaction rates"

Especially experiments with a larger series of different bentonites have shown that bentonites have higher variability in reaction than it could be assumed in cause of the dif-

ferent amount of smectite or certain reactive admixtures in these bentonites (e. g., /LAN 05/, /KAU 08a/, /KAU 08b/, /KAU10a/, /HER 11/, /NGU 12/.

/LAN 05/ reported already about an important reactivity contrast as a function of smectite crystal chemistry mirrored by octahedral Fe^{3+} (Fig. 2.18) and Na+-amount in the interlayer space. They proposed also a conceptual model for smectite destabilization. This model involves first the release of protons from smectite structure, $MeFe^{3+}OH$ groups being deprotonated preferentially and metal iron acting as proton acceptor. Corrosion of metal iron results from its interaction with these protons. Fe^{2+} cations resulting from this corrosion process sorb on the edges of smectite particles and lead to induce the reduction of structural Fe^{3+} and migrate into smectite interlayers to compensate for the increased layer charge deficit. Interlayer Fe^{2+} cations subsequently migrate to the octahedral sheet of smectite because of the extremely large layer charge deficit. This conceptual model explains also the high stability of trioctahedral smectites (like saponite) in comparison to dioctahedral smectites.

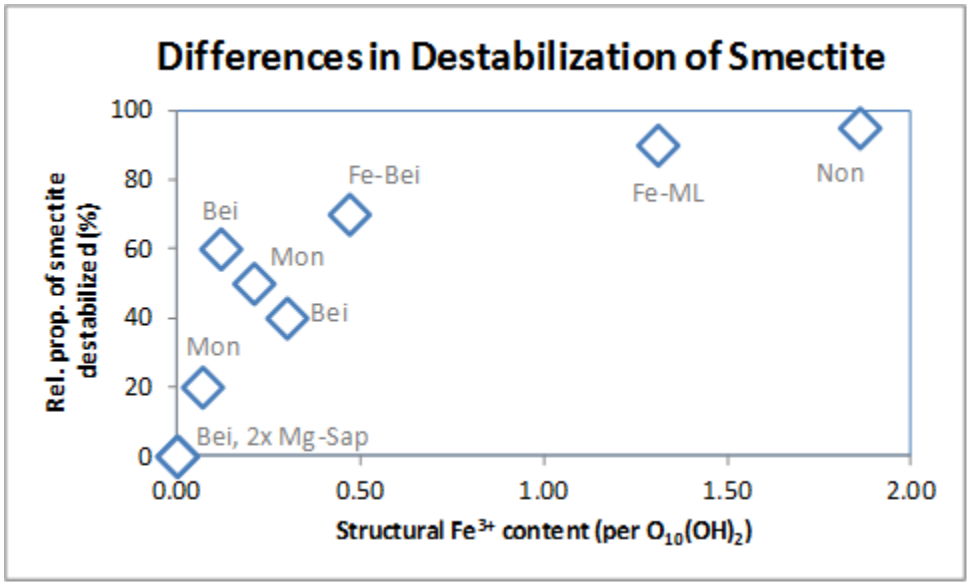

Fig. 2.18 Relation between structural Fe^{3+} content and degree of destabilization of smectite in 45 days experiments at 80 °C with Fe-powder (Fe^0/clay-ratio 1:1) adopted from /LAN 05/

In their experiments /LAN 05/, the cation composition of smectite interlayers appears as an additional parameter influencing the reactivity of dioctahedral smectites (concluded from experiments with exchanged interlayer compositions in samples SAz-1, SWy-2, and Garfield). The enhanced reactivity observed for the most hydrated samples

($Na^+ > Ca^{2+} > K^+$) indicates that the ability of solution cations to access smectite interlayers is a key parameter to smectite destabilization. The authors assumed that the reactivity contrast observed as a function of the interlayer cation composition is most likely related to the hydration of smectite which varies as a function of the interlayer cation (that means controlled by particle thickness).

Other authors /HER 11/, /NGU 12/ found also proofs for a different behavior of different smectite under comparable experimental conditions. They determined a specific dissolution potential for each smectite. The specific dissolution potential is controlled by Al/(Al+Fe+Mg)-ratio in octahedral layer and Na/(Na+Ca+Mg)-ratio in interlayer space of original smectite. High amount of Al in octahedral position and nearby full Na-occupation in interlayer space cause a low specific dissolution potential. Such smectites would be quite stable in any experiments. It seems that this specific dissolution potential defined by /HER 11/ and /NGU 12/ is also explaining the measured degree of smectite destabilization in the experiments of /LAN 05/. A comparison between the parameter for destabilized smectite /LAN 05/ and the specific dissolution potential /HER 11/, /NGU 12/ show a strong linear correlation for the most used smectites (circles in Fig. 2.19).

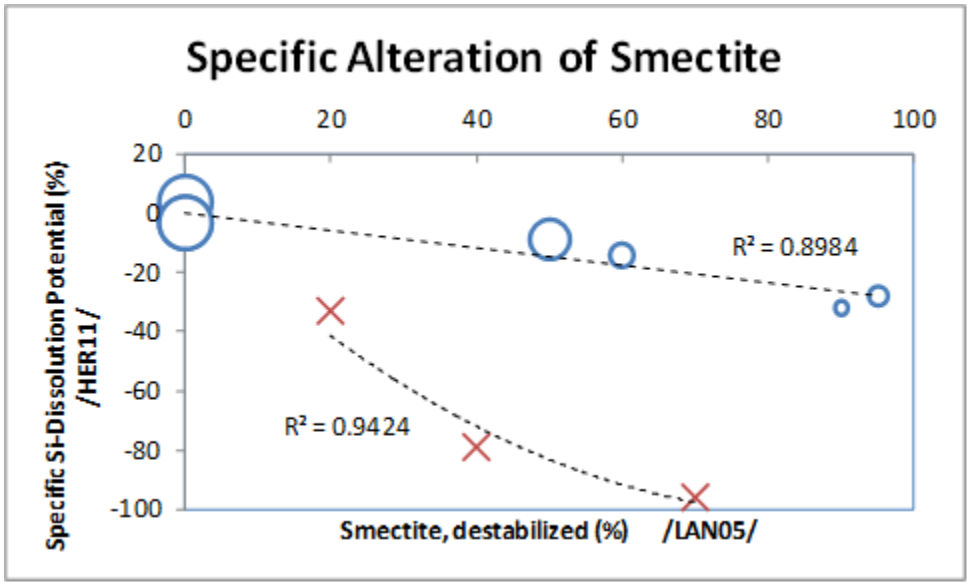

x-axis – ratio of destabilized smectite in % in according to /LAN 05/; y-axis – specific dissolution potential of Si from smectite in % calculated in according to /HER 11/, /NGU 12/; circles – bentonite samples without Si-precipitation potential, diameter of circle represents Na/(Ca+Mg)-ratio in interlayer space; red crosses – bentonite samples with Si-precipitation potential.

Fig. 2.19 Approach of dataset from /LAN 05/ in order to demonstrate relation between two different parameters describing specific alteration of smectite in contact with Fe^0

A higher dissolution potential (expressed with negative values) is causing also a higher degree of destabilization of smectite. But this comparison has identified also few exceptions (crosses in Fig. 2.19). Also these exceptions follow a strong correlation between the two parameters. The authors /HER 11/, /NGU 12/ described also a specific Si-buffer potential to incorporate dissolved Si again as smectitic layers. If the amount of dissolved Si is higher than the specific buffer potential then Si is precipitating and it leads to cementation of neighbored smectite particles. This situation is clearly to identify for three mentioned exceptions in Fig. 2.19 (Tab. 2.4). So, cemented particles by Si-precipitation are protected in a certain scale against destabilization processes. The exceptions show also that the specific dissolution potential is also here the controlling factor, but the occurrence of Si-precipitation generally is responsible for a lower degree of destabilization.

Tab. 2.4 Dataset for Fig. 2.19 to demonstrate relation between two different parameters describing specific alteration of smectite in contact with Fe^0 using the experimental data from /LAN 05/

	N	FS	B	B	M	S	S	B	B	M
	Garfield	SWa-1	SbId	SbS-1	SWy-2	SapCa-2	SapFe08	Drayton	CP4	SAz-1
/LAN05/-model										
Smectite destab. %	95	90	60	0	50	0	0	70	40	20
/HER11, NGU12/-model										
Specific Dissolution Potential (%)	-28	-32	-14	4	-9	-3	-3	-96	-79	-33
Montmorill. layers in smectite (%)	*27*	*29*	*51*	*45*	*91*	*35*	*39*	*49*	*37*	*100*
Potential of Si-Precipitation (%)	*0*	*0*	*0*	*0*	*0*	*0*	*0*	***40***	***10***	***33***

The very high specific dissolution potential for samples Drayton, CP4, SAz-1 exceeds their Si-buffer potential, what is causing the mentioned Si-precipitation. The lack of Si-buffer for sample SAz-1 in comparison to samples Garfield and SWa-1 is caused in the montmorillonite-like smectite of SAz-1

Summarizing, the behavior of smectite in experiments is controlled by two main keys: (i) specific experimental parameter mirrored by Fe-activity and (ii) specific material parameter mirrored by the specific dissolution potential of smectite.

Fe-activity is commonly determined by Fe^0-concentration expressed as Fe^0/clay-ratio as well as temperature of experiments. The Fe^0-corrosion is responsible for an increasing pH-range. Smectites are stable under middle to neutral pH-ranges, but a high basic pH-range could dissolve Al and Si from smectite. Middle and neutral pH-ranges protonate $MeFe^{3+}OH$ groups preferentially (e. g., /YAR 97/. Fe^{2+}-cations have no access to these groups and the key-process in the alteration model of /LAN 05/ is not active under these middle to neutral pH-ranges.

Furthermore, occupation of octahedral layers and the arrangement of particles caused by composition of interlayer cations are defining a specific dissolution potential for each smectite /HER 11/, /NGU 12/. Possible cementation of particles by precipitated Si is reducing additionally the degree of destabilization of smectite. Furthermore, the particle thickness distribution is controlling additionally the degree of alteration in case of exchanged interlayer cations in comparison to the original cations distribution /LAN 05/.

The conclusion is: The results from low temperature experiments will give also furthermore equivocal indications so long any future experiments would be not adjusted to the approached Fe-activity and specific dissolution potential.

2.4.2 Copper-induced impacts on alteration of smectite

Copper has been considered as a canister material by a number of radioactive waste management organizations (in Sweden, Finland, and Canada, for example). The recent literature about copper-induced impacts on alteration of smectite was summarized by /WIL 11/. They cited /PUS 82/ that diffusion of copper into bentonite is a slow process. It has been suggested that it could result in an increase in hydraulic conductivity (2 – 5 times), but given the extremely low hydraulic conductivity of compacted bentonite prior to any alteration, it may be considered to be insignificant. Finally, they concluded that alteration of 2:1 smectite layers due to the presence of copper is not envisaged.

Recalculations of Cu-Pourbaix-diagrams in copper-chlorine-water system /BEV 98/ at 100 °C have shown that under low oxygen-conditions Cu is corroding rarely in middle to neutral pH-ranges (Fig. 2.20). Like discussed for Fe-corrosion, no remarkable alteration of smectite is to expect caused by Cu-corrosion in this lower pH-range.

Otherwise, /KAS 12/ investigated the penetration of Cu into three different smectites in hydrothermal experiments with Cu-plates and compacted clay. Montmorillonite-rich MX-80 clay, Greek saponite with a minor amount of palygorskite, and Friedland clay were investigated in hydrothermal tests with dense samples confined in oedometers with 95 °C temperature at one end, which was made of copper, and 35 °C at the other, for 8 weeks. A 1 % $CaCl_2$ solution was circulated through a filter at the cold end. At the end of the tests the samples were sliced into three parts which were tested with respect to expandability, hydraulic conductivity, and chemical composition. The tests showed that while the saponite was nearby unchanged at all and did not take up any copper,

MX-80 underwent substantial changes in physical performance and adsorbed significant amounts of copper. The Friedland clay sample was intermediate in both respects (Fig. 2.21, Tab. 2.5). These results are in complete agreement with the outcome of other investigations of similar type /XIA 11/.

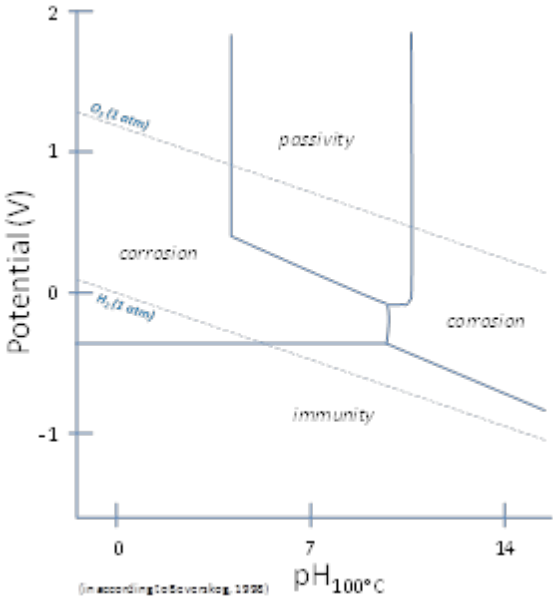

Fig. 2.20 Simplified Pourbaix diagram for copper species in the copper-chlorine-water system at 100 °C and [Cu(aq)]tot = 10^{-6} molal and [Cl(aq)]tot = 0.2 molal (adopted from /BEV 98/)

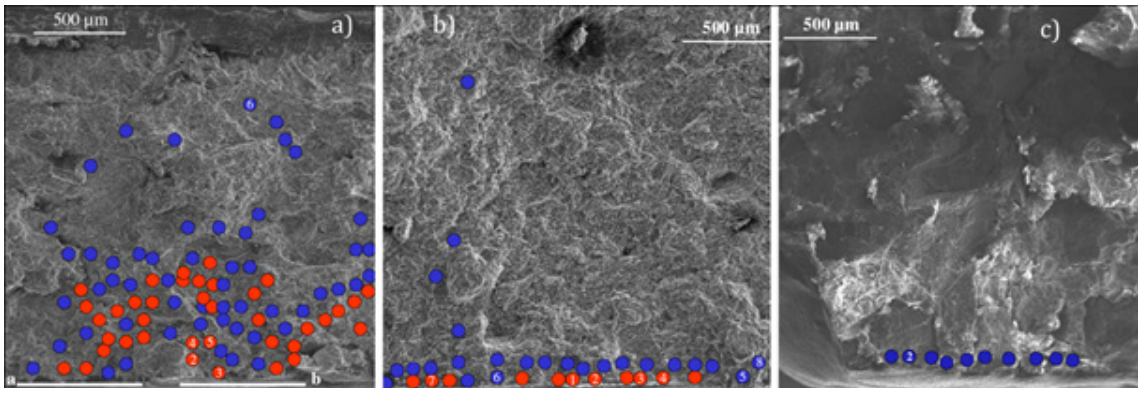

a) analyses of MX-80 clay; b) analyses of Friedland clay; c) analyses of saponite-rich DA0464 clay blue circles – Cu was not detected by SEM-EDX; red circles – Cu was detected by SEM-EDX that means Cu >>0.1 %)

Fig. 2.21 SEM-EDX analyses of three clays in contact with the copper plate at the bottom /KAS 12/

Tab. 2.5 Properties of MX-80, saponite-rich DA0464 and Friedland clays at different distance from the hot boundary (results from 8 weeks-experiments at 95 °C in contact with a Cu-plate) /KAS 12/

Clay	Distance from hot boundary [mm]	Density [kg/m^3]	Dry density [kg/m^3]	Hydraulic conductivity K [m/s]	Swelling pressure p_s [kPa]
MX-80	0 - 7	2000	1580	$2\cdot10^{-11}/2\cdot10^{-13}$	150/4000
	7 - 18	1850	1350	$2\cdot10^{-11}/5\cdot10^{-12}$	1020/1000
	18 - 32	1,800	1270	$1\cdot10^{-11}/8\cdot10^{-12}$	450/600
DA0464	0 - 10	1880	1380	$7\cdot10^{-11}/1\cdot10^{-12}$	1880/2000
	10 - 19	1790	1170	$1\cdot10^{-11}/5\cdot10^{-12}$	1280/1300
	19 - 32	1,800	1175	$8\cdot10^{-12}/4\cdot10^{-12}$	1170/1300
Friedland	0 - 8	2240	1725	$5\cdot10^{-11}/1\cdot10^{-12}$	240/> 1000
	8 - 21	2030	1545	$2\cdot10^{-11}/2\cdot10^{-11}$	445/630
	21 -3 2	1970	1360	$5\cdot10^{-11}/5\cdot10^{-11}$	300/450

Note: In the K and ps columns, pairs of A/B mean A is the experimental value while B represents untreated clays saturated with 1 % $CaCl_2$ solution. The initial dry density for MX-80, DA0464 and Friedland clay was 1353, 1237 and 1527 kg/m³, respectively.

The unaltered properties of saponite-rich bentonite should be in agreement with the observations from /LAN 05/ with Fe-experiments. Surprising is the high depth of penetration of copper into MX-80 bentonite (close to 1 mm) linked with the remarkable change of its physical performance in comparison to Friedland clay, an Fe^{3+}-rich illite-smectite mixed layers (%S = 70 %). Also strong effects of corrosion were visible on Cu-plate in contact with MX-80 bentonite. Both samples contain traces of sulfate that means the difference is not to find in this point.

The overall conclusion is that the saponite clay suffered less from the hydrothermal treatment than the montmorillonite clay and that the mixed-layer minerals-dominated clay was intermediate in this respect. The MX-80 clay sorbed substantial amounts of copper to a significant distance from the copper plate. Saponite did not take up any copper at all and FIM clay was similar in this respect. The distribution of Cu in MX-80 mirrored advective transport (also for FIM clay) and additionally local channel-type migration occurred. A possible explanation could be find in the approaching of the synthesized model between /LAN 05/ and /HER 11/, /NGU 12/ visualized in Fig. 2.19. Following this model, MX-80 would be characterized by 50 % destabilized smectite, Friedland clay by 15 % (low effect caused by Si-precipitation controlled cementation) and the saponite-rich clay by 0 % (real “zero” alteration). This comparison indicates that a high degree of dissolved particles is supporting the penetration of clay by heavy metals.

/SZA 07/ published studies about Cu-corrosion in anaerobic aqueous solutions.

$$Cu(0) + yH_2O \Rightarrow H_x\,Cu(I)O_y + (2y - x)H(0)ads \quad (2.8)$$

$$2H(0)ads + O(0)ads \Rightarrow H_2O \quad (2.9)$$

$$2H(0) \Rightarrow H_2(g) \quad (2.10)$$

Transforming the Fe-corrosion model of /LAN 05/, Cu(I)O- sorb on the edges of smectite particles (positive charge in middle and neutral pH-ranges) and lead to induce the reduction of structural Fe^{3+} and migrate into smectite interlayers to compensate for the increased layer charge deficit.

Summarizing, also for Cu-corrosion is to conclude: Studied literature shows equivocal indications from low temperature experiments concerning the impact of Cu on smectite. The different smectites show a different behavior especially for the penetration of heavy metal. A higher degree of dissolved particles seems to support a deeper penetration by heavy metals.

2.4.3 Gas formation

Specific studies have been performed that gas could be generated from the direct contact of possible repository brine and radioactive waste and could significant build-up of pressure in the repository. Four factors have been identified which influence the production of gases: radiolysis, microbial activity, corrosion, and evolved residual gas /MUE 97/, /HOL 98/. Furthermore, saline host rock could store some gas occurrence /MUE 97/.

The first mechanism, radiolysis of the water and material inherent in the waste and the brine, will result in the production of hydrogen (H_2), oxygen (O_2), nitrogen (N_2), carbon dioxide (CO_2), carbon monoxide (CO), nitrous oxide (N_2O), and smaller organic compounds. The corrosion mechanism will result from the electrochemical potential differences of various metals and will also result in the production of hydrogen gas. The bacterial degradation of organic and inorganic material in the waste is an additional mechanism that could result in the production of carbon dioxide (CO_2), carbon monoxide (CO), methane (CH_4), nitrogen (N_2), and nitrous oxide (N_2O). The final mechanism is the generation of air (N_2, O_2, and CO_2) in the waste that will evolve to some equilibri-

um concentration within the repository /HOL 98/. CO_2, CH_4, H_2S and water were reported from salt rocks /MUE 97/. Furthermore the distribution of gases in salt rocks was reported as very inhomogeneous. The differences in the amount of gases would be variable up to three magnitudes in the distance from few meters only.

/MUE 97/ cited results from experiments in rock salt and hydrated salt. 0.65 m³ H_2- and 0.3 m³ O_2-gas were produced in maximum per meter HLW-container in rock salt after 100 years, if more of 90 % of γ-energy would be involved in the processes. Hydrated salts, like $MgCl_2 \cdot 6H_2O$, have higher gas production (factor 20). An overview of gas generation in different media is given in Tab. 2.6 by /RUE 04/.

Tab. 2.6 Calculated volume of gas production by radiolysis in different media for a repository in Nm³ per meter coquille /RUE 04/

	V_I (term 0 – < 1,000 years) [$Nm^3 \cdot m^{-1}$]	**V_{II} (term > 10^3 – 10^6 years) [$Nm^3 \cdot m^{-1}$]**
Water	62.2	5.07
5n NaCl solution	297	24.2
Halite	0.122	0.01
Clay	3.1 – 15.8	0.25 – 1.29
Concrete	8.53 – 42.6	0.69 – 3.47
Granite	0.305	0.025
Bentonite	140	11.4

Hydrogen production by anaerobe corrosion of metals is the main mechanism for gas production and the gas-induced pressure development in the repository. The microbial gas production is considered as the second important process. Generally, the γ-radiolysis process of gas production is well understood /MUE 97/.

2.4.4 Effect of radiation and radionuclides on Bentonite

Radiolysis of porewater produces H-bearing radicals and oxygen compounds (including ozone and hydrogen peroxide). Radiolysis products may take part in chemical reactions affecting pH and oxidizing canister metals. Oxygen compounds (in gaseous form) may occupy wider voids and can delay or inhibit water saturation and contribute to the heat-induced desiccation of the buffer adjacent to the hot canisters. This is expected to have a particularly deleterious impact on the buffer in very tight repository host media, such as argillaceous rock and very fracture-poor crystalline rock. Relatively little atten-

tion seems to have been given to the impact of gases formed through radiolysis on overall gas pressure. Given that most disposal canisters are thick-walled and so provide substantial shielding, it is likely that the amount of gas produced by radiolysis will be small compared with the amount that will be produced as a result of corrosion of steel containers or cast iron inserts. Radiolysis on its own is unlikely to result in a significant build-up of pressure /WIL 11/.

Following /WIL 11/, the impact of alpha radiation on clay minerals (such as smectite) is related to changes in microstructural features and can be understood by considering the mechanisms for cation diffusion. Alpha radiation is expected to cause structural disintegration along the migration paths. For example, experiments have shown that montmorillonite that has been saturated with either of these elements, yielding around $5 \cdot 10^{18}$ α g^{-1}, is completely destroyed and converted to an amorphous, siliceous mass /BEA 84/. Other authors reported that an alpha dose of around $4 \cdot 10^{18}$ α g^{-1} is required to completely destroy the crystal structure of montmorillonite /GRA 86/.

Early research showed that the crystal structure of the clay mineral kaolinite undergoes destabilization when exposed to gamma radiation /JAC 77/, causing reduction of the size of the crystallites and a related increase in specific surface area. This effect may be similar or possibly more prevalent in smectite because of the large number of fragile hydrated layers that make up crystallites.

/WIL 11/ reviewed further experiments with bentonite under γ-radiation. The studies didn't identify any structural alteration of bentonites. Otherwise, they found quicker migration from iron plate into clay under radiation /PUS 93/, increasing CEC of montmorillonite /GRA 86/ and several properties of clay mineral (such as solubility, specific surface area, and exchange capacity) can be altered by local damage produced by radiation /ALL 09/, the effects on properties appear significant only for high doses and remain relatively limited. Structure breakdown can potentially result from radiolytic damage due to a severe ionizing irradiation and clay minerals can be amorphized under electron or ion beams /ALL 09/. The last authors consider that research effort is still required to obtain a consistent and comprehensive understanding concerning the evolution of specific surface area and CEC with the radiation dose.

Finally, /WIL 11/ summarized from different reports that only a small part of the buffer would be affected (and that this would not be substantial) and the effects on properties appear significant only for high doses and remain relatively limited.

2.4.5 Behavior of bentonites in contact with non-radioactive, chemotoxic substances

Different authors discussed in first steps also the option to use Geological Disposal Facilities also as storage for non-radioactive, chemotoxic substances.

/WIL 09/ presented a report on the treatment of chemotoxic species, aims to: provide a detailed assessment of the possible release of priority chemotoxic substances from a generic Geological Disposal Facility (GDF) and to quantitatively assess human exposures and allied health risks posed by such releases (in order to demonstrate that such approaches can be effectively used to inform post-closure safety assessments). Following chemotoxic substances would be considered as priority for human health risk assessment: beryllium, cadmium, chromium, lead and uranium. Their assessment focuses on the possible releases of chemotoxic substances from Intermediate and Low Level Waste (LLW and ILW). However, they have noted that a GDF could be developed in which there is co-disposal of these wastes with High Level Waste (HLW) and Spent Fuel (SF).

Other authors conducted experiments to the retardation potential of bentonite.

Removal of Pb(II), Cd(II), Zn(II), and Cu(II) from aqueous solutions using the adsorption process on bentonite has been investigated. For all these metals, maximum adsorption was observed at 20 °C in comparison to 30 and 50 °C. The rate of attaining equilibrium of adsorption of metal ions follows the order Zn(II) > Cu(II) > Cd(II) > Pb(II). Equilibrium modeling of the adsorption showed that adsorption of Pb(II), Cd(II), and Cu(II) were fitted to a Langmuir isotherm, while the adsorption of Zn(II) was fitted to a FREUNDLICH isotherm. Dynamic modeling of the adsorption showed that the first order reversible kinetic model was held for the adsorption process /BER 97/. /BAE 97/ deduced that two main sorption mechanisms were controlling the uptake of Ni and Zn onto Na-montmorillonite: (i) a pH-independent component, identified as cation exchange on the permanent charge sites, and (ii) a pH-dependent one, interpreted as surface complexation on the amphoteric surface hydroxyl groups. The non-linearity of the sorption isotherms indicated that at least two different ≡ SOH type sites were contributing to the overall sorption on Na-montmorillonite. /BRA 03/ developed a database of sorption values for a large series of cations from batch experiments with MX-80 bentonite under more oxidative conditions.

2.5 Special properties under highly saline solution

In salt formations but also in other geological host formations saline solutions may occur and can interact with the engineered barrier systems (EBS). High salinity and high pH in solutions put a high chemical stress on bentonites. These interactions may change the mineralogical composition and especially the swelling capacity of bentonites and thus the long term performance of the EBS /HER 08/.

2.5.1 Technical Properties

/KAR 98/ reported that several laboratory test series have been made in order to determine the effects on bentonite swelling of typical ground-water at repository depth, and of water solutions with considerably higher salt content /PUS 80/, /KAR 92/, /DIX 96/.

Experimental data and the performed calculations by /KAR 98/ indicate that swelling pressures may be expected also under repository conditions with a high content of NaCl in the ground water. The theoretical difference in effect from NaCl and $CaCl_2$ solutions is small according to this approach. However, the reduced swelling capacity in a brine type of ground-water significantly raises the lowest possible buffer density, and in practice, eliminates the positive effects of mixing bentonite into a backfill material. Calculations and experiments at different NaCl-solutions have shown that for montmorillonite compacted at high density (> 1.800 g/cm³ for saturated bentonite) the influence of the salinity of the solution on the value of the swelling pressure has been considered negligible or small.

Tests performed with FEBEX bentonite /CAS 07/ have shown than the swelling pressure of the bentonite compacted to dry density 1.65 g/cm³ decreases to almost half its initial value when $CaCl_2$ and NaCl solutions 2 M are used as saturating fluid. The bentonite develops slightly lower swelling strains upon saturation with low-concentrated saline water (0.8 percent salinity) than with deionized water, although this difference becomes less evident for the higher dry densities. The reduction of the swelling strains due to the increase of the concentration in the flooding solution can be explained by considering that the NaCl or $CaCl_2$ solutions cause an increase of electrolyte concentration near the clay particle surfaces, diminishing the thickness of the double layer and the swelling potential. In addition, samples wetted with $CaCl_2$ solutions swelled slightly

more than those wetted with NaCl. They observed also that the permeability increases when the concentration of the saline solutions increases, especially for high values of saline concentration. This higher permeability to saline water is more significant for low densities.

Other experiments were performed with MX-80 bentonite and saline solutions of different ion strength /HER 08/. These experiments have shown a clear development of swelling pressure in relation to ion strength of solution (Fig. 2.22). The highest swelling pressure was measured for MX-80 in contact with water (ion strength ~ 0). A moderate ion strength represented by Äspö-, Opalinus- and young cement pore solution caused a remarkable reduction of swelling pressure. The lowest swelling pressure was detected for MX-80 in contact with solutions like 1N NaCl, IP21, NaCl + cement or IP21 + cement mirroring high ion strength. The reduction of distances between the clay particles caused by higher concentration of electrolytes is generally reducing also the swelling pressure (double layer theory). Furthermore, the total charge of smectite particles could have an additional impact on swelling pressure. The total charge was calculated from the TEM-EDX analyses of smectite particles. The swelling pressure is decreasing with the total charge for low ion strength. In opposite to the situation of low ion strength, the swelling pressure seems to rise with decreasing total charge for moderate and high ion strength (Fig. 2.22).

A lower total charge of smectite in the same electrolyte concentration is also causing a reduction of double layer thickness. The repulsive forces would be reduced for lower total charge in case of low ion strength (Fig. 2.23, graph 1). Otherwise, moderate ion strength causes increasing repulsive forces for decreasing total charges (Fig. 2.23, graph 2). Finally, high ion strength shows in low distances an increasing but low repulsive forces (Fig. 2.23, graph 3). That means, the visualization of salt impact on development of ratio between repulsive and attractive forces offers a clear ex-planation of these experiments and the observed additional relation between total charge of smectite and swelling pressure under different ion strengths.

Experiments from /HER 11/ show also that the reduced swelling pressure is accompanied by in-creased permeability (Fig. 2.24). It seems to follow the general relation that higher swelling pressure is reducing the permeability.

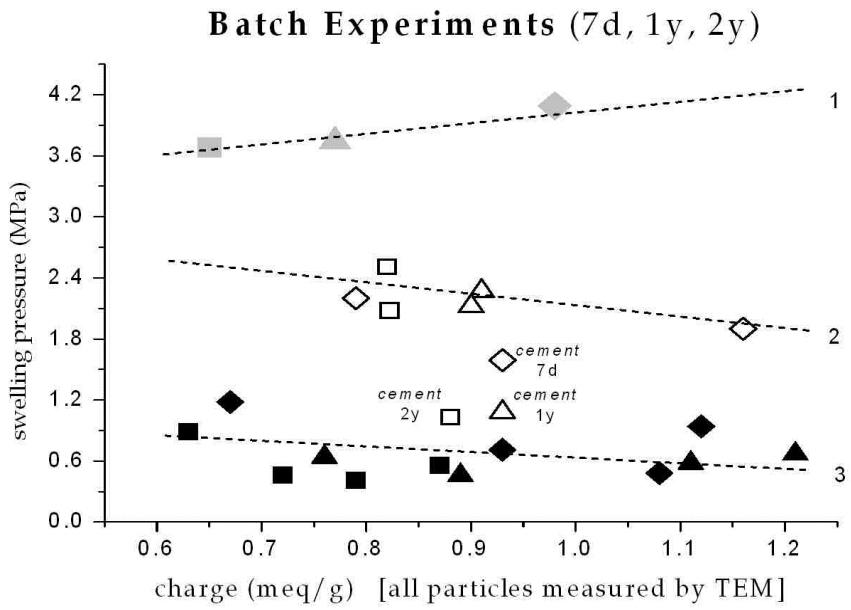

1 – low ion strength: MX-80 in contact deionized water; 2 – moderate ion strength: MX-80 in contact with Äspö-, Opalinus or young cement pore solution; 3 – high ion strength: MX-80 in contact with 1N NaCl, IP21, NaCl+ cement or IP21+cement solution; diamond – contact time with 7 days; triangle – contact time with 1 year; square – contact time with 2 years

Fig. 2.22 Correlation of swelling pressure and total charge for different classes of ion strength (batch experiments) /HER 08/

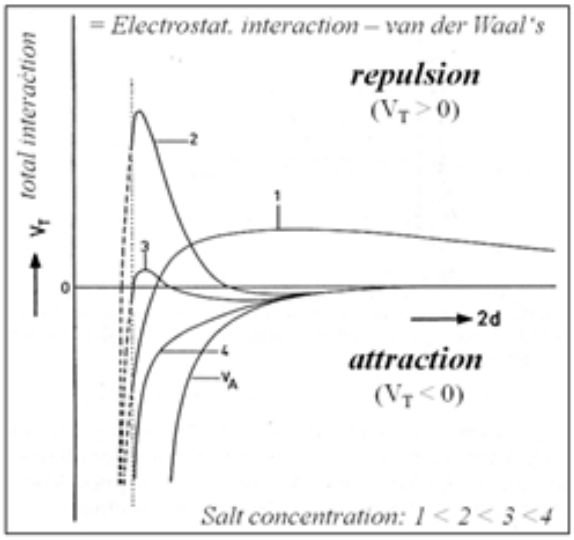

Fig. 2.23 Changing of repulsion forces in relation to increasing salt concentrations /JAS 93/

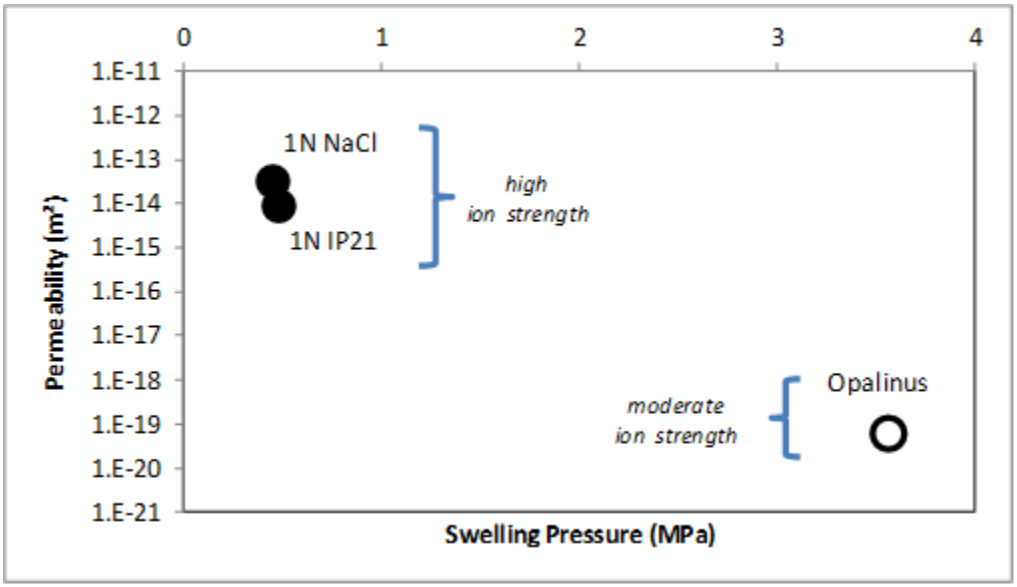

Fig. 2.24 Development of swelling pressure and permeability of compacted MX-80 bentonite in contact with different percolating solution (1N NaCl, 1N IP21; Opalinus) at 25 °C (dataset from /HER 11/)

Further experiments of /HER 11/ have also shown that the development of permeability and swelling pressure is drawing partially an equivocal behavior in case of higher chemical activities (higher concentration, higher temperature etc.).

Compacted MX-80 bentonite was percolated by Opalinus solution for 2 months at 25 °C, 60 °C and 90 °C. Higher temperature is acting like an increasing electrolyte concentration. In result of this experimental design, swelling pressure is increasing with temperature and also permeability increases (Fig. 2.25). This general trend is to understand under the view of already mentioned relation in the sense “swelling pressure ~ 1/permeability”. A complete different behavior is drawn in case of higher ion strength like 1N NaCl-solution as percolating agent. The highest swelling pressure and partially also the lowest permeability was identified for the experiments now at high temperature (Fig. 2.26). A further mechanism is overlapping now the effects explained by double layer theory.

Actually, it could be guessed only about the nature of this mentioned additional mechanism. It is remarkable that the high ion strength experiments with NaCl-solution show three different types of swelling pressure/permeability-relation: (i) increasing swelling pressure causes decreasing permeability (Fig. 2.26, box 1); (ii) different permeability at the same swelling pressure (Fig. 2.26, box 2) and (iii) reducing swelling pressure with also reducing permeability (Fig. 2.26, box 3).

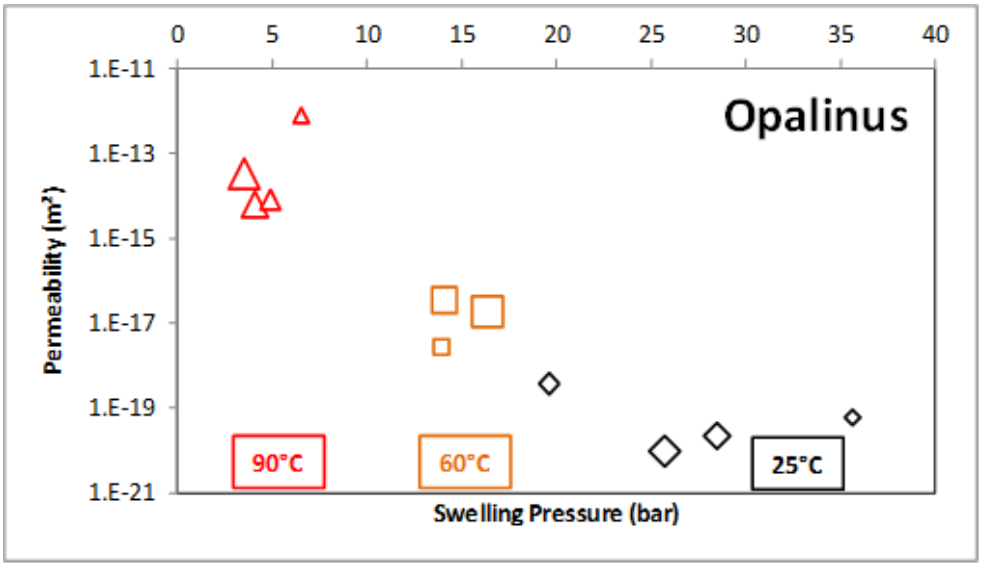

Different size of labels represents different concentration of additive $FeCl_2$-solution

Fig. 2.25 Development of swelling pressure and permeability of compacted MX-80 after 2 months percolation by Opalinus-solution at different temperatures (open system) /HER 11/

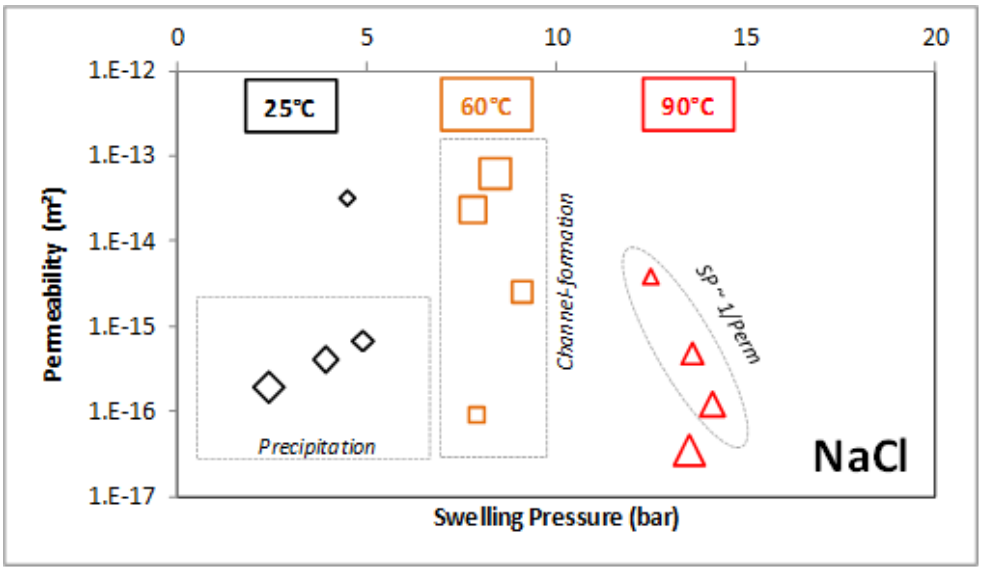

Different size of labels represents different concentration of additive $FeCl_2$-solution

Fig. 2.26 Development of swelling pressure and permeability of compacted MX-80 after 2 months percolation by 1N NaCl-solution at different temperatures (open system) /HER 11/

The first case represents the normally expected behavior that higher swelling pressure causes also reduced permeability. It is assumed that the higher temperature leads to a

certain degree of dis-solution and precipitation of smectite layers. The smaller particles increase the double layer zones: The swelling pressure is rising.

For the second case, it is assumed that precipitations reduce the available smectite by cementation. The swelling pressure is reduced by lower available expandable layers, but the permeability is improved because of the cementation. Fe-oxides should be such precipitations because of additionally involved $FeCl_2$-solution (identified also by XRD).

The temperature induced higher pressure could arrange a breaking of some cemented zones. This breaking would increase the permeability at a constant swelling pressure. This assumption would be the explanation for the third case.

Simplifying, dissolution/precipitation processes overlay the before mentioned aspects of double layer theory. With beginning cementation, the known behavior “swelling pressure ~ 1/permeability” is no longer valid.

The critical point between dissolution/precipitation without cementation to dissolution/precipitation with cementation is different between different ion strengths, but also different between different bentonites.

2.5.2 Mineralogical Alteration of Smectite

/HER 04/ and /HER 08/ proposed also some alteration processes of smectite as additionally factor on swelling pressure (Fig. 2.22). They observed in their experiments a trend to lower total charge of smectite as reaction product in close systems and to a higher total charge in open systems.

A typical example for this discussion is their batch experimental series with MX-80 bentonite and Äspö-solution at 25 °C (Fig. 2.27). This series is not overlapped by additional dissolution/precipitation processes like discussed before for higher temperatures. The octahedral Al-amount is drawing a remarkable increasing and the octahedral Fe-concentration is undergoing also a slight rising. A remarkable loss of octahedral Mg is balancing this development. The interlayer charge is decreasing with the time, because of the lower charge deficit in octahedral sheet. A slight smectitization is also to observe. Furthermore, the Na is substituted mainly by Ca after 1 year of reaction. This rearrangement of interlayer cation distribution is a typical process observed by /HER 04/,

/HER 08/, /HER 11/ for reaction products in close systems. The decreasing ratio of normal charged smectite in comparison to low charge smectite is the reason for that (Fig. 2.28). It seems that stepwise particles with higher amount of octahedral Mg (Mg has a larger cation diameter than Al^{3+} or Fe^{3+} and could cause that is why also a higher sheet stress) are easier removed than (Al^{3+}+Fe^{3+})-rich one.

Such differences in the mineralogy of smectite in the reaction products were to identify only by TEM-measurements. XRD is mostly not sensitive enough to mirror these small differences. That is why it is possible to find numerous publications, which could not identify any alteration in smectite under moderate pH. /KAU 09/ noted that literature data do not provide a homogenous picture, yet. They presented a study, where 36 bentonites from different deposit were reacted in a closed system with a 6 M NaCl solution at 60 °C for 5 months, respectively. Run products were washed and dialyzed and finally analyzed with respect to chemical and mineralogical changes by XRF, XRD, CEC, water uptake capacity, and amount of soluble silica. All significant chemical changes could be explained by the expected cation exchange (Na^+ for Ca^{2+}/Mg^{2+}).

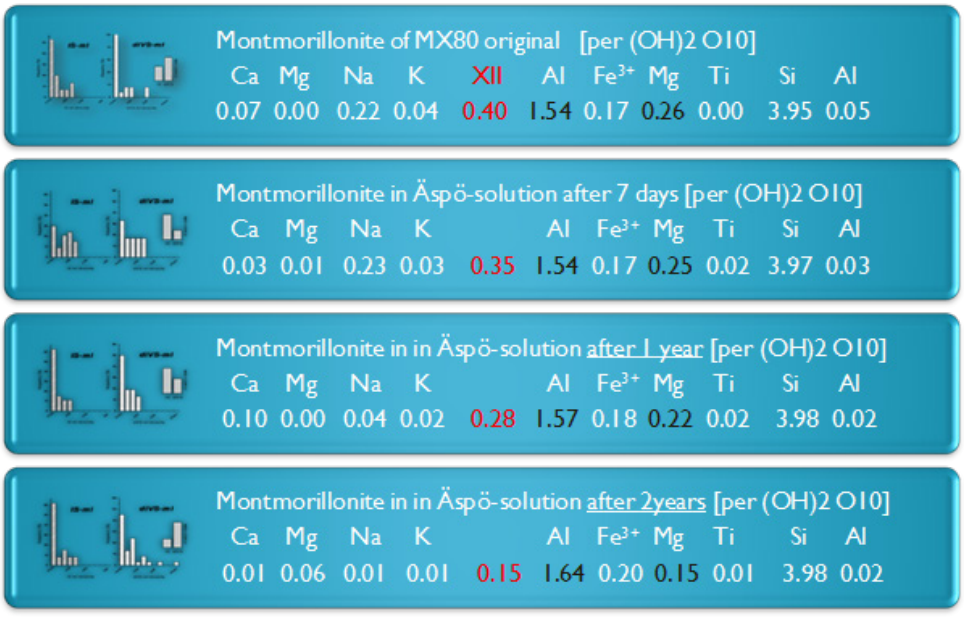

Structural formulae as result of TEM-EDX-measurements (dataset from /HER 08/)

Fig. 2.27 Alteration of MX-80 bentonite in batch experiments in contact with Äspö-solution for 7 days, 1 year, and 2 years at 25 °C in comparison to the original MX-80

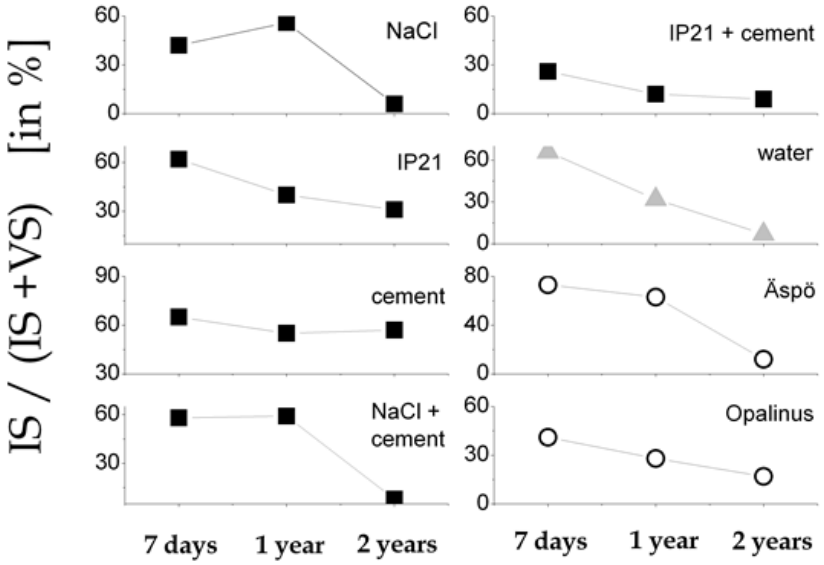

Fig. 2.28 The MX-80 and its reaction products contain two classes of montmorillonite: (i) normal charged and (ii) low charged. The ratio of normal charged montmorillonite in comparison to low charged is decreasing with the time in close reaction systems /HER 08/

After the experiment, however, the exchange sites were not completely occupied by Na^+ despite a 100 fold excess of Na+ compared to the CEC. The presence of carbonates, obviously, interferes with the exchange of Na^+ for Ca^{2+}/Mg^{2+}. The presence of gypsum proved to be even more effective and caused the opposite trend (Ca^{2+} was exchanged for Na^+). The cation exchange buffer capacity of carbonates is believed to be particularly effective during dialysis, where the Na+ excess is significantly reduced while carbonate/gypsum dissolution proceeds. The changes of the XRD patterns, particularly the position, shape, and intensity (area) of the basal reflections could not be attributed to mineral alteration but can be explained by cation exchange, differences of the hydration state, and/or different degrees of preferred orientation, the latter can be explained by particle arrangement. The results of the present study indicate that montmorillonites are stable in NaCl solutions of moderate pH up to 60 °C which is in agreement with other available studies. Literature data indicate that temperatures of > 100 °C can lead to irreversible montmorillonite alteration. The same, of course, holds true for extreme pH values, drying, or the presence of K^+.

The selected examples from literature have shown clearly: Highly saline solution is reducing the swelling pressure and its related technical parameter. This behavior is well

accepted by different experiments, from the general theoretical background (double layer theory) and by modeling. Additional impacts on swelling pressure or other technical parameters by mineralogical changes of smectite are still under strong discussion.

2.6 Summary - Long-term stability and functionality in the near field of repositories

2.6.1 Target: Safe disposal for HLW

Different authors conclude by their literature studies that the published experiments give only an equivocal indication to alteration processes of bentonite, especially for experiments under moderate pH-ranges (e. g. /KAU 09/, /WIL 11/. This situation is caused by generally low grade alteration of smectite under moderate pH-ranges and complex processes, which interact in different scale in the system “solution – bentonite – canister”.

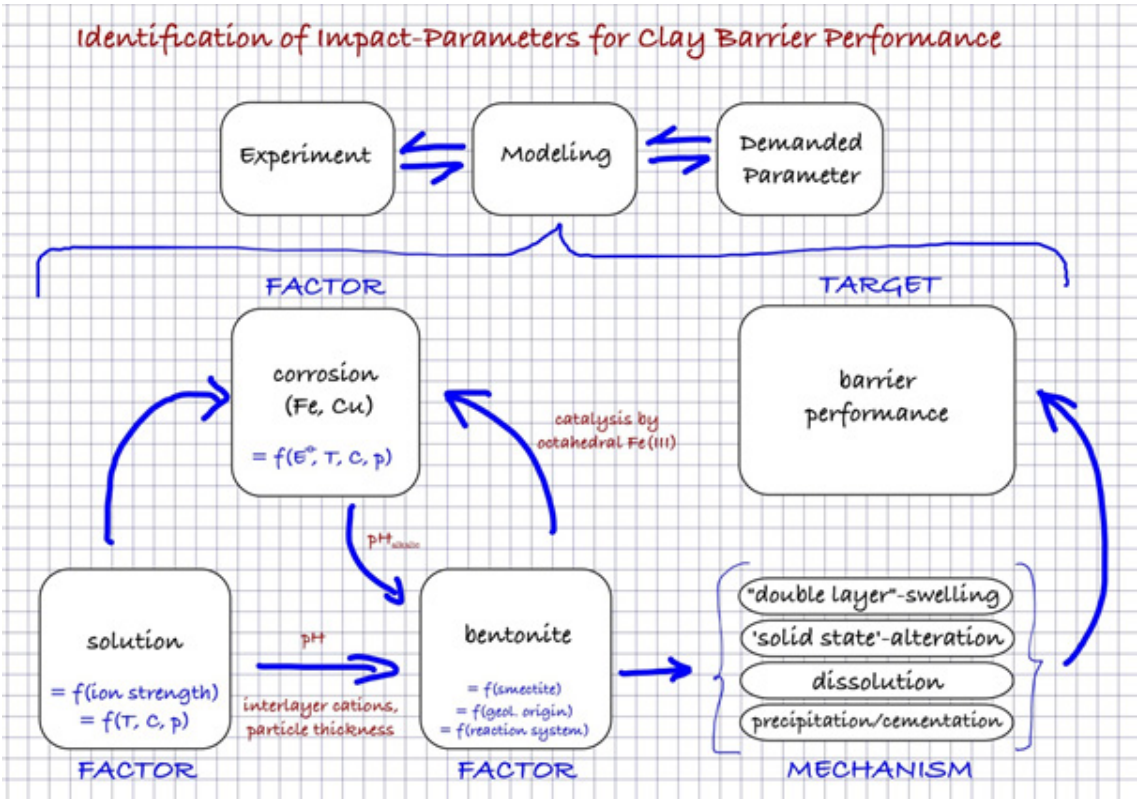

Fig. 2.29 Identification of impact-parameters for clay barrier performance – draft version

Additionally, it is missing actually also a transfer of detected small smectite alterations and identified mechanisms (e. g. /HER 04/, /HER 08/, /HER 11/) into a comprehensive thermodynamic and kinetic modeling to identify the practical meaning of these results for the long-term barrier performance.

Fig. 2.29 shall deliver first impression about the possible different interacting factors and mechanisms, which could affect the barrier performance. Alteration processes start, if bentonite comes in contact with aqueous solutions. Additionally, corrosion processes influence these alteration processes. Each of these three items has specific parameters affecting the interaction.

2.6.1.1 Factor corrosion (Fig. 2.29)

The alteration of smectite would be remarkable if high intensive corrosion processes change the pH into high alkaline ranges. The intensity of redox reaction depends for instant from standard electrode potential (EΘ) of corroding material, temperature (T), concentration (C) and pressure (p). The concentration is commonly expressed as iron/clay-ratio. Only high chemical activities of corroding material lead to basic pH-range and so to remarkable alteration of smectite mirrored by neoformation of 1:1 sheet silicates (e. g., /BIL 06/, /PER 08/, /MOS 10/, /HER 11/, /NGU 12/). The specific corrosion behavior of iron and copper is a typical example for before mentioned different acting mechanisms. Copper has a much lower redox potential than Fe^0. Additionally, copper is corroding only under moderate or acidic pH-environment. That is why the possible impact Cu is not only remarkable lower than iron. The moderate pH-range in case of Cu-interaction is also limiting sorbing of Cu-cations on edges from smectite, because of the positive charge of the edges under moderate or acidic pH-ranges. In this case, copper cannot act directly as deprotonator of octahedral Fe(III) in smectite like Fe(II). /LAN 05/ proposed this mechanism for Fe-corrosion as driving force for alteration of smectite. It is a good agreement with the results from /KAR 09/ and /KAR 09/ that they could not identify any Cu incorporated in the smectite structure in their long-term experiments with a MX-80 bentonite barrier surrounding a Cu-heater. Corroded copper occurred in the reaction material as individual phase /KAR 09/.

In opposite to high chemical activities of corroding metal, the liberated cations precipitate preferred as crust under low chemical activities and don’t enter smectite. So, this crust acts than as protecting shield against further corrosion.

2.6.1.2 Factor solution (Fig. 2.29)

The ionic strength of solution affects the arrangement of smectite particles in the barrier. The pro-cesses are well understood and following the principles of double layer theory. A collapsing of particles caused by high ion strength is general reducing the resulting swelling pressure in comparison to water regime (e. g., /DIX 96/, /KAR 98/, /CAS 07/, /HER 08/). Few authors described a general relation between charge of smectite and swelling pressure (e. g., /SAV 05/, /HER 08/). So, charge of smectite is to consider also as a further impact factor on swelling pressure. But also here, it is possible to find a different behavior for development of swelling pressure between solutions with very low or moderate/high ion strength /HER 08/. Decreasing total charge of smectite deals a decreasing swelling pressure under water-smectite system (very low ion strength). Saline solutions cause an increasing swelling pressure with decreasing charges of smectite (Fig. 2.22). Also this different behavior is to explain by the double layer theory.

Temperature, concentration and pressure are further parameter, which could enforce the impact of highly saline solutions on extreme acid or basic pH-ranges in the reaction system.

Additionally, saline solutions can accelerate the corrosion process. They act as additional electron acceptors.

2.6.1.3 Factor bentonite (Fig. 2.29)

'GEOLOGICAL ORIGIN': Especially experiments and analytical series included a series of different bentonites (e. g. /CIC 76/, /NOV 78/, /KAU 08a/, /KAR 09/, /KAU 10/, /KAU 11a/, /HER 11/, /NGU 12/) have shown: Each bentonite is reacting specifically, has a specific rate of alteration. /HER 11/ and /NGU 12/ identified a specific dissolution potential for each bentonite. This parameter bases on chemical composition of smectite measured by TEM-analytics and FT-IR-positions of selected octahedral cations signals. The specific dissolution parameter describes a relative order how fast or slow the certain smectites are reacting. It seems that this parameter is controlled by the geological origin of each bentonite characterized by kind of parent rocks, water environment during smectite formation and temperature effects.

2.6.1.4 Smectite

Experiments with di- and trioctahedral smectites have drawn a strong stability of trioctahedral smectites (e. g. /LAN 05/, /PUS 07b/, /KAS 12/). Especially the full occupation of all three octahedral positions and the low octahedral Fe3+-amount of until now involved trioctahedral smectite seem to be the reason for this stability under non-oxidative conditions. The total charge (e. g., expressed as CEC) affects also the swelling pressure. Lower charges could increase commonly the swelling pressure.

2.6.1.5 Reaction system

Furthermore, the bentonites react different under different reaction systems. The intensity of flow rate determines an open/dynamic or closed reaction systems. Dissolved elements from clay (e. g., Si) could migrate in an open system (flow rate >> 0). Smectite can undergo here also an 'illitization'. The total charge is rising by increasing tetrahedral and also octahedral charge deficit. Partially, trivalent Fe in the octahedral sheets could be substituted by bivalent cations. In opposite to the open system, dissolved elements of smectite precipitate again in the same stack or close in the neighborhood of dissolution in a closed system. This local dissolution/precipitation can lead to a further smectitization and it reduces the total charge of smectite caused also by progressing substitution of octahedral Mg by Al /HER 04/, /HER 08/, /HER 11/, /NGU 12/.

Different Mock Up-experiments indicate in case of fast reacting bentonites (e.g, Czech RMN-bentonite) that it is to consider rarely a pressure-controlled open reaction system close to the hot canister (< 10 cm in 2 years) and with decreasing temperature (about lower than 60 °C), also far from heater, the expected close system /PUS 10/.

The density of compacted bentonite is a further item of reaction system, which is controlling the activity of reaction. Dry densities higher than 1,800 g/cm³ reduce the different reaction in different saline solution (KAR98).

2.6.1.6 Mechanism alteration processes in smectite (Fig. 2.29)

The diverse parameters can affect in different level the 'double-layer'-swelling (e. g., controlled by ionic strength and charge of smectite). Possible 'solid-state'-alterations, dissolution of particles as well as precipitation controlled cementation can influence additionally the 'double-layer'-swelling.

2.6.1.7 Double-layer-swelling

Ionic strength and charge of smectite (important: expressed by total CEC) control mainly the development of swelling pressure (Fig. 2.30). The CEC-values show a lowering development under moderate pH-conditions and a rising behavior under basic pH-ranges. The different CEC-behavior has mainly two reasons: (i) higher impact by dissolution processes in basic pH-range (see further explanations in part 'dissolution') and (ii) additional impact of so called 'broken surfaces' in sense of /YAR 97/. The negative charged edges of clay particles (variable charge) under alkaline pH-conditions affect the increase of CEC by additional adsorbed cations (Fig. 2.31). That means the relation "charge ~ 1/swelling pressure" is full valid, only the behavior in water is different. The exception with deionized water was already above explained by double layer theory.

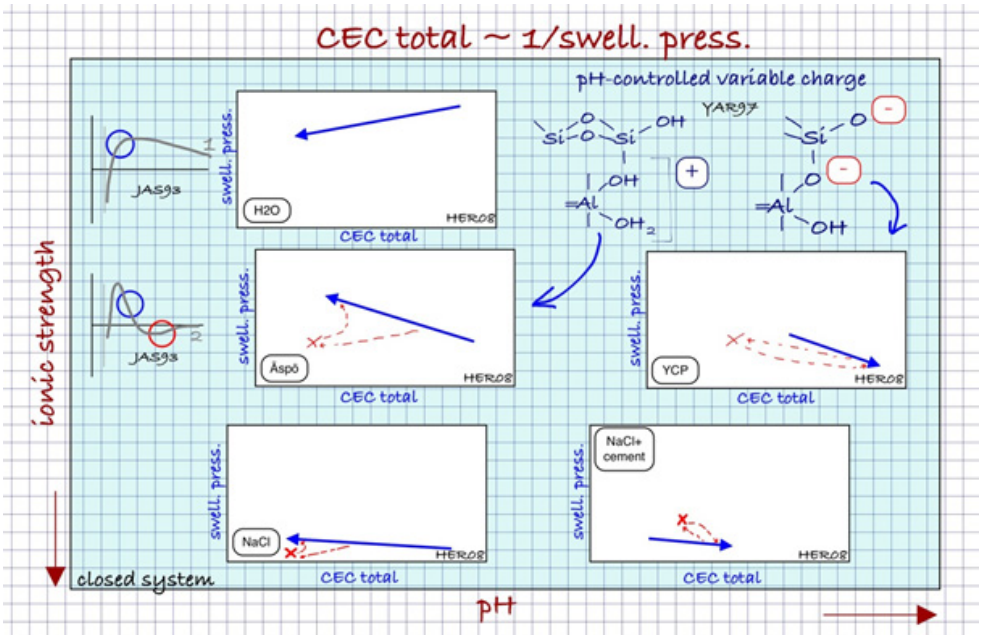

imaging of 'broken bond surfaces' in according to /YAR 97/; imaging of different development of repulsive/attractive forces by different ionic strength in according to /JAS 93/

Fig. 2.30 Generalized visualization of "Influence of total CEC on swelling pressure" based on data from /HER 08/ (see text for explanation)

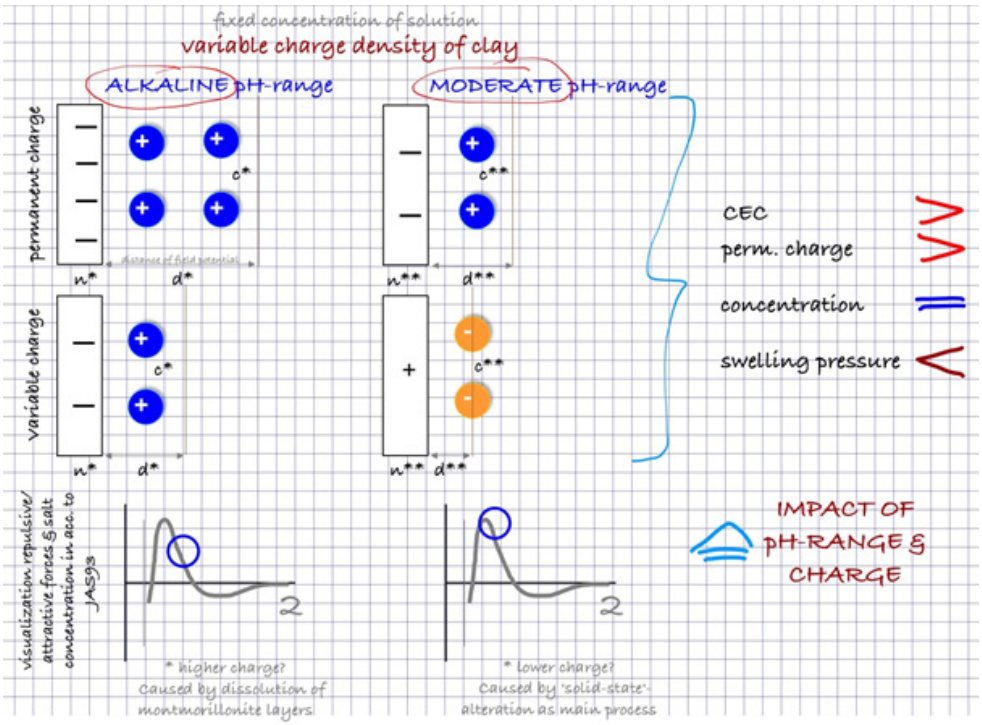

Shorter depth of field potential at moderate pH-range causes the higher swelling pressure in comparison to conditions in alkaline pH-range with higher CEC causing a larger depth of field potential.

Fig. 2.31 Visualization “Impact of pH-range & Charge on Swelling Pressure”

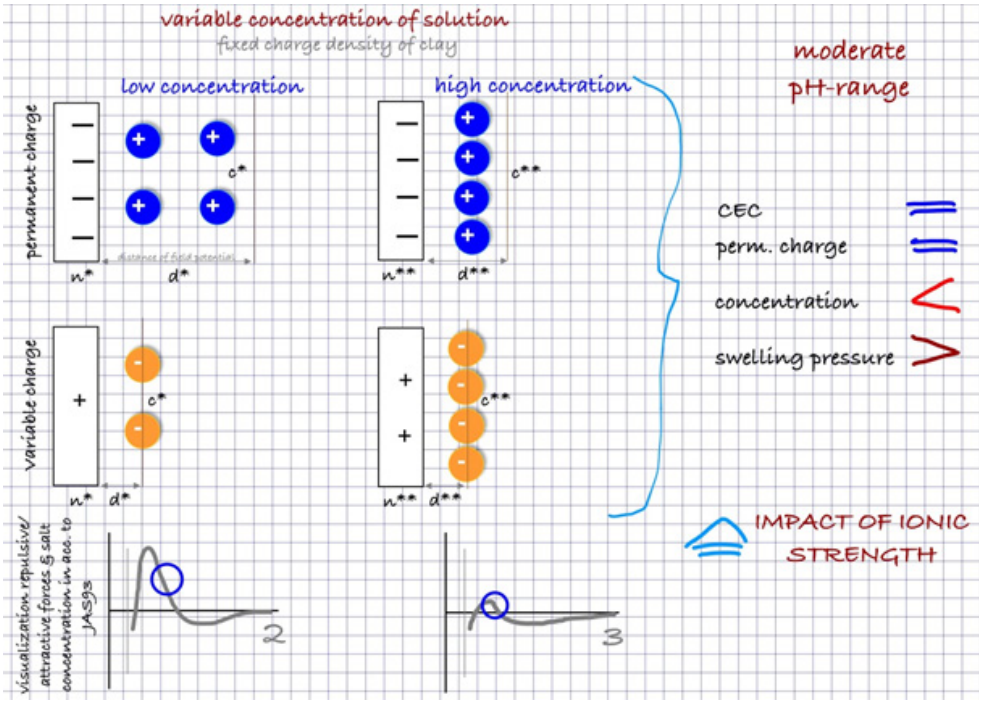

Fig. 2.32 Visualization “Impact of Ionic Strength on Swelling Pressure” at moderate pH-range approaching the graphical description in /JAS 93/

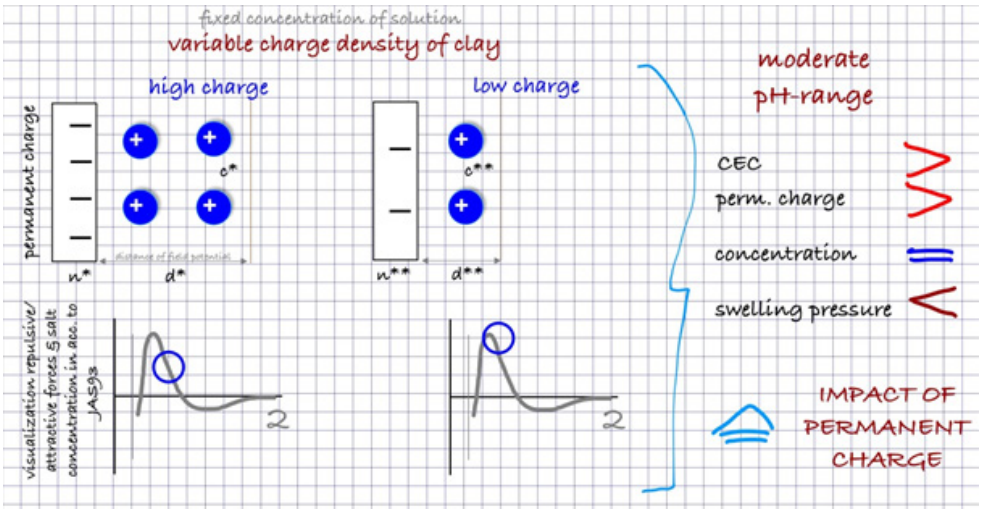

Fig. 2.33 Visualization "Impact of Permanent Charge on Swelling Pressure" at moderate pH-range approaching the graphical description in /JAS 93/

The general reduced swelling pressure by higher ionic strength is to explain by double layer theory (e. g., in sense of /JAS 93/ – see also Fig. 2.32). It is possible to demonstrate also the increasing swelling pressure with reduced smectite charges (Fig. 2.33) in the same manner like in case of variable concentration of solution.

2.6.1.8 Solid-state-alteration

The morphology, stack arrangement and chemical composition can be changed for all particles already in less than 10 days (e. g., for MX-80 bentonite in according to /HER 04/, /HER 08/. These authors proposed a 'solid-state'-alteration in sense of /ALT 97/. They assume dissolution/precipitation processes in the interlayer space of smectite that means an alteration without dissolution of the total stack. This should be also the main process for the already mentioned small changes in interlayer charge of smectite. It is important to distinguish between interlayer charge (calculated, e. g., from TEM-EDX-measurement) and total charge expressed by CEC. CEC contains also effects by edges, which have an additional impact to swelling pressure especially under alkaline pH-ranges (Fig. 2.31).

The parameter 'specific dissolution potential' described by /HER 11/ and /NGU 12/ seems to represent the intensity of 'solid-state'-alteration. These authors identified three different parameter settings for the activity of specific dissolution potential. It depends from energy input (e. g., temperature, Fe-activity etc.) and ionic strength of solution, where higher reaction activities increase also the specific dissolution potential.

2.6.1.9 Dissolution

Some authors described sudden changes in development of smectite charge in their experiments (e. g., under moderate pH-ranges: /HER 04/, /HER 08/; under alkaline pH-ranges: /HER 08/, /HER 11/, /NGU 12/). These changes interrupted the observed trends to lower charges of smectite during increasing experimental time in closed reaction systems. Dissolution processes were identified for the experiments under high basic pH-conditions. The mentioned changes were identified under moderate pH-ranges only in experiments after long terms (few years), high temperatures (> 60 °C) or high ionic strength. Also here, it is to assume the impact of starting dissolution processes.

The dissolution of smectite meets first the thinnest particles. Na-bearing low charge montmorillonite forms generally the thinnest smectite particles. A more intensive loss of such low charge smectites increases in sum the interlayer charge at the beginning of dissolution processes (Fig. 2.34 – see red line). Also the higher interlayer charge of alkaline experiments at same reaction time in comparison to experiments under moderate pH-range (Fig. 2.34) is to explain by earlier beginning of dissolution processes. This is caused by the higher solubility also of Si under high basic pH-conditions (Fig. 2.17). In further progress of chemical reaction, only particles with low sheet stress can resist a longer time the dissolution processes. That means the described trend to lower charges is now continued after dissolution of thinnest particles in starting material (Fig. 2.34).

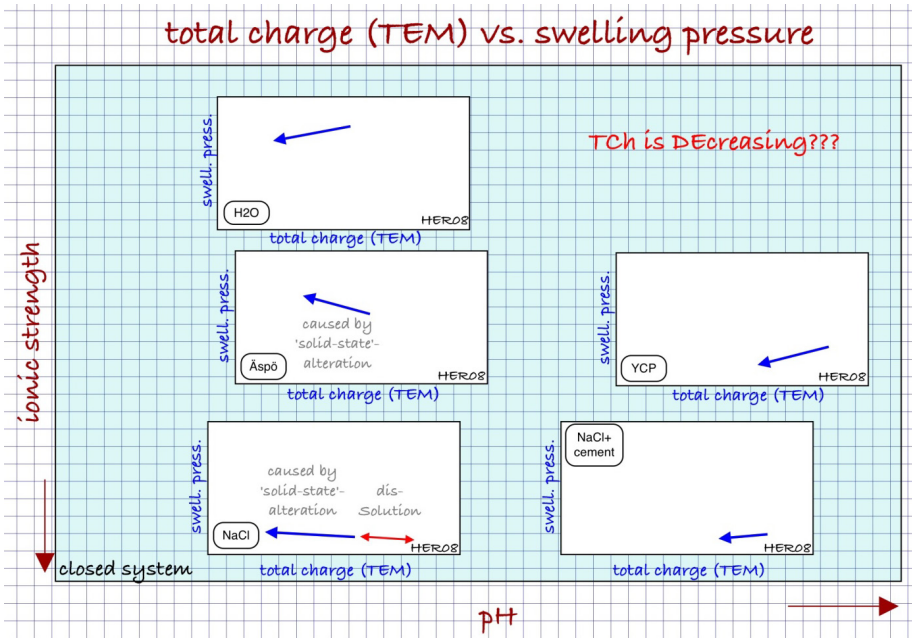

'solid-state'-alteration in closed reaction system is continuous reducing the interlayer charge of smectite – blue lines; exceptions occur (red lines) caused by additional impact by 'dissolution' at higher reaction activities - see text for explanation of impact by 'dissolution'

Fig. 2.34 Generalized visualization of "Influence of total charge (TEM) on swelling pressure" based on data from /HER 08/

/LAN 05/ described methodology by XRD and FT-IR to measure the amount of destabilized smectite identifying the degree of dissolution. Furthermore, a comparison between the parameter ‘de-stabilized smectite’ and the specific dissolution potential defined by /HER 11/ and /NGU 12/ indicates that the specific dissolution potential, the potential of Si-precipitation (see above) and the chemical activity of acting agents control the degree of destabilized smectite (Fig. 2.19).

2.6.1.10 Precipitation/cementation

/PUS 99/ has already introduced the relevance of changing micro-structures in smectite for barrier performance. Cementation effects caused by Si-precipitation are here the main reason. /HER 11/ and /NGU 12/ have shown that illite-smectite mixed layer phases have a natural buffer to sorb dissolved Si as neoformed montmorillonite layers in already existing stacks. A further surplus of dissolved Si will lead to Si-precipitation of neighbored particles in case of 100 % montmorillonite layers in the smectite. They found indications that so the Si-buffer of MX-80 could transform dissolved Si into additional montmorillonite layers so the relation “swelling pressure ~ 1/permeability” was also valid. Cemented areas interrupted this relation (Fig. 2.23 and Fig. 2.26).

2.6.1.11 Target ‘barrier performance’ (Fig. 2.29)

The scale of the three mentioned alteration mechanisms of smectite in bentonite barrier depends on the activity of the three factors ‘corrosion’, ‘solution’ and ‘bentonite’. The mechanism ‘double layer’-swelling is in any time active. Low reaction activities promote more ‘solid-state’-alterations with low degrees of smectite alteration and small changes only in swelling pressure, permeability and density. Higher activities of these three factors cause a higher impact of mechanism ‘dissolution’. /LAN 05/ measured in their experiments with MX-80 bentonite at 85 °C with 1:1 as very high Fe^0/clay-ratio that about 50 % of MX-80 smectite was destabilized. In an open system, such development is comparable with a loss of expandable phases and causes reduced swelling pressure and cations exchange capacity as well as increased permeability, but only so long if no cementation by precipitation occurs. Cementation reduces also the swelling pressure, but it can reduce simultaneously also the permeability linked with reduced strain. In a closed system, a higher degree of dissolution can promote first the neoformation of montmorillonite (Si-buffer function of IS-ml phases) including an increasing of swelling pressure and reducing of hydraulic conductivity. The known relation “swelling pressure

~ 1/permeability" will be broken again /HER 11/ with the occurrence of cementation (because of the limited Si-buffer potential).

2.6.1.12 What is the practical meaning of the different degree of alteration for the long-term performance of barrier? (Fig. 2.29)

It is an open question, what the indicated alteration mechanisms mean for the long-term performance of HLW-barrier. It needs further research to design experiments, which give sufficient data to understand the different interacting factors and mechanisms in a numerical manner. Furthermore, such experiments are to model than including variable thermodynamic and kinetic parameters to identify the practical meaning of indicated alterations.

2.6.2 Target: safe disposal for chemotoxic waste

Approaching the mentioned mechanisms (Fig. 2.30), mechanism 'Dissolution' seems to play a promoting role for uptake of heavy metals in smectite /KAS 12/ additionally to the known diffusion processes.

Authors like /WIL 09/ conducted a detailed study about possible release of priority chemotoxic sub-stances from a generic Geological Disposal Facility (GDF) and to quantitatively assess human ex-posures and allied health risks posed by such releases. Their report focuses on the possible releases of chemotoxic substances from Intermediate and Low Level Waste (LLW and ILW). Furthermore, they noted that a GDF could be developed in which there is co-disposal of these wastes with High Level Waste (HLW) and Spent Fuel (SF). As HLW and SF would exhibit very high integrity and resistance to leaching and would be likely to be disposed of in highly corrosion-resistant containers, it is unlikely that the HLW and SF would make a significant contribution to chemotoxic releases from the co-disposed wastes.

2.7 Further R&D topics

/WIL 11/ focused key points like:

- The evolution of bentonite under the conditions expected in a **G**eological **D**isposal **F**acility (GDF) is complex, and the processes affecting it are coupled, perhaps strongly.
- Most aspects of bentonite performance are likely to be specific to both the site (both groundwater flow rate and composition) and the particular bentonite that will be used.

The parameter systematics presented in former chapters that typical factors (corrosion, solution, bentonite) and alteration mechanisms ('double-layer'-swelling, dissolution, 'solid-state'-alteration, precipitation/cementation) influence the development of barrier performance (Fig. 2.30) would now additional tools for further research comparable to the focus of /WIL 11/. Furthermore, the literature study has shown that moderate pH-ranges confirm commonly with expected typical environment in final repository, but smectite shows the lowest degree of alteration even under in moderate pH-ranges.

Future research should approach the described 'factor and mechanism'-concept and should include experiments and modeling as unit. Following tasks are recommended for further research & development under moderate pH-ranges in order to obtain a basis for optimal selection of one specific candidate material:

- Assessment of clay materials with respect to coupled THMCB-processes (**T**hermal/**H**ydraulic/**M**echanical/**C**hemical/**B**iological behaviour)
  - use of a larger series of different bentonites (incl. Mg-saponite)
  - experiments in solutions with different ionic strength ('double-layer'-swelling)
  - + experiments with a low Fe/clay-ratio (remarkable lower than 1:1)
  - + experiments with temperatures at 90 – 100 °C (incl. to detect 'dissolution/precipitation'-effects and to understand the change of reaction system 'close to open system' – see Fig. 2.35)
  - experiments at room temperatures (to describe numerically the effects in a closed system)
- Assessment and standardization of analytical procedures to guarantee the identification and correct characterization of described factors and mechanism

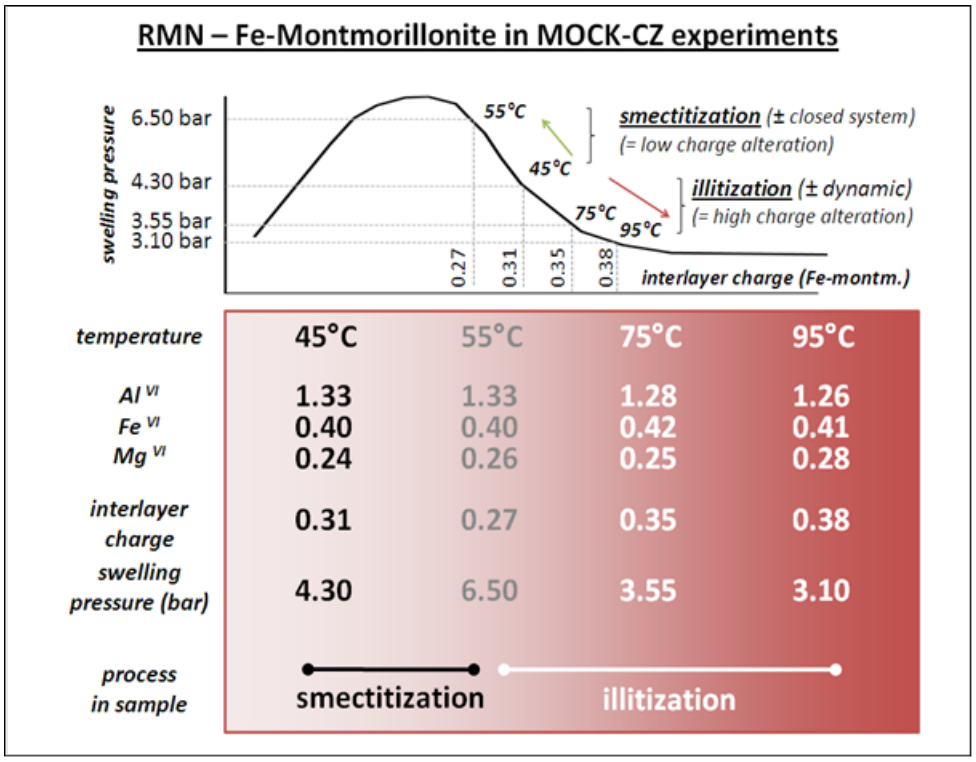

Data from Mock-CZ experiments with Czech Fe-rich RMN-bentonite indicate a different direction of charge and swelling pressure development close and far from heater

Fig. 2.35 The reaction product: smectite

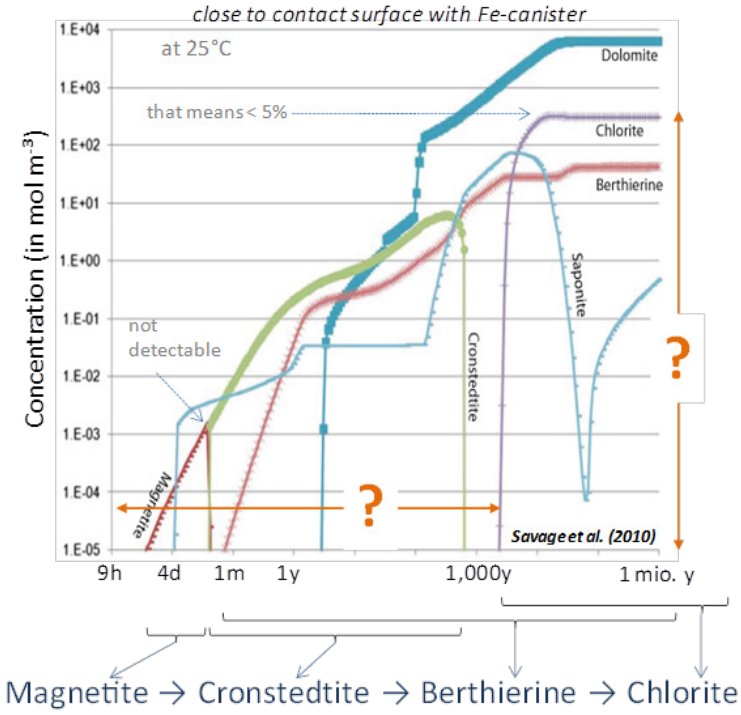

Fig. 2.36 Thermodynamic and kinetic modeling of smectite alteration in contact with Fe^0 at low temperature (/SAV10/)

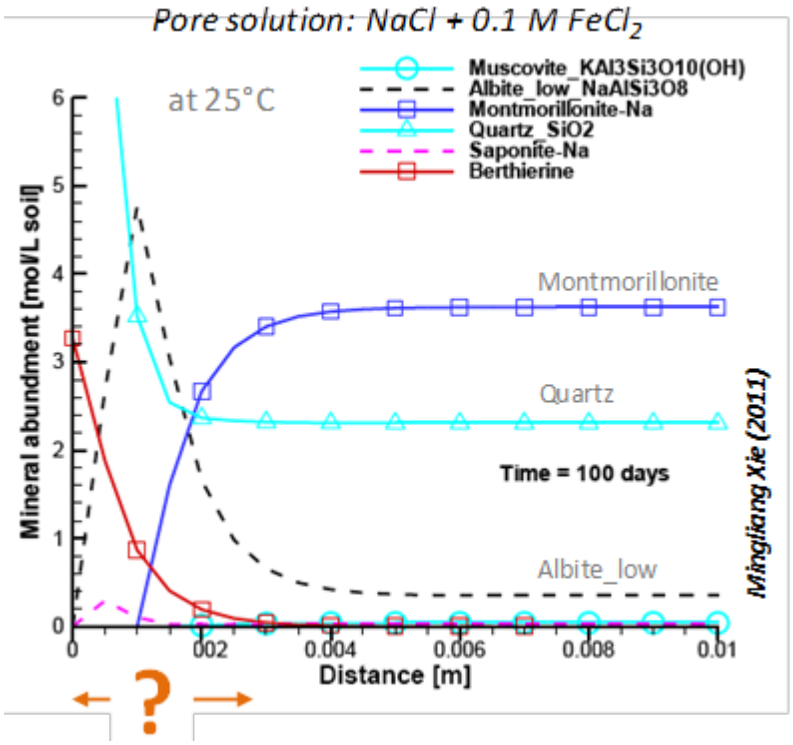

Fig. 2.37 Thermodynamic and kinetic modeling of smectite alteration in contact with 0.1 M $FeCl_2$-solution at low temperature (/HER11/)

Future research should offer answers, which variable impact could have factors like corrosion, solution and bentonite on time and concentration of smectite transformation into neoformed sheet silicates (see "?" on x-axis and y-axis for example chlorite in Fig. 2.36) and on time and intensity of smectite alteration (see "?" on x-axis in Fig. 2.37).

2.7.1 What is the practical meaning of the different degree of alteration for the long-term performance of barrier? (Fig. 2.29)

It is an open question, what the indicated alteration mechanisms mean for the long-term performance of HLW-barrier. It needs further research to design experiments, which give sufficient data to understand the coupling of different interacting factors and mechanisms in a numerical manner. Furthermore, such experiments are to model than including variable thermodynamic and kinetic parameters to identify the practical meaning of indicated alterations.

If it is possible in future to characterize sufficient correctly the described factors and mechanisms than it should be also possible to model the practical meaning of the detected differences of some bentonite properties for the long-term behavior of a geological disposal facility.

It should be possible a clarification: the detected small short-term performance differences have a remarkable impact on time (kinetic aspect) or phase development (thermodynamics) like visualized in Fig. 2.36 and Fig. 2.37.

3 Theoretical background of diffusion

3.1 Fick's laws

Diffusion or molecular diffusion is a mass transport process by spreading of particles through random motion from regions of higher concentration to regions of lower concentration. This kind of mass transport process can be mathematically decribed using Fick's laws of diffusion /FIC 1855/. Fick's first law relates the diffusive flux (J) to the concentration (C) under the assumption of steady state:

$$J = -D\nabla C \tag{3.1}$$

For one dimensional problem it can be simplified as:

$$J = -D\frac{\partial C}{\partial x} \tag{3.2}$$

in which J is the diffusive flux in [mol m^{-3} s^{-1}], D is the diffusion coefficient in [m^2 s^{-1}], C is the concentration in [mol m^{-3}] and x is the position or distance of the observation point in [m].

Fick's second law predicts how diffusion causes the concentration to change with time:

$$\frac{\partial C}{\partial t} = D\nabla^2 C \tag{3.3}$$

For one dimesional problem it can be simplified as:

$$\frac{\partial C}{\partial t} = D\frac{\partial^2 C}{\partial x^2} \tag{3.4}$$

in which *t* is the time in [s].

These equations are suitable for the description of particles moving in the free liquids driving by concentration gradient. In the hydrogeological science, the transport processes in the soil is much more complex owing to the hydraulic and concentration gradients, interaction of solutes with the solids through chemical reaction, sorption and surface complexation when passing through the pore systems.

3.2 Flux equation in porous media

In the natural porous media (e. g. soil, barrier layers of landfill sealing system), understanding the migration process (transport and retardation) of chemical species (solute or contaminants) is of crucial importance for the design of related facilities. The one dimensional equation for mass flux of a chemical species in a saturated porous medium under combined effect of hydraulic and concentration gradients can be described as the following /SHA 91/:

$$J = n\left(v_s C - D_h \frac{\partial C}{\partial x}\right) \tag{3.5}$$

in which J denotes the mass flux in [mol m^{-3} s^{-1}], n is the total porosity of the porous media (dimensionless), v_s is the seepage velocity of the solution in [m s^{-1}], D_h is the hydrodynamic dispersion coefficient in [m^2 s^{-1}]. The hydrodynamic dispersion coefficient is defined to account for mechanical dispersion and diffusive dispersion of a solute being transported:

$$D_h = D_m + D_0\tau \tag{3.6}$$

in which D_m is the mechanical dispersion coefficient in [m^2 s^{-1}]; D_0 is the molecular diffusion coefficient of the solute in a free solution in [m^2 s^{-1}]; τ is the tortuosity factor of the porous media, which is a dimensionless and purely geometric parameter. It accounts for the prolonged transport distance (tortuous pathway) (L_e) in the soil pore system in comparison to the straight –line, macroscopic distance between two points determining the flow path (L). It is commonly described as /BEA 72/:

$$\tau = \left(\frac{L}{L_e}\right)^2 \tag{3.7}$$

Owing to the fact that $L < L_e$ for porous media, τ is less than 1.

The mechanical dispersion effect can be neglected for low-permeable clayey materials under the working conditions of waste containment facilities, i. e. $D_m \approx 0$ /ROW 87/. In such case, the total flux can be calculated as:

$$J = n(v_s C - D_0\tau \frac{\partial C}{\partial x}) \tag{3.8}$$

If the flow velocity ν_s is too small, this equation can be simplified as a purely diffusion dominant flux (J_D) as:

$$J_D = -D_0 \tau\, n\, \frac{\partial C}{\partial x} \tag{3.9}$$

It is here of interest to evaluate the conditions for diffusion dominant transport processes. According to Gillham et al. /GIL 84/, ν_s should be less than 0.005 m year^{-1} ($1.59 \cdot 10^{-10}$ m s^{-1}). Therefore, the solute transport processes in highly compacted bentonite as barrier material can be treated as diffusion dominant problem.

3.3 Transient equations

The general balance equation for multicomponent mass transport in porous media is given by e. g. Kolditz /KOL 02/, /XIE 06/:

$$nS^{\gamma} \frac{\partial C_i^{\gamma}}{\partial t} = -v^{\gamma} \nabla C_i^{\gamma} + \nabla\left(nS^{\gamma} D_i^{\gamma} \nabla C_i^{\gamma}\right) + nS^{\gamma} Q_i^{\gamma} + nS^{\gamma} \Gamma_i^{\gamma}(C_1^{\gamma}, \ldots C_m^{\gamma}) \tag{3.10}$$

where C_i^{γ} is the concentration of the ith species of an m multi-species system in phase γ, S^{γ} is the saturation of phase γ, v^{γ} is the Darcy velocity of phase γ, D_i^{γ} is the diffusion-dispersion coefficient of component i in phase γ, Q_i^{γ} is the source/sink term and $\Gamma_i^{\gamma}(C_1^{\gamma} \ldots C_m^{\gamma})$ is the source/sink term of species i in phase γ due to temperature dependent equilibrium chemical reactions with all other species in the same phase. For fully saturated porous media, $S^{\gamma} = 1$.

However, this equation can be simplified if the chemical reactions of chemical species and the solid phases in the saturated porous media can be neglected.

For many practical applications involving contaminant transport through relatively thin, low-permeable clay material, the retardation effect (e. g. sorption) cannot be neglected. Therefore, the following equation for single solute transport is also commonly used to address such effect /FRE 79/:

$$\frac{\partial C}{\partial t} = \frac{D_h}{R_d} \frac{\partial^2 C}{\partial x^2} - \frac{v_s}{R_d} C \tag{3.11}$$

In which R_d is the dimensionless retardation factor. The retardation factor represents the relative rate of mass transport of a non-adsorbing (non-reactive) solute (i. e. Cl^-) to that of a adsorbing (reactive) solute subject to reversible sorption or equilibrium exchange reaction /FRE 79/. For non-adsorbing solutes is $R_d = 1$. The retardation coefficient R_d for the Henry isotherm is related to the Henry sorption coefficient k_d in the following way.

$$R_d = 1 + \frac{\rho_b}{n} K_d \tag{3.12}$$

where ρ_b is the bulk density of the porous media in [kg m^{-3}].

When the flow velocity ν_s is sufficiently low such that the advection and mechanical dispersion D_m can be negligible, the advection-diffusion equation (3.12) effectively reduces to a diffusion equation:

$$\frac{\partial C}{\partial t} = \frac{D_0 \tau n}{R_d} \frac{\partial^2 C}{\partial x^2} \tag{3.13}$$

This expression is the Fick's second law for solute diffusion in porous media.

In the literature there are several different expressions for Fick's second law of solute diffusion in porous media (Tab. 3.1) due to difference of (1) the definitions of effective diffusion coefficient D*, which is discussed in the following section; (2) the reference frame for the expression of the solute concentration; (3) the behaviour of the adsorbing solutes during transport relative to that of the non-adsorbing solutes. Therefore, special care should be taken when extracting diffusion parameters from literature since failure to account for them may affect conclusions drawn from the experimental or modelling results /SHA 91/.

The general mathematic form can be simplified as

$$\frac{\partial C}{\partial t} = D_a \frac{\partial^2 C}{\partial x^2} \tag{3.14}$$

The solution of this equation depends on the initial and boundary conditions /CRA 75/, /GRA 98/. In the case of diffusion across layers of low conductivity (e. g. mineral liner at waste disposal sites) in a thickness of d, it is usually assumed that the liner is initially

free of contaminants, and the concentration of the contaminant at the waste side is C_0 (constant) and the other side almost zero, the following initial and boundary conditions can be applied:

$$\begin{array}{llll} t = 0 & x > 0 & C = 0 \\ t > 0 & x = 0 & C = C_0 \\ t > 0 & x = d & C = 0 \end{array} \tag{3.15}$$

The concentration profile at time t in the layer can be described as /GRA 98/:

$$\frac{C}{C_0} = 1 - \frac{x}{d} - \frac{2}{\pi}\sum_{i=1}^{\infty}\frac{1}{i} sin\left[\frac{i\pi x}{d}\right] exp\left[\frac{-i^2\pi^2 D_a t}{d^2}\right] \tag{3.16}$$

The analytical solution for the contaminant mass (M) which has diffused through the liner per unit area (e. g. flowed out at x = d) is given by:

$$M = C_0(n + K_d\rho)d\left(\frac{D_a t}{d^2} - \frac{1}{6} - \frac{2}{\pi^2}\sum_{i=1}^{\infty}\frac{(-1)^i}{i^2} exp\left[\frac{-i^2\pi^2 D_a t}{d^2}\right]\right) \tag{3.17}$$

After long time periods, when the steady state diffusion condition arrives, equation (3.17) can be simplified by omitting the series expansion:

$$M = C_0(n + K_d\rho)d\left(\frac{D_a t}{d^2} - \frac{1}{6}\right) \tag{3.18}$$

Define effective diffusion coefficient $D_e = (n + k_d\rho) D_a$, equation (3.18) can be rewritten as:

$$M = C_0\left(\frac{D_e t}{d} - \frac{(n + K_d\rho)d}{6}\right) \tag{3.19}$$

The steady-state flux q_{stat} can be obtained by the time derivative of equation (3.19):

$$q_{stat} = D_e\frac{C_0}{d} \tag{3.20}$$

The interception of equation (3.19) with the time axis (M = 0) is usually denoted as lag-time (t_{lag}):

$$t_{lag} = \frac{d^2(n + K_d\rho)}{6D_e} \tag{3.21}$$

which is the theoretical basis for the time-lag diffusion method (section 6.1.2).

Tab. 3.1 Expressions of Fick's second law for solute diffusion in saturated porous media /SHA 91/

Definition of D^* or D_a	Definition of concentration	Adsorption	Form of Fick's second law
$D_0\tau$	C	no	$\frac{\partial C}{\partial t} = D^* \frac{\partial^2 C}{\partial x^2}$
	C'	no	$\frac{\partial C'}{\partial t} = D^* \frac{\partial^2 C'}{\partial x^2}$
	C	yes	$\frac{\partial C}{\partial t} = \frac{D^*}{R_d} \frac{\partial^2 C}{\partial x^2}$
	C'	yes	$\frac{\partial C'}{\partial t} = \frac{D^*}{R_d} \frac{\partial^2 C'}{\partial x^2}$
$D_0\tau n$	C	no	$\frac{\partial C}{\partial t} = \frac{D_a}{n} \frac{\partial^2 C}{\partial x^2}$
	C'	no	$\frac{\partial C'}{\partial t} = \frac{D_a}{n} \frac{\partial^2 C'}{\partial x^2}$
	C	yes	$\frac{\partial C}{\partial t} = \frac{D_a}{nR_d} \frac{\partial^2 C}{\partial x^2}$
	C'	yes	$\frac{\partial C'}{\partial t} = \frac{D_a}{nR_d} \frac{\partial^2 C'}{\partial x^2}$

3.4 Types of diffusion coefficients

Diffusion in porous media obeys Fick's first and second laws and is characterised by a diffusion coefficient. There are many different types of diffusion coefficient /GOO 07/. The first major distinction is the phase or phases accounted: gas, liquid or solid. Diffusion coefficients of gas, solute or solid are thus defined. For the same porous media, the gas diffusion coefficient is normally much higher than the solute diffusion coeffi-

cient. The second distinction defines the type of medium involved: (a) self-diffusion (one molecule amongst similar ones), (b) tracer diffusion (a minor constituent within a major one), (c) salt diffusion (salt diffuses towards different reservoir with distinct concentration gradient), or (d) counterdiffusion or interdiffusion (diffusion between two or more different reservoirs) (Fig. 3.1). Additionally, surface diffusion (migration through the diffuse double layer of clay minerals) is also discussed to explain the greater diffusion rates of some cations through materials like bentonite and fractured media /KIM 93/, /OSC 94/. Apart from this, gas transport through low permeable porous media by Knudsen diffusion (or free-molecule diffusion) /WEB 06/. Therefore, there is significant room for confusion over the meaning of the term diffusion coefficient. Several related parameters are in common use reflecting the different types of diffusion and the precise meaning of the term being used is often not clear.

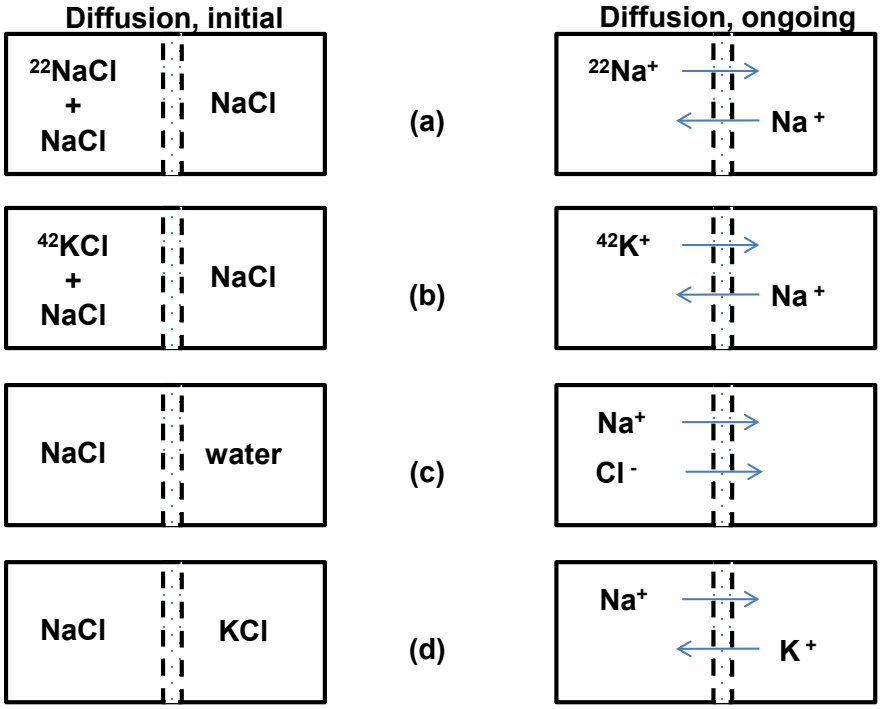

Fig. 3.1 Type of diffusions in porous media (after /SHA 88/ (a) self-diffusion, (b) tracer diffusion, (c) salt diffusion, (d) counter-diffusion

From the view point of practical application, two commonly used diffusion parameters (e. g. the effective diffusion coefficient D* and the apparent in-soil diffusion coefficient D*a*) are of interest. This is partly owing to the fact that currently there is no satisfactory method for determining independently the tortuosity factor. The term 'apparent in-soil diffusion coefficient' refers to a numerical coefficient that primarily describes movement

by diffusion but also contains secondary effects due to other mechanisms (e. g., adsorption, buoyancy, and solubility) and is a term that has been commonly used by others /BRU 86/, /FAR 80/. According to these definitions, the diffusion flux equation (3.9) can be rewritten as:

$$J_D = -D^* n \frac{\partial C}{\partial x} \tag{3.22}$$

$$J_D = -D_a \frac{\partial C}{\partial x} \tag{3.23}$$

3.5 Diffusion in unsaturated porous media

The diffusion flux of solute in unsaturated porous media can be mathematically described as:

$$J_D = -D_0 \theta \frac{\partial C}{\partial x} \tag{3.24}$$

In which θ is the volumetric water content defined as the following

$$\theta = nS_r \tag{3.25}$$

Where n is the total porosity of the porous media, Sr is the degree of liquid phase saturation of the porous media. As Sr ≤ 1, the maximal solute flux through-diffusion occurs in the case of fully saturation (Sr = 1).

3.6 Anion exclusion effect in compacted bentonite

Owing to the net negative charge of montmorillonite (the main minerals in bentonite up to 80 – 90 %), bentonite exhibit strong anion exclusion effects /BOL 82/, /PUS 90/. In the case of negatively charged surfaces, anions are expelled from the diffuse double layer (DDL) on the surface. Consequently, this leads to a negative adsorption (exclusion) of anions from this regions /BOL 82/. The higher the charge of the anion, the larger is the repulsion effect. Furthermore, the chemical composition of the pore water in contact with the surface also influences the anion exclusion effect. The ionic strength

of the pore solution, for instance, can strongly influence the anion exclusion effect. In the case of higher ionic strength (e. g. higher concentration) the thickness of DDL is thinner /XIE 06/, which leads to a higher interparticle porosity in general. On the other hand side, the higher ionic strength solution let the charges on the surface better shielded and thus resulting in a weaker repulsion of the anions by the negatively charged surface or lower anion exclusion effect /VAN 07/.

Moreover, the dry density of the compacted bentonite plays a crucial role for the solute diffusion. Because the density of the compacted bentonite represents the degree of the compaction and the diffusion accessible porosity /VAN 07/. Based on the special mineral structure of montmorillonite, the pore space in compacted bentonite is commonly divided into two groups – the interlayer porosity (i. e. the space between individual mineral layers – TOT-layers within the montmorillonite clay platelets), and the interparticle porosity (i. e. the rest space other than the interlayer porosity, normally the space between the montmorillonite clay platelets and/or impurities). For saturated bentonite, this space can be occupied by water/solution. Correspondingly, the water/solution is commonly named interlayer or interparticle water (Fig. 3.2). The interparticle water can be further divided into DDL-water and free water. For a given amount of bentonite, the total porosity changes with the degree of compaction. Generally the larger sized interparticle pore space is easier to be compacted than the interlayer space. It is reported that the interparticle pore space remains almost unchanged when the loose bentonite is being compacted up to a dry density of less than 1,300 kg m^{-3} /MUU 04/. The volume of interlayer water in a pure Na-montmorillonite is reported to be 10 % when compacted to a density of 350 kg m^{-3}, and above 90 % when further compacted to a density over 1,600 kg m^{-3} /PUS 90/. At high bulk density (over 1,300 kg m^{-3}), the interlayer space can also be compressed and leading to very narrow space within the interlayer. The diffuse double layers potentially to be formed from both sides of such narrow interlayer spaces overlap and the electric potential in the truncated layer turns to be large and tends to completely exclude anions from the interlayer /BOL 82/, /PUS 90/. The interlayer waters contain dominantly cations compensating the negative charge of the ton mineral surface. In contrast the interparticle pore space is much larger and leading to form DDL-layer more completely and even have more space for free water, thus showed less anion exclusion effect. In order to describe the anion exclusion effect in compacted bentonite, it is important to take all factors into consideration /TOU 11/.

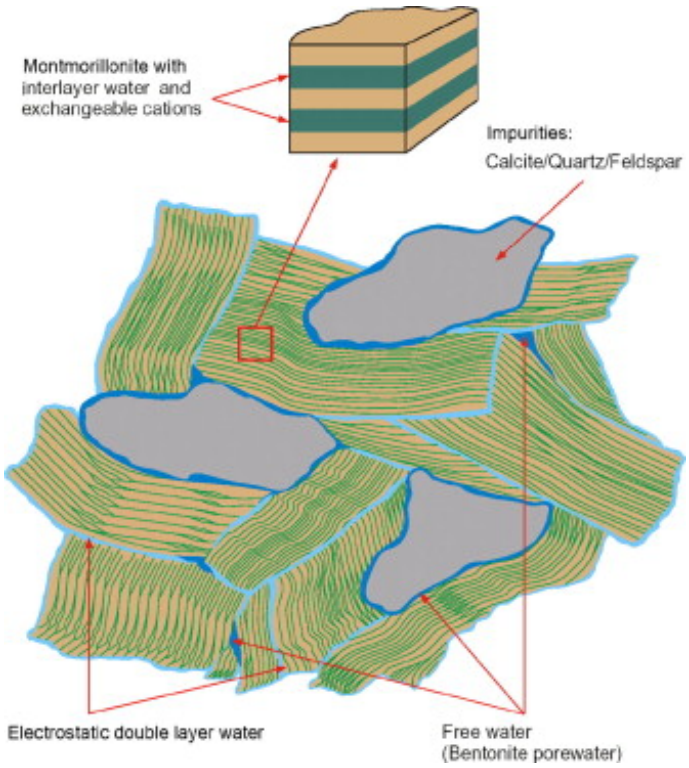

Fig. 3.2 Schematic description of the water types in compacted bentonite /TOU 11/

4 Gas and heavy metal in highly saline solution

4.1 Gas dissolution in saline solution

In order to investigate the diffusion of gases (hydrogen, methane, Carbon dioxide, sulfur hexafluoride) dissolved in different solutions (water, NaCl- and IP 21-solution) through MX-80, it was necessary to know the solubility of gases in the solutions. Since a study of literature showed no usable results, additional experiments were carried out to determine the concentration of the gases in the solutions. Fig. 4.1 shows the principle test set-up for the determination of gas dissolution in different solutions.

Fig. 4.1 Experimental set-up for the determination of gas dissolution

First, the whole system was purged with the gases to be investigated (hydrogen, methane, carbon dioxide, sulphur hexafluoride). Then the respective solutions (pure water, NaCl-solutions with different salinities, IP21-solution) were added and recirculated by a peristaltic pump. After dissolution, a defined fraction of the solution was filled in a sampling bag. The dissoluted gases were removed from the solution by heating and applied to the gas-phase chromatograph by a gas syringe pump. The results are summarized in Tab. 4.1 to Tab. 4.5.

The investigations on dissolubility in pure water and NaCl-solutions at different salinities have shown a decrease of the gas concentration in the solutions by increasing salinities. Over all, the concentrations of the dissolved gases were relatively low.

Tab. 4.1 Gas dissolution in pure water at 0.1009 MPa and 298.16 K

Gas	Solvent	Gas concentration [ppm]	Dissolubility [g/100 ml]	Ostwald-coefficient [v/v]
Hydrogen	pure water	2.5	0.000223	0.00025
Methane	pure water	3.20	0.0022811	0.0003232
Carbon dioxid	pure water	8100	15.1322	0.8585
Sulfur hexafluoride	pure water	151.5	0.96404	0.01578

Tab. 4.2 Gas dissolution in 15 % NaCl-solution at 0.1009 MPa and 298.16 K

Gas	Solvent	Gas concentration [ppm]	Dissolubility [g/100 ml]	Ostwald-coefficient [v/v]
Hydrogen	15% NaCl	2	0.000144	0.000249
Methane	15 % NaCl	2.90	0.0016609	0.0003646
Carbon dioxid	15 % NaCl	7450	14.2047	0.77365
Sulfur hexafluoride	15 % NaCl	140	0.70344	0.01847

Tab. 4.3 Gas dissolution in 50 % NaCl-solution at 0.1009 MPa and 298.16 K

Gas	Solvent	Gas concentration [ppm]	Dissolubility [g/100 ml]	Ostwald-coefficient [v/v]
Hydrogen	50 % NaCl	1.1	0.0000731	0.000148
Methane	50 % NaCl	1.36	0.000748	0.0001754
Carbon dioxid	50 % NaCl	3240	4.7152	0.44081
Sulfur hexafluoride	50 % NaCl	61	0.2944	0.0083

Tab. 4.4 Gas dissolution in 90 % NaCl-solution at 0.1009 MPa and 298.16 K

Gas	Solvent	Gas concentration [ppm]	Dissolubility [g/100 ml]	Ostwald-coefficient [v/v]
Hydrogen	90 % NaCl	0.8	0.00005453	0.000105
Methane	90 % NaCl	1.10	0.00054276	0.000161
Carbon dioxid	90 % NaCl	2840	3.9246	0.4069
Sulfur hexafluoride	90 % NaCl	53	0.2944	0.00788

Tab. 4.5 Gas dissolution in 90 % IP21-solution at 0.1009 MPa and 298.16K

Gas	Solvent	Gas concentration [ppm]	Dissolubility [g/100 ml]	Ostwald-coefficient [v/v]
Hydrogen	90 % IP 21	0.7	0.00003868	0.000114
Methane	90 % IP 21	0.90	0.0003728	0.0001564
Carbon dioxid	90 % IP 21	2280	2.5637	0.4015
Sulfur hexafluoride	90 % IP 21	45	0.1787	0.0075

The dissolubility is defined as the Ostwald`s solubility coefficient. The coefficient is the ratio of the millilitres of gas dissolved and the millilitres of liquid at atmosphere pressure of the gas and given temperature of 298.16 K ±1 K.

4.2 Heavy metal (Pb, Cd, Zn, Cs) properties in saline solution

Transition-metal ions in aqueous solution are often written with symbols such as Cr^{3+}, Cu^{2+}, and Fe^{3+} as though they were monatomic, but this is far from being the case. These ions are actually hydrated in solution and can be regarded as complex ions. Many chromium (III) salts when dissolved in H_2O is, for instance, due to the species $[Cr(H_2O)_6]^{3+}$ rather than to a bare Cr^{3+} ion /GEN 11/. However, not all salts of transition-metal ions yield the hydrated ion when dissolved in H_2O. Thus when $CuCl_2$ is dissolved in H_2O, a beautiful green color due mainly to the complex $[CuCl_2(H_2O)_2]$ is produced, which is obviously different from the sky-blue color of $[Cu(H_2O)_4]^{2+}$ obtained when Copper (II) sulfate or copper (II) nitrate are dissolved. This is because the Cl^- ion is a stronger Lewis base with respect to the Cu^{2+} ion than is H_2O. Thus, if there is a competition between H_2O and Cl^- to bond as a ligand to Cu^{2+}, the Cl^- ion will usually win out over the H_2O. Therefore, adding more Cl^- in the solution leads to gradual displacement of H_2O ligands by Cl^- ligands from $[Cu(H_2O)_4]^{2+}$ to $[Cu(H_2O)_3Cl]^+$, $[Cu(H_2O)_2Cl_2]$, $[Cu(H_2O)_2Cl_3]^-$ and finally $[CuCl_4]^{2-}$.

Some heavy metals like Pb, Cd, Hg, Cs and Zn are transition-metals and belong to the most toxic chemical substances in the natural system for the biosphere especially for the human beings. The toxicity of a heavy metal in solution to a microorganism depends not only on its concentration but also on pH and the concentrations of any aqueous complex ligands in the microorganism's environment /SAR 00/. Increasing the Cl^- concentration, for instance, increased also the complex concentration. In highly saline

solutions with high Cl^- concentration, transition-metals like Pb, Cd, Zn tend to form different such complexes. Detailed information for Pb complexes in highly saline solution can be found in /BYR 84/, /MIL 84/ and /HAG 99/. The stepwise formation of lead chloro complexes can be described:

$$Pb^{2+} + Cl^- \rightarrow [PbCl]^+ \quad (4.1)$$

$$[PbCl]^+ + Cl^- \rightarrow [PbCl_2]^0 \quad (4.2)$$

$$[PbCl_2]^0 + Cl^- \rightarrow [PbCl_3]^- \quad (4.3)$$

$$[PbCl_3]^- + Cl^- \rightarrow [PbCl_4]^{2-} \quad (4.4)$$

The formation and percentage of the lead chloro complexes in a highly saline solution with high Cl^- concentration depend mainly on the Cl^- concentration as well as other cation types /BYR 84/ and /HAG 99/. The experimental results of formation and fraction of each lead chloro complexes in Na Cl^- and $CaCl_2$-solutions are listed in Fig. 4.2. It is clear to see that almost half of the lead is form of lead chloro complexes at a Cl^- concentration of 0.1 mol/kg. Increase the Cl^- concentration to 1.0 mol/kg, almost all of the lead is in form of lead chloro complexes as $[PbCl]^+$, $[PbCl_2]^0$, $[PbCl_3]^-$ and $[PbCl_4]^{2-}$, in which more than half of them are anions. With the further increase of the Cl^- concentration, dominates the anion lead chloro complexes until almost no lead in cation forms. Similar lead sulfato complexes ($[PbSO_4]^0$ and $[Pb(SO_4)_2]^{2-}$) form when there is SO_4^{2-} in the solution. The complexing of lead in a solution with different anions is more complex. Generally the formation and amount of different complexes depend on the type and concentration of each anion. For example, in a chloride/sulfate mixing system including lead in NaCl solution and adding Na_2SO_4, both chloro and sulfato complexes exist in the solution when the background NaCl solution with a NaCl concentration of 0.4 mol/l (Fig. 4.3). However, if the NaCl concentration increased to 0.9 mol/l no sulfato complex can be detected (Fig. 4.4 /HAG 99/). Interesting is that at such higher NaCl concentration, the addition of Na_2SO_4 leads to the change of the fractions of lead chloro complexes and intensifies the monochloro complex formation (Fig. 4.4).

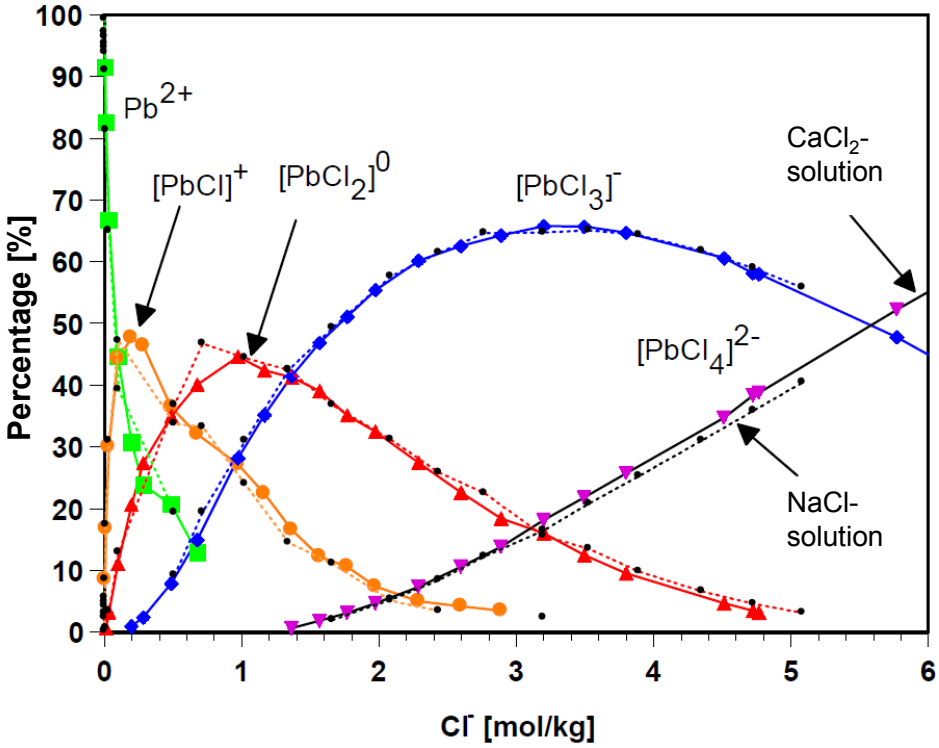

Fig. 4.2 Dependence of stepwise formation of lead chloro complexes on Cl^- concentration, solid lines – $CaCl_2$-solution, dotted lines – NaCl-solution /HAG 99/

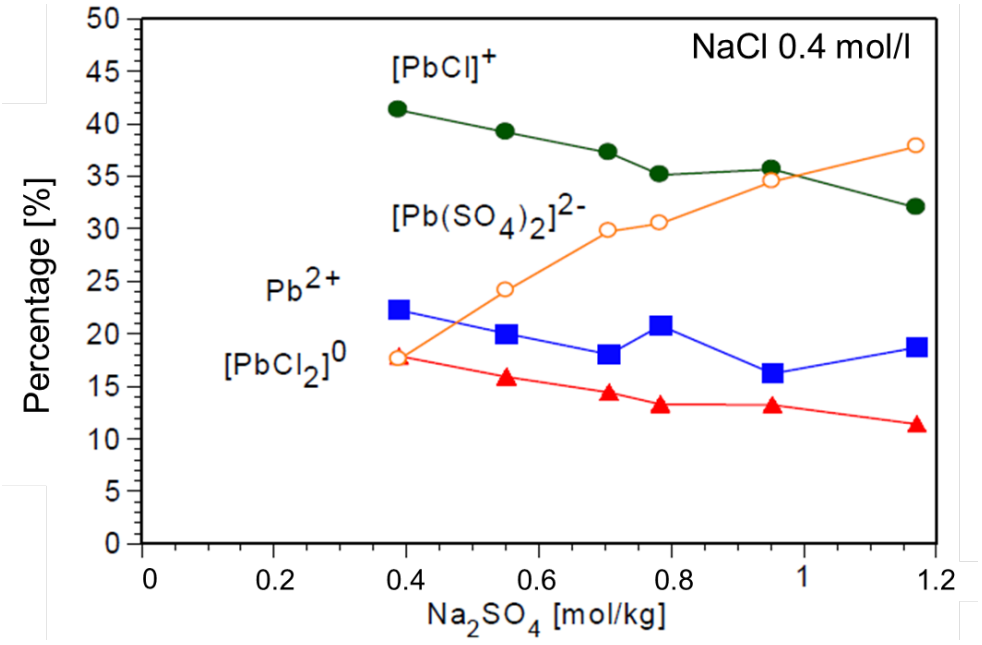

Fig. 4.3 Composition of lead chloro and sulfato complexes in a 0.4 mol/l NaCl solution adding Na_2SO_4

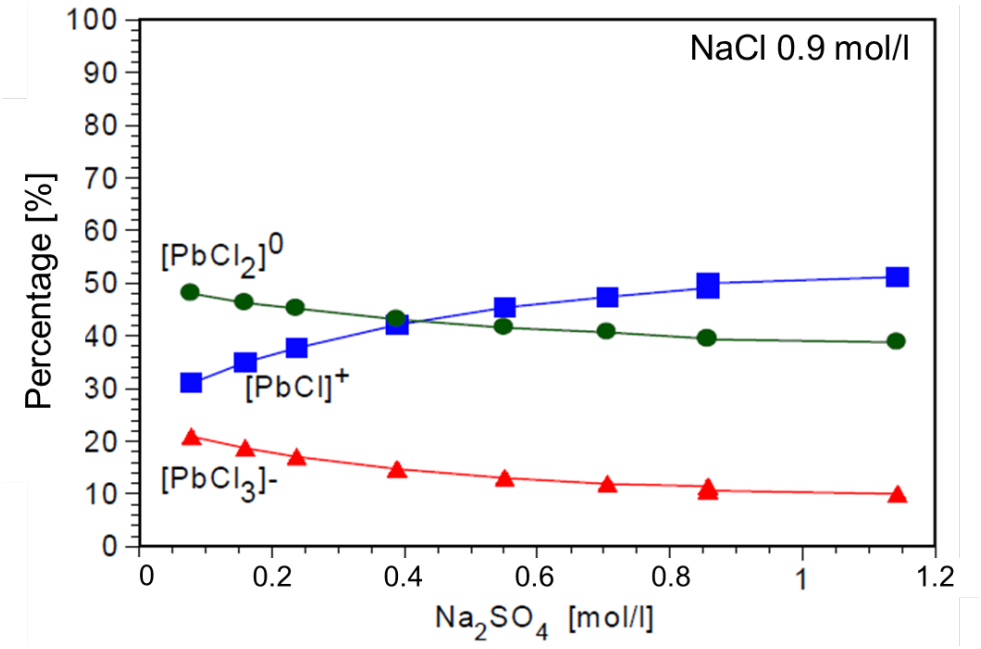

Fig. 4.4 Composition of lead chloro and sulfato complexes in a 0.9 mol/l NaCl solution adding Na_2SO_4

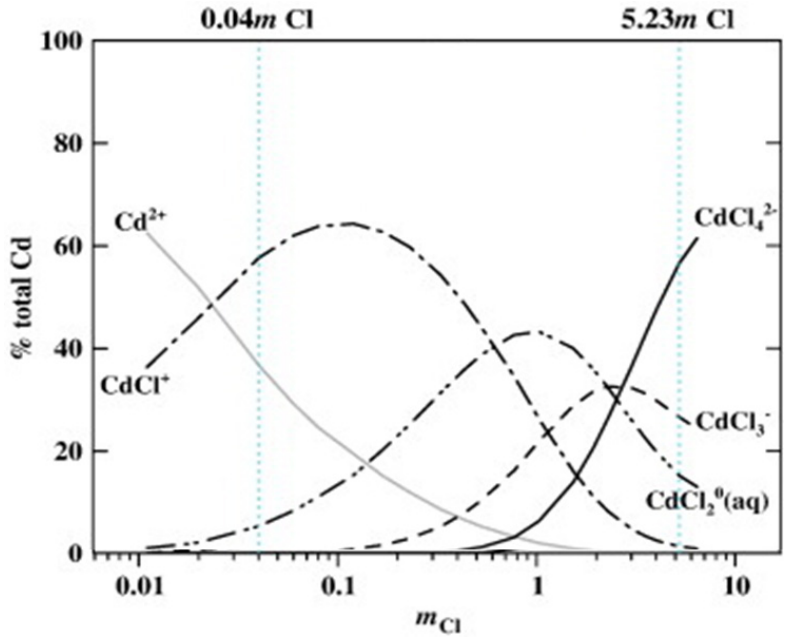

Fig. 4.5 Dependence of stepwise formation of Cd chloride complexes on Cl^- concentration at 20 °C and 1 bar /BAZ 10/

Similar cadmium chloride complexes are formed in cadmium chloride solution /VAN 53/, /BAZ 10/, which leads to its high solubility. Experimental results showed that aqueous Cd speciation is dominated by the cation $Cd(H_2O)_6^{2+}$ in acidic Cl^- free solutions and by chloride species $CdCl_m(H_2O)n^{2-m}$ (m = 1, 2, 3, 4, n = 2 – 6 /BAZ 10/. At relatively high

Cl^- concentration (> 2 mol/kg H_2O) Cd chloride complex is dominated in form of anions (Fig. 4.5).

If such solutions contract with or flow through clay materials, the interaction to the clay minerals is different to that in dilute solution. Because the sorption and diffuse double layer formation are all rooted to the fact that there is net negative charge of clay minerals and thus cations can be easily attracted and adsorbed on the surface. The main mineral montmorillonite in bentonite has the highest specific surface and thus the highest ionic exchange capacity and also usually the most efficient adsorption effect to most heavy metals. However, when the heavy metals exist in a solution with complexation with ligands like Cl, SO_4, the adsorption properties can be changed /BEN 82/. According to Benjamin /BEN 82/, interactions between metal ions and complexing ligands interacting with an adsorbent may be divided into three groups based on the origin and strength of the interactions: (1) Metal-ligand complexes form in the solution and lead to weak or no adsorption on a solid surface; (2) The species interact indirectly at the surfaces by altering the surface electric properties such as the point of zero charge, the isoelectric point and even the surface electrical potential. These changes may affect the Coulombic attraction between the surface and adsorbate ions; (3) The metal-ligand complexes adsorb strongly. For clay minerals like montmorillonite, there is permanent net negative charge on the minerals surface, anionic complexes are not sorbed /FAR 77/. Adsorption of cationic metal complexes is subject to competition from charged protonated ligand species.

5 Materials and methods

The MX-80 bentonite and following saline solutions were applied in the different experiments:

- MX-80 (Wyoming-bentonite, trade article from 2005)
- Saline solutions: NaCl solution in different saturation index (10 %, 30 %, 50 %, 90 % and 100 % NaCl solution), IP21 solution

5.1 MX-80

MX-80 bentonite was a commercial product of the Süd-Chemie AG (Moosburg, Germany) bought by GRS mbH in 2005. It originated from latitic or rhyolitic volcanic ash in the sea water in Mowry shale – Wyoming – USA /MOL 01/. The MX-80 starting material was characterised as Na bentonite, which was dominated in XRD of randomly oriented mounts (powder) by 13Å-montmorillonite (monovalent, 1 water layer in interlayer space).

The mineral matter of MX-80 starting material was nearly comparable to other published data about MX-80 bentonite (Tab. 5.1). On the other hand, it has to be pointed out that the smectite of the applied MX-80 starting material has shown remarkable treatment impacts by the seller in the chemical composition in comparison with literature data for MX-80 bentonite from Madsen /MAD 98/ and Ufer et al. /UFE 08/. The applied GRS-MX-80 bentonite (trade article from 2005) was more Al-rich smectite and had a lower total charge than in the mentioned analyses published on the former MX-80 series.

For the production of the samples with a thickness of 15 – 18 mm and a diameter of 50 mm, the MX 80-material was compacted under uniaxial pressure in a cylindrical compaction form. Samples with densities of 1,400 kg/m^3, 1,600 kg/m^3 and 1,800 kg/m^3 were produced. Originally it was foreseen to perform the diffusion experiments also of Zn through bentonite with a bulk dry density of 1,200 kg/m^3. Owing to the technical difficulties in the geochemical analysis of Zn in highly saline solution, Zn is replaced with Cs. The diffusion experiments with bentonite in 1,200 kg/m^3 were given up as canal formation in the bentonite sample during diffusion experiments. As a compensation

batch sorption experiments with heavy metals Cd, Pb and Cs in NaCl-solution with different degree of NaCl saturation were performed in order to obtain the sorption data needed for the numerical simulation.

Tab. 5.1 Semi-quantitative mineral composition of bulk samples of MX-80 bentonite by BGMN-Rietveld refinement (own measurements: bulk sample, random preparation, < 63 µm; semi-quantification by BGMN-Rietveld processing of X-ray diffractograms [1-rho = 9.53 %; Rwp = 9.48 %]) /HER 12/

Phases (wt%)	**Own Measurements**	**Literature Data**			
	Mineral composition by BGMN-Rietveld	/LAI 06/	VTT (1996)	/UFE 08/	/MAD 98/
Smectite	77	75	85 – 95	85.7	75.5
Cristobalite	3	15.2*	--	1.7	15*
Quartz	5		3 – 6	4.5	
Albite	13	5 – 8	1 – 3	5.4	5 – 8
Calcite	trace	1.4	1 – 3	0.4	1.4
Muscovite	1	--	--	1.8	--
Pyrite	--	--	1 – 3	--	0.3
Gypsum	--	--	--	0.6	--
Organic matter	--	0.4	--	--	0.4

* cristobalite + quartz; structural formula of smectite by BGMN–Rietveld refinement was $Ca_{0.01}\ Mg_{0.02}\ Na_{<0..01}\ K_{0.02}\ Al_{1.62}\ Fe_{0.43}\ Si_{3.96}Al_{0.04}\ O_{10}(OH)_2$ and $Ca_{0.06}\ Na_{0.02}\ K_{0.01}\ Mg_{0.29}\ Fe_{0.16}\ Al_{1.55}\ Si_{3.88}Al_{0.12}\ O_{10}(OH)_2$

The average mineral formula of all TEM-EDX-measured dioctahedral smectitic particles of fraction < 2 µm was:

MX-80 (average mineral formula)

$Ca_{0.04}\ Mg_{0.04}\ Na_{0.01}\ K_{0.02}\ Al_{1.59}\ Fe^{3+}_{0.21}\ Mg_{0.16}\ Ti_{0.04}\ (OH)_2\ Al_{0.05}\ Si_{3.95}\ O_{10}$
with Interlayer charge XII = 0.19

5.2 Solutions

The experiments were performed with several solutions of different ionic strength:

- Saturated NaCl solution, similar to the typical brine encountered in the Zechstein formations in Germany /HER 00/, /HER 08/

- Unsaturated NaCl solutions (10 %, 30 %, 50 %, 90 % NaCl solutions)
- IP21 solution, a $MgCl_2$-rich brine which may be encountered in the Zechstein potash beds in Germany. An IP21 solution is saturated with the salt minerals halite, carnallite, sylvite, kainite and polyhalite /HER 00/, /HER 08/ In the experiments, only 90 % IP21 solution is used owing to the precipitation induced clogging problem by small temperature changes.

The chemical composition of these brines is given in Tab. 5.2.

Tab. 5.2 Chemical composition of brines used in the experiments

Solution	Na	K	Mg	Ca	Cl	SO_4	Density	I
	[g/l]						[kg/m³]	[M]
10 % NaCl	12.25	--	--	--	18.88	--	1021.21	0.54
30 % NaCl	36.73	--	--	--	56.65	--	1060.84	1.65
50 % NaCl	61.22	--	--	--	94.41	--	1100.46	2.82
90 % NaCl	110.20	--	--	--	169.94	--	1179.71	5.36
100 % NaCl	122.45	--	--	--	188.83	--	1199.52	6.04
90 % IP21	8.14	12.92	79.11	$7.2 \cdot 10^{-4}$	241.89	21.7575	1185.30	13.04

All basic solutions were prepared according to the GRS Standard Operation Procedure (SOP):

1. Solutions: NaCl saturated and unsaturated solutions with saturation grades (10 % – 90 %)
2. Solution: 90 % IP21

With the increase of the ionic strength of the saline solution, the physical parameters of the solution change. The density, viscosity and electric conductivity of the solution increase. Consequently the hydraulic parameters vary accordingly. The chemical properties especially the corrosion behavior will also change. This is beyond the scope of current project.

For the diffusion experiment, three solutions (mentioned above are prepared and then added with heavy metals Cd, Cs, Pb to the required concentrations, which are described in the related sections.

5.3 Gases

For determine the gas diffusivity a gas mixture of hydrogen, Carbon dioxide, methane and sulfur hexafluoride with an initial concentration of about 1 % each was used. The back end of the sample was purged with pure nitrogen. In the gas flow at the back end, the gas concentrations of the components were determined with the use of a GC (Type Ultratrace, Thermo Elektron) (Fig. 5.1).

Fig. 5.1 Experimental setup for the investigation on diffusion in compacted MX-80 samples (left: diffusion cell; right: gaschromatograph)

5.4 Chemical analysis for heavy metals in highly saline solution

The chemical analysis of the low concentrated heavy metals Pb, Cd and Cs in highly saline solutions mentioned above is the ICP-MS Spectrometry, which is proved to be very suitable and accurate for such solution types /GWI 98/, /HAG 99/.

5.4.1 Method description

The ICP-MS instrument measures more than 75 elements in the periodic table, most of them at the detection limits less than 1 part pro billion. Most analyses performed on ICP-MS are quantitative.

5.4.2 Technical equipment

The Thermo Scientifc XSERIES 2 Quadrupole Inductively Coupled Plasma Mass Spectrometer (ICP-MS) provides reliable interference removal in all sample types with a single collision gas and Kinetic Energy Discrimination. This ICP-MS consists of the following components:

This ICP-MS consists of the following components:

- Sample introduction system – composed of nebulizer and spray chamber (with Peltier cooling)
- ICP torch and RF coil RF
- Interface with special cones (Xt,Xs)
- Vacuum system- composed of a single rotary pump and a split flow turbo pump
- Collision/reactor cell (CCT mode)
- Ion optics (Protective Ion Extraction and Infinity II ion opticts)
- Mass spectrometer (quadrupole) – acts as a mass filter
- Detector-simultaneous analog/PC detector with real time multi-channel analyser
- Data handing and system controller (PlasmaLab software)

Each gas is controlled by mass flow device.

5.4.3 Laboratory Methods

The content of cadmium, caesium and lead in different salt solutions with different salt concentrations was analysed.

5.4.4 General

It is important to adapt the calibration to the background salt solution (salt type and salt concentration).

5.4.5 Analysis

In order to determine the concentration of the tracer elements a multi element 6 level calibration was prepared (certified element standards).

- Working range (prepared Blank, 2 – 10 ng/ml)
- Sample preparation
- Sample dissolution 1/200 include 2 % nitric acid
- Sample measuring
- Continuous calibration verification and blank verification are performed continuously during measurement
- LOQ
- The LOQ depends on the background salt quality and quantity
- Lead: 0,039 mg/l $1 \cdot 10^{-9}$ mol/l
- Caesium:0,008 mg/l $6 \cdot 10^{-8}$ mol/l
- Cadmium: 0,0026 mg/l

6 Review of diffusion experimental methods

Diffusion is an important and dominant transport process in very fine-grained and highly compacted bentonite/clay as engineered barrier system (e. g. /DES 86/, /SHA 91/, /MAD 98/, /SAM 09/). This finding can have a significant effect on the design and evaluation of waste containment facilities. Consequently a laboratory diffusion experiment is a necessary component of the overall design and evaluation processes associated with toxic waste disposal practice.

In the practice for the determination of the diffusion coefficient of barrier material like clay substance especially highly compacted bentonite, some difficulties occurred: extremely long test duration. This is mainly owing to the extremely low permeability induced long saturation process, high sorption coefficient and thus strong retardation effect.

In general, there are many experimental methods for the determination of diffusion coefficient in porous media. However, currently suitable methods for measuring the effective coefficients of chemical species in clay liners fall in two categories: steady state and transient methods.

6.1 The steady state based methods

The steady state based method can be described by the Fick's first law (equation (3.2)). When the diffusion field reaches the steady state, the diffusion coefficient can be calculated:

$$D^* = -\frac{J}{\frac{\Delta C}{\Delta x}} \tag{6.1}$$

with:

D*	effective diffusion coefficient
J	diffusive flux, which should be constant at steady state diffusion condition
C	concentration of the species to be determined
x	distance or Δx the thickness of the sample
$\frac{\Delta C}{\Delta x}$	concentration gradient

6.1.1 Steady-state method

The application of the steady-state method for determining the effective diffusion coefficient of bentonite can be traced back to Husted and Low in the 50's /HUS 54/. It is also widely used for the soil science practice /HUS 54/, /DUT 62/, /OLS 65/, /MUU 90/, /GLA 07/. The principal of the method is normally undertaken as the following: The soil sample is contained between two reservoirs – a source reservoir with the solution of interest (e. g. an actual or simulated solution containing solutes, which diffusion coefficient is to be determined), and a collection reservoir, from which samples are withdrawn for chemical analysis of specified chemical species. Detailed descriptions can be found in section 8.2.

6.1.2 Time-lag method

The time-lag method is commonly used for obtaining the diffusion coefficient, the permeability constant and the solubility of a gas flowing through a porous membrane /JOS 60/, /CRA 75/, /COM 85/, /ROG 85/, /SHA 91/, /GRA 98/. This method starts with zero concentration in the sample, which connects with two reservoirs similar like the steady-state method. The experiment continues until a steady state diffusion flux is reached. The difference is that the cumulative mass curve of the collection reservoir is used for the calculation of the effective diffusion coefficient. The theoretical basis of the method is described with equation (3.21) in section 3.3. When the lag-time t_{lag} is calculated, the effective diffusion coefficient D_e can be obtained:

$$D_e = \frac{d^2(n + K_d\rho)}{6t_{lag}} \tag{6.2}$$

in which n is the porosity, k_d is the adsorption coefficient, ρ is the bulk density of the soil.

The advantage of this method is that less control of the test is required in comparison to the traditional steady-state method since steady-state condition only has to be established, not maintained. However, the retardation parameter and accessible porosity has to be known in order to use this method for calculating the effective coefficient. If the adsorption coefficient is high, the time required to establish steady-state conditions can be extremely long.

6.2 The transient methods

Apart from the steady-state based methods, there are many other kinds of diffusion test methods in the literature based on the transient diffusion theory. A thorough overview can be found in the review paper by Schackelford /SHA 91/. In the currently project, the steady-state based method is applied after some modifications, therefore the in-depth description of various transient based test methods is beyond the scope of the current report.

7 Gas diffusion experiments

The planned experimental approach, to couple the investigations on heavy metals and gas diffusion was not successful, because a reaction between the ionic heavy metals (Cd^{2+}, Pb^{2+} und Zn^{2+}) with the hydrogen occurred. A reaction of the contaminants caused a decrease of the initial concentrations of the ionic and the gaseous components in the initial solution. At the beginning of the experiments the MX-80- sample was saturated with a NaCl-solution. Over a period of test time no gas was observed at the back end of the sample. For this reason, the experiments were separated.

For the characterisation of the hydraulic condition of the samples, the gas permeability was determined. For the evaluation, the Darcy's law for compressible media was applied for steady-state flow as follows:

$$k_g = \frac{2 \cdot q_g \cdot \mu_g \cdot l \cdot p_0}{A \cdot (p_1^2 - p_0^2)} \tag{7.1}$$

with:

k_g	permeability measured with gas	[m^2]
q_g	flow rate of the gas	[m^3/s]
p_1	injection pressure	[Pa]
p_0	atmospheric pressure	[Pa]
μ_g	viscosity of the gas	[Pa·s]
l	sample length	[m]
A	cross-section of the sample	[m^2]

Gas diffusion is described as a particle movement from a region of higher concentration to region of lower concentration. The diffusion concept is based on a mass transport driven by a concentration gradient. At steady state condition the diffusivities of the different gas components can be calculated by Fick's first law /JOC 01/, /JOS 72/:

$$D = \frac{J \cdot l}{\Delta c \cdot A} \tag{7.2}$$

with:

D	diffusion coefficient	[m^2/s]
J	diffusion rate $= j \cdot c_{II}$	[kg/s]
j	purging rate at the back end	[m^3/s]
c_{II}	concentration of the gas component at the back end	[kg/m^3]
l	length of the sample	[m]
Δc	concentration gradient between both ends of the sample	[kg/m^3]
A	cross-section of the sample	[m^2]

The instationary case the diffusion is described by the Fick's second law /GER 74/:

$$\frac{\partial c}{\partial t} = D \frac{\partial^2 c}{\partial x^2} \tag{7.3}$$

with:

c	concentration	kg/m^3
D	diffusions coefficient	m^2/s
t	time	s
x	position	m

and represents the temporal and local concentration distribution.

First, it was foreseen to calculate the diffusion coefficient by a numerical description of the concentration history at the back side of the sample at decreased concentration on the front side.

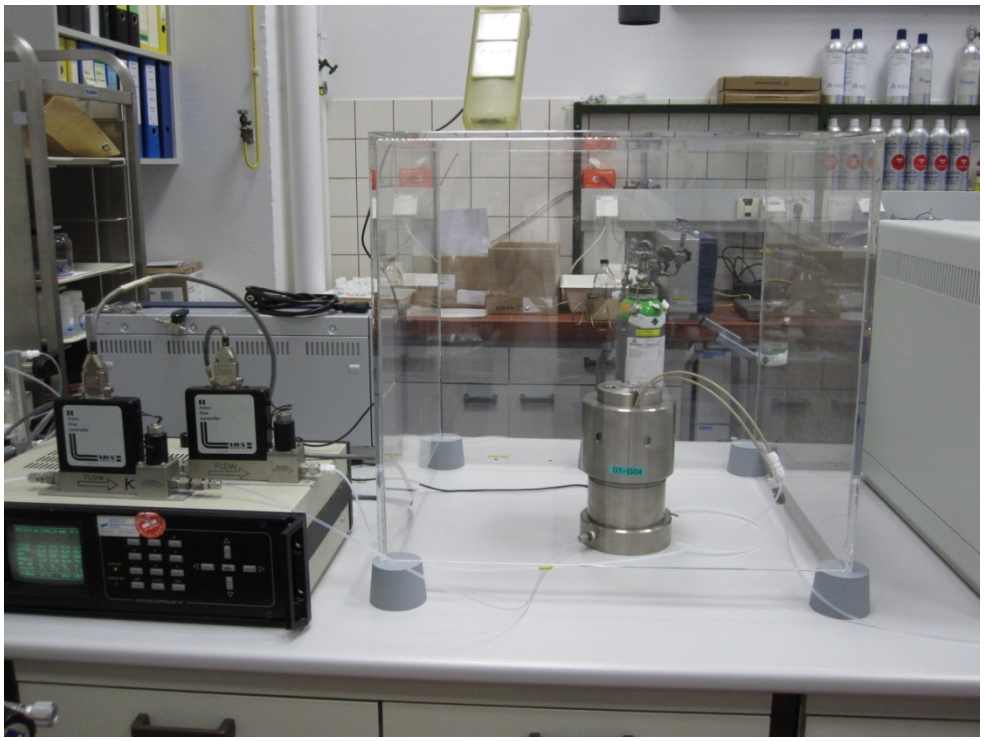

Left: Two mass-flow controller with data acquisition unit. Right: measuring device with an acrylic glass hood

Fig. 7.1 Experimental setup for the investigation at steady state condition

For comparison of the investigations at decreasing initial gas concentrations, one test at steady state conditions was performed. Since the gas flows were equal at both ends

and the configuration was symmetrical, no pressure gradient occurred between the two ends of the sample and the diffusivity can calculated using Fick's first law.

7.1 Gas diffusion through bentonite

At the beginning, the permeability to gas (argon) was determined to $2.8 \cdot 10^{-15}$ m^2. Afterwards, the measurements for the determination of the diffusion of hydrogen were performed at first.

A 90 % NaCl-solution saturated with hydrogen was connected to the front end of the testing cell and were pumped in a closed loop by a peristaltic pump. The MX-80 sample in the cell was 10 mm high. At the back end, a continuous nitrogen flow was applied. Gas samples were taken once a day. The test has shown that a thickness of 10 mm of the sample was not suitable, because fissures were generated. No diffusion measurements were possible. For the further experiments, the thickness of the samples was enlarged to 15 mm.

With the modification of the sample dimension, another experiment using a 90 % NaCl-solution saturated with hydrogen was started. Even after a longer test period, no diffusion of the hydrogen was observed.

Based on the observations of the hydrogen with a saturated NaCl solution and because of the long test times, further experiments with other gases and solutions have been omitted. The tests were continued by only using the pure gas phases on samples prepared with MX-80 in state of delivery. Since the concentration of the gas components should be similar to the relatively low concentration of the dissoluted gases in the solutions, a mixture of the envisaged gases of 1 % was applied. In comparison, /JOC 00/ und /JOC 01/ the initial concentration amounted to 25 %.

Despite of the modifications of the test, none gas components were found at the back end of the sample. It was assumed, that the time for passing of the gases through the sample was very long. For this reason, the sample was filled with the gas components by injecting at low pressure. The gas mixture was injected to the specimen by a peristaltic pump. This forced convective passage led to a significant reduction of the test time. After the pressure was reduced, the diffusion experiments were started, and diffusion to the back end was observed.

The variation of the measuring signals was relatively high, what may be explained by variation in temperatures. For protection, the test setup was added by an acrylic glass hood. In addition, the gas flow at the back end was controlled by a mass-flow controller was led to a constant volume flow. After the modification of the test setup, the variations of the measuring signals were lower.

At an unsaturated sample, particularly hydrogen, and sulfur hexafluoride were detected. The amount of methane was relatively low and Carbon dioxide was not detectable.

Investigations on partially water saturated samples, showed higher diffusion coefficients than at the unsaturated samples at state of delivery. Carbon dioxide was not detectable. In both cases the diffusion coefficients of sulfure hexafluorid showed the highest values.

Assuming an initial gas concentration of about 1 %, an estimation using the data immediately after the detection of the gas components resulted in diffusion coefficient in a range between 10^{-11} m^2/s to 10^{-10} m^2/s for the unsaturated samples and between 10^{-10} m^2/s and 10^{-9} m^2/s for the partially saturated samples. After decreasing of the gas concentration on the front end of the specimen of about one-tenth for Carbon dioxide, methane as well as sulfur hexafluoride and of about one-hundredth for hydrogen in respective to the initial concentrations, further diffusion could not detected or was lower than the limit of detection of the gas-phase chromatograph.

Furthermore, the gas circulation on the back end led to a drying of the sample to a water content of only 2.1 %.

Other experiments of gas diffusion in clay containing materials have shown higher diffusion coefficients. Jockwer et al /JOC 01/ have investigated dried Boom clay backfill with 60 % Foca clay, 35 % sand and 5 % graphite, as well as 95 % Foca clay with 5 % sand. The diffusion coefficients of the dry material were about 10^{-7} m^2/s. Another experiment was performed on samples of the same mixtures and at the same test conditions. These tests resulted in lower diffusion coefficients which were smaller by a factor of ten to twenty. The reason for this difference was not known /JOC 01/. This result is an advice of the complexity of these tests. The gas permeability amounted to 10^{-13} m^2/s. The diffusion coefficient of saturated samples were significant lower with values lower than 10^{-10} m^2/s /JOC 01/.

Volckaert et al. /VOL 95/ have determined the diffusion coefficient of hydrogen and methane in Boom Clay by using two methods, the in-diffusion and the through-diffusion method. The diffusion coefficient varied over a large rang. For hydrogen the values were $4 \cdot 10^{-12}$ m^2/s to $5 \cdot 10^{-10}$ m^2/s and for methane $6 \cdot 10^{-10}$ m^2/s to $2 \cdot 10^{-9}$ m^2/s /VOL 95/, /ORT 02/.

Investigations on gas diffusion, sand-clay mixtures at different clay ratios between 10 %, 25 % and 50 % Calcigel and different compaction pressures between 25 MPa and 100 MPa showed a decrease with increasing clay content and increasing compaction pressures /JOC 00/. The diffusion coefficients ranged between 10^{-8} m^2/s to 10^{-7} m^2/s. At clay contents of 25 % and 50 %, the diffusion coefficients were about 2 to 3 times smaller than the samples with 10 % clay. An increase of compaction pressure led to a decrease by a factor of 5 to 30. At saturated samples the diffusion was controlled significantly by the clay content and the compaction pressure. The diffusion coefficients of samples with 10 % clay and a compaction pressure of 25 MPa ranged between 10^{-10} m^2/s to 10^{-9} m^2/s. At higher clay contents and compaction pressures, the diffusion coefficients were below the limit of detection of 10^{-10} m^2/s. The gas permeabilities ranged between $6 \cdot 10^{-14}$ m^2 to $3 \cdot 10^{-13}$ m^2, and were nearly independent of the clay contents and the compaction pressure /JOC 00/. Compared to the investigations of /JOC 00/ and /JOC 01/, the described tests above, were performed at in stationary conditions, that means with decreasing initial gas concentrations.

According to the investigations of /JOC 00/ and /JOC 01/, one test was performed at steady state conditions on a sample prepared of dry MX-80. Because the sample with a thickness of 15 mm was not stable, the thickness was changed to 18 mm. This test has shown a distinct gas concentration at the back side of the samples for all gases. In this case Carbon dioxide was detected too. After a relative short time of about 14 days the concentration of the gases at the back end was nearly constant. The diffusion coefficients evaluated after Fick`s 1. law were summarized in Tab. 7.1.

Tab. 7.1 Diffusion coefficient of the gases determined by test at steady state condition in comparison to the molecular weight

Gas	Diffusion coefficient [m^2/s]
H_2	$3.40 \cdot 10^{-7}$
CO_2	$2.30 \cdot 10^{-7}$
CH_4	$1.41 \cdot 10^{-7}$
SF_6	$3.38 \cdot 10^{-8}$

7.2 Adsorption of gases in contact with MX-80

To check whether the used gases are adsorbed on MX-80, the gases with a defined concentration were brought in contact with a defined mass of MX-80 powder. The changes of the initial gas concentrations were determined. The initial concentration for each gas was 1 %. The aim of this experiment is to investigate the adsorption of hydrogen, carbon dioxide, methane and sulfur hexafluoride on bentonite

According to the instruction, 4 glass bottles were filled with 100 g bentonite (Fig. 7.2). Before starting the experiment, the whole system was purged by nitrogen in order to prevent influencing adherent gases.

Every single glass bottle had been charged with 1 per cent of the gas that was analyzed. For analyzing, a gas chromatograph (GC) was used.

The gas chromatography (GC) is a partition chromatography, which is used as an analytical method for separate mixtures into individual chemical compounds. The GC is only applicable to gaseous or vaporized compounds. During the transport in a gas stream through a column the separation takes place. The mobile phase is given by using an inert gas, usually nitrogen, helium or argon.

After separation, the detection of the compounds is done by different detectors like a FID or an ECD.

A gas chromatographic system with following specification was used:

- Unit designation: Trace GC Ultra
- Manufacturer: Thermo Scientific

- System Components – Pneumatic Compartment
  - Analytical Unit
  - Column oven
  - Injector and detector compartment
  - Detector: Pulsed Discharge Detector (PDD)
  - Detection range: low pg

Fig. 7.2 Experimental set-up

The following results were described in Tab. 7.2.

Tab. 7.2 Result of adsorption experiments

Time of analysis	Hydrogen [%]	Methane [%]	Carbon dioxide [%]	Sulfur hexafluoride [%]
After 7 days	0.44	0.50	0.09	0.56
After 14 days	0.26	0.44	0.08	0.55
After 21 days	0.05	0.44	0.05	0.50

The very low values of carbon dioxid might be explained by a natusural adsorped gas of the MX-80 at initial state.

8 Development of a new through-diffusion method

8.1 Introduction

Bentonite is being increasingly used as barrier material in the design of disposal facilities for hazardous wastes. The sorption and diffusion coefficients of chemotoxic and radionuclides under its working conditions are crucial parameter in the safety analysis of high-level nuclear waste repositories. Numerous studies on the theory and experimental methods have been undertaken /KRA 70/, /CHO 93/, /GRA 98/, /COR 03/, /VOP 06/. However, the actual range of diffusion coefficients remains still uncertain according to Yu and Nertnieks /YUN 97/ based on a systematic literature study. The main reasons are:

1. There is no standard method for measuring the sorption and diffusion coefficients of highly compacted bentonite /VOP 06/;

2. There are many factors strongly influence the adsorption and diffusion processes in bentonite. The impurities in bentonite may react with the contaminants to be determined, and result in mineral dissolution/precipitation other than normal absorption. The existing cations on the bentonite may exert ionic exchange and thus retard/accelerate the diffusion/precipitation.

3. The diffusion coefficients of contaminants are normally very low in highly compacted bentonite;

4. The traditional methods for diffusion coefficient determination are based on the 1D analytical solutions with one side to be kept as constant as 0, which is technically difficult to maintain with the traditional method in the praxis.

8.2 The classic steady state method

As it is mentioned in the above sections, through-diffusion experiment as a steady state method is one of the most reliable and the most widely used techniques for the determination of the diffusion coefficient of contaminants through porous media. The principle set-up of the classic through-diffusion method is schematically described in Fig. 8.1.

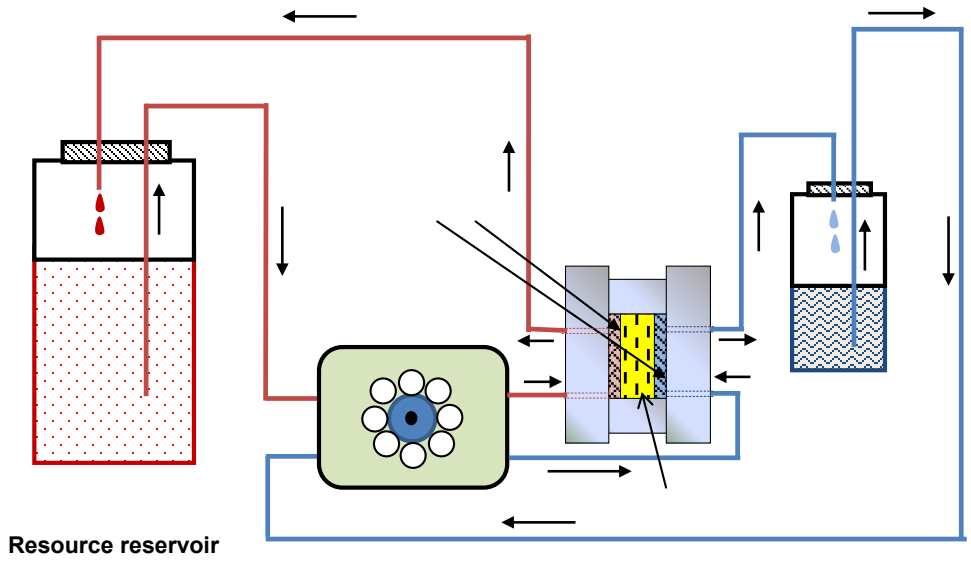

Fig. 8.1 Schematic description of a classic through-diffusion experiment /VAN 05/

The general mathematic equation for the diffusion process can be described by equation (3.14) in section 3.3. The boundary and initial condition together with the analytical solution of the equation is also given at the end of section 3.3.

With the diffusion process the heavy metal diffuses into the sample and the concentration profile evolution is illustrated in Fig. 8.2. When a steady state diffusion condition is reached (Fig. 8.2), the diffusion flux remains constant. The effective diffusion coefficient can be calculated by rewriting equation (3.20).

$$D_e = q_{stat}\frac{d}{C_0} \tag{8.1}$$

The advantage of the steady-state method is that the effective diffusion coefficient of reactive solutes can be measured without even having the adsorption properties of the solute to the porous media, because there is no retardation of a solute species at steady state condition. Such parameter doesn't thus even appear in the Fick's first law equation. That means it is reliable to determine the effective diffusion coefficient independently. However, there are several disadvantages of the method especially by using the classic through-diffusion apparatus for the determination of chemical species with high adsorption coefficient migrating through clay material with extremely low permeability as shown in Fig. 8.1.

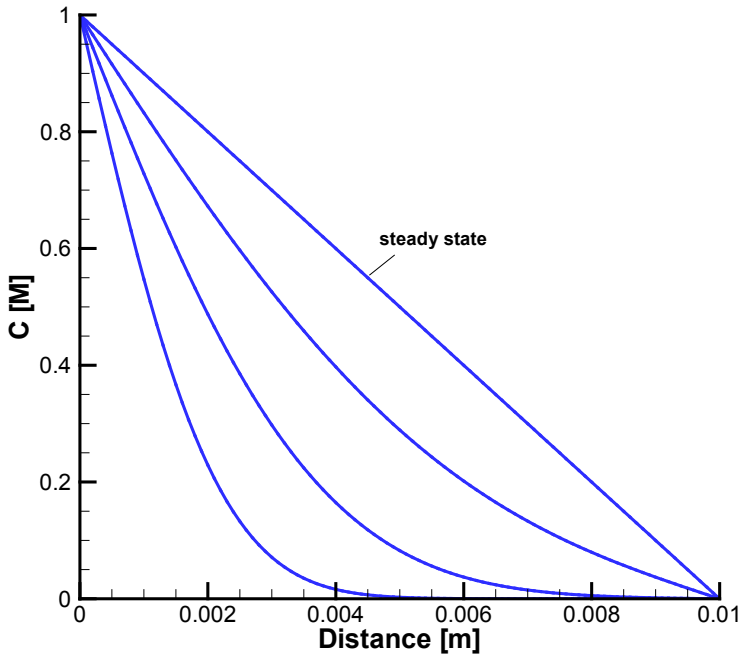

Fig. 8.2 Diffusion profile evolution and steady state diffusion

The time needed to establish steady-state diffusion conditions for reactive chemical species could be very long, the higher the sorption coefficient, the longer time will be required.

The concentration in the resource reservoir can decrease with the time because the contaminants migrate into the sample. As bentonite has a very high sorption coefficient to heavy metals in general, such effect is apparent. The concentration in the resource reservoir could decreases in such an extent that the actual concentration gradient differs far from the designed one. The migration turns to be much slower than expected so that the time for establishing a steady-state condition will extend accordingly. In the practice, the reservoir volume of 200 ml is commonly used and can be replaced for several times. In such cases, the theoretical requirement with “constant boundary concentration” is not fulfilled.

The concentration in the collection reservoir is also changing with the time. There are two ways to take samples for chemical analysis: (a) directly taking samples from the reservoir (i. e. use a syringe through a needle); (b) Regularly changing the reservoir with a fresh solution. For the first way, the amount of the solution decreases with the time if no compensation amount of solution is injected into the sample. Even if the exact amount of compensation solution is injected, the concentration of the chemical species to be determined decreases with the injection and accumulates until the next injec-

tion. For the second way the concentration of the solutes to be determined changes with the replacement, which disturbs the establishment of the steady-state diffusion condition. In both cases it is difficult to maintain the “zero concentration” condition as the theoretical requirement. The “zero concentration” requirement for the diffusion experiment according the classic through-diffusion is unrealisable in the classic through-diffusion experiment.

For the evaluation and design of environmental facilities like landfill, it is reasonable and accurate enough to determine the diffusion coefficient of the liner with initially contaminant free condition and thus maintain the zero concentration at other side. However, for some special environmental facilities like landfill for chemotoxic substance or HLW (high-level nuclear waste), the evaluation has to consider not only the first stage migration at the initially contaminant free condition but also the migration after the contaminants migrate through the barrier layer with limited thickness, which can be named as the long-term diffusion process. Little work is however known at the moment.

8.3 The new steady-state through-diffusion method

Based on the observations to the classic through-diffusion coefficient, some modifications were undertaken and thus a new through-diffusion method is developed. The schematic description of the method is shown in Fig. 8.3.

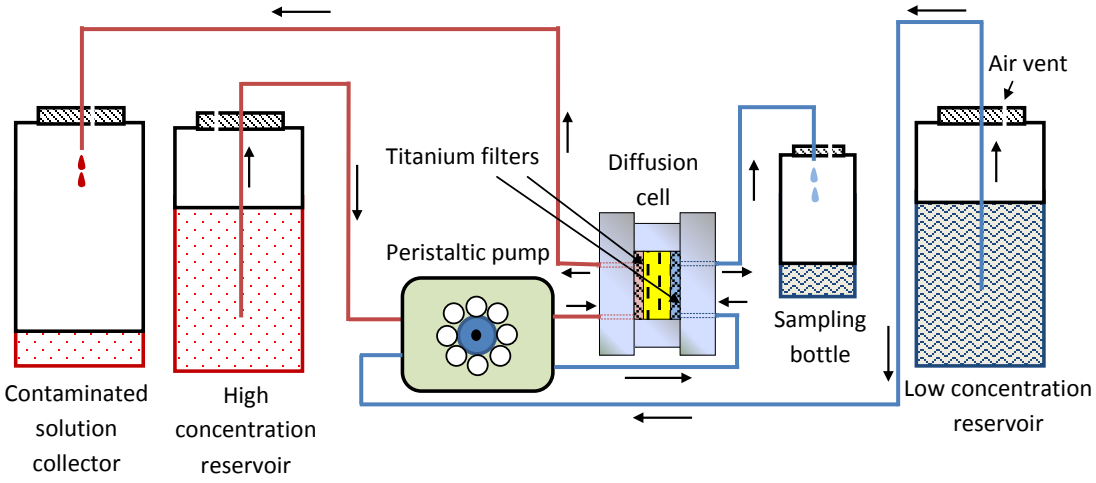

Fig. 8.3 Schematic description of a modified through-diffusion experiment

The key points of the new method are:

1. The bentonite sample is flashed with solution containing a small amount of heavy metals of interest (using the solution to be supplied to the collection side). By this measurement, the sample is partially equilibrated with the contaminants of interest, in other words, the sorption process is partially completed before the actual diffusion experiment begins. Some uncertainties influencing the retardation process owing to some reactive impurities in the natural sample might be avoided through such process. Consequently the time for the establishment of steady-state condition by applying the new method should be much faster than that using the classic through-diffusion experiment.

2. The samples are saturated with the solution to be supplied to the collection side for the diffusion experiment. After that the samples are compacted to the designed dry density. This procedure shortens once again the saturation process. For the current project for the determination of the migration parameters of heavy metals through compacted bentonite in salt rock formations, this procedure is necessary. This is because the natural pore water is different from highly saline solutions to be expected in salt rock formations. It can be reasonably assumed that such highly saline solution should firstly penetrate through bentonite before contacting the containers of chemotoxic waste, setting off the corrosion process followed by releasing chemotoxic species. That means the chemotoxic migration in bentonite should occur after the saturation process. As the liquid permeability increases with the concentration or ionic strength, fully saturation condition is mostly to be expected. However, this pre-treatment is only suitable for highly compacted bentonite in saline solution, which ensures a high permeability for the compaction.

3. The resource boundary remains constant by the continuous supply of solutions containing the heavy metals of interest (the high concentration reservoir).

4. The same method is applied to the collection side except the concentration of heavy metal in the solution (about two magnitudes lower than those solution supplied to the source boundary).

5. Through the measurement of the solution amount at both collection bottles at the same time interval, the diffusion only condition for the experiment can be checked. This is interesting for material with high permeability, i. e. bentonite with low density by highly saline solution. In such cases small hydraulic difference might lead to advective transport from one side to the other side of the sample.

In the diffusion experiments for current project all solutions (for the pre-treatment, for the resource or collection reservoirs) have the same background chemical composition (i. e. 50 % NaCl, 90 % NaCl or 90 % IP21 solutions) at least for each individual diffusion experiment. Therefore the chemical reactions between bentonite and the chemical species in the background solution can be neglected during the experimental time frame.

The mathematic description for the modified through-diffusion method remains the same as the classic method (equation (3.14) in section 3.3). But the initial and boundary conditions are different, which leads to a different solution of the equation.

In the case of diffusion across layers of low conductivity in a thickness of d, it is assumed that the liner is initially contaminated and can be represented as f(x), and the concentration of the contaminant at the waste side is C_1 (constant) and the other side C_2 (constant), the following initial and boundary conditions can be applied:

$$\begin{array}{llll} t = 0 & x > 0 & C = f(x) \\ t > 0 & x = 0 & C = C_1 \\ t > 0 & x = d & C = C_2 \end{array} \qquad (8.2)$$

The concentration profile at time t in the layer can be described in the trigonometrical series as /CRA 75/:

$$C = C_1 + (C_2 - C_1)\frac{x}{d} + \frac{2}{\pi}\sum_{i=1}^{\infty}\frac{C_2\cos(i\pi) - C_1}{i} sin\left[\frac{i\pi x}{d}\right] exp\left[\frac{-i^2\pi^2 D_a t}{d^2}\right] + \frac{2}{d}\sum_{j=1}^{\infty} sin\left[\frac{j\pi x}{d}\right] exp\left[\frac{-j^2\pi^2 D_a t}{d^2}\right]\int_0^d f(x')sin\left[\frac{j\pi x'}{d}\right]dx' \qquad (8.3)$$

Ideally the initial condition of the contaminants in the bentonite after the pre-treatment and flash with solutions containing the contaminants in the concentration of C_2 should create an initial condition of C_2 as shown in Fig. 8.4.

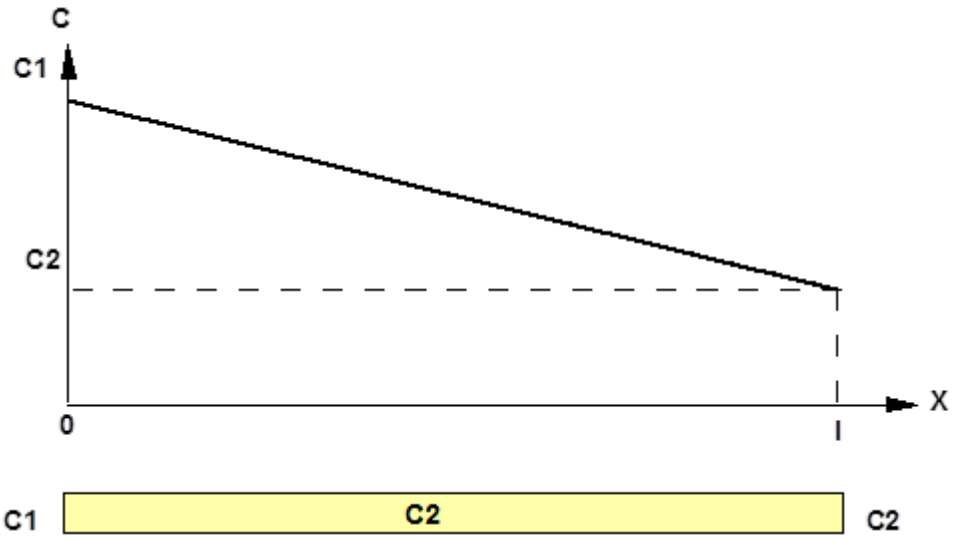

Fig. 8.4 Initial and boundary conditions of the modified through-diffusion method

In such case, f(x) = C_2, the equation (8.3) can be simplified as

$$C = C_1 + (C_2 - C_1)\frac{x}{d} + \frac{2}{\pi}\sum_{i=1}^{\infty}\frac{C_2\cos(i\pi) - C_1}{i} sin\left[\frac{i\pi x}{d}\right] exp\left[\frac{-i^2\pi^2 D_a t}{d^2}\right]$$
$$+ \frac{2}{d}\sum_{j=1}^{\infty} sin\left[\frac{j\pi x}{d}\right] exp\left[\frac{-j^2\pi^2 D_a t}{d^2}\right]\frac{C_2 d}{j\pi}[1 - \cos(j\pi)] \qquad (8.4)$$

However, in the experiment, it is found that the concentrations of the contaminants in the pore water are lower than C_2. This is mainly because the sample can adsorb part of the contaminants and thus leading to the lower concentration in the pore water. The flashing in the sample is also not long enough to reach the concentration C_2 along the sample. Consequently the initial concentration along the sample remains less than C_2. In such situation, the contaminants diffuse even into the sample from the collection reservoir. The migration of contaminants out of the sample can only be detected if there is a net positive increase of the concentration of the contaminants. This effect can be schematically described in Fig. 8.5. When the concentration of a contaminant on the collection end is higher than its initial concentration in the sample, the diffusion begins with in-diffusion into the sample from both ends. This can be easily detected by the change of the concentration at the collection side.

The disadvantage of the modified through-diffusion method is that much more solution is needed in comparison of the traditional method and results in more contaminated solution. This can be minimized by the combination of both methods.

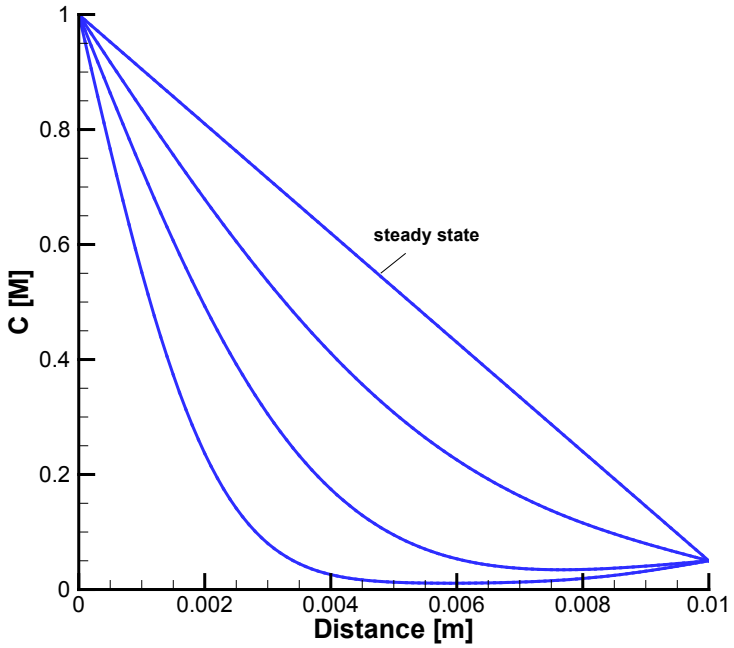

Fig. 8.5 Evolution of the concentration profile with the modified through-diffusion method

When the steady-state diffusion condition is reached, the diffusion flux (J) can be described withFick's first law:

$$J = -D_e \frac{\partial C}{\partial x} = -D_e \frac{C_2 - C_1}{d} \tag{8.5}$$

The diffusion coefficient can be obtained:

$$D_e = \frac{Jd}{C_1 - C_2} \tag{8.6}$$

9 Heavy metal diffusion experiments

The diffusion experiments of heavy metals (Pb, Cd and Cs) in three different background solutions (50 % NaCl-solution, 90 % NaCl-solution and 90 % IP21-solution) were conducted with compacted bentonite in different densities (1,200 kg/m^3, 1,400 kg/m^3, 1,600 kg/m^3 and 1,800 kg/m^3) (Tab. 9.1). However, the experiment of compacted bentonite with the low density 1,200 kg/m^3 encountered difficulties like canal formation along the contact zone of the sample and the container, or advection induced by very small hydraulic head difference of both sides. This is because that the swelling capacity of bentonite is much smaller in contact with highly saline solution and the hydraulic conductivity is higher with highly saline solution. On the other hand side, it is also unlikely to use bentonite at such a small density as sealing material in storage facilities for wastes especially chemotoxic wastes. Therefore, only one of the planned experiments on bentonite with density 1,200 kg/m^3 was conducted.

Tab. 9.1 Overview of the diffusion experiments

Test-No.	Dry density [kg m^{-3}]	Solution type	Heavy metals		
			Pb	Cd	Cs
D1_S06	1,200	90 %. NaCl		✓	
D1_S02	1,400	90 %. NaCl	✓	✓	
33363	1,400	50 %. NaCl			✓
33658	1,400	90 %. IP21	✓	✓	✓
33897	1,400	90 %. NaCl	✓	✓	✓
34045	1,400	50 %. NaCl	✓	✓	✓
D1_S01	1,600	90 %. NaCl	✓	✓	
33029	1,600	90 %. NaCl	✓		
33472	1,600	90 %. NaCl	✓	✓	✓
33199	1,600	50 %. NaCl	✓		
33233	1,600	50 %. NaCl			✓
33234	1,600	50 %. NaCl	✓	✓	✓
33475	1,600	90 %. IP21	✓	✓	✓
33381	1,800	50 %. NaCl	✓		✓
33557	1,800	90 %. IP21	✓	✓	✓
33657	1,800	90 %. NaCl	✓	✓	✓

An overview of the measured diffusion coefficients can be found in Fig. 9.1. The values are between $5.0 \cdot 10^{-12}$ m^2/s and $5.0 \cdot 10^{-10}$ m^2/s. Generally the diffusion coefficient values of each heavy metal decrease with the increase of the dry density of the compacted

bentonite. It is very interesting that the background solution strongly influences the diffusion coefficient of heavy metals within it. The details can be found in the following subsections.

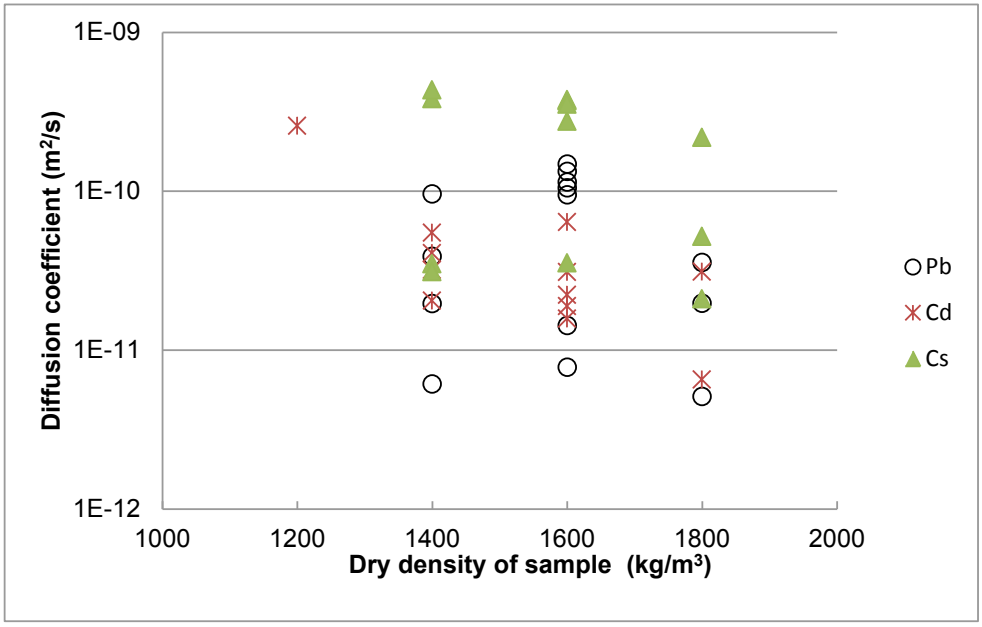

Fig. 9.1 Overview of measured diffusion coefficients of Pb, Cd and Cs measured in three different saline solutions (50 % NaCl-solution, 90 % NaCl-solution and 90 % IP21-solution) through compacted bentonite with different dry densities

9.1 Materials

The materials used for the experiments are MX-80 bentonite, different background solutions (50 %- and 90 %-NaCl solutions, 90 %-IP21 solution), heavy metals (Pb, Cd and Cs). Details can be found in section 5.

9.2 Description of diffusion experiments

Within the project the diffusion coefficient was determined on pre-compacted bentonite (MX-80), using a test equipment designed by GRS (see Fig. 8.3). The basic idea of the test design is to penetrate a bentonite-plug from two sides, simultaneously with the same test solution spiked with low, respectively high concentrations of the same tracer.

The change of tracer concentrations in the solution is assumed to be representative for the particle diffusion in the bentonite. Applied on the test concept the tracer of higher concentration – bottom line at the cell – is forced to diffuse through the plug to the solution of lower tracer concentration – top line of the cell. To minimize interactions of the brine solutions and to prevent corrosion effects, autoclaves (test cells) of titanium were used, manufactured by INFRASERV/Wiesbaden.

The test procedure started with the compaction of the moistened bentonite plug to a given bulk density in the future test cell. In the second step the circulation of the spiked test solution at the bottom line and at the top line of the bentonite plug was initiated. The sampling of the test solutions and analytical determination of the residual tracer concentration was part of the final step. The change of tracer concentration measured by time was taken to determine the specific diffusion coefficients.

Three types of test solutions (1) NaCl, (2) IP21 and (3) PEARSON-water, OCPW[1] spiked with three tracers (A) Cadmium, (B) Cesium and (C) Lead were used as fluid reservoirs within the diffusion experiments (see chapter 5.2).

The NaCl-concentration of solution (1) was of 50 mol %, respectively 90 mol % sodium chloride. The concentration with magnesium chloride of solution (2) was at 90 mol % (see Tab. 5.2). The OCPW-solution was less ionic strength /PEA 03/.

The (A), (B), (C)-tracer cocktail (Cd, Cs, Pb) concentration at the top line was adjusted to 10^{-5} mol kg^{-1}; at the bottom line to 10^{-3} mol kg^{-1} (see chapter 9.4).

Assembling of components of the test equipment (see Fig. 8.3)

- Bottom section, containing the inlet and outlet for the solution
- Primary flange to fix the assembling
- Piece of metal to adjust the distance between plug and piston
- Top section, consisting of a piston with an integrated inlet and outlet for the solution
- secondary flange to fix the piston

[1] Opalinus clay pore water (OCPW) with the composition of the pore water of the argillaceous formation Opalinus Clay at Mon Terry Rock Laboratory in Switzerland /PEA 03/

Procedural method

- The technical components described above were assembled to achieve a system of high mechanically stiffness. An AMSLER Digicon 2000 machine was applied for pre-compaction of the loose bentonite material and to form a plug of defined length and bulk density. The electronic control panel of the AMSLER machine–generally used to measure elastic parameters- guaranteed to achieve a high accuracy of the geometry of the plug.
- 62.832 g of loose dry material of bentonite were necessary to prepare a pre-compacted plug of 20 mm length with a density between 1.2 to 1.8 g cm^{-3}. To achieve a homogeneous moistening of the plug, the material was penetrated with the specific test solution spiked with a tracer concentration of 10^{-5} mol kg^{-1}, in advance. Possible excess of moisture was squeezed out during the procedure of compaction. In general a mechanical load up to 40 KN – induced by the AMSLER machine – was needed to get the defined plug geometry.
- Using a High- Pressure-Liquid-Chromatographic pump, (HPLC) the residual free gas fraction in the pore space was removed from the plug by flooding the ready test cell for at least 24 hours using the specific test solution spiked with the low tracer concentration (10^{-5} molar) to reach hydraulic and chemical equilibrium before starting the test.
- The final test equipment consists of the prepared test cell, a pulse free peristaltic pump (type ISMATEC) and two 5-litre-bottles containing the specific test solution and the tracer cocktails (10^{-3} and 10^{-5} mol). All components were connected by transparent 1/8" PFA-(perfluoralkoxy)-tubes. After the pump rate was set to 50.1 µl min^{-1} the top and the bottom of the bentonite plug was penetrated by the tracer cocktail permanently. The eluate of the top line was sampled daily, weighted and analyzed with respect to the change of the tracer concentrations. For control, the outflow of the bottom line was random sampled and stored.

9.3 Comparison experiment of the traditional and modified method

Comparison experiments for the traditional and the modified through-diffusion methods were undertaken with compacted bentonite in density 1,600 kg/m^3, background solution 50 % NaCl-solution. The results are schematically described in Fig. 9.2 for the traditional method and in Fig. 9.3 for the modified method. In the traditional method, the so-

lution on the resource side has been changed several times to ensure the designed concentration (0.69 mmol/L of Cs) by considering the migration and sorption induced concentration decrease. It is clear to see that the break through time of Cs through the 20 mm sample is about 70 days. After 120 days, steady-state condition is still not arrived yet. Only after about 160 days, the steady-state diffusion condition is reached. The diffusive flux of Cs is about $1.2 \cdot 10^{-8}$ mol/(m^2 s). The thickness of the sample is 20 mm. The calculated diffusion coefficient according to equation (6.1) is $3.54 \cdot 10^{-10}$ m^2/s.

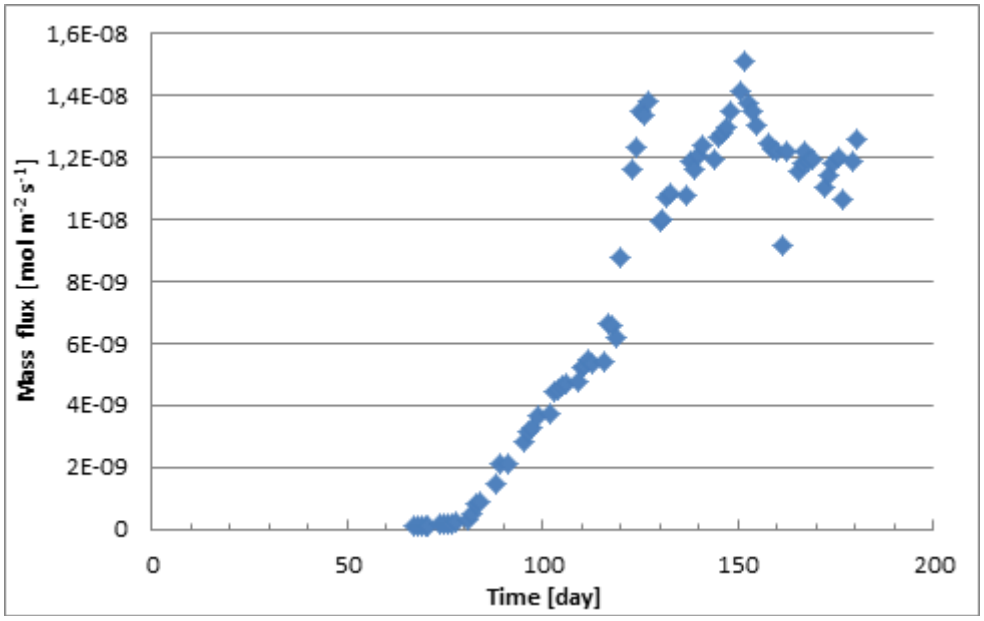

Fig. 9.2 Mass flux of Cs measured by using the traditional through-diffusion method

The comparison experiment was undertaken with bentonite in the same dry density and background solution. The concentration at the resource side is 0.34 mmol/L. The difference is that before the experiment, the sample was flushed with a solution including $1.1 \cdot 10^{-2}$ mmol/L Cs for several days with a minimal pressure from one side. After that the injection side was connected to the resource bottle including Cs in 0.34 mmol/L, and the other side connected with the collection circulation system including Cs in $1.1 \cdot 10^{-2}$ mmol/L. The time evolution of the mass flux rate measured through the collection circulation can be found in Fig. 9.3. At the beginning the mass flux rate is negative, which means that Cs flows into the sample even from the collection circulation system. This indicates that the sample is still not in equilibrium with the Cs in the transport solution. Nevertheless, after about 16 days, the mass flux of Cs turned into positive value, indicating a break through migration of Cs. After about 50 days, the

mass flux is almost constant: a steady-state diffusion state is reached. The diffusive flux of Cs is about $6.8 \cdot 10^{-9}$ mol/(m^2 s). The thickness of the sample is 20 mm. The calculated diffusion coefficient according to equation (6.1) is $3.53 \cdot 10^{-10}$ m^2/s. In comparison to the value obtained with the traditional method, the result is almost identical. But the time needed for the experiment with the modified method was only less than 1/3 of that with the traditional method.

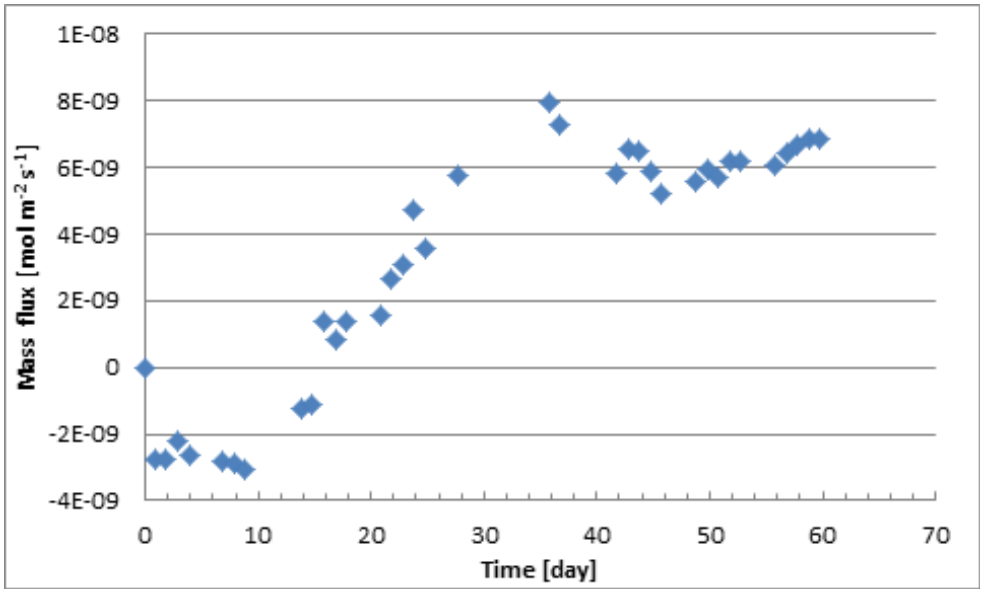

Fig. 9.3 Mass flux of Cs measured by using the modified through-diffusion method

Therefore the modified method is adopted for the further diffusion coefficient determinations.

9.4 Solution type and diffusion coefficient

The diffusion experiments of heavy metals Pb, Cd and Cs in three different background solution types (50 % NaCl, 90 % NaCl and 90 % IP21) were undertaken with compacted bentonite in different dry densities (1,400 kg/m^3, 1,600 kg/m^3 and 1,800 kg/m^3). The results are described in Fig. 9.4 to Fig. 9.6, Tab. 9.2 to Tab. 9.4. In the following subsections, the effects of background solutions on the diffusion coefficient of heavy metals through bentonite are discussed in three different dry densities of the compacted MX-bentonite.

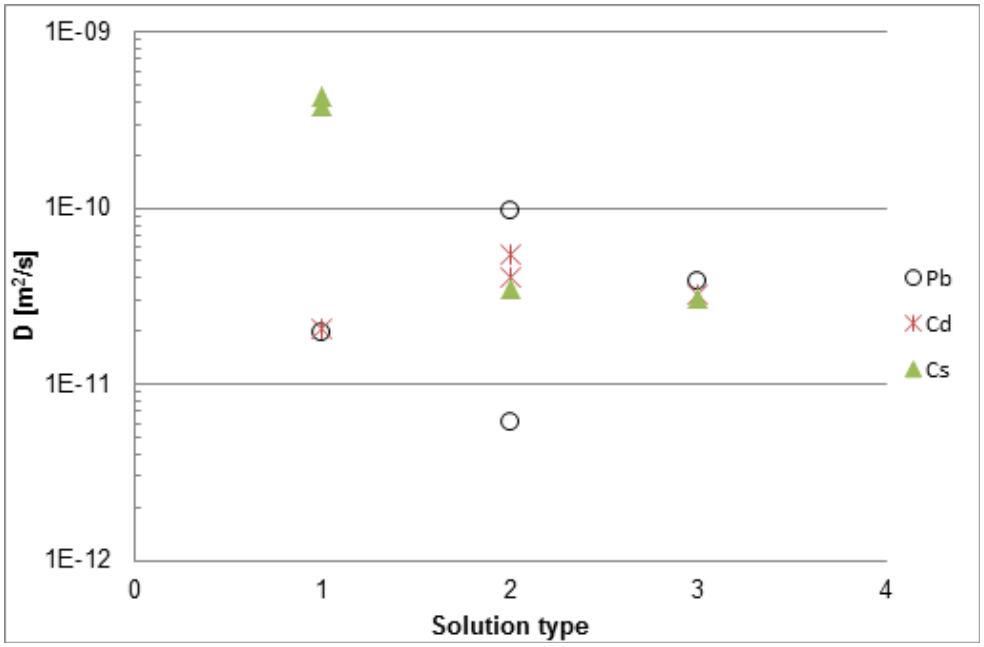

Fig. 9.4 Measured diffusion coefficient values (D) and correlation to the background solution types (1 – 50 % NaCl, 2 – 90 % NaCl and 3 – 90 % IP21) for compacted MX-bentonite with dry density 1,400 kg/m^3

9.4.1 Dry density of 1,400 kg/m^3

For the samples with dry density of 1,400 kg/m^3 as shown in Fig. 9.4, the diffusion coefficient of Cs decrease from $4.09 \cdot 10^{-10}$ m^2/s in 50 % NaCl solution to $3.5 \cdot 10^{-11}$ m^2/s in 90 % NaCl solution (Tab. 9.2). The diffusion coefficient of Cs in 90 % IP21 solution is $3.11 \cdot 10^{-11}$ m^2/s. The averaged diffusion coefficients of Cd and Pb are quite similar, i. e. $2.0 \cdot 10^{-11}$ m^2/s in 50 % NaCl solution and $5.0 \cdot 10^{-11}$ m^2/s in 90 % NaCl solution. The diffusion coefficients of all three heavy metals Pb, Cd and Cs are almost the same in the background solution of 90 % IP21. The trends of Cd and Pb in the relatively low dry density are thus not very clear for the background solution owing to the limited measurements.

Tab. 9.2 Measured diffusion coefficient of Pb, Cd and Cs in different background solutions through compacted MX-80 bentonite with dry density of 1,400 kg/m^3

Contaminant		Diffusion coefficient [m^2/s]		
Background solution type		50 % NaCl solution	90 % NaCl solution	90 % IP21 solution
Number of experiments		2	2	1
Pb	minimum	$1.96 \cdot 10^{-11}$	$6.12 \cdot 10^{-12}$	
	maximum	$1.96 \cdot 10^{-11}$	$9.61 \cdot 10^{-11}$	
	averaged	$1.96 \cdot 10^{-11}$	$5.11 \cdot 10^{-11}$	$3.89 \cdot 10^{-11}$
Cd	minimum	$2.05 \cdot 10^{-11}$	$4.08 \cdot 10^{-11}$	
	maximum	$2.05 \cdot 10^{-11}$	$5.48 \cdot 10^{-11}$	
	averaged	$2.05 \cdot 10^{-11}$	$4.78 \cdot 10^{-11}$	$3.20 \cdot 10^{-11}$
Cs	minimum	$3.82 \cdot 10^{-10}$	$3.50 \cdot 10^{-11}$	
	maximum	$4.35 \cdot 10^{-10}$	$3.50 \cdot 10^{-11}$	
	averaged	$4.09 \cdot 10^{-10}$	$3.50 \cdot 10^{-11}$	$3.11 \cdot 10^{-11}$

9.4.2 Dry density of 1,600 kg/m^3

More experiments have been undertaken on bentonite compacted to 1,600 kg/m^3, because it is the most likely density of compacted bentonite to be applied in the practice. The influence of the background solution on the diffusion coefficient is more apparent as shown in Fig. 9.5 and Tab. 9.3. The diffusion coefficients decrease with the increase of the salinity in the background solution for all three heavy metals Pb, Cd and Cs. The diffusion coefficient of Cd decreases from $6.4 \cdot 10^{-11}$ m^2/s in 50 % NaCl background solution to $2.50 \cdot 10^{-11}$ m^2/s in 90 % NaCl background solution and $1.58 \cdot 10^{-11}$ m^2/s in 90 % IP21 background solution. The diffusion coefficient of Pb decreases from $1.10 \cdot 10^{-10}$ m^2/s in 50 % NaCl background solution to $7.83 \cdot 10^{-11}$ m^2/s in 90 % NaCl background solution, and $1.42 \cdot 10^{-11}$ m^2/s in 90 % IP21 background solution. The diffusion coefficient of Cs decreases from $3.74 \cdot 10^{-10}$ m^2/s in 50 % NaCl background solution to $2.76 \cdot 10^{-11}$ m^2/s in 90 % NaCl background solution, and $3.55 \cdot 10^{-11}$ m^2/s in 90 % IP21 background solution. The diffusion coefficients of Pb, Cd and Cs in 90 % IP21 background solutions are very close.

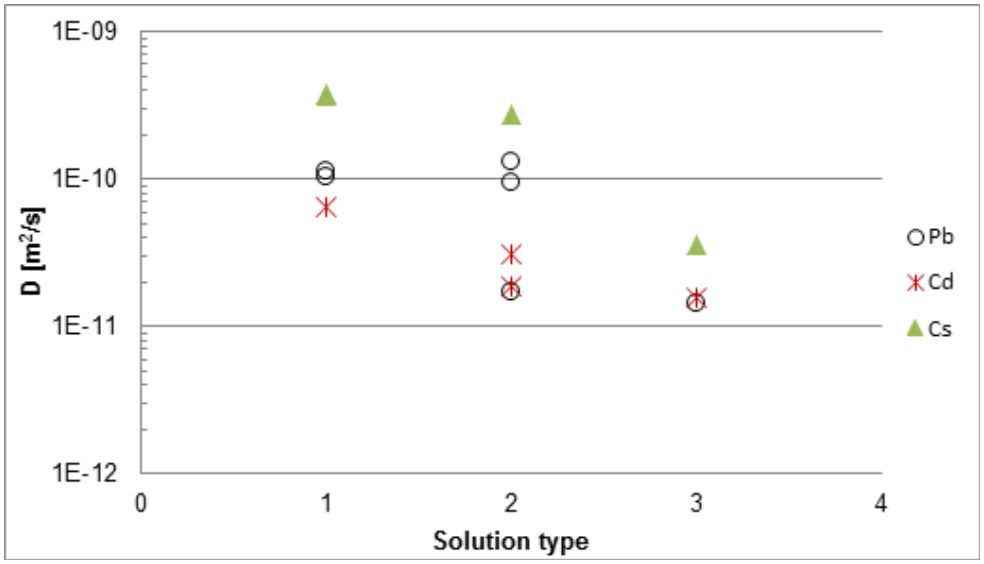

Fig. 9.5 Measured diffusion coefficient values (D) and correlation to the background solution types (1 – 50 % NaCl, 2 – 90 % NaCl and 3 – 90 % IP21) for compacted MX-bentonite with dry density of 1,600 kg/m^3

Tab. 9.3 Measured diffusion coefficient of Pb, Cd and Cs in different background solutions through compacted MX-80 bentonite with dry density of 1,600 kg/m^3

Contaminant		Diffusion coefficient [m^2/s]		
Background solution type		50 %. NaCl solution	90 %. NaCl solution	90 %. IP21 solution
Number of experiments		3	3	1
Pb	minimum	$1.05 \cdot 10^{-10}$	$7.80 \cdot 10^{-12}$	
	maximum	$1.14 \cdot 10^{-10}$	$1.33 \cdot 10^{-10}$	
	averaged	$1.10 \cdot 10^{-10}$	$7.83 \cdot 10^{-11}$	$1.42 \cdot 10^{-11}$
Cd	minimum	$6.40 \cdot 10^{-11}$	$1.89 \cdot 10^{-11}$	
	maximum	$6.41 \cdot 10^{-11}$	$3.10 \cdot 10^{-11}$	
	averaged	$6.41 \cdot 10^{-11}$	$2.50 \cdot 10^{-11}$	$1.58 \cdot 10^{-11}$
Cs	minimum	$3.71 \cdot 10^{-10}$	$2.76 \cdot 10^{-10}$	
	maximum	$3.77 \cdot 10^{-10}$	$2.76 \cdot 10^{-10}$	
	averaged	$3.74 \cdot 10^{-10}$	$2.76 \cdot 10^{-10}$	$3.55 \cdot 10^{-11}$

9.4.3 Dry density of 1,800 kg/m^3

Further diffusion experiments were undertaken for densely compacted MX-80 bentonite with dry density in 1,800 kg/m^3. The test durations of each experiment are much longer

than the other experiments with lower densities mentioned above owing to the much lower hydraulic permeability. Therefore, only one experiment for each heavy metal in three different background solutions except Cd in 50 % NaCl solution was successfully performed. The test results are shown in Fig. 9.6 and Tab. 9.4. The diffusion coefficient of Cs decreases with the increase of the ionic strength of the background solution. The diffusion coefficient of Cs decreases from $2.18 \cdot 10^{-10}$ m^2/s in 50 % NaCl background solution to $5.19 \cdot 10^{-11}$ m^2/s in 90 % NaCl background solution, and $2.10 \cdot 10^{-11}$ m^2/s in 90 % IP21 background solution. The diffusion coefficient of Pb decreases from $3.56 \cdot 10^{-11}$ m^2/s in 50 % NaCl background solution to $5.10 \cdot 10^{-11}$ m^2/s in 90 % NaCl background solution, but increased to $2.10 \cdot 10^{-11}$ m^2/s in 90 % IP21 background solution. The diffusion coefficient of Cd is $6.54 \cdot 10^{-12}$ m^2/s in 90 % NaCl background solution and $3.12 \cdot 10^{-11}$ m^2/s in 90 % IP21 background solution. The diffusion coefficients of Pb, Cd and Cs in 90 % IP21 background solutions are also very close to each other. The diffusion coefficients of Cs in NaCl background solutions (50 % - and 90 %-NaCl solutions) are higher than those of Pb and Cd.

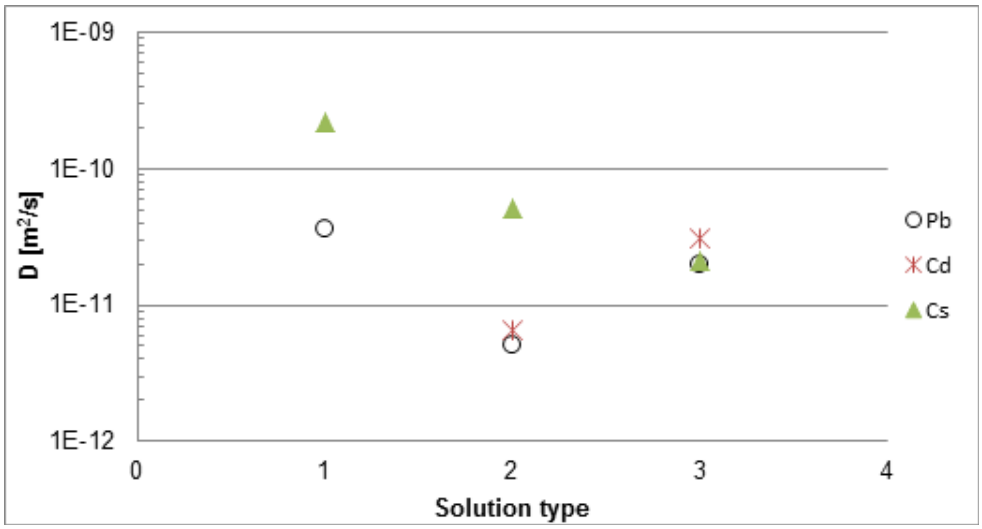

Fig. 9.6 Measured diffusion coefficient values and correlation to the background solution types (1 – 50 % NaCl, 2 – 90 % NaCl and 3 – 90 % IP21) for compacted MX-bentonite with dry density of 1,800 kg/m^3

Based on the measured diffusion coefficients mentioned above, it is interesting to note that the diffusion coefficients of heavy metal Cs decrease with the ionic strength of the background solutions; the averaged diffusion coefficients of heavy metals Pb and Cd migrating through compacted MX-80 bentonite with the same dry density decrease with

the ionic strength values of the background solutions for samples with densities up to 1,600 kg/m^3. Nevertheless, this trend is also valid for Pb in the NaCl solutions.

Tab. 9.4 Measured diffusion coefficient of Pb, Cd and Cs in different background solutions through compacted MX-80 bentonite with dry density of 1,800 kg/m^3

Contaminant	**Diffusion coefficient [m^2/s]**		
Background solution type	50 %. NaCl solution	90 %. NaCl solution	90 %. IP21 solution
Number of experiments	1	1	1
Pb	$3.56 \cdot 10^{-11}$	$5.10 \cdot 10^{-12}$	$1.97 \cdot 10^{-11}$
Cd	n. d.	$6.539 \cdot 10^{-12}$	$3.12 \cdot 10^{-11}$
Cs	$2.18 \cdot 10^{-10}$	$5.19 \cdot 10^{-11}$	$2.10 \cdot 10^{-11}$

n. d. – not determined

9.5 Dry density of bentonite on the diffusion coefficient

Dry density determines the pore volume in the bentonite and influences the migration of contaminates through it. Generally, higher porosity favours the migration of contaminants. Therefore, the diffusion coefficient of bentonite decreases with the increase of dry density of the samples. On the other hand side, the surface diffusion phenomena in highly compacted bentonite is also discussed in the literature /KIM 93/, /OSC 94/. In the following subsections the diffusion parameters and their dependence on the dry density are discussed in three groups based on their background solution types.

9.5.1 Diffusion of heavy metals in 50 % NaCl solution

Diffusion experiments of heavy metals Pb, Cd and Cs in 50 % NaCl background solution were undertaken with compacted MX-80 bentonite in different dry densities (i. e. 1,400 kg/m^3, 1,600 kg/m^3 and 1,800 kg/m^3 respectively). The results are shown in Fig. 9.7 and Tab. 9.5. The experiment with 1,400 kg/m^3 unexpectedly encountered difficulties in pure diffusion set-up owing to its relatively higher porosity and higher permeability. Small difference in the hydraulic gradient might result in advective transport in the sample. The flow direction depends on the hydraulic gradient. Therefore, if the hydraulic gradient is opposite to the concentration gradient, total mass transport will be

reduced in comparison to the pure diffusion case. The diffusion coefficients of Cs decrease with the increase of the density of the bentonite samples. The diffusion coefficients of Pb decrease with the increase of the density of the bentonite samples except for the value with the dry density of bentonite in 1,400 kg/m^3 Fig. 9.7.

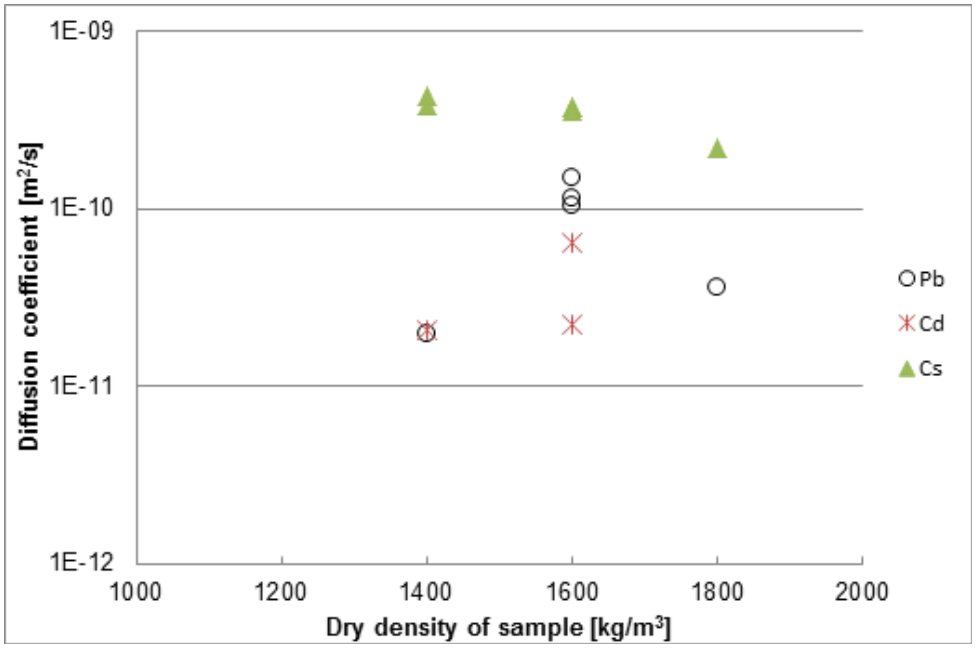

Fig. 9.7 Diffusion coefficients of Pb, Cd and Cs measured in 50 % NaCl-solution through compacted bentonite with different dry densities

Tab. 9.5 Measured diffusion coefficient of Pb, Cd and Cs in 50 % NaCl background solutions through compacted MX-80 bentonite with different dry densities

Contaminant		**Diffusion coefficient in [m^2/s]**		
MX-80 bentonite dry density		1,400 kg/m^3	1,600 kg/m^3	1,800 kg/m^3
Number of experiments		2	4	1
Pb	minimum		$1.05 \cdot 10^{-10}$	
	maximum		$1.48 \cdot 10^{-10}$	
	averaged	$1.96 \cdot 10^{-11}$	$1.22 \cdot 10^{-10}$	$3.56 \cdot 10^{-11}$
Cd	minimum		$2.05 \cdot 10^{-11}$	
	maximum		$6.40 \cdot 10^{-11}$	
	averaged	$2.05 \cdot 10^{-11}$	$4.23 \cdot 10^{-11}$	n. d.
Cs	minimum	$3.82 \cdot 10^{-10}$	$3.53 \cdot 10^{-10}$	
	maximum	$4.35 \cdot 10^{-10}$	$3.77 \cdot 10^{-10}$	
	averaged	$4.09 \cdot 10^{-10}$	$3.67 \cdot 10^{-10}$	$2.18 \cdot 10^{-10}$

n. d. – not determined

9.5.2 Diffusion of heavy metals in 90 % NaCl solution

The Diffusion experiments of heavy metals Pb, Cd and Cs in 90 %. NaCl background solution were undertaken with compacted MX-80 bentonite in different dry densities (i. e. 1,200 kg/m^3, 1,400 kg/m^3, 1,600 kg/m^3 and 1,800 kg/m^3 respectively). The results are shown in Fig. 9.8 and Tab. 9.6. The experiments on 1,200 kg/m^3 samples encountered difficulties owing to the high porosity related canal formation by the intrusion of highly saline solution. Another problem is the blockage in the sample and/or in the apparatus owing to salt precipitation induced by small thermodynamic condition changes (i. e. temperature in winter) for the nearly saturated solution. On the other hand side it is also very unlikely to use bentonite in such low density as engineered sealing material. Therefore, only one experiment was undertaken for the determination of the diffusion coefficient of Cd with $2.58 \cdot 10^{-10}$ m^2/s as shown in Fig. 9.8.

The results showed that the diffusion coefficients of Cd decreases with the increase of the dry densities of the MX-80 bentonite samples from $2.58 \cdot 10^{-10}$ m^2/s by a dry density of 1,200 kg/m^3 to $6.54 \cdot 10^{-12}$ m^2/s by a dry density of 1,800 kg/m^3. The diffusion coefficients of Cs decreases with the increase of the dry densities of the MX-80 bentonite samples from $2.76 \cdot 10^{-10}$ m^2/s by a dry density of 1,600 kg/m^3 to $6.5.19 \cdot 10^{-11}$ m^2/s by a dry density of 1,800 kg/m^3. The averaged diffusion coefficients of Pb decreases with the increase of the dry densities of the MX-80 bentonite samples from $7.85 \cdot 10^{-11}$ m^2/s by a dry density of 1,600 kg/m^3 to $5.10 \cdot 10^{-12}$ m^2/s by a dry density of 1,800 kg/m^3.

Tab. 9.6 Measured diffusion coefficient of Pb, Cd and Cs in 90 % NaCl background solutions through compacted MX-80 bentonite with different dry densities

Contaminant		**Diffusion coefficient in [m^2/s]**		
MX-80 bentonite dry density		1,400 kg/m^3	1,600 kg/m^3	1,800 kg/m^3
Number of experiments		2	3	1
Pb	minimum	$6.12 \cdot 10^{-12}$	$1.70 \cdot 10^{-11}$	-
	maximum	$9.61 \cdot 10^{-11}$	$1.33 \cdot 10^{-10}$	-
	averaged	$5.11 \cdot 10^{-11}$	$7.85 \cdot 10^{-11}$	$5.10 \cdot 10^{-12}$
Cd	minimum	$4.08 \cdot 10^{-11}$	$1.89 \cdot 10^{-11}$	-
	maximum	$5.48 \cdot 10^{-11}$	$3.10 \cdot 10^{-11}$	-
	averaged	$4.78 \cdot 10^{-11}$	$2.50 \cdot 10^{-11}$	$6.54 \cdot 10^{-12}$
Cs	minimum	-	$2.76 \cdot 10^{-10}$	-
	maximum	-	$2.76 \cdot 10^{-10}$	-
	averaged	$3.50 \cdot 10^{-11}$	$2.76 \cdot 10^{-10}$	$5.19 \cdot 10^{-11}$

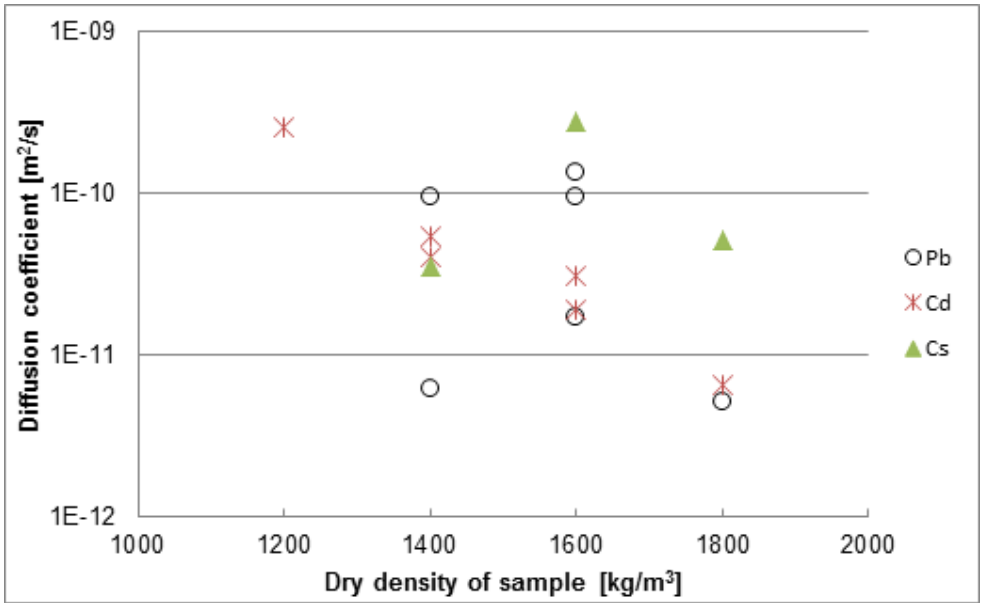

Fig. 9.8 Diffusion coefficients of Pb, Cd and Cs measured in 90 % NaCl-solution through compacted bentonite with different dry densities

9.5.3 Diffusion of heavy metals in 90 % IP21 solution

The Diffusion experiments of heavy metals Pb, Cd and Cs in 90 %. IP21 background solution were undertaken with compacted MX-80 bentonite in different dry densities (i. e. 1,400 kg/m^3, 1,600 kg/m^3 and 1,800 kg/m^3 respectively). The results are shown in Fig. 9.9 and Tab. 9.7. The main problem is the blockage in the sample and/or in the apparatus owing to salt precipitation induced by small thermodynamic condition changes (i. e. temperature in winter) for the extremely high ionic strength of the IP21 solution.

Tab. 9.7 Measured diffusion coefficient of Pb, Cd and Cs in 90 % IP21 background solutions through compacted MX-80 bentonite with different dry densities

Contaminant	**Diffusion coefficient [m^2/s]**		
MX-80 bentonite dry density	1,400 kg/m^3	1,600 kg/m^3	1,800 kg/m^3
Number of experiments	1	1	1
Pb	$3.89 \cdot 10^{-11}$	$1.42 \cdot 10^{-11}$	$1.97 \cdot 10^{-11}$
Cd	$3.20 \cdot 10^{-11}$	$1.58 \cdot 10^{-11}$	$3.12 \cdot 10^{-11}$
Cs	$3.11 \cdot 10^{-11}$	$3.55 \cdot 10^{-11}$	$2.10 \cdot 10^{-11}$

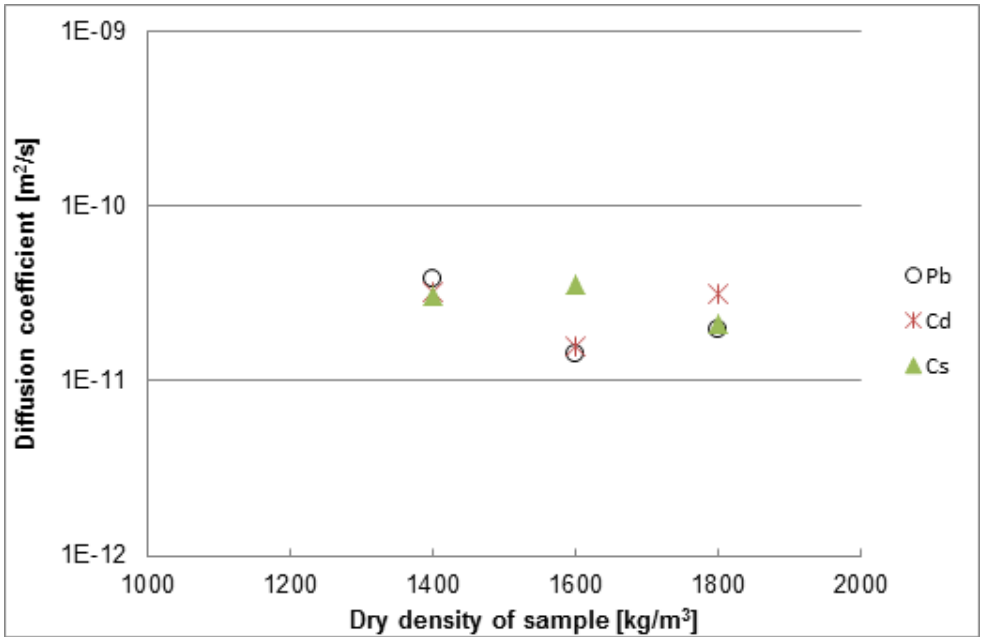

Fig. 9.9 Diffusion coefficients of Pb, Cd and Cs measured in 90 % IP21-solution through compacted bentonite with different dry densities

The results showed that the diffusion coefficients of all three heavy metals in the 90 % IP21 background solution are almost the same for the same dry density level and decrease slightly with the increase of the density. All measured diffusion coefficients are within the narrow range between $1.4 \cdot 10^{-11}$ m^2/s and $3.89 \cdot 10^{-11}$ m^2/s.

10 Heavy metal adsorption batch experiments

In order to find the sorption properties of heavy metals Pb, Cd and Cs from highly saline solutions by MX-80 bentonite, a systematic sorption batch experiment were undertaken.

10.1 Materials

MX-80 bentonite and solutions of NaCl with different saturation degree were used for the batch experiment.

10.2 Preparation of batch experiments

The test series were prepared with sodium chloride concentrations of 100 %, 90 %, 50 %, 30 %, 10 % and magnesium chloride (IP21) concentration of 90 %. The solutions were filled into bottles of glass and mixed with a defined mass of bentonite (see Tab. 5.2). The concentration of the added tracer cocktail (Cadmium, Cesium, Lead) varied between 10^{-6} to 10^{-3} mol kg^{-1}. To reach equilibrium, the mixtures were shaken by turning head over for at least 2 weeks. Then die equilibrium solution was eluted, centrifuged and the chemical composition analyzed.

10.3 Adsorption of heavy metals in NaCl background solutions by bentonite

The batch experiments on the adsorption of Pb, Cs and Cd from NaCl background solutions in different saturation degrees (10 %, 30 %, 50 %, 90 % and 100 %) were undertaken. The concentrations of the heavy metals Pb, Cs and Cd for each background solution are varied in four levels with 10^{-3} mol/L, 10^{-4} mol/L, 10^{-5} mol/L and 10^{-6} mol/L. At equilibrium the concentration of each heavy metal in the solution is measured. The sorbed amount of each heavy metal can be obtained by calculating the decrease of the heavy metal concentration times the amount of the solution. The sorption coefficient and sorption model of each heavy metal is obtained by plotting the equilibrium sorbed concentration vs. the equilibrium heavy metal concentration in the solution, and followed by regression calculation. All measurements can be well described by the con-

stant sorption model and/or FREUNDLICH sorption model, which are described in the following sections.

As the concentration of the background solution increases, cation Na^+ competes with heavy metals for the sorption sites of bentonite. It is thus common that with the increase of the background solution, the sorption coefficient of heavy metals decreases. Some of them might totally disappear. In the pure NaCl solution series at the current project, the same trend is observed: with the increase of the salinity, the adsorption coefficient of Pb, Cs or Cd decreases but not totally disappear. This proved that MX-80 bentonite has fairly strong sorption of Pb, Cs and Cd in saline NaCl.

10.3.1 Sorption in 100 % NaCl background solution

The batch experiments on the adsorption of Pb, Cs and Cd from 100 % NaCl background solutions were undertaken. The actual concentrations of Pb varied in four levels with 166.1 mg/L, 20.24 mg/L, 2.498 mg/L and 0.1506 mg/L. The results of the sorption experiments are plotted in Fig. 10.1. The calculated sorption models are LINEAR (R^2 = 0.96) and FREUNDLICH (R^2 = 0.95) models and the corresponding sorption coefficients are listed in Tab. 10.1. The k_d of Pb in 100 % NaCl solution is 6.8 ml/g.

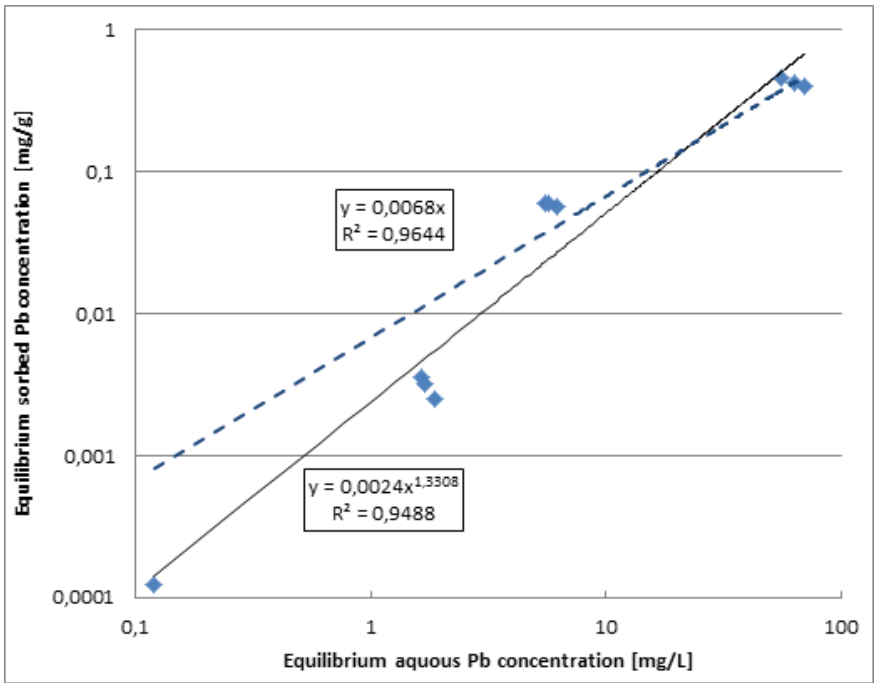

Fig. 10.1 Sorption of Pb in 100 % NaCl-solution by MX-80 bentonite

Tab. 10.1 Model and measured sorption coefficient of Pb, Cs and Cd in 100 % NaCl background solution by MX-80 bentonite

Contaminant	LINEAR		FREUNDLICH		
	k_d [L/g]	R^2	Kf [(mg/g)/(mg/L)^n]	n [-]	R^2
Pb	0.0068	0.96	0.0024	1.3308	0.95
Cs	0.0056	0.98	0.0122	0.8021	0.98
Cd	0.0003	0.50	0.0038	0.4085	0.96

The actual concentrations of Cs varied in four levels with 78.59 mg/L, 10.13 mg/L, 1.406 mg/L and 0.0715 mg/L. The results of the sorption experiments are plotted in Fig. 10.2. The calculated sorption models are LINEAR (R^2 = 0.98) and FREUNDLICH (R^2 = 0.98) models and the corresponding sorption coefficients are listed in Tab. 10.1. The k_d of Cs in 100 % NaCl solution is 5.6 ml/g, slightly lower than that of Pb.

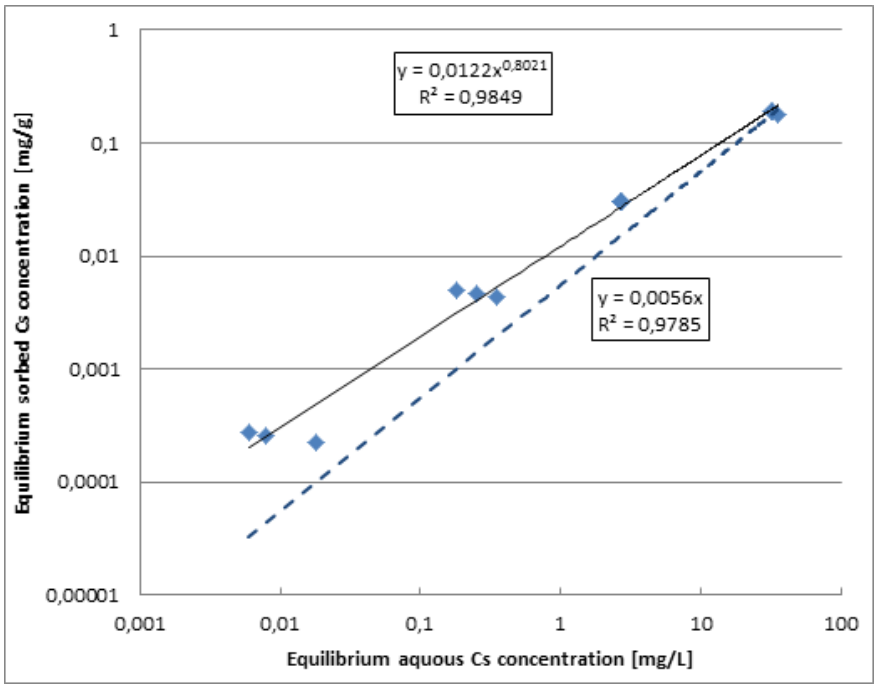

Fig. 10.2 Sorption of Cs in 100 % NaCl-solution by MX-80 bentonite

The actual concentrations of Cd varied in four levels with 92.7 mg/L, 17.63 mg/L, 2.237 mg/L and 0.09067 mg/L. The results of the sorption experiments are plotted in Fig. 10.3. The calculated sorption models are LINEAR (R^2 = 0.50) and FREUNDLICH (R^2 = 0.96) models. Therefore, the FREUNDLICH sorption model is more suitable for

Cd. The corresponding sorption coefficients are listed in Tab. 10.1. The k_d of Cd in 100 % NaCl solution is 0.3 ml/g, much lower than that of Pb or Cs.

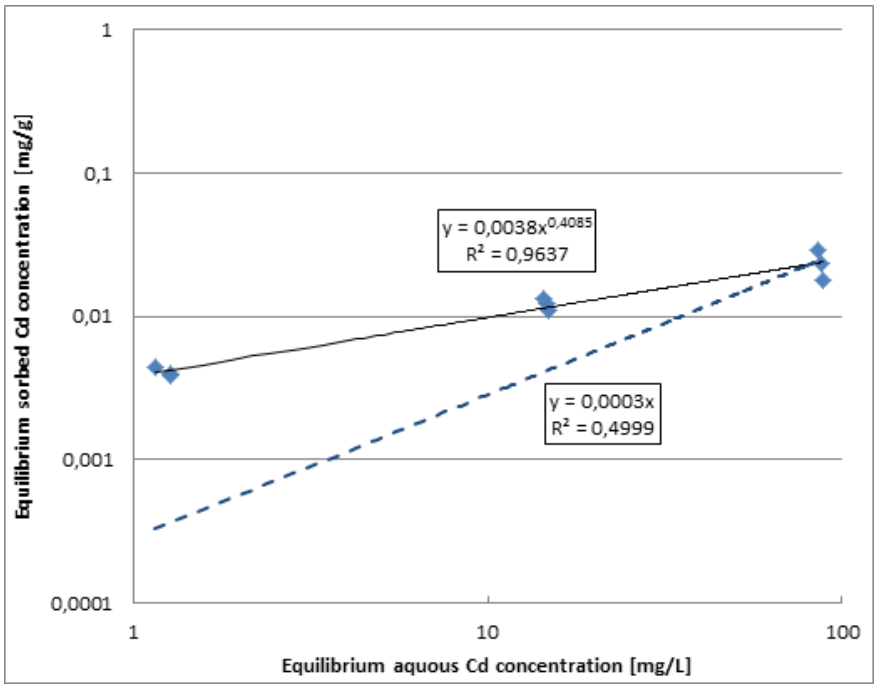

Fig. 10.3 Sorption of Cd in 100 % NaCl-solution by MX-80 bentonite

Based on the experiment results, MX-80 bentonite showed relatively high sorption of heavy metals Pb, Cs and weak sorption of Cd in 100 % saturated NaCl.

10.3.2 Sorption in 90 % NaCl background solution

The batch experiments on the adsorption of Pb, Cs and Cd from 90 % NaCl background solutions were undertaken. The actual concentrations of Pb varied in four levels with 203.7 mg/L, 18.04 mg/L, 1.853 mg/L and 0.630 mg/L. The results of the sorption experiments are plotted in Fig. 10.4. The calculated sorption models are LINEAR (R^2 = 0.96) and FREUNDLICH (R^2 = 0.92) models and the corresponding sorption coefficients are listed in Tab. 10.2. The k_d of Pb in 90 % NaCl solution is 11.8 ml/g, almost doubled than that in 100 % NaCl solution.

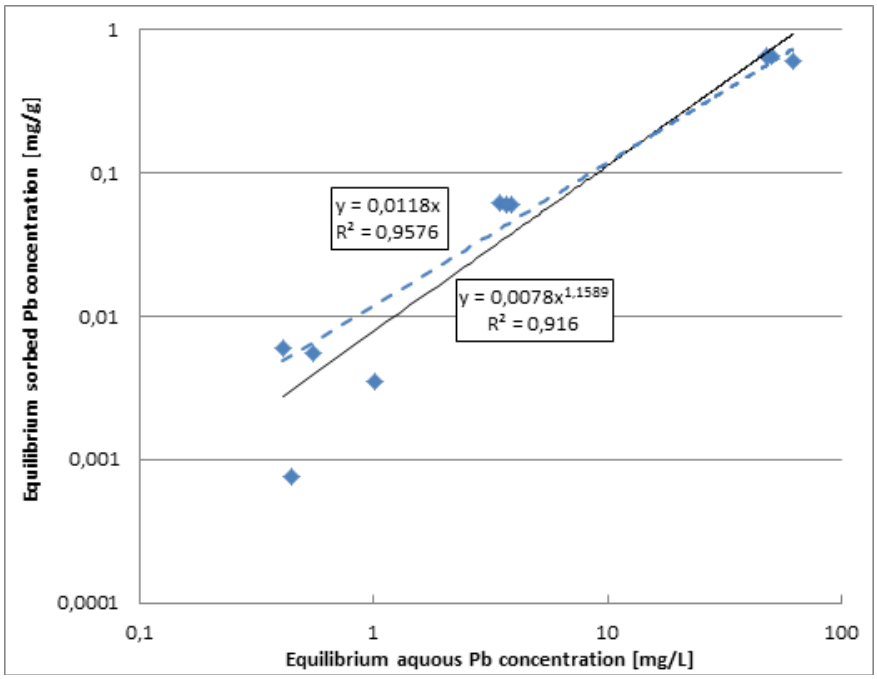

Fig. 10.4 Sorption of Pb in 90 % NaCl-solution by MX-80 bentonite

The actual concentrations of Cs varied in four levels with 85.41 mg/L, 11.21 mg/L, 0.905 mg/L and 0.1058 mg/L. The results of the sorption experiments are plotted in Fig. 10.5. The calculated sorption models are LINEAR (R^2 = 0.99) and FREUNDLICH (R^2 = 0.99) models and the corresponding sorption coefficients are listed in Tab. 10.2. The k_d of Cs in 90 % NaCl solution is 5.2 ml/g, much lower than that of Pb and almost the same as that in 100 % NaCl solution.

Tab. 10.2 Model and measured sorption coefficient of Pb, Cs and Cd in 90 % NaCl background solution by MX-80 bentonite

Contaminant	**LINEAR**		**FREUNDLICH**		
	k_d [L/g]	**R^2**	**Kf [(mg/g)/(mg/L)^n]**	**n [-]**	**R^2**
Pb	0.0118	0.96	0.0078	1.1589	0.92
Cs	0.0052	0.99	0.0123	0.7834	0.99
Cd	0.0010	0.98	0.0004	1.0551	0.90

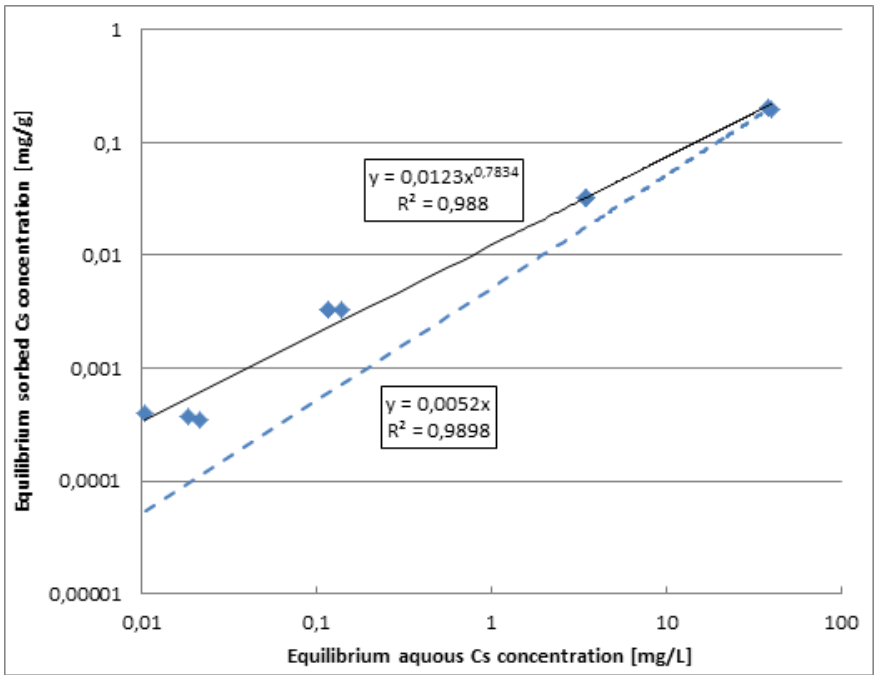

Fig. 10.5 Sorption of Cs in 90 % NaCl-solution by MX-80 bentonite

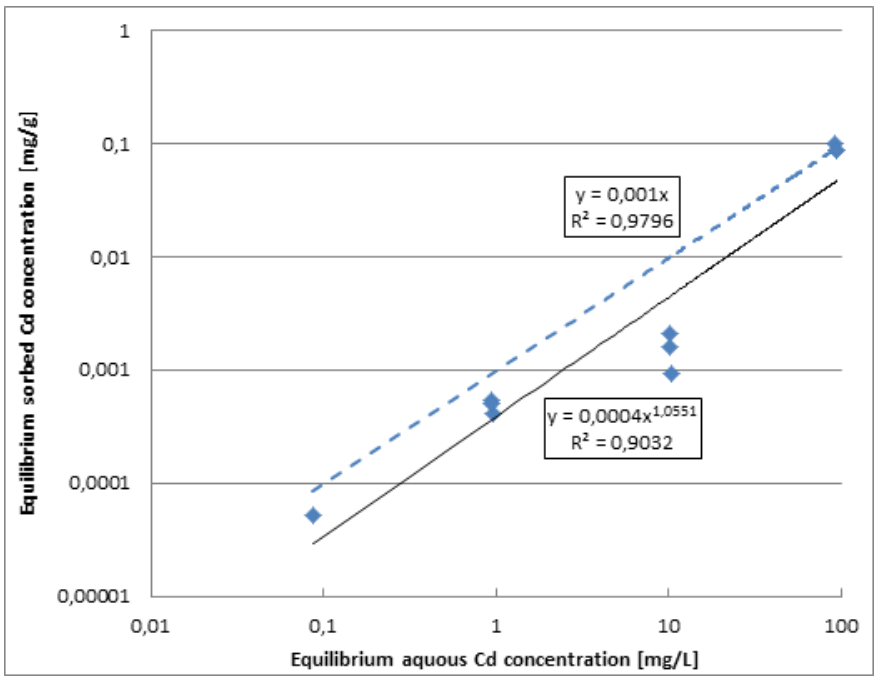

Fig. 10.6 Sorption of Cd in 90 % NaCl-solution by MX-80 bentonite

The actual concentrations of Cd varied in four levels with 114.5 mg/L, 10.55 mg/L, 1.069 mg/L and 0.09957 mg/L. The results of the sorption experiments are plotted in Fig. 10.6. The calculated sorption models are LINEAR (R^2 = 0.98) and FREUNDLICH (R^2 = 0.90) models. The corresponding sorption coefficients are listed in Tab. 10.2. The

k_d of Cd in 90 % NaCl solution is 1.0 ml/g, much lower than that of Pb or Cs but higher than that of Cd in 100 % NaCl solution.

Based on the experiment results, it is clear to see that the sorption coefficients of Pb and Cd increase with the 10 % decrease of the background NaCl solution. The k_d value of Pb almost doubles, while the k_d value of Cd increases from 0.3 ml/g to 1.0 ml/g. The k_d value of Cd is much lower than those of Pb and Cs.

10.3.3 Sorption in 50 % NaCl background solution

The batch experiments on the adsorption of Pb, Cs and Cd from 50 % NaCl background solutions were undertaken. However, the experiments of Pb were not successful.

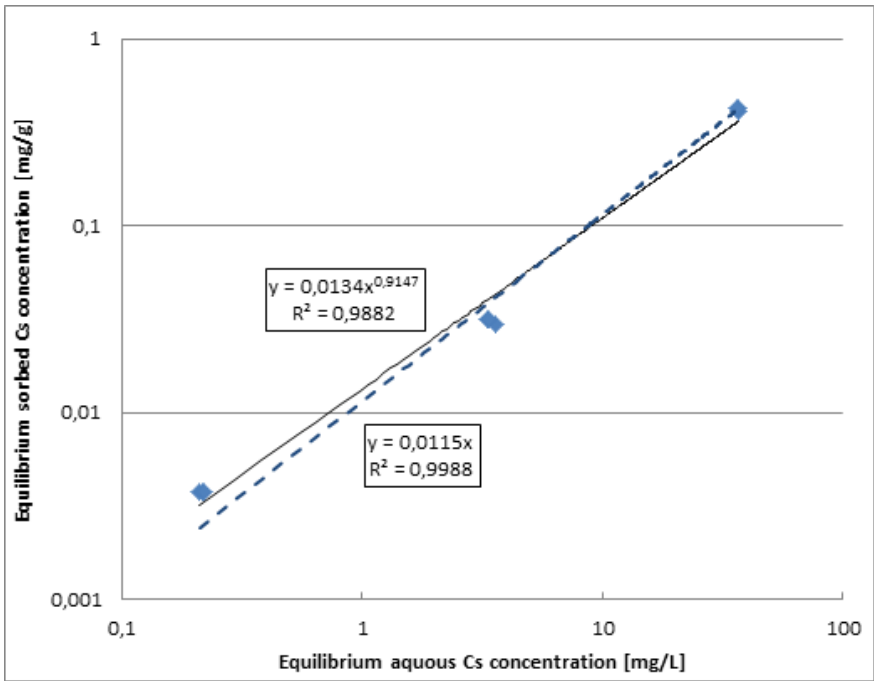

Fig. 10.7 Sorption of Cs in 50 % NaCl-solution by MX-80 bentonite

The actual concentrations of Cs varied in four levels with 128.7 mg/L, 10.38 mg/L, 1.053 mg/L and 0.058 mg/L. The results of the sorption experiments are plotted in Fig. 10.7. The calculated sorption models are LINEAR (R^2 = 1.00) and FREUNDLICH (R^2 = 0.99) models and the corresponding sorption coefficients are listed in Tab. 10.3. The k_d of Cs in 50 % NaCl solution is 11.5 ml/g, much higher than that in 100 % NaCl solution in 5.6 ml/g.

Tab. 10.3 Model and measured sorption coefficient of Pb, Cs and Cd in 50 % NaCl background solution by MX-80 bentonite

Contaminant	LINEAR		FREUNDLICH		
	k_d [L/g]	R^2	Kf [(mg/g)/(mg/L)^n]	n [-]	R^2
Pb	-		-	-	
Cs	0.0115	1.00	0.0134	0.9147	0.99
Cd	0.0026	0.99	0.0031	0.9758	0.98

The actual concentrations of Cd varied in four levels with 109.8 mg/L, 11.47 mg/L, 1.222 mg/L and 0.1173 mg/L. The results of the sorption experiments are plotted in Fig. 10.8. The calculated sorption models are LINEAR (R^2 = 0.99) and FREUNDLICH (R^2 = 0.98) models. The corresponding sorption coefficients are listed in Tab. 10.3. The k_d of Cd in 50 % NaCl solution is 2.6 ml/g, much lower than that of Cs but much higher than that of Cd in 100 % NaCl solution.

Based on the experiment results, it is clear to see that the sorption coefficients of Cs and Cd increase further with the decrease of the background NaCl solution.

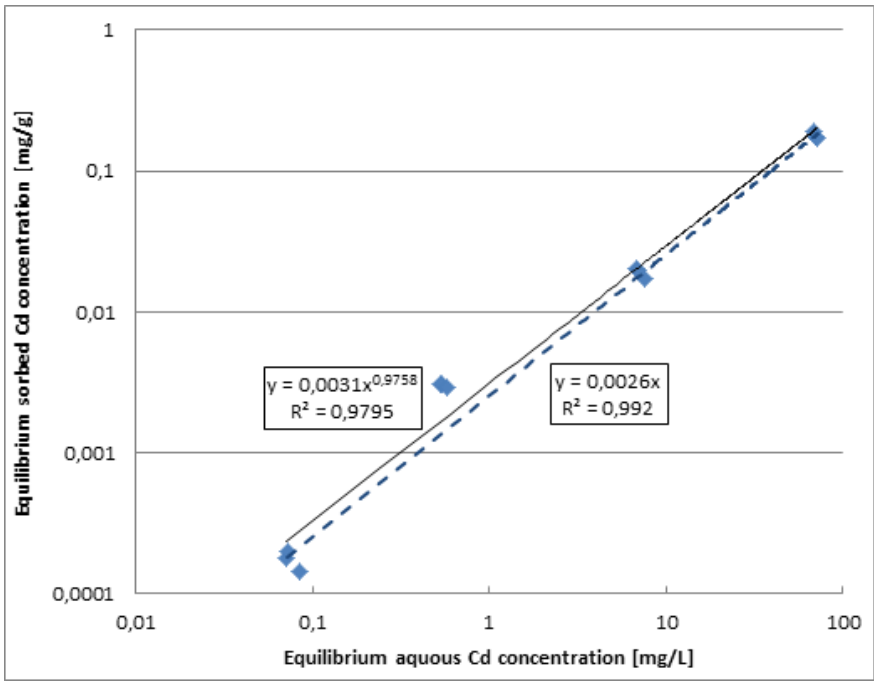

Fig. 10.8 Sorption of Cd in 50 % NaCl-solution by MX-80 bentonite

10.3.4 Sorption in 30 % NaCl background solution

The batch experiments on the adsorption of Pb, Cs and Cd from 30 % NaCl background solutions were undertaken. The actual concentrations of Pb varied in four levels with 216.9 mg/L, 24.61 mg/L, 3.315 mg/L and 0.243 mg/L. The results of the sorption experiments are plotted in Fig. 10.9. The calculated sorption models are LINEAR (R^2 = 0.96) and FREUNDLICH (R^2 = 0.80) models and the corresponding sorption coefficients are listed in Tab. 10.4. The k_d of Pb in 30 % NaCl solution is 49.6 ml/g, much higher than that in 100 % NaCl solution with 6.8 ml/g.

Tab. 10.4 Model and measured sorption coefficient of Pb, Cs and Cd in 30 % NaCl background solution by MX-80 bentonite

Contaminant	LINEAR		FREUNDLICH		
	k_d [L/g]	R^2	Kf [(mg/g)/(mg/L)^n]	n [-]	R^2
Pb	0.0496	0.96	0.0349	1.0076	0.81
Cs	0.0087	1.00	0.0119	0.9323	1.00
Cd	0.0111	0.99	0.0144	0.9485	1.00

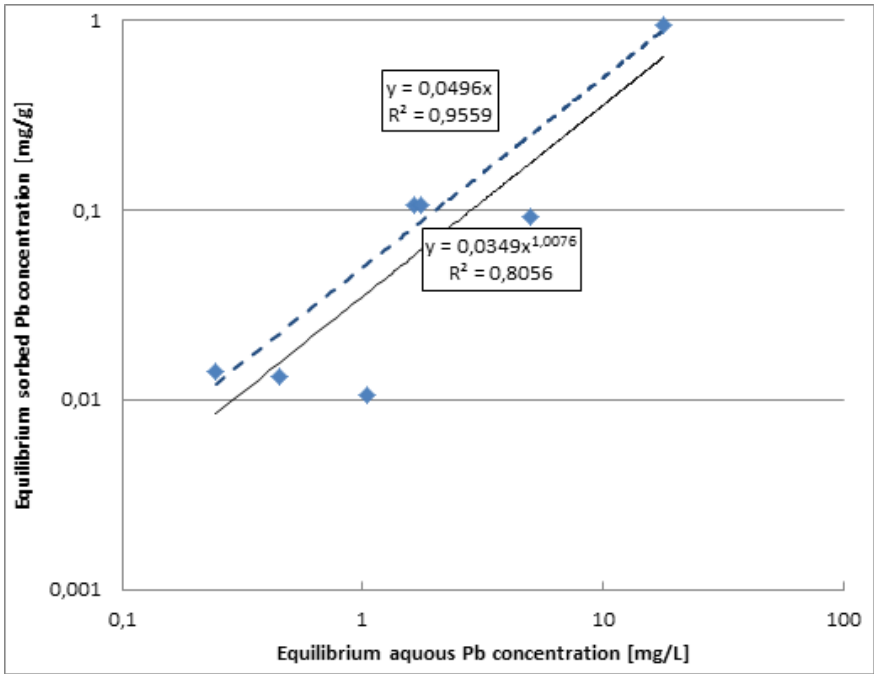

Fig. 10.9 Sorption of Pb in 30 % NaCl-solution by MX-80 bentonite

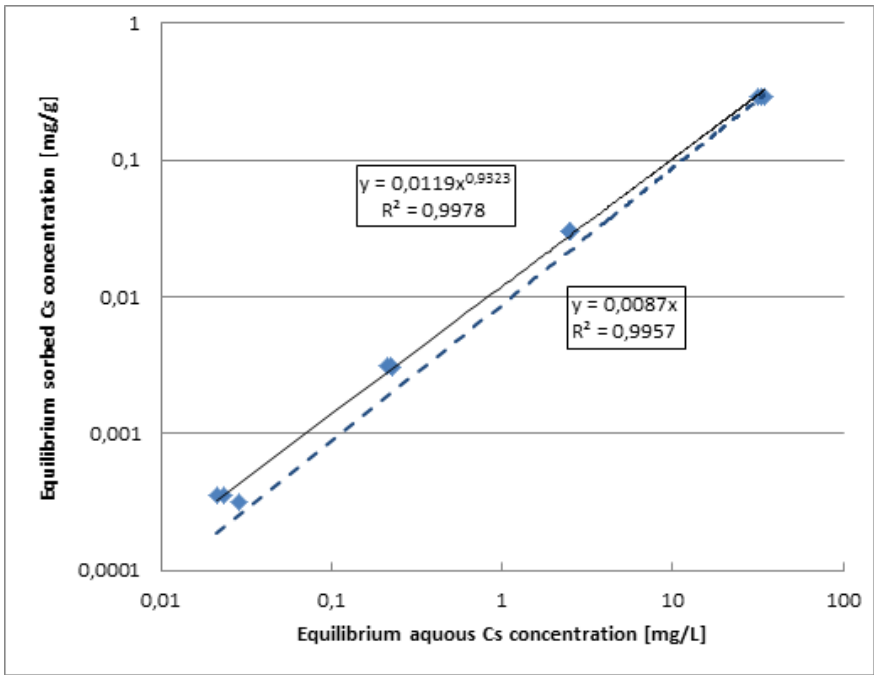

Fig. 10.10 Sorption of Cs in 30 % NaCl-solution by MX-80 bentonite

The actual concentrations of Cs varied in four levels with 95.81 mg/L, 8.951 mg/L, 0.8956 mg/L and 0.0972 mg/L. The results of the sorption experiments are plotted in Fig. 10.5. The calculated sorption models are LINEAR (R^2 = 1.00) and FREUNDLICH (R^2 = 1.00) models and the corresponding sorption coefficients are listed in Tab. 10.4. The k_d of Cs in 30 % NaCl solution is 8.7 ml/g, much lower than that of Pb.

The actual concentrations of Cd varied in four levels with 111.3 mg/L, 14.72 mg/L, 1.498 mg/L and 0.1272 mg/L. The results of the sorption experiments are plotted in Fig. 10.11. The calculated sorption models are LINEAR (R^2 = 0.99) and FREUNDLICH (R^2 = 1.00) models. The corresponding sorption coefficients are listed in Tab. 10.4. The k_d of Cd in 30 % NaCl solution is 11.1 ml/g, higher than that of Cs and much higher than that of Cd in 100 % NaCl solution.

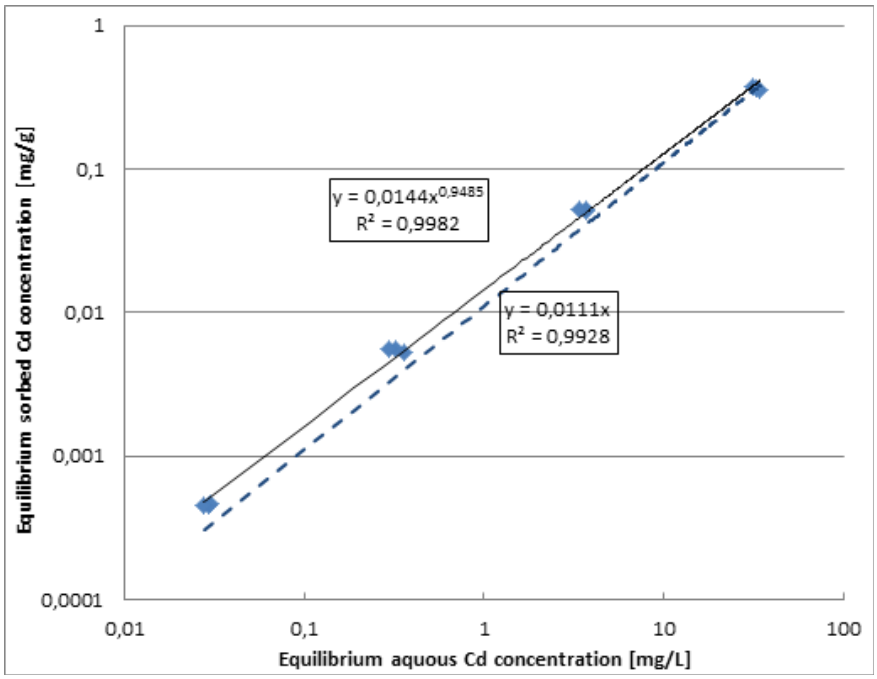

Fig. 10.11 Sorption of Cd in 30 % NaCl-solution by MX-80 bentonite

Based on the experiment results, it is clear to see that the sorption coefficients of Pb, Cs and Cd increase further with the decrease of the background NaCl solution. The k_d value of Cd increases dramatically from 0.3 ml/g in 100 % NaCl solution to 2.6 ml/g in 50 % NaCl solution to 11.1 ml/g in 30 % NaCl solution.

10.3.5 Sorption in 10 % NaCl background solution

The batch experiments on the adsorption of Pb, Cs and Cd from 50 % NaCl background solutions were undertaken. However, the experiments of Pb were not successful. The reason is not clear, might be the rapid sorption effect by such lower background solution, which leads to the measured results as no Pb in the solution can be detected.

The actual concentrations of Cs varied in four levels with 91.37 mg/L, 10.22 mg/L, 0.9587 mg/L and 0.1097 mg/L. The results of the sorption experiments are plotted in Fig. 10.12. The calculated sorption models are LINEAR (R^2 = 0.99) and FREUNDLICH (R^2 = 1.00) models and the corresponding sorption coefficients are listed in Tab. 10.5. The k_d of Cs in 10 % NaCl solution is 16.7 ml/g, much higher than that in 100 % NaCl solution in 5.6 ml/g.

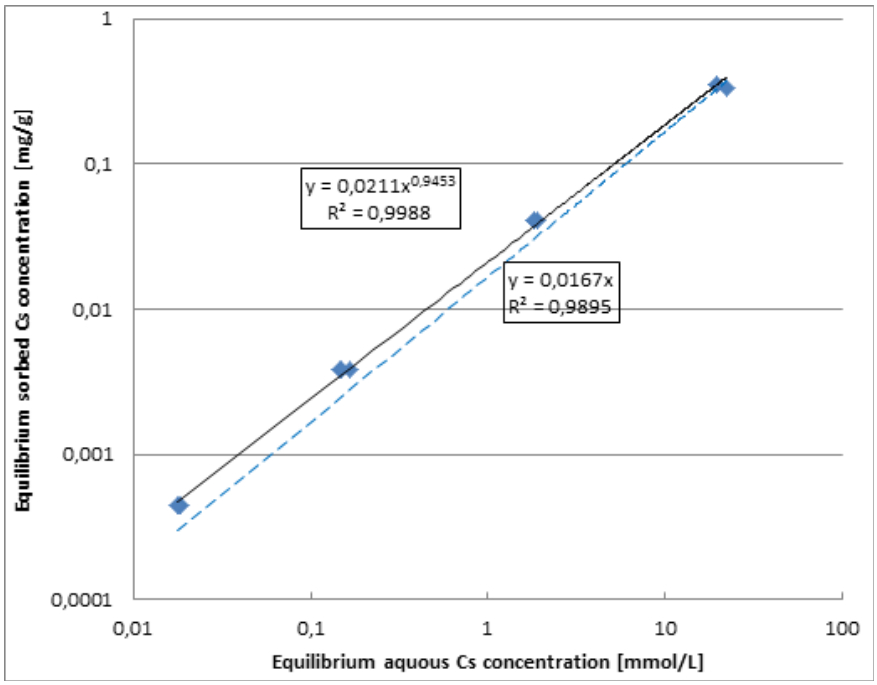

Fig. 10.12 Sorption of Cs in 10 % NaCl-solution by MX-80 bentonite

Tab. 10.5 Model and measured sorption coefficient of Pb, Cs and Cd in 10 % NaCl background solution by MX-80 bentonite

Contaminant	LINEAR		FREUNDLICH		
	k_d [L/g]	R^2	Kf [(mg/g)/(mg/L)^n]	n [-]	R^2
Pb	-		-	-	
Cs	0.0167	0.99	0.0211	0.9453	1.00
Cd	0.149	0.99	0.1683	1.0275	0.98

The actual concentrations of Cd varied in four levels with 128.3 mg/L, 10.64 mg/L, 1.07 mg/L and 0.1031 mg/L. The results of the sorption experiments are plotted in Fig. 10.13. The calculated sorption models are LINEAR (R^2 = 0.99) and FREUNDLICH (R^2 = 0.98) models. The corresponding sorption coefficients are listed in Tab. 10.5. The k_d of Cd in 10 % NaCl solution is 149.0 ml/g, higher than that of Cs and much higher than that of Cd in 100 % NaCl solution.

Based on the experiment results, it is clear to see that the sorption coefficients of Cs and Cd increase further with the decrease of the background NaCl solution. The k_d value of Cd increases dramatically from 0.3 ml/g in 100 % NaCl solution to 2.6 ml/g in 50 % NaCl solution to 11.1 ml/g in 30 % NaCl solution and 149.0 ml/g in 10 % NaCl solution.

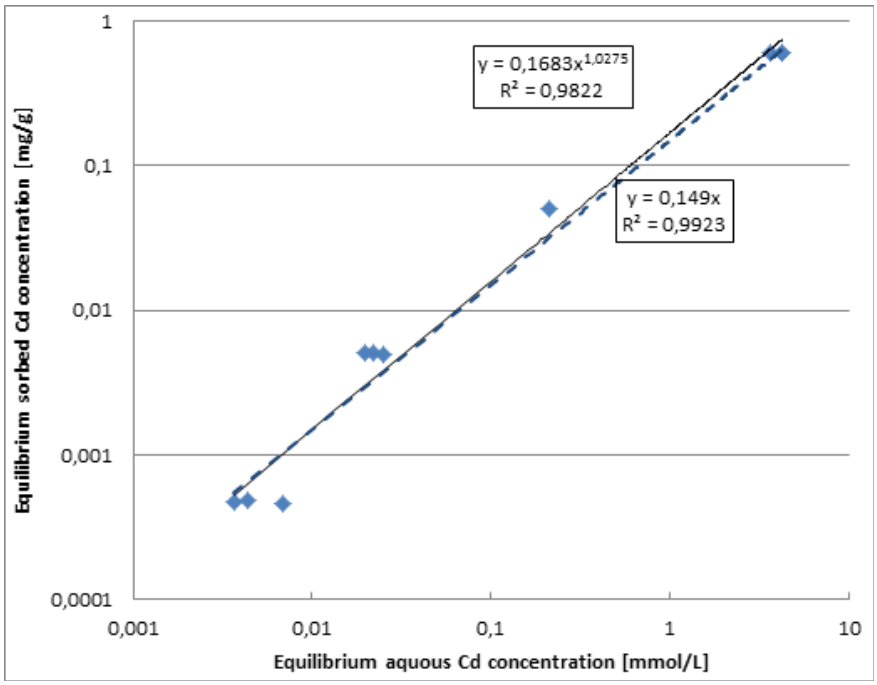

Fig. 10.13 Sorption of Cd in 10 % NaCl-solution by MX-80 bentonite

10.4 Sorption coefficient and concentration of NaCl background solution

The systematic sorption batch experiments demonstrated that the sorption capacity of heavy metals Pb, Cs and Cd by MX-80 decreases with the increase of the background NaCl solution concentration. This effect is extremely apparent for Cd and Pb. The element Cs is less sensitive. Therefore, it is interesting to find out the correlation of sorption coefficient of each individual heavy metal and the NaCl concentration as background solution.

10.4.1 Cd

The sorption coefficients of element Cd in NaCl-solutions by MX-80 bentonite strongly depends on the concentration of NaCl (Tab. 10.6 and Fig. 10.14). The k_d value at low concentrated solution is fairly high with 0.149 L/g or 149 ml/g in 10 % NaCl background solution, but decreases dramatically to 11.1 ml/g in 30 % NaCl solution. In 100 % NaCl solution, the k_d value is only 0.3 ml/g. The reason should be the ionic exchange of Na^+/Cd^{2+} and the complex formation in highly saline solution, which leads to the formation of $CdCl^+$, $CdCl_2(0)$, $CdCl_3^-$ and $CdCl_4^{2-}$. Bentonite has negative charge on the surface, therefore it prefers to adsorb cations.

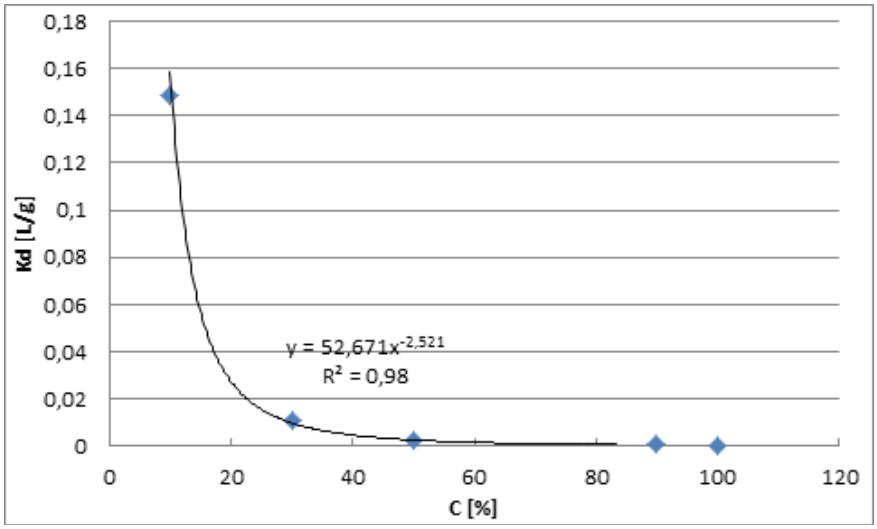

Fig. 10.14 Effect of concentration of the NaCl-solution on the Cd sorption coefficient (k_d) by MX-80 bentonite

Tab. 10.6 Dependence of the sorption coefficients of Cd in NaCl solutions by MX-80 bentonite on the degree of NaCl saturation

Degree of NaCl saturation	LINEAR		FREUNDLICH		
	k_d [L/g]	R^2	Kf [(mg/g)/(mg/L)^n]	n [-]	R^2
100 % NaCl	0.0003	0.50	0.0038	0.4085	0.96
90 % NaCl	0.0010	0.98	0.0004	1.0551	0.90
50 % NaCl	0.0026	0.99	0.0031	0.9758	0.98
30 % NaCl	0.0111	0.99	0.0144	0.9485	1.00
10 % NaCl	0.1490	0.99	0.1683	1.0275	0.98

10.4.2 Pb

Similar to Cd, the sorption coefficients of element Pb in NaCl-solutions by MX-80 bentonite strongly depends on the concentration of NaCl (Tab. 10.7 and Fig. 10.15). Unfortunately two batch experiments with Pb 10 % and 50 % NaCl solutions were not successful. However, the sorption coefficient values are higher than those of Cd in the other NaCl solutions. By the end of the batch experiments in 10 % NaCl solution, no Pb in the solution can be detected, which might be a sign of the very strong sorption characteristics of MX-80 bentonite on Pb. In such concentrations much more Pb has to be provided. Nevertheless, the sorption of Pb depends strongly on the degree of saturation of the NaCl background solution. Even in 100 % NaCl solution, MX-80 bentonite

showed still a relatively high sorption capacity of Pb. The complex formations of Pb-Clx (x = 1, 2, 3, 4) should contribute to the decrease of the sorption coefficient of Pb on MX-80 benonite.

Tab. 10.7 Correlation of measured sorption coefficients of Pb by MX-80 bentonite and the degree of NaCl saturation in background solution

Degree of NaCl saturation	LINEAR		FREUNDLICH		
	k_d [L/g]	R^2	Kf [(mg/g)/(mg/L)^n]	n [-]	R^2
100 % NaCl	0.0068	0.96	0.0024	1.3308	0.95
90 % NaCl	0.0118	0.96	0.0078	1.1589	0.92
30 % NaCl	0.0496	0.96	0.0349	1.0076	0.81

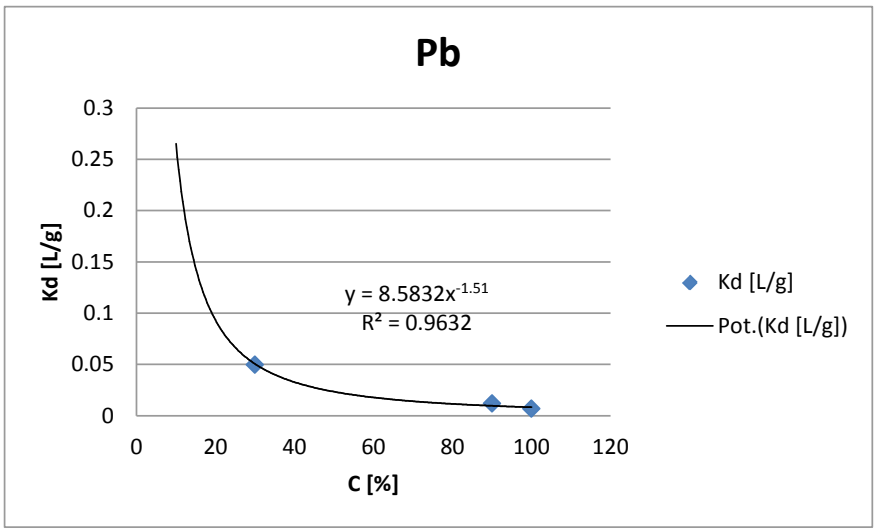

Fig. 10.15 Effect of concentration of the NaCl-solution on the Pb sorption coefficient (k_d) by MX-80 bentonite

10.4.3 Cs

The sorption coefficient of Cs decreases with the increase of the degree of saturation of the NaCl background solution (Tab. 10.8 and Fig. 10.16). However, it is less sensitive to the change of the NaCl concentration than those of Cd and Pb.

Tab. 10.8 Correlation of measured sorption coefficients of Cs by MX-80 bentonite and the degree of NaCl saturation in background solution

Degree of NaCl saturation	LINEAR		FREUNDLICH		
	k_d [L/g]	R^2	Kf [(mg/g)/(mg/L)^n]	n [-]	R^2
100 %. NaCl	0.0056	0.98	0.0122	0.8021	0.98
90 %. NaCl	0.0052	0.99	0.0123	0.7834	0.99
50 %. NaCl	0.0115	1.00	0.0134	0.9147	0.99
30 %. NaCl	0.0087	1.00	0.0119	0.9323	1.00
10 %. NaCl	0.0167	0.99	0.0211	0.9453	1.00

The batch sorption experiments of three heavy metals Cd, Pb and Cs showed that the sorption coefficient decreases with the increase of the degree of saturation of the NaCl background solution. The complex formations of Cd and Pb influence their sorption properties by the MX-80 bentonite, which should be taken into consideration by the evaluation of the retardation processes where highly saline solution exists.

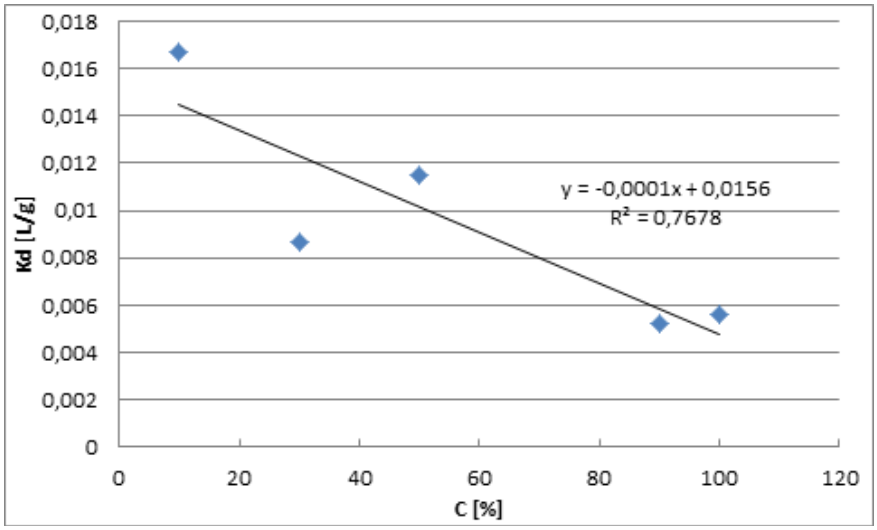

Fig. 10.16 Effect of concentration of the NaCl-solution on the Cs sorption coefficient (k_d) by MX-80 bentonite

11 Numerical simulations

Numerical simulations of the diffusion processes were undertaken to simulate the diffusion experiment on heavy metals in saline solution through compacted bentonite. The software for the simulation is OpenGeoSys (OGS) /KOL 10/. OpenGeoSys is a scientific open source project for the development of numerical methods for the simulation of thermo-hydro-mechanical-chemical (THMC) processes in porous and fractured media. OGS is implemented in C++, it is object-oriented with an focus on the numerical solution of coupled multi-field problems (multi-physics).

11.1 General assumptions of geochemical reaction calculation

The general assumptions of the geochemical batch reaction calculation are:

1. The temperature and pressure conditions were assumed to be constant (25 °C and 1 bar) for all simulations;
2. The samples are assumed to be saturated;
3. There is no bulk flow for the diffusion experiment; Diffusion is the only mass transport process;
4. All main ions in the solution are considered, however no chemical reactions are considered;
5. The diffusion coefficients of each heavy metals measured in the diffusion experiments are used for the simulations;
6. The sorption coefficients obtained from the batch experiments are used for the simulation, which might somewhat higher than the compacted bentonite. Because in highly compacted bentonite, the interaction of part of the clay minerals and the solution in the pore space is limited and leads to lower sorption coefficient than that measured in batch experiment.

11.2 Experimental results for the simulation

In section 9, the measured diffusion coefficients and some influencing parameters were discussed. For the numerical simulation, it is interesting to simulate the time evolution of the diffusion experiment, especially the mass flux of each heavy metal during the experiment. In this subsection, one representative example is selected with a bulk dry density of 1,600 kg/m^3 and in 90 % NaCl solution, which is the most potential density to be used and the nearly saturated condition. The highly compacted bentonite sample is in cylinder form with 2 cm in height and 5 cm in diameter, both sides contact with filter made of titan (see Fig. 8.3 in section 8.3). Both filters connect with a separated solution circulation system with the same flow rate driven by one peristaltic pump.

The sample was first mixed with a small amount of 90 % NaCl solution including Cs, Cd and Pb, which are to be used as transport solution for the first phase as listed in Tab. 11.1. It was then compacted into 1,600 kg/m3 and some solution was pressured out. The sample remains confined in the diffusion cell and connected with the transport solution to one side. With small pressure in range of 5 bar, which was the minimal pressure needed to force the solution to flow through the sample in a very small velocity, in order to saturated the sample faster but avoid the disturbing the pore structure of the sample. The saturation lasted about two days until no gas bubble emerges. The sample is then removed from the saturation instrument and connected with the diffusion apparatus for diffusion experiment using the modified diffusion method (Fig. 8.3) described in section 8.3.

Tab. 11.1 Boundary conditions (BC) for model set up

Element	BC source		BC Transport	
	Time [day]	Concentration [mol/kg H_2O]	Time [day]	Concentration [mol/kg H_2O]
Cs	0 – 50	$5.74 \cdot 10^{-4}$	0 – 50	$7.34 \cdot 10^{-6}$
	> 50	$6.19 \cdot 10^{-4}$	> 50	$7.28 \cdot 10^{-6}$
Cd	0 – 50	$9.28 \cdot 10^{-4}$	0 – 50	$1.09 \cdot 10^{-5}$
	> 50	$1.02 \cdot 10^{-3}$	> 50	$1.31 \cdot 10^{-5}$
Pb	0 – 50	$8.07 \cdot 10^{-4}$	0 – 50	$8.24 \cdot 10^{-6}$
	> 50	$9.93 \cdot 10^{-4}$	> 50	$9.92 \cdot 10^{-6}$

The concentration values of the contaminants Cs, Cd and Pb listed in Tab. 11.1 for the first 50 days have slightly changed because the solution was totally used, but the steady state diffusion condition was not reached.

The heavy metal concentrations in the solutions collected every day from the transport side were analysed. According to the data, the net change of the concentration of each heavy metal can be calculated and thus also the accumulated mass and mass flux.

The results of diffusion experiment on Cs are shown in Fig. 11.1. The curve of the net mass flux (in the middle) showed that the flux is negative at the beginning, which means that Cs diffuse into the sample. This indicates that the sample is not equilibrated with the transport solution even after the previous treatments. This leads to the negative total net accumulated mass amount as shown on the top figure in Fig. 11.1. Nevertheless, the flux turns to positive shortly after 20 days and increases continuously for around 60 days until the steady state diffusion condition arrived.

The results of diffusion experiment on Cd are shown in Fig. 11.2. The curve of the net mass flux (in the middle) showed that the flux is negative at the beginning, which means that Cd diffuse into the sample. This indicates that the sample is not equilibrated with the transport solution even after the previous treatments. This leads to the negative total net accumulated mass amount as shown on the top figure in Fig. 11.2. In comparison with Cs, this effect remains much longer time. After about 50 days the net Cd flux turns to positive and increases continuously until 90 days to reach the steady state diffusion condition. The reason for such effect is the much higher sorption coefficient of Cd than that of Cs. More Cd has to be provided for reaching sorption equilibrium.

Similar effects for the results of diffusion experiment on Pb are shown in Fig. 11.3. The curve of the net mass flux (in the middle) showed that the flux is negative at the beginning, which means that Pb diffuse into the sample. The flux remains negative for a long period indicates that the sample is far from equilibrated with the transport solution even after the previous treatments. This leads to the negative total net accumulated mass amount as shown on the top figure in Fig. 11.3. In comparison with Cs, this effect remains much longer time. After about 70 days the net Pb flux turns to positive and increases continuously until 95 days to reach the steady state diffusion condition. The reason for such effect is the much higher sorption coefficient of Pb than those of Cs and Cd. More Pb has to be provided for reaching sorption equilibrium.

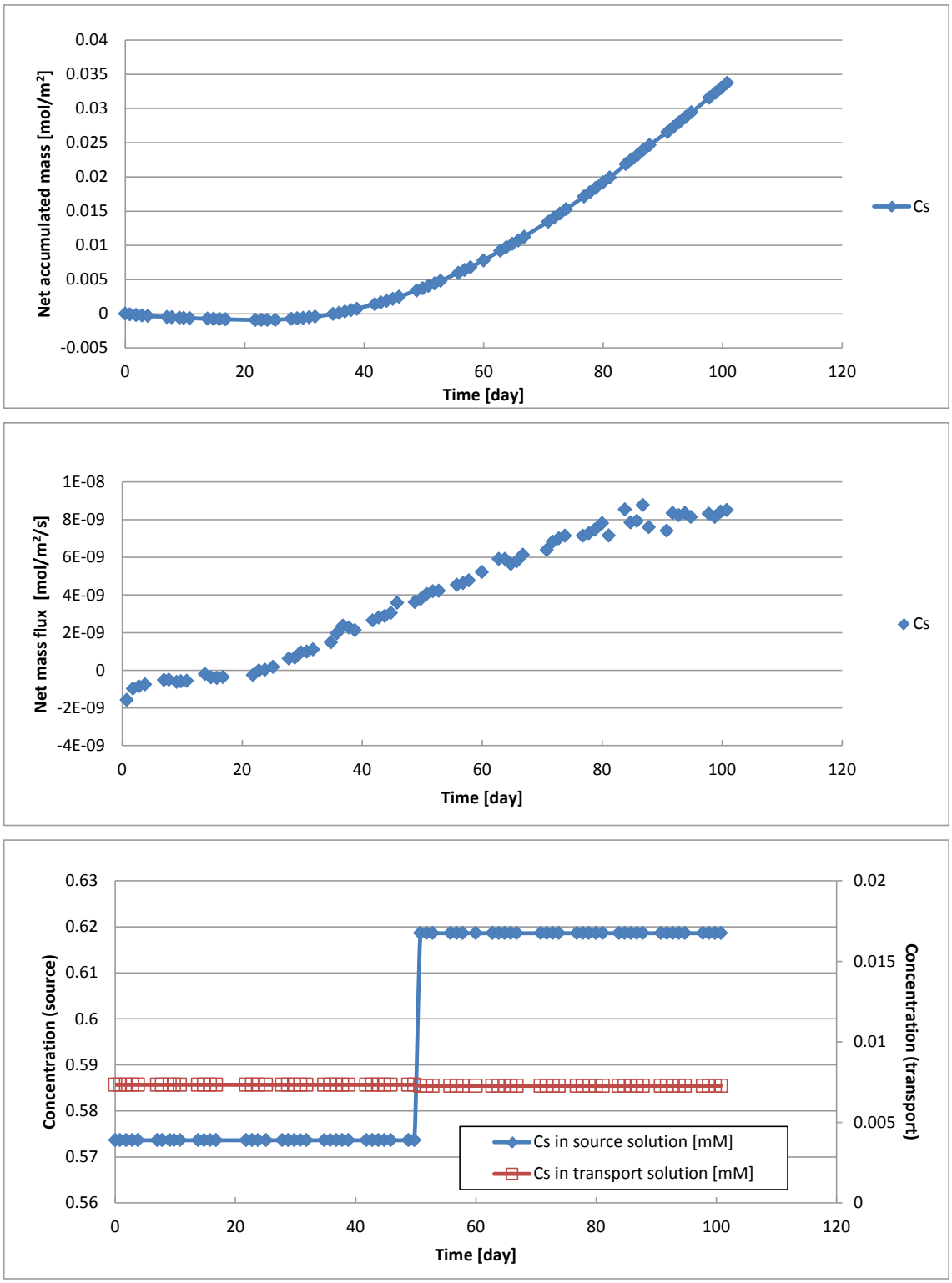

Top: net accumulated Cs mass amount; Middle: net Cs mass flux; Bottom: Cs concentration at source and transport boundaries

Fig. 11.1 Results of the diffusion experiment of Cs in 90 % NaCl solution through MX-80 bentonite with dry density 1,600 kg/m^3

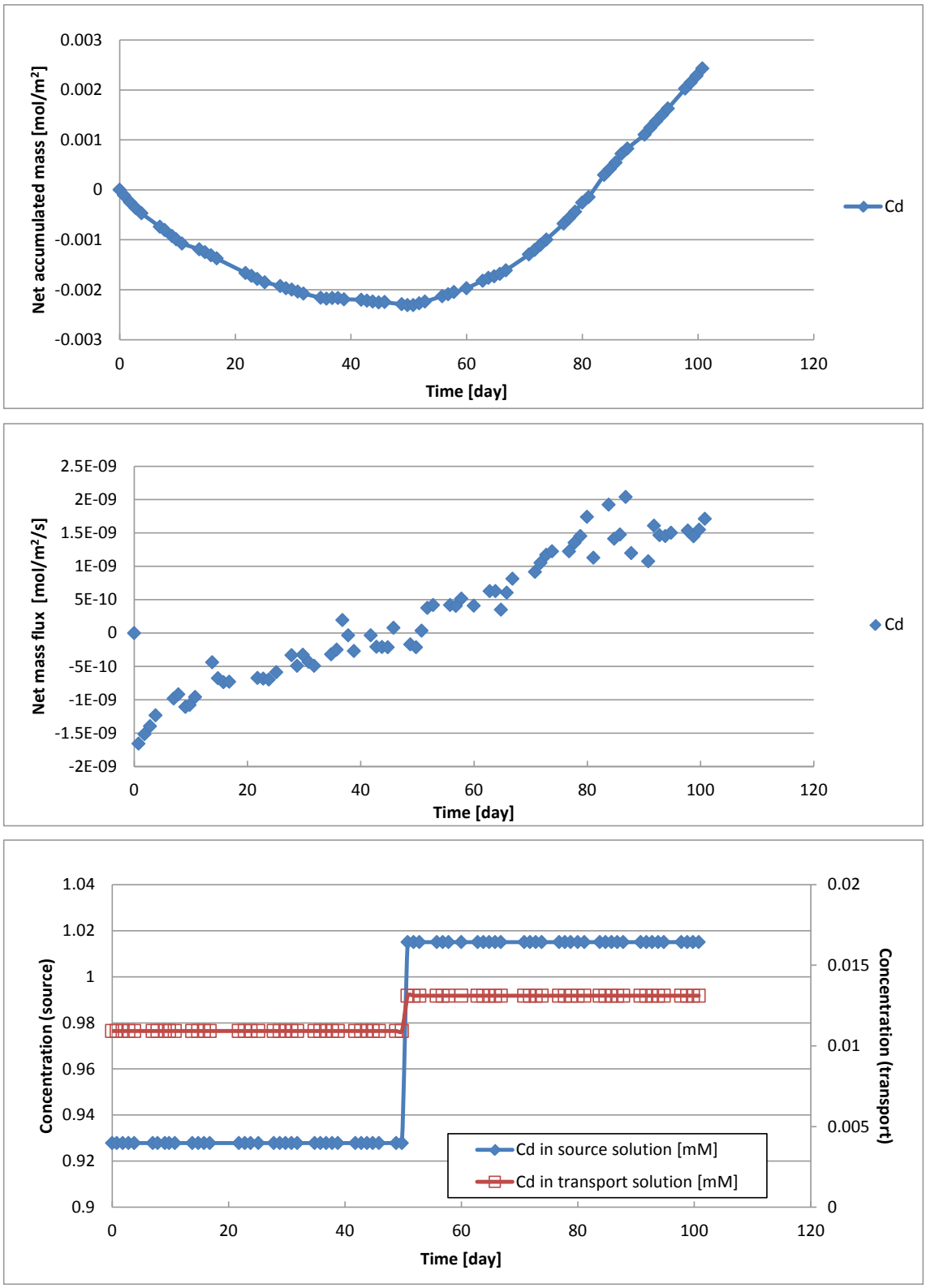

Top: net accumulated Cd mass amount; Middle: net Cd mass flux; Bottom: Cd concentration at source and transport boundaries

Fig. 11.2 Results of the diffusion experiment of Cd in 90 % NaCl solution through MX-80 bentonite with dry density 1,600 kg/m^3

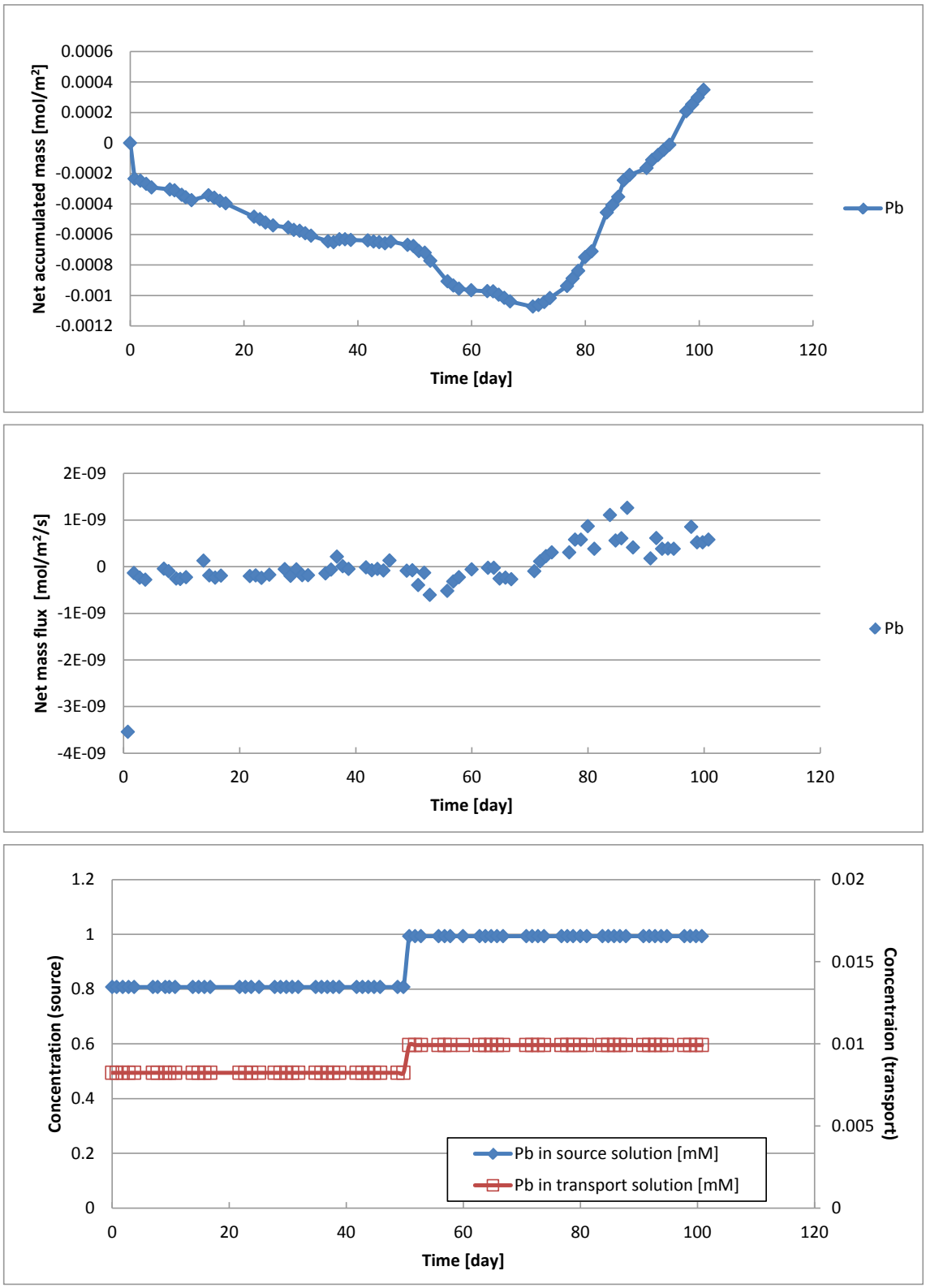

Top: net accumulated Pb mass amount; Middle: net Pb mass flux; Bottom: Pb concentration at source and transport boundaries

Fig. 11.3 Results of the diffusion experiment of Pb in 90 % NaCl solution through MX-80 bentonite with dry density 1,600 kg/m^3

11.3 Model setup

The model for the simulation is set up based on the experiment described above. Owing to the symmetric geometry and boundary conditions the model is simplified as one dimensional case along the axis of symmetry.

Material properties of the sample are bulk dry density 1,600 kg/m^3, porosity 0.36 [-], grain density 2500 kg/m^3. All other parameters are listed in Tab. 11.2 and the boundary conditions in Tab. 11.1. The initial condition (IC) values refer to the concentration of each heavy metal in the pore water at the beginning of the simulation. Through the pretreatment such values are impossible to be exactly measured and thus are estimated based on the concentrations in the solution provided for the saturation phase and the sorption coefficient and are set as homogeneous for the whole domain.

Tab. 11.2 Parameters and initial condition (IC) for model set up

Element	Diffusion coefficient [m^2/s]	k_d batch [m^3/kg]	k_d fitted [m^3/kg]	IC [mol/kg H_2O]
Cs	$2.76 \cdot 10^{-10}$	0.0052	0.00416	$6.9 \cdot 10^{-6}$
Cd	$3.10 \cdot 10^{-11}$	0.0010	0.0003	$7.7 \cdot 10^{-7}$
Pb	$1.70 \cdot 10^{-11}$	0.0118	$1.18 \cdot 10^{-4}$	$2.8 \cdot 10^{-6}$

11.4 Simulated results

The simulations were undertaken in two steps: The first step is the simulation with the measured diffusion coefficients, and sorption values obtained by batch experiments. It is common that the sorption coefficients differ from those in column experiments, in which the interaction of solution and the clay minerals is limited. Therefore the second step simulations are undertaken by fitting the experimental curves by adjusting the k_d values. Such values with best fit to the experimental curves are listed in Tab. 11.2.

11.4.1 Step I: measured diffusion and sorption coefficients

In the first simulation with OGS, the parameters for the material properties used for the numerical simulation are measured data (Tab. 11.1 and Tab. 11.2). The simulated con-

centration profiles are shown in Fig. 11.4 at 2 days and Fig. 11.5 at 200 days. It is clear to see that the diffusion of Cd and Pb occurs from both ends of the sample (Fig. 11.4). After about 200 days, steady state diffusion conditions for Cd and Cs have reached. However, the diffusion of Pb is far from the steady state (Fig. 11.5). On the contrary, the diffusion of Pb continues from both ends into the sample even after 200 days, which is not the case in the experimental observations as showed in Fig. 11.3. The exact reason is not very clear. However, the overestimation of the sorption effect by the directly application of the sorption coefficient obtained through the batch sorption experiment should be the main cause.

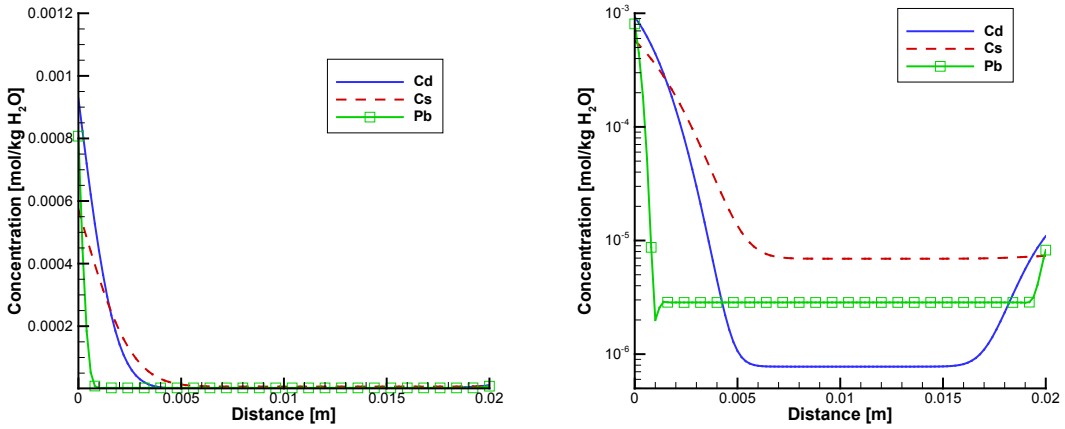

Fig. 11.4 Concentration profile of Cs, Cd and Pb at 2 days (the same results in normal (left) and LOG (right) axis scale)

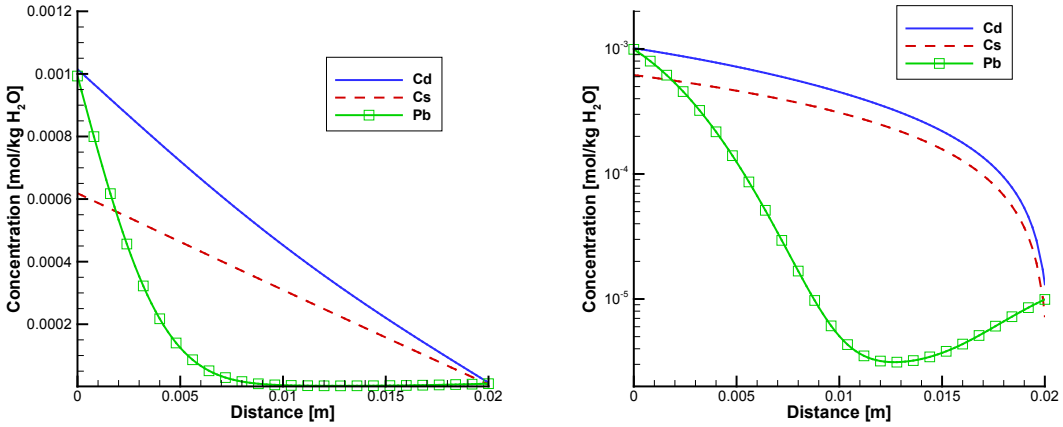

Fig. 11.5 Concentration profile of Cs, Cd and Pb at 200 days (the same results in normal (left) and LOG (right) axis scale)

Compare the simulated and observed net mass flux data, the results for Cs fits relatively well (Fig. 11.6). The comparison of the experimental and simulated results for Cd is less promising but showed similar trends (Fig. 11.7). The comparison of the experimental and simulated results for Pb is not satisfactory (Fig. 11.8). The overestimation of the sorption coefficients of Cd and Pb by using the batch experiment data should be the main reason. It is interesting to note that the change of the Pb concentration at 50 days results in the drop of Pb concentration in the transportation solution, which can be observed by the simulation.

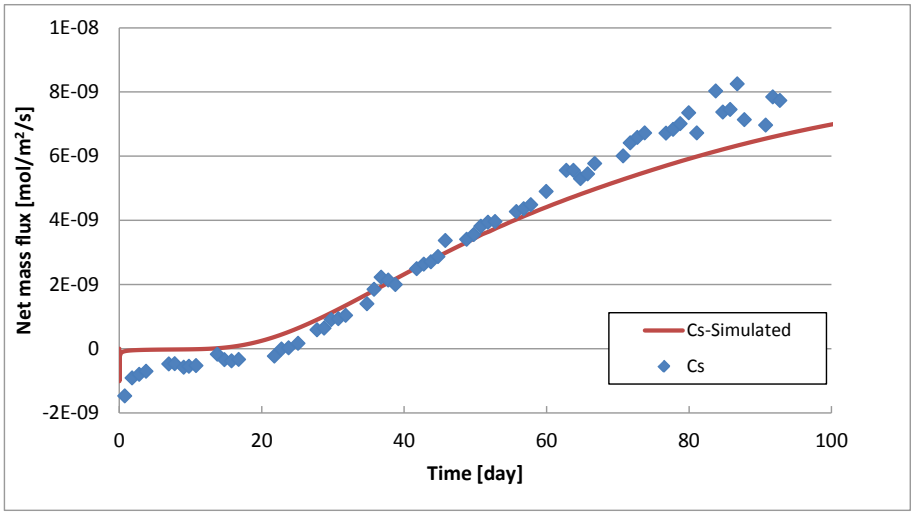

Fig. 11.6 Comparison of the experimental net Cs mass flux (symbol) with the simulated result (solid line) with measured diffusion and batch sorption coefficient

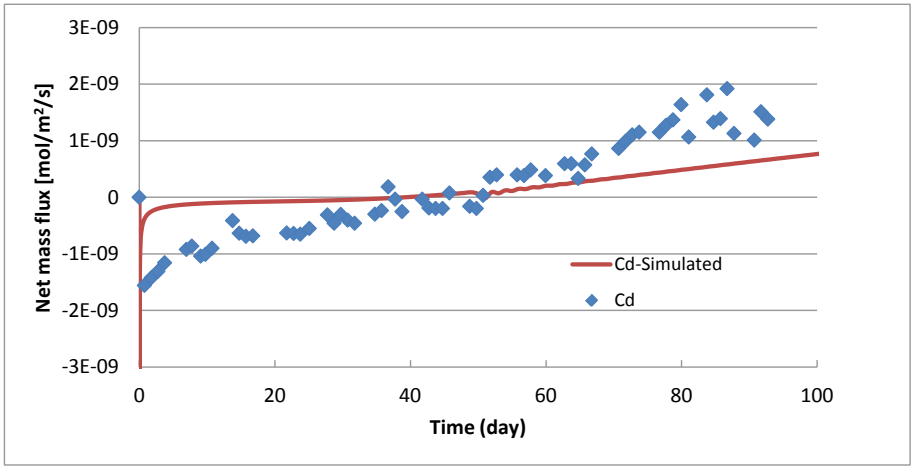

Fig. 11.7 Comparison of the experimental net Cd mass flux (symbol) with the simulated result (solid line) with measured diffusion and batch sorption coefficient

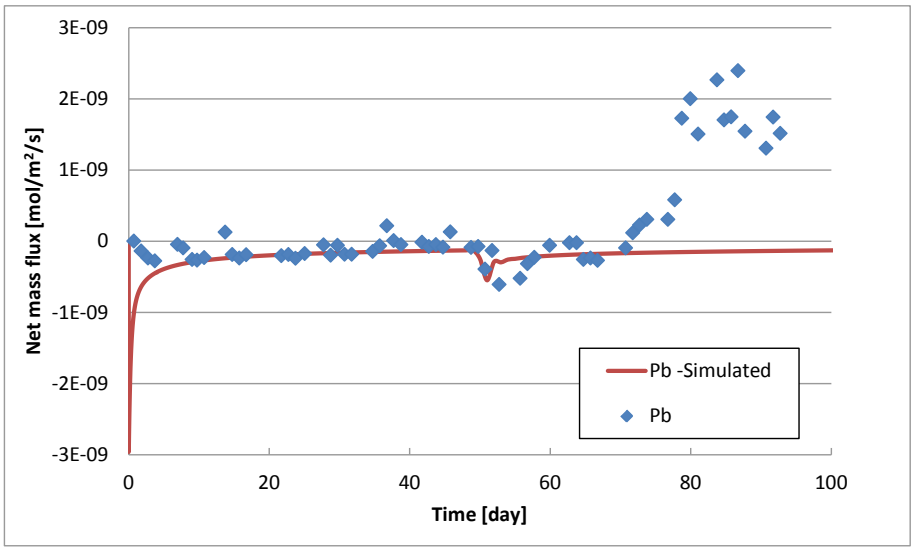

Fig. 11.8 Comparison of the experimental net Pb mass flux (symbol) with the simulated result (solid line) with measured diffusion and batch sorption coefficient

11.4.2 Step II: measured diffusion but modified sorption coefficients

The second step simulations were undertaken on the basis of the first step simulations. The only modification is the k_d values of each heavy metals.

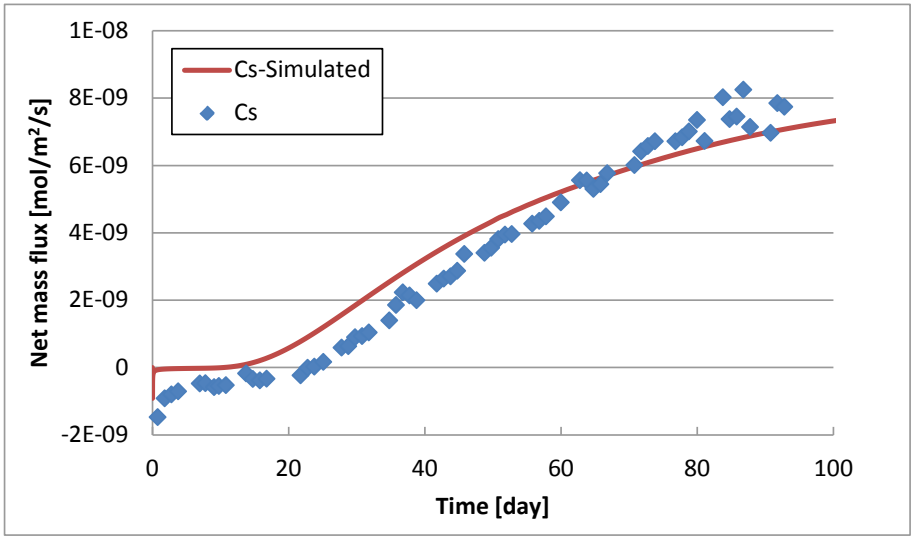

Fig. 11.9 Comparison of the experimental net Cd mass flux (symbol) with the simulated result (solid line) with measured diffusion and 80 % of the batch sorption coefficient

By decreasing the sorption coefficient, the simulated data at the steady state diffusion condition is getting closer to the experimental data, especially the steady state flux and the time for reaching the steady state (Fig. 11.9, Fig. 11.10 and Fig. 11.11). The best fitting k_d values are about 90 % of the batch experiment data for Cs, 30 % of that for Cd and about 1 %. for Pb (Tab. 11.2).

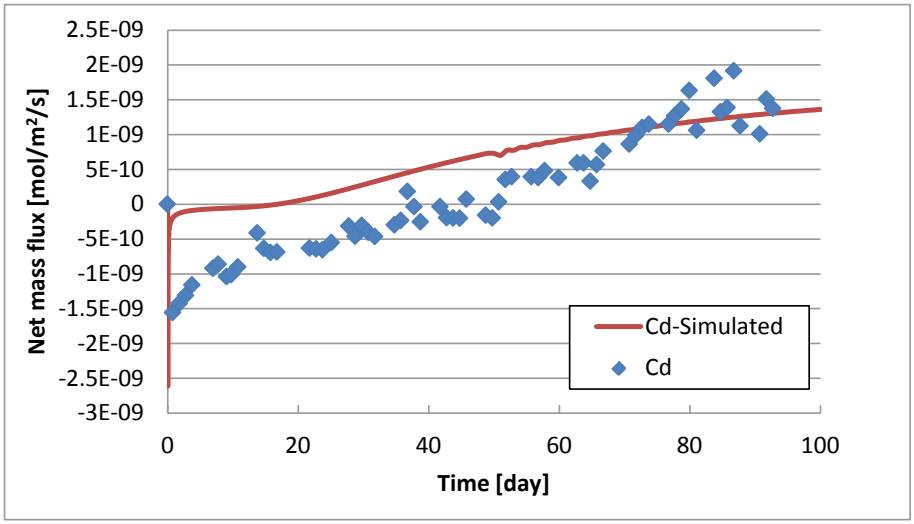

Fig. 11.10 Comparison of the experimental net Cd mass flux (symbol) with the simulated result (solid line) with measured diffusion and 30 % of the batch sorption coefficient

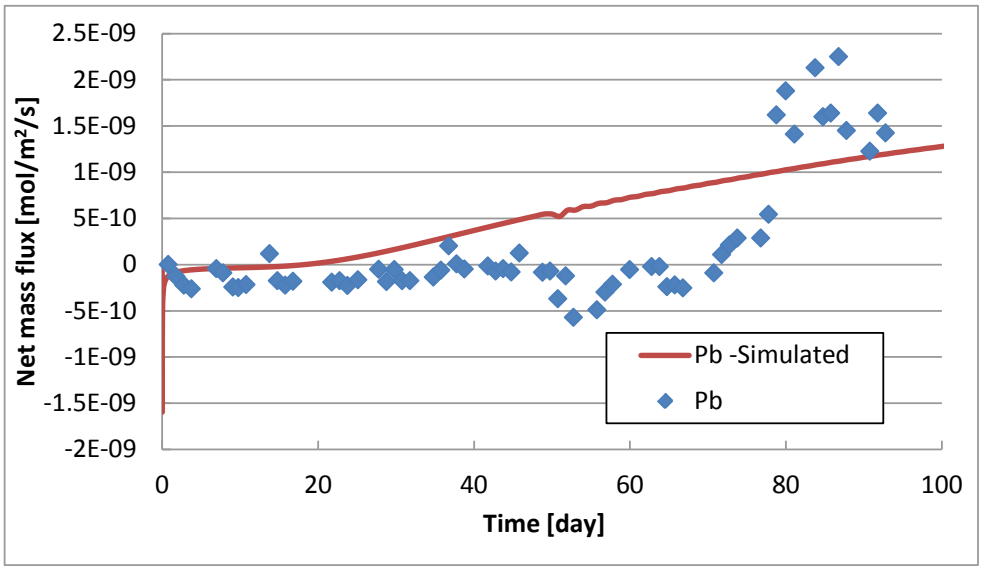

Fig. 11.11 Comparison of the experimental net Pb mass flux (symbol) with the simulated result (solid line) with measured diffusion and 1 % of the batch sorption coefficient

The simulated results showed that the diffusion process of Cs can be well simulated through directly using the measured diffusion coefficient and the batch sorption coefficient, which showed the suitability of the newly modified method for diffusion coefficient determination. The simulation of the diffusion experiment on Cd is also fairly well after the lowering the sorption coefficient down to 30 %. The simulation of Pb showed good trend to reach the flux approaching steady state condition. The reasons for such differences might be the ionic interaction in the highly saline solution, the complex formation of Cd and Pb in the solution with very high Cl^- concentration and thus changed the charge of the contaminants, which leads to other mechanism in the diffusion including ion exclusion by the net negatively charged clay mineral system.

12 Discussion

Through the current project a modified through-diffusion method is developed and can be used to shorten the experiment time and get more reliable diffusion coefficient data. However, there are still some remaining issues to be discusses in the following subsections.

12.1 Influence of concentration change on the diffusion experiment

The traditional through-diffusion method uses two closed circulation systems attached to both sides of a sample. In one system there is contaminant in the solution and provides the source of elements, whose diffusion coefficients are to be determined. In the other circulation system, it is pursued to keep a “zero” concentration boundary condition. However, this is impossible. As long as the diffusion front reaches from one end to the other, the concentration of the element of interest accumulates with the circulation until the solution is replaced. The change of the concentration is small if the solution can be replaced in relatively short time. But the influence of the concentration increase in the collection side on the diffusion coefficient determination cannot be found in the literature. Using the new method, such effect can be quantified. To demonstrate such effect, two observations are selected and discussed.

The first observation is the diffusion experiment on Cd in 90 % NaCl solution through highly compacted MX-80 bentonite with a bulk dry density of 1,800 kg/m^3. During the experiment time for about 140 days, the Cd concentration at the source solution remains constant in $1.02 \cdot 10^{-3}$ M till the end of the experiment; the Cd concentration in the 90 % NaCl solution provided to the other side of the sample is also constant for the first 45 days in $9.51 \cdot 10^{-6}$ M, which is replaced by another similar 90 % NaCl solution with slightly different Cd concentration in $9.554 \cdot 10^{-6}$ M and remains constant for the rest of the experiment time period (Fig. 12.1 bottom). The increase of the Cd is only $4.4 \cdot 10^{-8}$ M. However, the small Cd concentration increase dramatically changed the diffusion process. The concentration gradient is slightly increased; the local concentration gradient has changed its direction and leads to the back diffusion from the transport solution into the bentonite and the net Cd mass flux decreases and later on turns from positive to negative (Fig. 12.1 middle). This process continues and lasts for about

50 days until the total recovery or a new balance for the new Cd concentration boundary conditions.

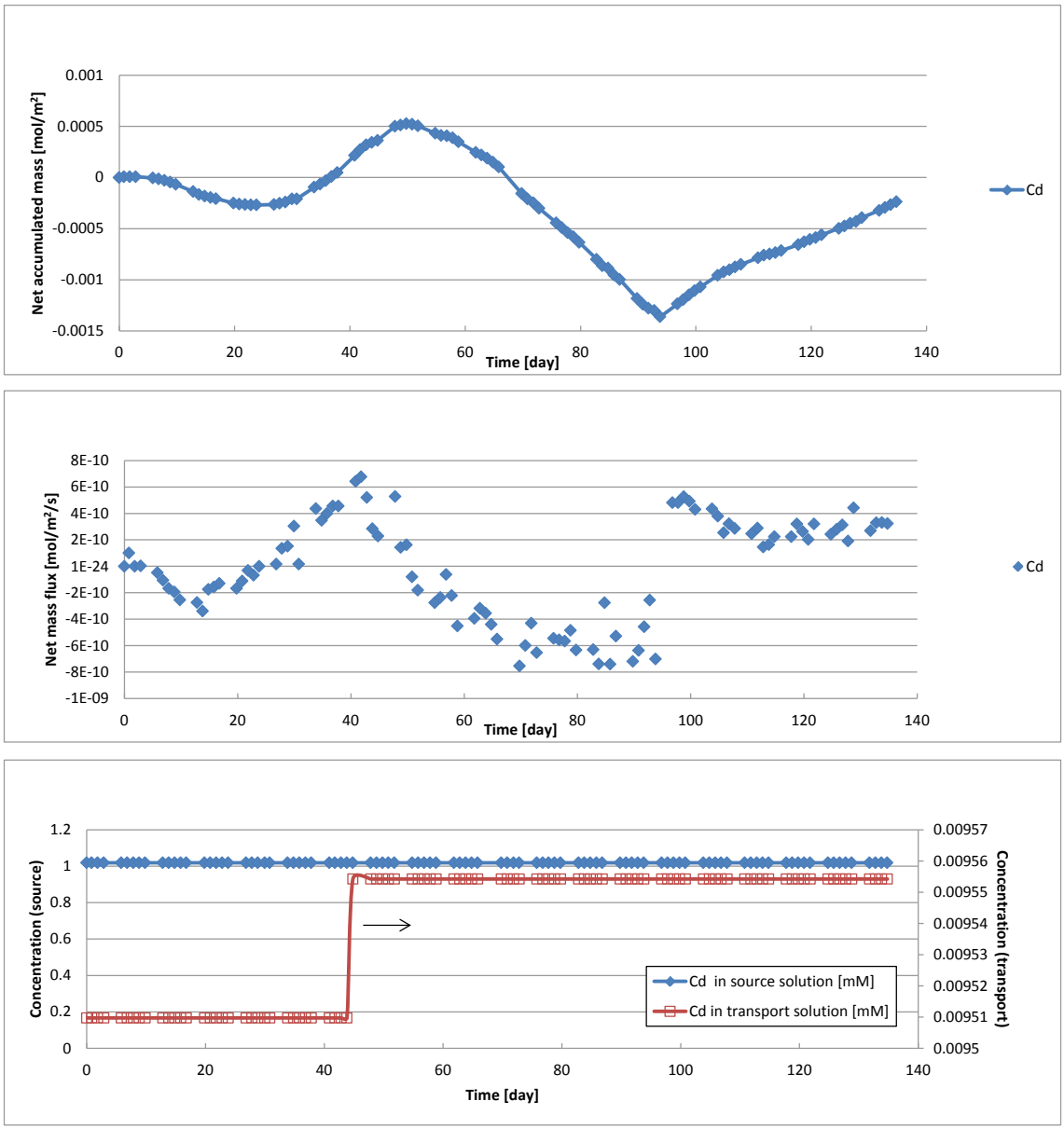

Fig. 12.1 Results of the diffusion experiment of Cd in 90 % NaCl solution through MX-80 bentonite with dry density 1,800 kg/m^3 (Top – net accumulated Cd mass amount, Middle – net Cd mass flux, Bottom – Cd concentration at source and transport boundaries)

It is interesting to note that the diffusion coefficient calculated based on the Cd mass flux at about 45 days of the experiment is $9.03 \cdot 10^{-12}$ m^2/s, the diffusion coefficient calculated based on the final Cd mass flux is $8.78 \cdot 10^{-12}$ m^2/s. Both values are very close, which indicates that the steady state diffusion of Cd at 45 days is almost reached.

However, through the sudden increase of the Cd concentration in the transport solution, the previous diffusion process is disturbed and another steady state diffusion has to be newly established to match the new boundary conditions.

Another example of Cs diffusion experiment showed similar effect. It is the diffusion experiment on Cs in 90 % NaCl solution through highly compacted MX-80 bentonite with a bulk dry density of 1,800 kg/m^3. The sample is far from equilibrated to the solution with a concentration of $6.811 \cdot 10^{-6}$ M provided on the collection side for transporting the Cs coming out of the sample through diffusion process. After 45 days, the solution was replaced by another very similar solution with a concentration of $6.818 \cdot 10^{-6}$ M (Fig. 12.2 bottom). The increase is $7 \cdot 10^{-9}$ M. At the same time, the Cs concentration in the source solution provided to the other side of the solution is also replaced from the Cs concentration of $6.43 \cdot 10^{-4}$ M to $7.21 \cdot 10^{-4}$ M, which increases the concentration gradient of Cs. Nevertheless, the disturbance of the diffusion can also be observed for about 10 days.

According to these observations, it is clear that the small variation of the transport solution can strongly influence the diffusion process. It is thus important to keep the concentration of the candidate element at both ends of the sample constant for the through diffusion experiment. Otherwise the experiment will last longer. Therefore, the dynamic changing of the candidate element in the solution for the collection circle in the classic through-diffusion process makes it technically difficult to maintain specific steady state diffusion.

12.2 Comparison of experimental results with literature data

The measured diffusion coefficients for heavy metals Cs, Pb and Cd are in good agreement with the data published in the literature (Tab. 12.1 and Fig. 12.3), even though the background solution is much higher in the concentration or ionic strength than those value published in the literature. Additionally the permeabilities of bentonite for solutions of high ionic strength are much higher than solutions in lower ionic strength, which indicates much higher effective porosity for flow with higher ionic strength. The reason is still unclear. One reason might be the lower sorption coefficient of the heavy metals, which keeps more ions in the solution for migration. The diffusion coefficients of Cd and Pb might be related to the complex formation as discussed in the next section.

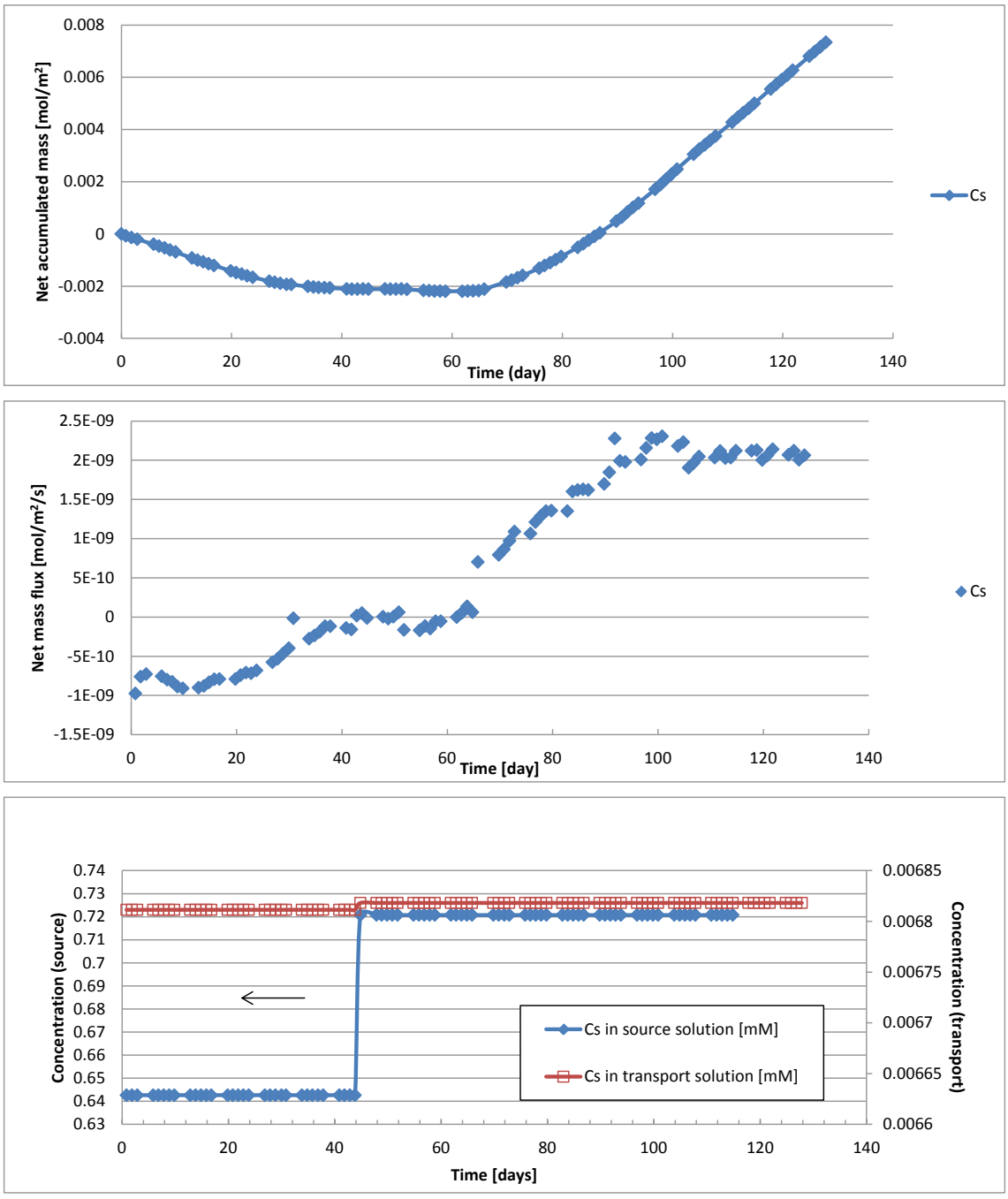

Fig. 12.2 Results of the diffusion experiment of Cs in 90 % NaCl solution through MX-80 bentonite with dry density 1,800 kg/m^3 (Top – net accumulated Cs mass amount, Middle – net Cs mass flux, Bottom – Cs concentration at source and transport boundaries)

Tab. 12.1 Comparison of the diffusion coefficient of MX-80 bentonite measured in current work and data in the literature

Element	Diffusion Coefficient (current work) [m^2/s]			Remarks
	Averaged	upper limit	lower limit	
Cs	$2.76 \cdot 10^{-10}$	$3.77 \cdot 10^{-10}$	$3.55 \cdot 10^{-11}$	dry density 1,600 kg/m^3
Pb	$1.14 \cdot 10^{-10}$	$1.33 \cdot 10^{-10}$	$7.80 \cdot 10^{-12}$	
Cd	$3.10 \cdot 10^{-11}$	$6.40 \cdot 10^{-11}$	$1.58 \cdot 10^{-11}$	
Element	**Diffusion Coefficient /OCH 04/ [m^2/s]**			**Remarks**
	Averaged	upper limit	lower limit	
Cs(I)	$3.0 \cdot 10^{-10}$	$3.00 \cdot 10^{-10}$	$4.94 \cdot 10^{-11}$	dry density 1590 kg/m^3
Pb(II)	$1.2 \cdot 10^{-10}$	$1.91 \cdot 10^{-10}$	$4.94 \cdot 10^{-11}$	

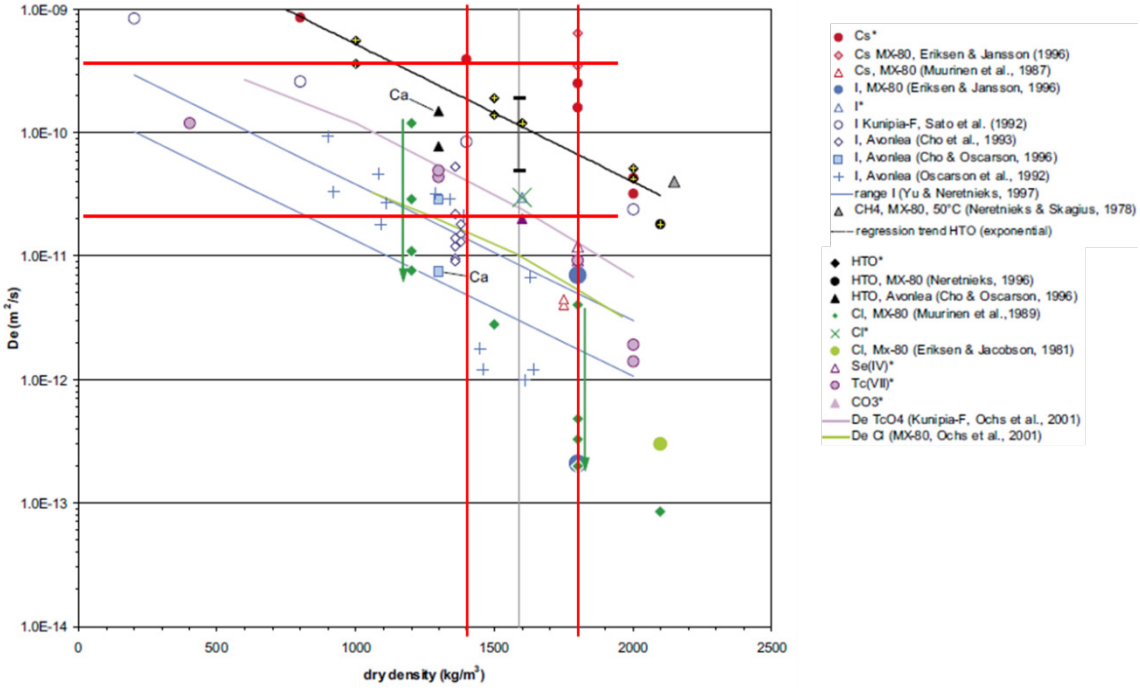

Fig. 12.3 Diffusion coefficient of Cs in MX-80 bentonite in the literature /OCH 04/ and the range of measured values in current work (within the range between red lines)

Tab. 12.2 Permeability and swelling pressure of MX-80 bentonite compacted in bulk dry density of 1,600 kg/m^3 in contact with different solutions /HER 12/

T [°C]	Permeability [m^2]			Swelling pressure [bar]		
	NaCl	IP21	OPCW	NaCl	IP21	OPCW
25	$1.70 \cdot 10^{-16}$	$9.83 \cdot 10^{-17}$	$8.46 \cdot 10^{-20}$	4.9	4.8	15.6

NaCl – saturated NaCl solution; IP21 – IP21 solution; OPCW – Opalinus pore water

12.3 Complex formation and diffusion

Anion exclusion by net negatively charged clay minerals leads to low diffusion coefficients of anions than those of cations /BOL 82/, /VAN 07/. The mechanism of such effect is numerically demonstrated by /HED 12/. Some heavy metals like Pb and Cd form complexes with Cl in highly saline solution including high concentration of Cl^-. Consequently the Pb and Cd complexes will change the charge of the hydrated complexes and thus the ion radius. Therefore, it is important to take these effects into consideration especially for the numerical simulation. As the fraction of the complexes varies with the concentration of Cl^- in the solution, the diffusion processes of each individual complex distinguish from each other by the pace and influencing factors. Precise determination can thus only be achieved if the diffusion coefficient, sorption coefficient and the actual fraction of each individual complex can be determined separately.

12.4 Bentonite alteration and diffusion property

Bentonite alteration is possible in highly saline solution for long term period as to be considered in the HLW repository or underground landfill for chemotoxic waste. The potential alteration mechanisms are chemical reaction like dissolution/precipitation, mineral transformation. Such effects are normally very slow processes and kinetically controlled. Nevertheless, the surface properties of such minerals will be modified and thus the sorption, diffusion processes, which is out of the scope of the current project.

13 Summary and conclusion

Bentonite is intensively investigated from many institutes for its properties and feasibility as engineering barrier material for many environmental facilities like landfill, underground landfill for chemotoxic waste and also HLW repositories. A summary of the current state of knowledge regarding the origin of bentonites and different processes through bentonite is provided together with the potential further research and development needs.

Diffusion experiments with gas (CO_2, H_2, CH_4 and SF_6) and heavy metals Pb, Cd and Cs in highly saline solution (50 % and 90 % NaCl solutions, 90 % IP21 solution) at room temperature and atmosphere pressure conditions through compacted MX-80 bentonite with three different bulk dry densities (1,400 kg/m^3,1,600 kg/m^3 and/or 1,800 kg/m^3) were performed. Numerical simulations of some experiments were undertaken.

13.1 Laboratory experiments on heavy metal diffusion

A new through-diffusion experiment method was developed on the basis of the traditional through-diffusion method described in the literature. The new method can keep the concentration of both ends constant and control the identification of the steady-state diffusion condition. Through some pre-treatment measures like pre-saturation of the bentonite with the candidate element of interest, the determination time can be shortened. The comparison test experiments with both methods for the determination of the diffusion coefficient of Cs under the same conditions with the same diffusion coefficient value proved the feasibility of the new method. The time needed with the new method was only less than 1/3 of that required with the traditional method, which showed its advantage for the diffusion coefficient determination especially for elements with high sorption coefficients. It is also advantageous for the determination of samples including small amounts of elements to be determined.

The measured diffusion coefficients of Pb, Cs and Cd depend on the bulk density of the MX-80 bentonite and the type and concentration of the background solutions. The diffusion coefficient values for each element showed the trend of decrease with the increase of bentonite dry densities.

For MX-80 bentonite compacted in dry density of 1,400 kg/m^3, the diffusion coefficient of Cs decreases with the increase of the NaCl concentration from $4.09 \cdot 10^{-10}$ m^2/s for 50 % NaCl solution to $3.50 \cdot 10^{-11}$ m^2/s 90 % NaCl solution. The diffusion coefficient of Cs in 90 % IP21 solution is $3.11 \cdot 10^{-11}$ m^2/s. The diffusion coefficient of Cd increases with the increase of the NaCl concentration from $2.05 \cdot 10^{-11}$ m^2/s for 50 % NaCl solution to $4.78 \cdot 10^{-11}$ m^2/s 90 % NaCl solution. The diffusion coefficient of Cd in 90 % IP21 solution is $3.20 \cdot 10^{-11}$ m^2/s. The diffusion coefficient of Pb increases with the increase of the NaCl concentration from $1.96 \cdot 10^{-11}$ m^2/s for 50 % NaCl solution to $5.11 \cdot 10^{-11}$ m^2/s 90 % NaCl solution. The diffusion coefficient of Pb in 90 % IP21 solution is $3.89 \cdot 10^{-11}$ m^2/s.

For MX-80 bentonite compacted in dry density of 1,600 kg/m^3, the diffusion coefficient of Cs decreases with the increase of the NaCl concentration from $3.74 \cdot 10^{-10}$ m^2/s for 50 % NaCl solution to $2.76 \cdot 10^{-11}$ m^2/s 90 % NaCl solution. The diffusion coefficient of Cs in 90 % IP21 solution is $3.55 \cdot 10^{-11}$ m^2/s. The diffusion coefficient of Cd decreases with the increase of the NaCl concentration from $6.41 \cdot 10^{-11}$ m^2/s for 50 % NaCl solution to $2.50 \cdot 10^{-11}$ m^2/s 90 % NaCl solution. The diffusion coefficient of Cd in 90 % IP21 solution is $1.58 \cdot 10^{-11}$ m^2/s. The diffusion coefficient of Pb decreases with the increase of the NaCl concentration from $1.10 \cdot 10^{-10}$ m^2/s for 50 % NaCl solution to $7.83 \cdot 10^{-11}$ m^2/s 90 % NaCl solution. The diffusion coefficient of Pb in 90 % IP21 solution is $1.42 \cdot 10^{-11}$ m^2/s.

For MX-80 bentonite compacted in dry density of 1,800 kg/m^3, the diffusion coefficient of Cs decreases with the increase of the NaCl concentration from $2.18 \cdot 10^{-10}$ m^2/s for 50 % NaCl solution to $5.19 \cdot 10^{-11}$ m^2/s 90 % NaCl solution. The diffusion coefficient of Cs in 90 % IP21 solution is $2.10 \cdot 10^{-11}$ m^2/s. The diffusion coefficient of Cd is $6.54 \cdot 10^{-12}$ m^2/s 90 % NaCl solution. The diffusion coefficient of Cd in 90 % IP21 solution is $3.12 \cdot 10^{-11}$ m^2/s. The diffusion coefficient of Pb decreases with the increase of the NaCl concentration from $3.56 \cdot 10^{-11}$ m^2/s for 50 % NaCl solution to $5.10 \cdot 10^{-12}$ m^2/s 90 % NaCl solution. The diffusion coefficient of Pb in 90 % IP21 solution is $1.97 \cdot 10^{-11}$ m^2/s.

13.2 Batch experiments on heavy metal adsorption

The batch adsorption experiments on Cd, Cs and Pb in NaCl solutions with various degree of saturation (10 % to 100 %) by MX-80 bentonite showed that the sorption coefficients of all heavy metals decrease with the increase of the degree of saturation. Almost all adsorption results can be well described with both LINEAR and FREUNDLICH models. The sorption of Cd strongly depends on the NaCl concentration. Similar results

were observed for Pb. The sorption of Cs is less sensitive to the NaCl background concentration.

13.3 Numerical simulation

Numerical simulations were performed with the software OpenGeoSys (OGS) to simulate the experiment with the evolution of diffusion processes of Pb, Cd and Cs in 90 % NaCl solution through compacted MX-80 with a bulk dry density of 1,600 kg/m^3. The simulations were conducted in two steps. The first step modelling was the simulation of the diffusion process by directly using the measured diffusion coefficient and the sorption coefficient obtained by batch experiment. Simulated results of the net diffusive flux of Cs agree very well with the experimental observations. The simulations of the other two heavy metals Cd and Pb with higher sorption coefficient and complex formation fit not well to the experimental data. By adjusting the sorption coefficients of each individual elements (Pb, Cd and Cs), the steady-state diffusive flux and time needed to reach the steady-state observed in the experiments can be better fitted with the simulated results, which can serve as the method for calculating the effective sorption coefficient in the column.

Acknowledgements

This work was funded by the German Federal Ministry of Education and Research (BMBF) under Project Number 02 C 1638. The authors are grateful for this support. Special thanks are given to the project managers and many of our colleges, to name a few Dr. Helge C. Moog, Dr. Sven Hagemann, Udo Ziesche, and Nadine Zilling for their support.

References

/ADA 09/ Adamcová, R., Frankovská, J., Durmeková, T. (2009): Engineering geological clay research for a radioactive waste repository in Slovakia, Acta Geologica Slovaca, vol. 1: 71 – 82

/ALL 09/ Allard, T., Calas, G. (2009): Radiation effects on clay mineral properties. Applied Clay Science 43, 143-149

/ALT 97/ ALTANER, S. P.; YLAGAN, R. F. (1997): Comparison of structural models of mixed-layer illite/smectite and reaction mechanisms of smectite illitization.- Clays and Clay Minerals 45(4), 517-533

/ANT 03/ Antunes, R.A., Costa, I., de Faria, D.L.A. (2003): Characterisation of corrosion products formed on steels in the first months of atmospheric exposure. Materials Research 6, 403-408

/BAE 97/ Baeyens, B., Bradbury, M.H. (1997): A mechanistic description of Ni and Zn sorption on Na-montmorillonite Part I: Titration and sorption measurements. Journal of Contaminant Hydrology 27, 199-222

/BAZ 10/ Bazarkinaa, E.F, Pokrovskia, G.S., Zotovb, A.V., Hazemann, J.-L. (2010): Structure and stability of cadmium chloride complexes in hydrothermal fluids, Chemical Geology, 276(1-2),1-17

/BEA 72/ Bear, J. (1972): Dynamics of Fluids in Porous Media. American Elsevier, New York, NY, 764pp

/BEA 84/ Beall, G. W. (1984): The implications of alpha radiation damage for bentonites utilized in high-level waste disposal. Smectite alteration. SKB Technical Report TR-84-11. Swedish Nuclear Fuel and Waste Management Company, Stockholm, Sweden

/BEN 82/ Benjamin, M. M. (1982): Effects of complexation by Cl, SO_4 and S_2O_3 on adsorption behavior of Cd on oxide surfaces, Environ. Sci. Technol., 16:162-170

/BER 97/ Bereket, G., Zehra Aroguz, A., Zafer Özel, M. (1997): Removal of Pb(II), Cd(II), Cu(II), and Zn(II) from Aqueous Solutions by Adsorption on Bentonite. Journal of Colloid and Interface Science 187, 338–343

/BER 99/ Berry, R. (1999): Eocene and Oligocene Otay-type waxy bentonites of San Diego County and Baja California: chemistry, mineralogy, petrology and plate tectonic implications. Clays Clay Miner 47: 70-83

/BEV 98/ Beverskog, B., Puigdomenech, I. (1998): Pourbaix diagrams for the system copper-chlorine at 5-100 °C. SKI Rapport 98:19, Swedish Nuclear Power Inspectorate

/BIL 06/ Bildstein, O., Trotignona, L., Perronneta, M., Jullien, M (2006): Modelling iron – clay interactions in deep geological disposal conditions. Parts A/B/C. Physics and Chemistry of the Earth 31, pp. 10-14

/BOL 82/ G.H. Bolt, F.A.M. de Haan (1982): Anion exclusion in soil, In: G.H. Bolt (Ed.): Soil Chemistry: B. Physico-chemical Models, Elsevier, Amsterdam

/BÖR 03/ Börgesson, L., Johannesson, L.-E., Gunnarsson, D. (2003): Influence of soil structure heterogeneities on the behavior of backfill materials based on mixtures of bentonite and crushed rock. Applied Clay Science 23, 121–131

/BÖR 05/ Börgesson, L., Sandén, T., Fälth, B., Åkesson, M., Lindgren, E. (2005): Behavior of the buffer in KBS-3H. SKB Rapport R-05-50, Svensk Kärnbränslehantering AB

/BRA 03/ Bradbury, M.H., Baeyens, B. (2003): Near Field Sorption Data Bases for Compacted MX-80 Bentonite for Performance Assessment of a High-Level Radioactive Waste Repository in Opalinus Clay Host Rock. PSI Bericht 03-07, Paul Scherrer Institut, Villigen, Schweiz

/BRU 86/ Brusewitz, A.M. (1986): Chemical and physical properties of Paleozoic potassium bentonites from Kinnekulle, Sweden. Clays and Clay Minerals, 34, 4, 442-454

/BYR 84/ Byrne; R. H. and Millero; F.J. (1984): Medium composition dependence of lead (II) complexation by chlorite ion. Amer. J. Sci. 77: 5844-5848

/CAB 05/ Caballero, E., Jiménez de Cisneros, C., Huertas, F.J., Huertas, F., Pozzuoli, A., Linares, J. (2005): Bentonite from Cabo de Gata, Almería, Spain: a mineralogical and geochemical overview. Clay Miner. 40, 463-480

/CAR 08/ Carlson, L., Karnland, O., Olsson, S., Rance, A., Smart, N. (2008): Experimental studies on the interactions between anaerobically corroding iron and bentonite. SKB Rapport R-08-28, Svensk Kärnbränslehantering AB

/CAS 07/ Castellanos, E., Villar, M.V., Romero, E., Lloret, A., Gens, A. (2007): Chemical influence on the hydro-mechanical behavior of high-density FEBEX bentonite. International Meeting, September 17-18, 2007, Lille, France, Clays in Natural & Engineered Barriers for Radioactive Waste Confinement, 115-116

/CHA 71/ Chamley, H. (1971): Recherches sur la sédimentation argileuse en Méditerranée. Sci Géol, Strasbourg, Mém 35, 225 pp

/CHA 89/ Chamley H (1989): Clay sedimentology. Springer, Berlin Heidelberg New York, 623 pp

/CHO 93/ Cho, W. J., Oscarson, D. W. and Hahn; P. S. (1993): The measurement of apparent diffusion coefficients in compacted clays: an assessment of methods, Applied Clay Science, 82(8):283-294.

/CHR 06/ Christidis, G.E. (2006): Genesis and compositional heterogeneity of smectites. Part III: Alteration of basic pyroclastic rocks – A case study from the Troodos Ophiolite Complex, Cyprus. American Mineralogist 91, 685-701

/CHR 07/ Christidis, G.E., Makri, P. (2007): Distribution of layer charge and charge distribution of smectites in bentonite deposits: Implications for bentonite genesis. Euroclay ’07, Aveiro, Portugal, Abstracts

/CHR 08/ Christidis, G.E. (2008): Do bentonites have contradictory characteristics? An attempt to answer unanswered questions. Clay Minerals 43: 515-529

/CHR 09/ Christidis, G.E.; Huff, W.D. (2009): Geological Aspects and Genesis of Bentonites. Elements, Vol. 5, 93-98

/CHR 95/ Christides, G.E.; Scott, P.W.; Macropoulos, T. (1995): Origin of the bentonite deposits of eastern Milos, Aegean, Greece: Geological, mineralogical and geochemical evidence. Clays and Clay Minerals, 43(1), 63-77

/CHR 98/ Christidis, G.E. (1998): Comparative study of the mobility of major and trace elements during alteration of an andesite and a rhyolite to bentonite, in the islands of Milos and Kimolos, Aegean, Greece. Clays and Clay Minerals 46: 379-399

/CIC 76/ Cicel, B., Novak, I (1976): Dissolution of smectites in hydrochloric acid. I. Half-time of dissolution as a measure of reaction rate. 7th Conference on Clay Mineralogy and Petrology, Karlovy Vary, p. 163

/COM 85/ Comyn, J. (1985): Introduction to polymer permeability and the mathematics of diffusion. In: J. Comyn (Editor), Polymer Permeability, Ch. 1. Elsevier Applied Science Publ., London, pp. 1-10

/COR 03/ Cormenzanaa, J. L., García-Gutiérrez, M. Missanab, T. and Junghanns; A. (2003): Simultaneous estimation of effective and apparent diffusion coefficients in compacted bentonite, Applied Clay Science, 61, 63-72

/CRA 75/ Crank, J. (1975): The Mathematics of Diffusion. Clarendon Press, Oxford, 2nd ed., 414pp

/DEC 96/ Decher A, Bechtel A, Echle W, Friedrich G, Hoernes S, (1996): Stable isotope geochemistry of bentonites from the island of Milos (Greece). Chemical Geology, Volume 129, Number 1, 14 June 1996, pp 101-113(13) Elsevier

/DEL 10/ Delage, P., Cui, Y. J., Tang, A. M. (2010): Clays in radioactive waste disposal. Journal of Rock Mechanics and Geotechnical Engineering, 2010, 2 (2): 111-123

/DES 86/ Desaulniers, D.E., Kaufman, R.S., Cherry, J.A. and Bentley, H.W., (1986): 37C1-35C1 variations in a diffusion-controlled groundwater system. Geochim. Cosmochim. Acta, 50: 1757-1764

/DIX 96/ Dixon, D.A., Gray, M.N., Graham, J. (1996): Swelling and hydraulic properties of bentonites from Japan, Canada and the USA. Environmental Geotechnics, Kamon (ed), Balkema, Rotterdam

/DUT 62/ Dutt, G.R. and Low, P.F. (1962): Diffusion of alkali chloride in clay-water systems. Soil Science, 93:233-240

/ELZ 89/ Elzea J M, Murrey H H, (1989): Trace element composition of the Cretaceous Clay Spur bentonite and implications for its alteration history. 9th Int. Clay Conference, Strasbourg

/ELZ 94/ Elzea, J., Murray, H.H. (1994): Bentonite. Pp. 233-246 in: Industrial Minerals and Rocks (D.D. Can', editor). Society for Mining, Metallurgy, and Exploration, Littleton, Colorado

/EPA 99/ EPA (U.S. Environmental Protection Agency) and DOE (U.S. Department of Energy) (1999): Understanding Variation in Partition Coefficient, Kd, Values, Volume I: The Kd Model, Methods of Measurement, and Application of Chemical Reaction Codes, Technical Report: EPA 402-R-99-004A

/FAR 77/ Farrah, H. and Pickering, W.F. (1977): The sorption of lead and cadmium species by clay minerals, Australian Journal of Chemistry 30(7) 1417-1422

/FAR 80/ Farmer. W. J., Yang, M. S., Letey, J., and Spencer, W. F. (1980): Land Disposal of Hexachlorobenzene Wastes-Controlling Vapor Movement in Soil. EPA-600/2-80-119, Cincinnati, OH, U.S. EPA

/FER 04/ Fernández, A.M., Baeyens, B., Bradbury, M. and Rivas, P. (2004): Analysis of the porewater chemical composition of a Spanish compacted bentonite used in an engineered barrier. Phys. Chem. Earth. 29, 105-118

/FER 10/ Fernández, R., Rodríguez, M., Vigil de la Villa, R. and Cuevas, J. (2010): Geochemical constraints on the stability of zeolites and C-S-H in the high pH reaction of bentonite. Geochim. Cosmochim. Acta 74, 890-906

/FIC 1855/ Fick, A. (1855): Über Diffusion, Annalen der Physik, 170(1):59-86, DOI: 10.1002/andp.18551700105 (in German)

/FRE 26/ Freundlich, H. (1926): Colloid and Capillary Chemistry. Methuen, London, England

/FRE 79/ Freeze, R.A. and Cherry, J.A., (1979): Groundwater. Prentice-Hall, Englewood Cliffs, NJ, 604pp

/GAR 65/ Garrels, R. M.; Christ, C. L. (1965): Solutions, Minerals, and Equilibria. Harper, London

/GEN 11/ GenChem website (Last visit 2011-11-29): http://chemed.chem.wisc.edu/chempaths/GenChem-Textbook/Transition-Metal-Ions-in-Aqueous-Solutions-1055.html

/GER 74/ Gerthsen, Ch., Kneser, H. O., Vogel, H. (1974): Physik. – 12. neu bearbeitete Auflage von H. Vogel, Springer Verlag, Berlin, Heidelberg, New York

/GIL 84/ Gillham, R.W., Robin, M. L. J., Dytynyshyn, D. J. and Johnston, H.M., (1984): Diffusion of nonreactive and reactive solutes through fine-grained barrier materials. Can. Geotech. J., 21: 541-550

/GLA 07/ Glaus, M. A., B. Baeyens, M. H. Brandbury, A. Jakob, L.R. van Loon and A. Yaroshchuk (2007): Diffusion of ^{22}Na and ^{85}Sr in montmorillonite: Evidence of interlayer diffusion being the dominant pathway at high compaction, Environ. Sci. Technol., 41:478-485

/GOO 07/ Goody D. C., Kinniburgh, D. G., Barker J.A. (2007): A rapid method for determining apparent diffusion coefficients in Chalk and other consolidated porous media, J. Hydrology 343:97-103

/GRA 86/ Grauer, R. (1986): Bentonite as a backfill material in the high-level waste repository: chemical aspects, Nagra Technical Report 86-12E, Nagra, Baden, Switzerland

/GRA 97/ Grathwohl, P. (1997): Diffusion in natural porous media: Contaminant Transport, Sorption/Dissolution kinetics, Kluwer Academic Publishers, Boston/Dordrecht/London

/GRA 98/ Grathwohl, P. (1998): Diffusion in Natural Porous Media: Contaminant Transport, Sorption/Desorption and Dissolution Kinetics. Kluwer Academic Publishers, Boston, 224 p

/GRI 68/ Grim, R.E. (1968): Clay Mineralogy, 2nd edn. McGraw Hill, New York, 596 pp

/GWI 98/ Gwiazda, R., Woolard, D. and Smith, D. (1998): Improved lead isotope ratio measurements in environmental and biological samples with a double focusing magnetic sector inductively coupled plasma mass spectrometer (ICP-MS), J. Anal. At. Spectrom., 13, 1233-1238, DOI: 10.1039/A804062A

/HAG 99/ Hagemann S. (1999): Thermodynamische Eigenschaften des Bleis in Lösungen der ozeanischen Salze, PhD-thesis, Braunschweig, Germany

/HED 12/ Hedström, M. and Karnland, O. (2012): Donnan equilibrium in Na-montmorillonite from a molecular dynamics perspective, Geochimica et Cosmochimica Acta 77 (2012) 266-274

/HEN 98/ Henning, K.-H.; Kasbohm, J. (1998): Mineralbestand und Genese feinkörniger quartärer und präquartärer Sedimente in NE-Deutschland unter besonderer Berücksichtigung des “Friedländer Tones”.- Berichte der DTTG, Bd. 6: S. 147-167; Greifswald

/HER 00/ Herbert, H.-J. (2000): Zur Geochemie und geochemischen Modellierung hochsalinarer Lösungen mineralischer Rohstoffe, Geol. Jahrbuch, Reihe D, Heft SD1, Hannover

/HER 04/ Herbert, H.-J.; Kasbohm, J.; Moog, H. C.; Henning, K.-H. (2004): Long-term behavior of the Wyoming bentonite MX-80 in high saline solutions. Applied Clay Science 26: 275-291

/HER 08/ Herbert, H.-J., Kasbohm J., Sprenger, H., Fernandez, A. M., Reichelt, C. (2008) Swelling pressured of MX-80 bentonite in solutions of different ionic strength. Physics and Chemistry of the Earth 33, pp. S327-S342

/HER 11/ Herbert, H.-J., Kasbohm, J., Nguyen, T. L., Mayer, L., Hoang, T. and Xie, M. (2012): Fe-Bentonite, Experiments and Modelling of the Interactions of Bentonites with Iron, GRS-295

/HER 12/ Herbert, H.-J., Kasbohm, J., Nguyen, T. L., Mayer, L., Hoang, T. and Xie, M. (2012): Fe-Bentonite, Experiments and Modelling of the Interactions of Bentonites with Iron, GRS-295

/HIC 09/ Hicks, T. W., White, M. J., Hooker, P. J. (2009): Role of bentonite in determination of thermal limits on Geological Disposal Facility design. Galsons Sciences Ltd., Report 0883-1 (v 2.0) for Nuclear Decommissioning Authority, Harwell

/HOL 98/ Hollis, W. K., Velarde, K., Lashley, J., Bustos, L., Cournoyer, M. Villarreal, M. (1998): Gas generation from contact of radioactive waste and brine. Journal of Radioanalytical and Nuclear Chemistry, 235(1-2), 235-239

/HUS 54/ Husted, R. F. and Low, P. F. (1954): Ion diffusion in bentonite. Soil Sci., 77(5): 343-353

/INO 95/ Inoue, A. (1995): Formation of clay minerals in hydrothermal environments. In: Velde, B. (Edtr.): Origin and mineralogy of clays. Springer-Verlag Berlin Heidelberg, p. 268-331

/ISH 90/ Ishikawa, H.; Amemiya, K.; Yusa, Y.; Sakaki, N. (1990): Comparison of fundamental properties of Japanese bentonite as buffer material for waste disposal. Proc. 9th Int. Clay. Conf. Sci. Geol. Mem. 87, pp. 107-115

/JAC 77/ Jacobsson, A., Pusch, R. (1977): Deponering av högaktivt avfall i borrhål med buffert-substans. Högskolan I Luleå Tekn. Rapport 77-05-27

/JAS 93/ Jasmund, K. (1993): Bildung und Umbildung von Tonmineralen. In: Jasmund, K.; Lagaly, G. (Edt.): Tonminerale und Tone – Struktur, Eigenschaften, Anwendung und Einsatz in Industrie und Umwelt. Steinkopff Verlag Darmstadt

/JOC 00/ Jockwer, N.; Miehe, R.; Müller-Lyda, I. (2000): Untersuchungen zum Zweiphasenfluss und diffusiven Transport in Tonbarrieren und Tongesteinen. Abschlussbericht. – GRS-167, Braunschweig, Germany

/JOC 01/ Jockwer, N., Wieczorek, K. (2001): Gas Release and Migration in the Boom Clay of Mol within the Project 'Corrrosion of Active Glass in the Underground Conditions' (CORALUS). Abschlussbericht, GRS-171, Braunschweig, Germany

/JOC 97/ Jockwer, N, Hertes, U. und Sprenger, H. (1997): Gaserzeugung und -freisetzung in Abfällen und deren Ausbreitung im umgebenden Gebirge – Abschlussbericht zu den BMBF-Vorhaben 02 C 01636 und 02 C 04453, GRS-A-2539, 68 S.

/JON 88/ Jones, B.F., Galan, E. (1988): Sepiolite and palygorskite. In: Bailey, SW. (ed) Hydrous phyllo-silicates (exclusive of micas). Rev Mineral 19: 631-674

/JOS 60/ Jost, W. (1960): Diffusion in Solids, Liquids and Gases. Academic Press, New York, NY, 558 pp

/JOS 72/ Jost, W.; Haufe, K. (1972): Diffusion, Steinkopf Verlag, Darmstadt

/KAR 06/ Karnland, O.; Olsson, S., Nilsson, U. (2006): Mineralogy and sealing properties of various bentonites and smectite-rich clay materials. Technical Report TR-06-30, Svensk Kärnbränslehantering AB

/KAR 06b/ Karnland, O. (2006): In Wersin P. and Mettler S. (2006): Workshop on Fe-clay interactions in repository environments, a joint initiative by Andra, SKB and Nagra. Basel 9-10 May 2006. NAB-06-15. Nagra, Wettingen, Switzerland

/KAR 09/ Karnland, O., Olsson, S., Dueck, A., Birgersson, M., Nilsson, U., Hernan-Håkansson, T., Pedersen, K., Nilsson, S., Eriksen, T. E., Rosborg, B. (2009): Long term test of buffer material at the Äspö Hard Rock Laboratory, LOT project - Final report on the A2 test parcel, Technical Report TR-09-29, Svensk Kärnbränslehantering AB

/KAR 10/ Karnland, O. (2010): Chemical and mineralogical characterization of the bentonite buffer for the acceptance control procedure in a KBS-3 repository. Technical Report TR-10-60, Svensk Kärnbränslehantering AB

/KAR 92/ Karnland, 0., Pusch, R., Sanden, T. (1992): Electrolytens betydelse for de fysikaliska egenskapema hos MX-80 bentonit. SKB AR 92-35

/KAR 98/ Karnland, O. (1998): Bentonite swelling pressure in strong NaCl solutions - Correlation of model calculations to experimentally determined data, POSIVA 98-01, POSIVA OY

/KAS 12/ Kasbohm, J., Pusch, R., Nguyen Thanh Lan, Hoang Thi Minh Thao (2012): Lab-scale performance of selected expandable clays under HLW repository near-field view. Environmental Earth Sciences, submitted (ENGE-D-11-00869R1)

/KAU 08a/ Kaufhold, S., Dohrmann, R. (2008): Detachment of colloidal particles from bentonites in water. Applied Clay Science, 39, 50-59

/KAU 08b/ Kaufhold, S., Dohrmann, R., Koch, D., Houben, G. (2008): The pH of aqueous bentonite suspensions. Clays and Clay Minerals, 56, 338-343

/KAU 09/ Kaufhold, S., Dohrmann, R. (2009): Stability of bentonites in salt solution | sodium chloride. Applied Clay Sciences 45(3), 171-177

/KAU 10/ Kaufhold, S., Dohrmann, R. (2010): Stability of bentonites in salt solutions II. Potassium chloride solution - Initial step of illitisation? Applied Clay Science 49, 98-107.

/KAU 11a/ Kaufhold, S., Dohrmann, R. (2011): Stability of bentonites in salt solutions III – Calcium hydroxide. Applied Clay Science 51, 300-307

/KAU 11b/ Kaufhold, S., Dohrmann, R., Stucki, J.W., Anastácio, A.S. (2011): Layer charge density of smectites closing the gap between the structural formula method and the alkyl ammonium method. Clays and Clay Minerals, 59/2, 200-211

/KIE 55/ Kiersch, G.A., Keller, W.D. (1955): Bleaching clay deposits, Sanders-Defiance Plateau District, Navajo County, Arizona. Economic Geology, 50: 469-494

/KIM 93/ Kim, H.T., Suk, T.-W., Park S.-H., Lee, C.-S. (1993): Diffusivities for ions through compacted Na-bentonite with varying dry bulk density. Waste Management 13:303-308

/KIN 08/ King, F. (2008): Corrosion of carbon steel under anaerobic conditions in a repository for SF and HLW in Opalinus Clay. Nagra Technical Report 08-12

/KOC 08/ Koch, D. (2008): European Bentonites as alternatives to MX-80. Science & Technology Series, 334 (2008), ANDRA

/KOL 02/ Kolditz, O., (2002): Computational Methods in Environmental Fluid Mechanics. Springer

/KOL 10/ Kolditz, O and Shao, H. (2010): OpenGeoSys, Developer-Benchmark-Book OGS-DBB 4.10.07. (to be published)

/KON 86/ Konta J, (1986): Textural variation and composition of bentonite derived from basaltic ash. Clays and Clay Minerals; June 1986; v.34; no. 3; p.257-265

/KRA 70/ Crank, J. (1970): The mathematics of diffusion, Oxford University Press, London

/KRU 01/ Kruger, J. (2001): Electrochemistry Encyclopedia - Electrochemistry of corrosion; downloaded from http://electrochem.cwru.edu/encycl/art-c02-corrosion.htm (July 26, 2012)

/LAI 06/ Laird, D. A. (2006): Influence of layer charge on swelling of smectites, Applied Clay Science, 34, 74–87

/LAN 05/ Lantenois, S., Lanson, B., Muller, F., Bauer, A., Jullien, M. and Plançon, A. (2005): Experimental study of smectite interaction with metal Fe at low temperature: 1. Smectite destabilization. Clays and Clay Minerals 53, 597-612

/LAN 18/ Langmuir, I. (1918): The adsorption of gases on plane surfaces of glass, mica and Platinum, J. Am. Chem. Soc. 40, 1361-1403

/MAD 98/ Madsen, F. T. und Kahr, G. (1991): Diffusion of iron and iodine ions in highly densified bentonite – NAGRA-NTB-91-28

/MAR 08/ Martin, F.A., Bataillon, C., Schlegel, M.L. (2008): Corrosion of iron and low alloyed steel within a water saturated brick of clay under anaerobic deep geological disposal conditions: An integrated experiment. Journal of Nuclear Materials 379, 80-90

/MEU 04/ Meunier, A., Lanson, B., Velde, B. (2004): Composition variation of illite-vermiculite-smectite mixed-layer minerals in a bentonite bed from Charente (France), Clay Minerals 39: 317-332

/MEU 05/ Meunier, A. (2005): Clays. Springer Berlin Heidelberg New York

/MIL 64/ Millot, G (1964): Geologie des argiles. Masson, Paris, 510pp

/MIL 70/ Millot, G. (1970): Geology of Clays. Springer, New York Heidelberg Berlin

/MIL 84/ F.J. Millero and R. H. Byrne (1984): Use of Pitzer's equations to determine the media effect on the formation of lead chloro complexes, Geochimica et Cosmochimica Acta, 48(5):1145-1150

/MIS 99/ Misaelides P., Macášek F., Pinnavaia TJ, Colella C. (1999): Natural Microporous Materials in Environmental Technology – NATO Science Series, Series E: Applied Sciences, Vol. 362, Kluwer Academic Press

/MOL 01/ Moll, W.F (2001): Baseline studies of the clay minerals society source clays: geological origin. Clays and Clay Minerals 49 (5), pp. 374-380

/MOS 10/ Mosser-Ruck, R., Cathelineau, M., Guillaume, D., Charpentier, D., Rousset, D., Barres, O., Michau, N. (2010): Effects of temperature, pH, and iron/clay and liquid/clay ratios on experimental conversion of dioctahedral smectite to berthierine, chlorite, vermiculite, or saponite. Clays and Clay Minerals, 58(2) 280-291

/MOT 83/ Mottl, M.J. (1983): Metabasalts, axial hot springs, and the structure of hydrothermal systems at mid-oceanic ridges. Bull. Geol. Soc. Am. 94: 161-180

/MUE 12/ Müller-Hoeppe, N. (2012): Vorläufige Sicherheitsanalyse Gorleben. Materialspezifikationen für Filter/Aufsättigungs- und Widerlager/Speicherelemente sowie eines Langzeitdichtelementes für die Planung von Schacht- und Streckenverschlüssen (Arbeitspaket 9.1.2), DBE Technology GmbH

/MUE 97/ Müller-Lyda, I. (Edt.) (1997): Erzeugung und Verbleib von Gasen in einem Endlager für radioaktive Abfälle, Bericht über den GRS-Workshop vom 29. und 30. Mai 1996 in Braunschweig, GRS-129, Braunschweig, Germany

/MÜL 90/ Müller-Vonmoos, M., Kahr, G., Bucher, F., Madsen, F.T. (1990): Investigation of Kinnekulle K. bentonite aimed at assessing the long-term stability of bentonites under repository conditions. Eng. Geol., 28: 269-280

/MÜL 91/ Müller-Vonmoos, M., Bucher, F., Kahr, G., Madsen, F.T., Mayor, P.A. (1991): Wechsellagerungen und Quellverhalten von Kalium-Bentoniten. Technischer Bericht 91-13, NAGRA

/MUU 04/ Muurinen, A., O. Karnland and J. Lehikoinen (2004): Ion concentration caused by an external solution into the porewater of compacted bentonite Phys. Chem. Earth, 29, pp. 119-127

/MUU 90/ Muurinen, A. (1990): Diffusion of uranium in compacted sodium bentonite. Eng. Geol., 28, 359-367

/NGU 12/ Nguyen Than Lan (2012): Mineralogical Characterization of Fe-driven Alteration in Smectites. PhD-thesis, University of Greifswald

/NOV 78/ Novák, I., Cicel, B (1978): Dissolution of smectites in hydrochloric acid: II Dissolution rate as a function of crystallochemical composition. Clays and Clay Minerals 26, 341-344

/OCH 04/ Ochs, M. and Talerico, C. (2004): SR-CAN: Data and uncertainty assessment. Migration parameters for the bentonite buffer in the KBS-3 concept SKB Technical Report TR-04-18, SKB, Stockholm

/OLS 65/ Olsen, S.R., Kemper, W.D. and van Schaik, J.C., (1965): Self-diffusion coefficients of phosphorus in soil measured by transient and steady-state methods. Proc. Soil Sci. Soc. Am., 29, 154-158

/ORT 02/ Ortiz, L., Volckaert, G. Mallants, D. (2002): Gasgeneration and migration in Boom Clay, a potential host rock formation for nuclear waste storage.- Engineering Geology 64, 287-296

/OSC 92/ Oscarson, D.W., Hume, H.B., Sawatsky, N.G., Cheung, S.C.H., (1992): Diffusion of iodide in compacted bentonite. Soil Sci. Soc. Am. J. 56, 1,400-1406

/OSC 94/ Oscarson, D.W. (1994): Surface diffusion: Is it an important transport mechanism in compacted clays? Clays and Clay Minerals, 42(5):534-543

/PAP 03/ Papillon, F., Jullien, M., Bataillon, C. (2003): Carbon steel behaviour in compacted clay: two long term tests for corrosion prediction. In “Prediction of the long term corrosion behavior in nuclear waste systems”. Féron and MacDonald (Eds.), European Federation of Corrosion Publications, 36, 439-454, Maney Publishing, UK

/PEA 03/ Pearson, F.J., Arcos, D., Bath, A., Boisson, J.-Y., Fernàndez, A. M., Gäbler, H.E., Gaucher, E., Gautschi, A., Griffault, L., Hernàn, P., Waber, H.N. (2003): Mont Terri Project- Geochemistry of water in the Opalinus Clay Formation at the Mont Terri rock laboratory. Berichte des BWG, Serie Geologie No.5., Bundesamt Wasser und Geologie, Bern

/PER 08/ Perronnet, Jullien, M., Villiéras, F., Raynal, J., Bonnin, D., Bruno, G. (2008): Evidence of a critical content in Fe(0) on Foca7 bentonite reactivity at 80 °C. Applied Clay Science, 38, 187-202

/PRI 02/ Přikryl R, Woller F, (2002): Going underground: A new market for Czech bentonite in nuclear waste disposal. Industrial Minerals 415, 72-77

/PUS 01/ Pusch, R. (2001): The Buffer and Backfill Handbook, Part 2: Materials and techniques. Technical Report TR-02-12, Svensk Kärnbränslehantering AB

/PUS 07a/ Pusch, R., Kasbohm, J., Pacovsky, J., Cechova, Z. (2007): Are all smectite clays suitable as “buffers”? Physics and Chemistry of the Earth, Parts A/B/C, 32(1-7): 116-122, [Clay in natural and engineered barriers for radio-active waste confinement - Part 1]

/PUS 07b/ Pusch, R., Kasbohm, J., Hoang-Minh Thao (2007): A laboratory study of expandable clays in a simulated HLW repository. Lund Workshop, Sweden

/PUS 10/ Pusch, R., Kasbohm, J, Hoang-Minh, T (2010): Chemical stability of montmorillonite buffer clay under repository-like conditions - A synthesis of relevant experimental data. Applied Clay Science 47, 113-119

/PUS 80/ Pusch, R. (1980): Swelling pressure of highly compacted bentonite. SKB TR 80-13

/PUS 82/ Pusch, R. (1982): Copper/bentonite interaction. SKBF/KBS Technical Report 82-07

/PUS 90/ Pusch, R., Karnland, O., Hökmark, H., (1990): GMM – a general micro-structural model for qualitative and quantitative studies of smectite clays. SKB Technical Report 90-43, Swedish Nuclear Fuel and Waste Management Corporation, Stockholm, Sweden

/PUS 93/ Pusch, R. (1993): Waste Disposal in Rock. Developments in Geotechnical Engineering, 76, Elsevier

/PUS 95/ Pusch, R., Madsen, F. (1995): Aspects on the illitization of the Kinnekulle bentonites. Clays and Clay Minerals, 43, 3: 261-270

/PUS 98/ Pusch, R., Hiroyasu Takase, Benbow, S. (1998): Chemical processes causing cenetation in heta-affected smectite – the Kinnekulle bentonite. Technical Report TR-98-25, Svensk Kärnbränsle-hantering AB

/PUS 99/ Pusch, R. (1999): Microstructural evolution of buffers. Engineering Geology 54, 32-42

/REF 03/ Refait, P., Memet, J.B., Bon, C., Sabot, R. and Genin, J.M.R. (2003): Formation of the Fe,II–Fe,III hydroxysulphate green rust during marine corrosion. Corrosion Science 45, 833-845

/ROG 85/ Rogers, C.E. (1985): Permeation of gases and vapors in polymers. In: J. Comyn (Editor), Polymer Permeability, Ch. 2. Elsevier Applied Science Publ., London, pp. 11-74

/ROW 87/ Rowe, R.K. (1987): Pollutant transport through barriers. In: R.D. Woods (Edt.), Geotechnical Practice for Waste Disposal. Am. Soc. Civ. Eng., Spec. Publ. No. 13, pp.159-181

/RUE 04/ Rübel, A., Noseck, U., Müller-Lyda, I., Kröhn, K.-P., Storck, R. (2004): Konzeptioneller Umgang mit Gasen im Endlager. GRS-205, Gesellschaft für Anlagen und Reaktorsicherheit (GRS) mbH, Braunschweig, Germany

/SAM 09/ Samper, J.; Dewonck, S., Theng, L., Yang, Q. and Naves, A. (2008): Normalized sensitivities and parameter identifiability of in situ diffusion experiments on Callovo-Oxfordian clay at Bure site, Physics and Chemistry of the Earth. 33(14-16), pp 1000-1008

/SAR 00/ Sarin, C., Hall, J. M., Cotter-Howells, J., Killham, K. and Cresser, M. S. (2000): Influence of complexation with chloride on the responses of a lux-marked bacteria bioassay to cadmium, copper, lead, and mercury. Environmental Toxicology and Chemistry, 19: 259-264. doi: 10.1002/etc.5620190202

/SAV 05/ Savage, D. (2005): The effects of high salinity groundwater on the performance of clay barriers. SKI Report 54

/SAY 77/ Sayles, F.L., Mangelsdorf, P.C. (1977): The equilibration of clay minerals with seawater: ex-change reactions. Geochim. Cosmochim. Acta 41:951-960

/SCH 08/ Schade, H. (2008): Reverse mining–The development of deep geologic isolation of hazardous (chemotoxic) waste in Germany and its international prospects, Reviews in Engineering Geology, 19, p. 23-30

/SCH 98/ Schon, T.H.; Heidendael, M. (1998): Wasserstoffbildung durch Metallkorrosion. Bericht des Forschungszentrums Jülich Nr. 3495, Januar

/SEI 90/ Seim, R., Tischendorf, G. (1990): Grundlagen der Geochemie. VEB Deutscher Verlag für Grundstoffindustrie, Leipzig

/SEN 84/ Senkayi, A. L.; Dixon, J. B.; Hossner, L. R.; Abder-Ruhman, M.; Fanning, D. S. (1984): Mineralogy and genetic relationships of tonstein, bentonite, and lignitic strata in the Eocene Yegua Formation of East-Central Texas, Clays & Clay Miner. 32: 259-271

/SHA 88/ Shackelford, C. D. (1988): Diffusion of inorganic chemical wastes in compacted clay, thesis presented to the University of Texas, at Austin, Tex., in partial fulfillment of the requirements for the degree of Doctor of Philosophy

/SHA 91/ Schackelford, C. D. (1991): Laboratory diffusion testing for waste disposal – A review, J. Contaminant Hydrology, 7: 177-217

/SHA 97/ Shah N R, (1997): Indian bentonite – focus on the Kutch region, Industrial Minerals, no. 359, pp 43-47

/SHI 02/ Shibata, M. et al. (2002): ANDRA International Meeting, 2002, Reims, Abstract pp.151-152, O-10b-4

/SIL 61/ Sillén, L.G. (1961): The physical chemistry of sea water. In: Sears, M. (Edt.) Oceanography. Am. Assoc. for the Advancement of Science, Washington, DC, pp 549-581

/SLA 65/ Slaughter, M., Early, J. W. (1965): Mineralogy and Geological Significance of the Mowry Bentonites, Wyoming. Geol.Soc. Am. Spec. Pap., 83

/SOM 09/ Somelar, P., Kirsimäe, K., Środoń, J. (2009): Mixed-layer illite-smectite in the Kinnekulle K-bentonite, northern Baltic Basin. Clay Minerals, 44, 4: 455-468

/STR 09/ Stríček I, Šucha V, Uhlík, P, Madejová J, Galko, I. (2009): Mineral stability of Fe-rich bentonite in the Mock-Up-CZ experiment. Geologica Carpathica, October 2009, 60, 5, 431-436, DOI: 10.2478/v10096-009-0031-2

/STU 96/ Stumm, W. and Morgan, J. J. (1996): Aquatic chemistry: chemical equilibria and rates in natural waters, 3rd Edition, John Wiley & Sons, Inc., New York

/ŠUC 05/ Šucha, V., Adamcová, R., Bujdák, R., Haasová, Z., Honty, M., Komadel, P., Kufčáková, J., Madejová, J., Rajec, P., Stríček, I., Uhlík, P. Valúchová, J. (2005): Fyzikálne a mechanické vlastnosti tesniacich materiálov pre úložisko RAO, Čiastková úloha projektu SP 26/028 0C 00/028 0C 02 Štátneho programu výskumu a vývoja Záverečná správa, Univerzita Komenského, Prírodovedecká fakulta, Bratislava, 281 p

/SZA 07/ Szakalos, P., Hultquist, G., Wikmark, G. (2007): Corrosion of Copper by Water. Electro-chemical and Solid-State Letters 10 (11), C63-C67

/TAA 91/ Zweite allgemeine Verwaltungsvorschrift zum Abfallgesetz (TA-Abfall) Teil 1: Technische Anleitung zur Lagerung, chemisch/physikalischen, biologischen Behandlung, Verbrennung und Ablagerung von besonders überwachungsbedürftigen Abfällen vom 12.03.1991 (GMBl 1991, S. 139, ber. S.467)

/TAM 84/ Tamaura, Y., Yoshida, T. and Katsura, T. (1984): The synthesis of green rust II, FeIII–FeII and its spontaneous transformation to Fe3O4. Bulletin of the Chemical Society of Japan 57, 2411–2416

/TIN 69/ Tinker, P. B. (1969): A steady-state method for determining diffusion coefficients in soil. Journal of Soil Science, 20: 336–345. doi: 10.1111/j.1365-2389.1969.tb01582.x

/TOU 11/ Tournassat, C., Appelo, C.A.J. (2011): Modelling approaches for anion-exclusion in compacted Na-bentonite, Geochim. Cosmochim. Acta 75:3698–3710

/TRA 77/ Trauth, N. (1977): Argiles évaporitiques dans la sedimentation carbonatée continentale et épicontinentale tertiaire. Bassins de Paris, de Mormoiron et de Salinelle (France), Jbel Ghassoul (Maroc): Sci. Géol. Mém. 19, 195 pp

/UFE 08/ Ufer, K., Stanjek, H., Roth, G., Dohrmann, R., Kleeberg, R., Kaufhold, S (2008): Quantitative phase analysis of bentonites by the Rietveld method. Clays and Clay Minerals 56 (2), pp. 272-282

/VAN 05/ Van Loon, L.R., Baeyens, B., Bradbury, M.H. (2005): Diffusion and retention of sodium and strontium in Opalinus clay: Comparison of sorption data from diffusion and batch sorption measurements, and geochemical calculations, Applied Geochemistry 20(12): 2351-2363

/VAN 07/ van Loon, L.R., Glaus, M. A., and Müller, W. (2007): Anion exclusion effects in compacted bentonites: Towards a better understanding of anion diffusion, Applied Geochemistry, 22:2536-2552

/VAN 53/ Vanderzee, C. E. and Dawson, H. J. (1953): The Stability Constants of Cadmium Chloride Complexes: Variation with Temperature and Ionic Strength, J. Am. Chem. Soc., 75 (22), pp 5659-5663

/VEL 92/ Velde, B. (1992): Introduction to clay minerals – Chemistry, Origin, Uses and Environmental Significance. Chapman & Hall, London

/VIL 09/ Vilks, P. (2009): Sorption in highly saline solutions – State of the science review, Technical report, NWMO TR-2009-18, Canada

/VIL 11/ Vilks, P., Miller, N. H. and Felushko, K. (2011): Sorption experiments in Brine solutions with sedimentary rock and bentonite, Technical report, NWMO TR-2011-11, Canada

/VOG 80/ Vogt, K. (1980): Bentonite deposits in lower Bavaria. Geol. Jb. D 39, 47-68

/VOL 95/ Volckaert, G., Ortiz, L., De Cannière, P., Put, M., Horseman, S. T., Harrington, J. F., Fiovanante, V., Impey, M. D., (1995): MEGAS: Modelling and experiments on GAS migration in repository host rocks. Final report phase 1, Eur. Comm. [Rep]. EUR 16235 EN

/VOP 06/ Vopálka, D., Filipská, H., and Vokál, A. (2006): Some methodological modifications of determination of diffusion coefficients in compacted bentonite, in: Scientific basis for nuclear waste management XXIX, Mat. Res. Soc. Symp. Proc., vol. 932, edited by P. Van Isheghem, pp. 983-990, Warrendale, PA

/WAR 94/ Warnecke, E., Hollmann, A., Tittel, G., and Brennecke, P. (1994): Gorleben radionuclide migration experiments: more than 10 years of experience. Radiochimica Acta, 66/67, 821-827

/WEA 77/ Weaver, C.E., Beck, K.C. (1977): Miocene of the S.E. United States: A model for chemical sedimentation in a peri-marine environment. Sediment. Geol. 17, 1-234

/WEB 06/ Webb, S.W. (2006): Gas transport mechanism, In: Ho, C.-K. and Webb, S.W. (eds): Gas transport in porous media, Chapter 2. Springer, pp 5-20

/WER 03/ Wersin, P., Johnson, L.H., Schwyn, B., Berner, U., and Curti, E. (2003): Redox Conditions in the Near Field of a Repository for SF/HLW and ILW in Opalinus Clay, Nagra Technical Report 02-13, Switzerland

/WER 08/ Wersin, P., Birgersson, M., Olsson, S., Karnland, O., Snellman, M., Saanio Oy and Riekkola Oy (2008): Impact of corrosion-derived iron on the bentonite buffer within the KBS-3H disposal concept The Olkiluoto site as case study. SKB Rapport R-08-34, Svensk Kärnbränslehantering AB

/WIL 03/ Wilson, J.C. (2003): The effect of iron on bentonite stability. PhD Thesis, University of Bristol, UK

/WIL 04/ Wilson, J., Cuadros, J., Cressey, G. (2004): An in-situ time-resolved XRD-PSD investigation into sodium-montmorillonite interlayer and particle rearrangement during dehydration. Clays and Clay Minerals 52, 180-191

/WIL 06a/ Wilson, J., Savage, D., Cuadros, J., Shibata, M., and Ragnarsdottir, K.V. (2006): The effect of iron on montmorillonite stability. (I) Background and thermodynamic considerations; Geochim. Cosmochim. Acta 70, 306-322

/WIL 06b/ Wilson, J., Cressey, G., Cressey, B., Cuadros, J., Ragnarsdottir, K.V., Savage, D. and Shibata, M. (2006): The effect of iron on montmorillonite stability. (II) Experimental investigation. Geochimica et Cosmochimica Acta, 70, 323–336

/WIL 09/ Wilson, J., Thorne, M., Towler, G. (2009): Treatment of Chemotoxic Species (1) Quantitative Human Health Risk Assessment. QRS-1378M-1, Quintessa

/WIL 11/ Wilson, J.; Savage, D.; Bond, A.; Watson, S.; Pusch, R.; Bennett, D. (2011): Bentonite – A Review of key properties, processes and issues for consideration in the UK context. Quintessa Ltd., Henley-on-Thames

/XIA 11/ Xiaodong L, Prikryl, R., and Pusch, R. (2011): THMC-testing of three expandable clays of potential use in HLW repositories. App Clay Sci 52:419-427

/XIE 06/ Xie, M., Bauer, S., Kolditz, O., Nowak, T., and Shao, H. (2006): Numerical simulation of reactive processes in an experiment with partially saturated bentonite, J. Contam. Hydrol. 83, 122-147

/YAR 97/ Yraiv, S., Michaelian, K.H. (1997): Surface acidity of clay minerals, Industrial examples. Schriftenreihe für angewandte Geowissenschaften 1, 181-190

/YUN 97/ Yu, J. W., and Neretnieks, I. (1997): Diffusion and sorption properties of radianuclides in compacted bentonite, Technical Report 97-12, SKB, Sweden

/ZIE 83/ Zierenberg, R.A., Shanks, III W.C. (1983): Mineralogy and geochemistry of epigenetic features in metalliferrous sediment, Atlantis II Deep, Red Sea, Econ Geol 78:57–72

List of figures

List of tables

Gesellschaft für Anlagen- und Reaktorsicherheit (GRS) mbH

Schwertnergasse 1
50667 Köln
Telefon +49 221 2068-0
Telefax +49 221 2068-888

Forschungszentrum
85748 Garching b. München
Telefon +49 89 32004-0
Telefax +49 89 32004-300

Kurfürstendamm 200
10719 Berlin
Telefon +49 30 88589-0
Telefax +49 30 88589-111

Theodor-Heuss-Straße 4
38122 Braunschweig
Telefon +49 531 8012-0
Telefax +49 531 8012-200

www.grs.de

ISBN 978-3-939355-79-3